Phosphorus Ligands Derived From Terpene Alcohols
as Stereochemical Probes

by

Jihong Wang
B.Sc., Beijing University, 1989

A Dissertation Submitted in Partial Fulfilment of the
Requirements for the Degree of

DOCTOR OF PHILOSOPHY

in the Department of Chemistry

We accept this dissertation as conforming
to the required standard

_____
Dr. S.R. Stobart, Supervisor (Department of Chemistry)

_____
Dr. R.H. Mitchell, Departmental Member (Department of Chemistry)

_____
Dr. G.W. Bushnell, Departmental Member (Department of Chemistry)

_____
Dr. C.E. Picciotto, Outside Member (Department of Physics and Astronomy)

_____
Dr. W.R. Cullen, External Examiner (Department of Chemistry, University of British
Columbia)

© Jihong Wang, 1995
University of Victoria

Supervisor: Dr. S.R. Stobart

Abstract

A series of optically active tertiary phosphorus ligands, $P(OR)_n Ph_{3-n}$ (R = bornyl, menthyl, or isopinocamphyl; n = 1, 2, or 3, $\underline{1}$ - $\underline{9}$), containing chiral alkoxy groups derived from natural terpene alcohols, menthol, borneol, and isopinocampheol, are synthesized and characterized by various spectroscopic techniques. The reactions of these ligands with iron and cobalt carbonyl complexes are carried out, giving monomeric mono- and di-substituted iron(0) and dimeric di-substituted cobalt carbonyl complexes ($Fe(CO)_4L$, $Fe(CO)_3L_2$, and $[Co(CO)_3L]_2$, L = $\underline{1}$ - $\underline{9}$). The characterization of these complexes by IR and NMR spectrometries is discussed. Results of preliminary studies on hydroformylation reaction under oxo conditions catalysed by several cobalt complexes are presented.

Pyrazolyl bridged di-iridium(I) systems, $[Ir(CO)L(\mu\text{-pz})]_2$ (L = $P(OMen)Ph_2$, $\underline{40}$, $P(OBor)Ph_2$, $\underline{41}$, and $P(OMen)_2Ph$, $\underline{42}$), are prepared as diastereomers with unequal thermodynamic distribution. The X-ray crystal structure of $\underline{41}$ shows cocrystallization of the two diastereomers in the same unit cell, which provides 1:1 kinetic distribution of the two isomers. Kinetic studies of the interconversion from the kinetic ratio to the thermodynamic ratio of the two diastereomers in $\underline{41}$ indicates the existence of a slow inversion process of the six-membered central metallocycle in $\underline{41}$. Oxidative addition of MeI to $\underline{41}$ generates a pair of diastereomeric adducts ($\underline{43}$) in kinetic distribution, which is slowly converted to its thermodynamic distribution, implying a very slow reductive

elimination of MeI.

Oxidative additions of *exo-* and *endo*-norbornyl iodide to $[Ir(CO)_2(\mu\text{-pz})]_2$ results in same product (44). Possible mechanisms for this process are discussed.

Bisdiphenylphosphinoalkylsilane containing chiral menthoxy group $((o\text{-}PPh_2C_6H_4CH_2)_2(MenO)SiH$, 47) is prepared and characterized. Its four-coordinate square planar platinum complex $(Pt[Si(o\text{-}PPh_2C_6H_4CH_2)_2(OMen)]Cl$, 48) and five-coordinate iridium(I) complex $(IrH[Si(o\text{-}PPh_2C_6H_4CH_2)_2(OMen)]Cl$, 49) are synthesized. Isomerizations of 49 and its CO adducts, $Ir[Si(MenO)(CH_2C_6H_4PPh_2)_2](CO)HCl$ (55 and 56), are studied in relation to their methyl analogues.

Examiners:

_____

Dr. S.R. Stobart, Supervisor (Department of Chemistry)

_____

Dr. R.H. Mitchell, Departmental Member (Department of Chemistry)

_____

Dr. G.W. Bushnell, Departmental Member (Department of Chemistry)

_____

Dr. C.E. Picciotto. Outside Member (Department of Physics and Astronomy)

_____

Dr. W.R. Cullen, External Examiner (Department of Chemistry, University of British Columbia)

Table of Contents

List of Tables

i

List of Figures

List of Schemes

List of Compounds

1. $P(OMen)Ph_2$

2. $P(OBor)Ph_2$

3. $P(OPin^i)Ph_2$

4. $P(OMen)_2Ph$

5. $P(OBor)_2Ph$

6. $P(OPin^i)_2Ph$

7. $P(OMen)_3$

8. $P(OBor)_3$

9. $P(OPin^i)_3$

10. $Fe(CO)_4[P(OMen)Ph_2]$

11. $Fe(CO)_4[P(OBor)Ph_2]$

12. $Fe(CO)_4[P(OPin^i)Ph_2]$

13. $Fe(CO)_4[P(OMen)_2Ph]$

14. $Fe(CO)_4[P(OBor)_2Ph]$

15. $Fe(CO)_4[P(OPin^i)_2Ph]$

16. $Fe(CO)_4[P(OMen)_3]$

17. $Fe(CO)_4[P(OBor)_3]$

18. $Fe(CO)_4[P(OPin^i)_3]$

19. $Fe(CO)_3[P(OMen)Ph_2]_2$

20. $Fe(CO)_3[P(OBor)Ph_2]_2$

21. $Fe(CO)_3[P(OPin^i)Ph_2]2$

22. $Fe(CO)_3[P(OMen)_2Ph]_2$

23. $Fe(CO)_3[P(OBor)_2Ph]_2$

24. $Fe(CO)_3[P(OPin^i)_2Ph]_2$

25. $Fe(CO)_3[P(OMen)_3]_2$

26. $Fe(CO)_3[P(OBor)_3]_2$

27. $Fe(CO)_3[P(OPin^i)_3]_2$

28. $\{Co(CO)_3[P(OMen)Ph_2]\}_2$

29. $\{Co(CO)_3[P(OBor)Ph_2]\}_2$

30. $\{Co(CO)_3[P(OPin^i)Ph_2]\}_2$

31. $\{Co(CO)_3[P(OMen)_2Ph]\}_2$

32. $\{Co(CO)_3[P(OBor)_2Ph]\}_2$

33. $\{Co(CO)_3[P(OPin^i)_2Ph]\}_2$

34. $\{Co(CO)_3[P(OMen)_3]\}_2$

35. $\{Co(CO)_3[P(OBor)_3]\}_2$

36. $\{Co(CO)_3[P(OPin^i)_3]\}_2$

37. $[Ir(COD)(\mu\text{-}pz)]_2$

38. $[Ir(CO)_2(\mu\text{-}pz)]_2$

39. $[Ir(CO)(PPh_3)(\mu\text{-}pz)]_2$

40. $\{Ir(CO)[P(OMen)Ph_2](\mu\text{-}pz)\}_2$

41. $\{Ir(CO)[P(OBor)Ph_2](\mu\text{-}pz)\}_2$

42. $\{Ir(CO)[P(OMen)_2Ph](\mu\text{-}pz)\}_2$

43. $Ir_2(CO)_2[P(OBor)Ph_2]_2(\mu\text{-}pz)_2(Me)(I)$

44. $Ir_2(CO)_4(\mu\text{-}pz)_2(norbornyl)(I)$

45. biPSiH

46. mcbiPSiH

47. mcbiPSi*H

48. Pt(mcbiPSi*)Cl

49. IrH(mcbiPSi*)Cl

50. IrH(biPSi)Cl

51. IrH(mcbiPSi)Cl

52. RhH(biPSi)Cl

53. RhH(mcbiPSi)Cl

54. RhH(mcbiPSi*)Cl

55. IrH(mcbiPSi*)(CO)Cl

56. IrH(mcbiPSi*)Cl(CO)

57. IrH(biPSi)(CO)Cl

58. IrH(biPSi)Cl(CO)

59. IrH(mcbiPSi)(CO)Cl

60. IrH(mcbiPSi)Cl(CO)

Abbreviations

alk	alkyl	Men	menthyl
ar	aromatic	mol. equiv.	molar equivalence
b	broad	MS	mass spectrum
Bor	bornyl	NMR	nuclear magnetic resonance
Bu	butyl	Ph	phenyl
Bu^t	*tert*-butyl (1,1-dimethylethyl)	Pin^i	isopinocamphyl
COD	1,5-cyclooctadiene	ppm	parts per million
cosy	correlation spectroscopy	Pr^i	isopropyl
Cp	cyclopentadienyl	pz	pyrazolyl
Cp^*	pentamethylcyclopentadienyl	Ref.	reference
d	doublet	s	singlet
e.e.	enantiomeric excess	sh.	shoulder
Et	ethyl	st.	strong
IR	infra-red	t	triplet
m	multiplet	THF	tetrahydrofuran
m. st.	medium strong	tol	tolyl
Me	methyl	V.T.	variable temperature

BINAP	2,2'-bis(diphenylphosphino)-1,1'-binaphthyl
BINAPHOS	(2-(diphenylphosphino)-1,1'-binaphthalen-2'-yl)-(1,1'-binaphthalen-2,2'-yl)phosphite
DIOP	2,3-*O*-isopropylidene-2,3-dihydroxy-1,4-bis(diphenylphosphino)butane
DIPAMP	1,2-ethanediylbis[(*o*-methoxyphenyl)phenylphosphine]

biPSiH	bis-(1-diphenylphosphinopropyl)methylsilane
mcbiPSiH	bis-(2-diphenylphosphinobenzyl)methylsilane
mcbiPSi*H	bis-(2-diphenylphosphinobenzyl)menthoxysilane
mcbiP*SiH	bis-(2-dimenthoxyphosphinobenzyl)methylsilane

Acknowledgements

to my parents

Chapter 1

INTRODUCTION

1.A. Tertiary Phosphorus Ligands and Homogeneous Catalysis

During the past several decades there has been a spectacular growth in the chemistry of metal complexes that contain tertiary phosphorus ligands. This is directly related to the accelerated development of homogeneous catalysis over the same period. A homogeneous catalytic reaction is one in which all the constituents (including both the reactants and the catalyst) are present in the same phase, normally a solution. On the contrary, a heterogeneous catalyst is usually present as a solid while the reactants are liquids or, more frequently, gases, and the reaction then takes place at the catalyst surface. Heterogeneous catalysts are normally easier to separate, easier to regenerate and thermally more stable than homogeneous catalysts, but they are less active, less selective and more difficult to study or modify. It is because of its high activity and selectivity that homogeneous catalysis is potentially so useful: high activity is essential for economically competitive industrial processes, while high selectivity is crucial in the production of speciality chemicals. The latter include specialized polymers for electronic applications, intermediates for high performance structural materials, and many biologically active compounds. Preparation of compounds such as certain pharmaceuticals, insecticides, food additives, *etc.*, has relied on homogeneously catalyzed asymmetric synthesis to generate specific stereogenic conformation.

Transition metal complexes are of great importance in homogeneous catalytic reactions, due to the unique properties of both the metal centres and the ligands:[1]

(a) The metal centres. The nine valence shell orbitals - one *s*, three *p*, and five

d orbitals - in each *d*-block metal not only can accommodate its valence electrons but also provide the proper energy and compatible symmetry to form both σ- and π- hybrid molecular orbitals in bonding with other groups. Thus, the transition metals can readily form strong *p*π- or *d*π- bonds with compounds such as olefins or phosphines or essentially σ-bonds with several highly reactive species, such as hydride or alkyl groups. By so doing, transition metal complexes can activate stable functional groups such as a C-H bond under relatively mild conditions, and influence their subsequent behaviour in order to obtain the desired product. Transition metal elements can form complexes in different oxidation states with variable coordination numbers. This is essential to complete the catalytic cycles, which often involve species with different oxidation states and coordination numbers.

(b) The ligands. Transition metals can readily form linkages with almost every other element in the periodic table. This offers us the possibility of tuning the metal properties by ligand electronic and steric effects. In theory, the desired activity and selectivity of the catalyst can be obtained by modifying the electronic and structural properties of the ligands.

Due to these reasons, research on soluble transition metal complexes flourished during the last few decades, along with which, the ligand development surged as well. One class of most important ligands in this area is tertiary phosphorus ligands. Extensive investigations on such ligands were carried out, mainly due to their versatility. The electronic property of these ligands can vary from being similar to a CO ligand with very good π accepting ability, such as PF_3,[2] to very good σ donor with little π acidity, such as $P(OMe)_3$.[3] The steric bulk of these ligands can be as small as in PH_3,[4] or as big as in some poly-dentate ligands, such as in $C_6H_4[CH_2P(CH_2CH_2PPh_2)_2]_2$.[5] The vast pool of available tertiary phosphorus ligands with different properties and the relative readiness of modifying existing ligands or designing new ones provide an obvious

choice for transition metal chemists.

1.B. Asymmetric Synthesis

An important and rapidly growing branch of homogeneous catalysis is its application to asymmetric synthesis. By definition, asymmetric synthesis is one in which a prochiral unit in substrate molecule is transformed to a stereogenit unit in such a way that the possible stereoisomers are formed in unequal amounts. It is directly related to chirality, which is a fundamental symmetry property of three-dimensional objects. An object is said to be chiral if it cannot be superimposed upon its mirror image. In a chemical context, many compounds may be obtained in two different forms in which the molecular structures are constitutionally identical but differ in the three-dimensional arrangement of atoms such that they are related as mirror images. In such a case the two possible forms are called enantiomers. Enantiomers have identical chemical and physical properties in the absence of an external chiral influence, except the direction in which they rotate the plane of plane-polarised light. This phenomenon of optical activity provides the basis for the nomenclature of enantiomers. Thus, the molecule which rotates the plane of plane-polarised light (sodium D-line emission, wavelength = 589 nm) in a clockwise direction is denoted (+)-isomer, while its mirror image which has an equal and opposite rotation under the same conditions is denoted (-)-isomer.

Chirality in molecules is associated with the presence of one or more stereogenic units within the molecule, leading to the existence of stereoisomers. Simple chiral molecules can be classified into three types according to the type of stereogenic unit present: central, axial and planar (Figure 1-1).[6] A centrally chiral molecule is chiral by virtue of the arrangement of atoms or groups about a stereogenic centre. The most familiar example is a tetrahedral molecule of type I and this is the most common class

of chiral molecules. An axially chiral molecule is chiral by virtue of the arrangement of atoms or groups about a stereogenic axis. An example is provided by the biaryl (II). This class of chiral compounds also occurs quite commonly. The final type is planar chirality, in which the chirality is due to the arrangement of atoms or groups with respect to a stereogenic plane. This is illustrated by dibenzene metal complex with different substitutions on the same ring (III).
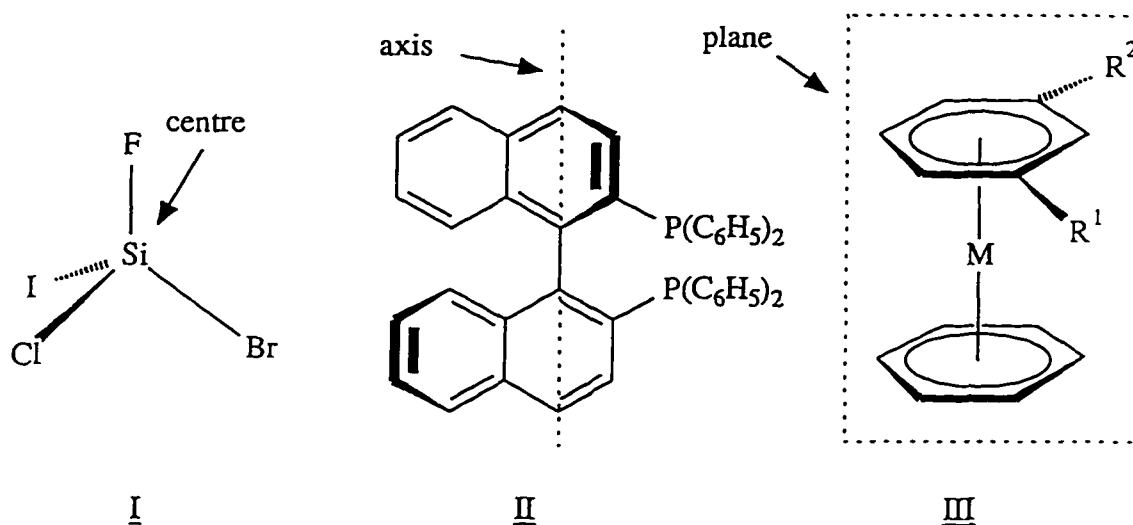
Figure 1-1. Types of stereogenic units.

If there are n stereogenic units there will be up to 2^n stereoisomers. If two of these stereoisomers are mirror images of each other, they are enantiomers; if not, they are diastereomers.

The absolute configuration at a given stereogenic centre is specified using the Cahn-Ingold-Prelog system.[7] For a tetrahedral centre, the procedure first involves placing the four groups in order of priority, which is based on atomic number or atomic weight for isotopes. Then the centre is viewed with the lowest priority group at the back. If the remaining three groups lie in order of decreasing priority in a clockwise

arrangement the configuration is denoted *R* and if the arrangement is counterclockwise the configuration is *S* (Figure 1-2).
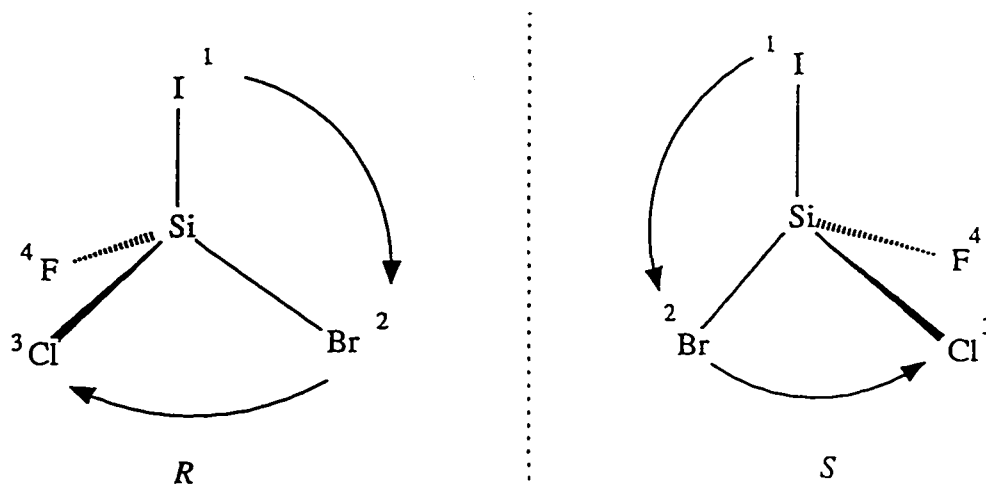
Figure 1-2. *R* and *S* configurations for a tetrahedral chiral centre.

For an axially chiral compound, the four groups attached to the stereogenic axis that are in tetrahedral arrangement are used to determine its configuration (in the case of a biaryl, the groups considered are the ones on the *ortho* positions): The group with the lower priority on one end of the axis is placed at the back (it does not matter which end is chosen, and this end is referred to as the back end while the other as the front end). The arrangement of the remaining groups is considered in the order: high priority (front) > low priority (front) > high priority (back). As before if this appears clockwise the configuration is *R* and otherwise it is *S* (Figure 1-3).

For a molecule having planar chirality, the chiral plane has to be located first. This would be a plane of symmetry if certain different groups were made identical, and also contains the greatest number of atoms including, if a choice of plane remains, the one that has the highest priority. After choosing the stereogenic plane, one side of plane, on which lies the group with the highest priority, is examined. The arrangement among
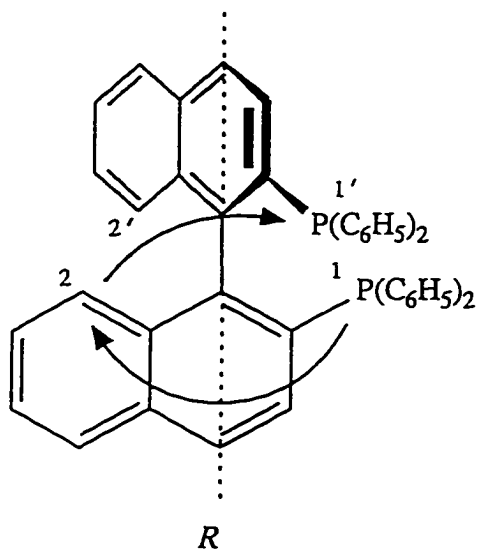
Figure 1-3. Configuration definition for axially chiral compounds.

the atoms that are on this side of the plane and directly attached to the plane by chemical bonds is considered in the order: the highest priority (1) > high priority next to 1 (2) > high priority next to 2. Again, if this appears clockwise the configuration is
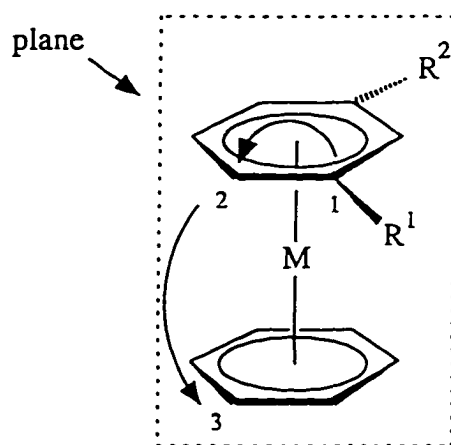
S, if R^1 has higher priority than R^2.

Figure 1-4. Configuration definition for compound with planar chirality.

R and otherwise it is *S* (Figure 1-4).

For a molecule with more than one stereogenic unit the absolute configuration can be specified by giving the configuration of each unit. Thus each diastereomer can be distinguished unambiguously.

Since most of the important building-blocks make up the biological macromolecules of living systems using one enantiomeric form only, it should come as no surprise that the two enantiomers of a biologically active chiral compound, such as a drug, a sweetener, a hormone, or a insecticide, *etc*, interact differently with its chiral receptor site and may lead to different effects. The importance of asymmetric synthesis is, therefore, obvious. For instance, (-)-propanolol was introduced in the 1960s as a β-blocker for the treatment of heart disease, but the (+)-enantiomer acts as a contraceptive;[6] (+)-estrone is a hormone, whereas the (-)-enantiomer has no hormonal activity; *R*-isomer of thalidomide is a sleeping aid, while the *S*-isomer is teratogenic.[8]

There are several known methods of asymmetric synthesis, among which the catalyzed processes are particularly attractive because of their high efficiency and low cost. Although heterogeneous catalysts are being developed, their homogeneous counterparts are undoubtably playing a far more important role in this area. Among the latter, enzymes are definitely the most efficient, but they are limited by their availability and narrow application. This leaves the transition metal complexes to be the best choices, and the subject of intensive research. Some of the research results have been converted into important industrial processes. A few examples are as follows:

(a) Enantioselective isomerization of olefins. Olefin isomerization (double-bond migration) is one of the simplest and most thoroughly studied catalytic reactions.[9] Soluble catalysts are used industrially to isomerize olefins that are involved as intermediates in other homogeneous catalytic processes. Enantioselective olefin isomerization has also been achieved. A good example is the (BINAP)Rh catalyzed

enantioselective isomerization of an allylic amine in the synthesis of L-menthol, a major

fragrance chemical (Scheme 1-1).[10] Compound IV is boiled in THF containing 0.1

mole % [Rh(-)-BINAP(COD)](ClO$_4$) for 21 hours to give a 94% yield of V.

β-Pinene   IV   V   L-Menthol
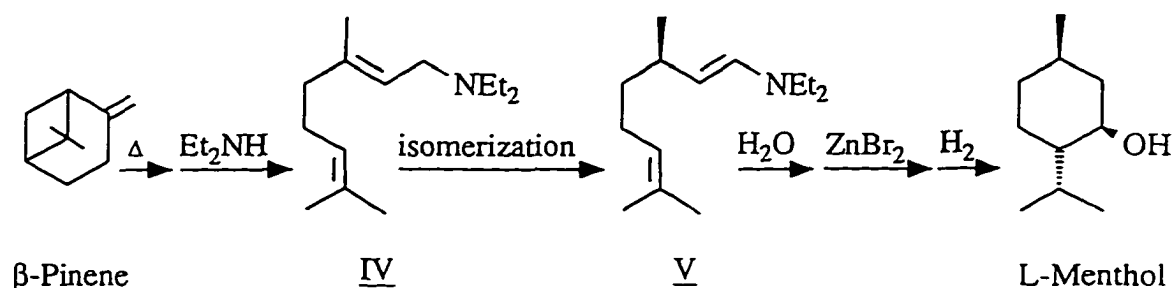
Scheme 1-1. Synthesis of L-menthol.

(b) Asymmetric hydrogenation of olefins. Some of the most thoroughly studied

homogeneous catalytic processes are the additions of H$_2$, HSiR$_3$, and HCN to a C=C

bond. In the past, hydrogenation was mostly performed with convenient heterogeneous

catalysts such as palladium metal on charcoal (Pd/C). Recently, however,

enantioselective hydrogenations with soluble chiral catalysts have become important in

the pharmaceutical industry and to the synthetic organic chemist. The first commercial

application of transition metal complex catalyzed asymmetric synthesis was the

enantioselective hydrogenation involved in Monsanto's synthesis of L-dopa (Scheme 1-

2), a drug used in the treatment of Parkinson's disease.[11] The catalyst used in the

hydrogenation is prepared by reacting the [Rh(COD)$_2$]$^+$ cation with DIPAMP in aqueous

ethanol or isopropanol. The hydrogenation is carried at about 50 °C and 3 atmospheres

pressure by adding solid VI to the catalyst solution. It slowly dissolves and reacts, after

which chiral VII crystallizes and is isolated with 95% e.e..

(c) Asymmetric hydroformylation. The oldest and largest homogeneous reaction

of olefins catalyzed by transition metal complexes is hydroformylation. This reaction
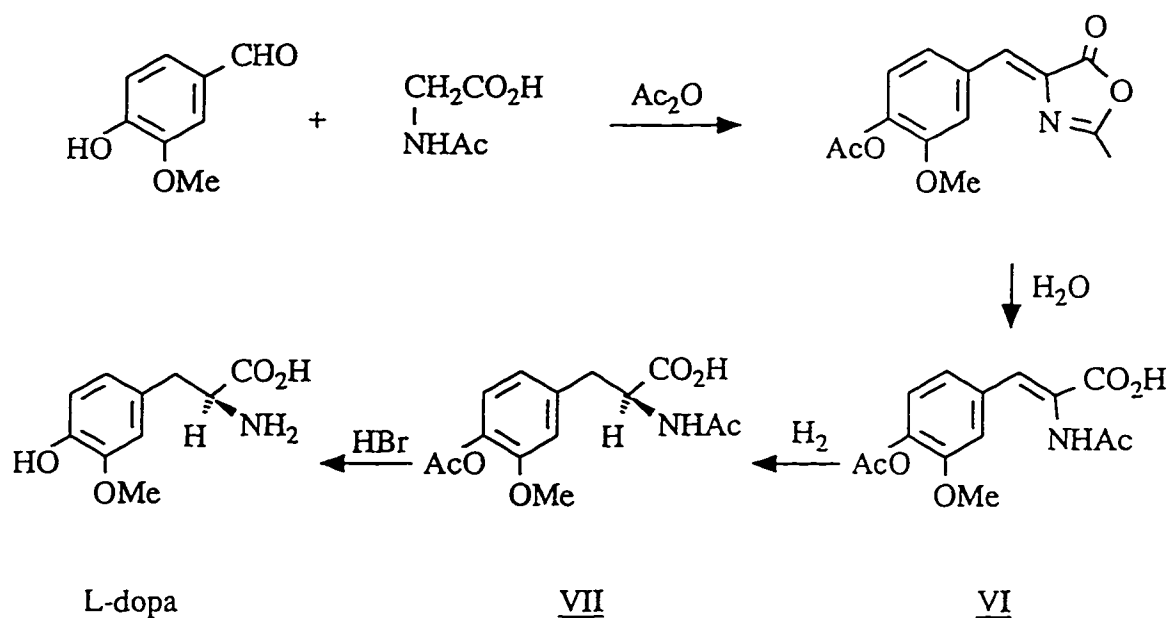
Scheme 1-2. Synthesis of L-dopa.

involves the addition of CO and hydrogen to a C=C to produce aldehydes. Aldehydes are very versatile chemical intermediates since they can be oxidized, reduced or condensed to produce different organic compounds. Naturally, asymmetric hydroformylation has become an important role in synthetic organic chemistry, since it may result in chiral formyl derivatives of importance as chiral building blocks or biologically active compounds. Although there has not been any commercial application of asymmetric hydroformylation so far, some very promising catalysts have been reported. An example is illustrated in Scheme 1-3. Using [Rh-BINAPHOS(acac)(CO)$_2$] as catalyst, a series of substituted ethylene were converted to chiral aldehydes with up to 88/12 branch/linear ratio and 94% e.e..[12]

Other processes involving transition metal catalyzed homogeneous catalysis, such as asymmetric hydrosilylation,[13] hydrocyanation,[14] oxidation of olefins,[15] or cyclopropanation[16] are also industrialized.

$$CH_2 = CHR \xrightarrow[\text{benzene}]{\substack{Rh(acac)(CO)_2- \\ BINAPHOS \\ H_2/CO(1:1,\ 100\ atm)}} CH_3 - \overset{*}{C}HR \underset{CHO}{|} + CH_2 - CH_2R \underset{CHO}{|}$$

a: R = OCOCH$_3$ e: R = p-CH$_3$OC$_6$H$_4$

b: R = $\underline{\text{NC(O)C}_6\text{H}_4\text{C(O)}}$ f: R = p-ClC$_6$H$_4$

g: R = p-(CH$_3$)$_2$CHCH$_2$C$_6$H$_4$

c: R = C$_6$H$_5$ h: R = n-C$_4$H$_9$

d: R = p-CH$_3$C$_6$H$_4$
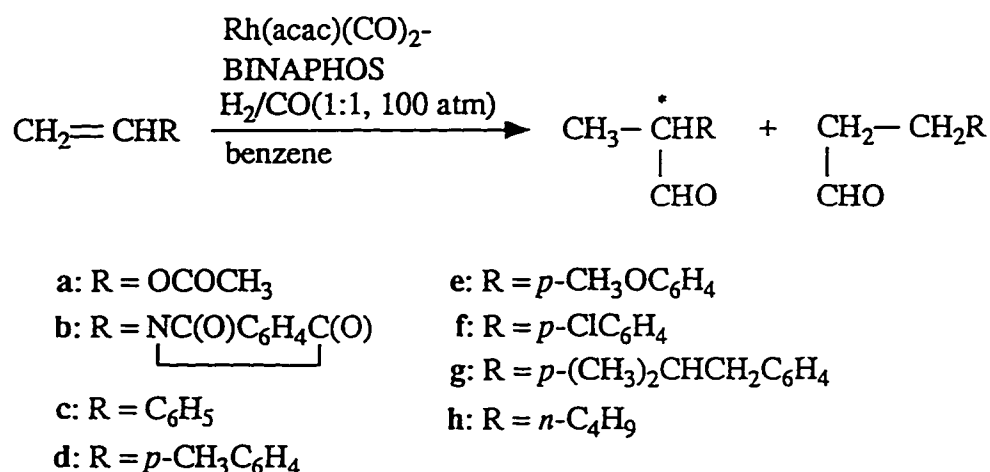
Scheme 1-3. Asymmetric hydroformylation of olefins.

1.C. Chiral Tertiary Phosphorus Ligands.

As shown in the examples in the previous section, many different chiral tertiary phosphorus ligands have been used in various transition metal complex catalyzed reactions. Since the first acyclic chiral tertiary phosphorus ligands were synthesized in early 1960s by Horner and coworkers,[17] a great number of chiral phosphorus ligands have been produced. These ligands can be categorized into three classes according to the different types of chirality they possess.

(a) P-chiral. This class of chiral phosphorus ligands have three different groups attached to the phosphorus atom. Since inversion of the phosphorus centre does not occur under normal conditions,[18] these ligands can be resolved into optically pure enantiomers. Examples include PEt(n-Bu)(C$_{12}$H$_{25}$), PMePhBz, PEtPhBz, the first three acyclic chiral tertiary phosphorus ligands to be made, and PMePrPh (VIII), which was employed in the first reported homogeneous asymmetric catalysis.[19, 20]

(b) Backbone chiral. In this class of chiral phosphorus ligands, the phosphorus

$$\underset{Me}{\overset{\ddot{P}\text{''''''''''''}Ph}{\diagup\diagdown}}\underset{Pr}{}$$
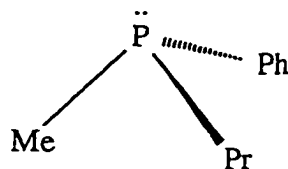
VIII. (*S*)-PMePrPh

centre is achiral because it is bonded to two or three identical groups. However, at least one of three substituents is an optically active unit. This chiral auxiliary makes the whole molecule asymmetric, although the phosphorus atom itself is achiral. The Diop (**IX**) ligand, derived form optically active tartaric acid, is a famous example of this type.
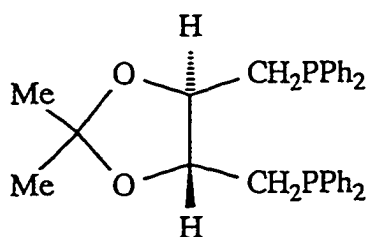
IX. (*R*,*R*)-Diop

(c) Axially chiral. This class of phosphorus ligands does not contain any conventional tetrahedral chiral units, but the molecules are axially chiral. A very important ligand in this class is BINAP (**X**). Similar to the Diop system in that they
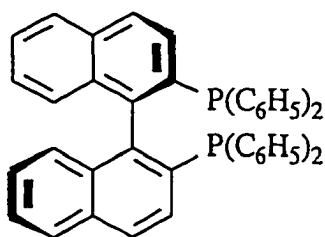
X. (*R*)-(+)-BINAP

both possess C_2 symmetry, the binaphthyl skeleton is known to have superior chirality recognition and induction abilities,[21] especially in ruthenium catalyzed hydrogenation reactions.[22]

Although the scope of chiral phosphine chemistry has grown rapidly during the last three decades,[23] the synthesis of such compounds has continued to pose a considerable challenge.[24, 25] Many synthetic schemes, especially those for the P chiral or axially chiral phosphorus compounds, involve multi-step reactions including resolution of optically pure enantiomers, which frequently causes low overall yields. A good example is the synthesis of BINAP as shown in Scheme 1-4.[26] The overall reaction yield after resolution is only about 20%.

The syntheses of backbone chiral phosphorus ligands usually have the advantage
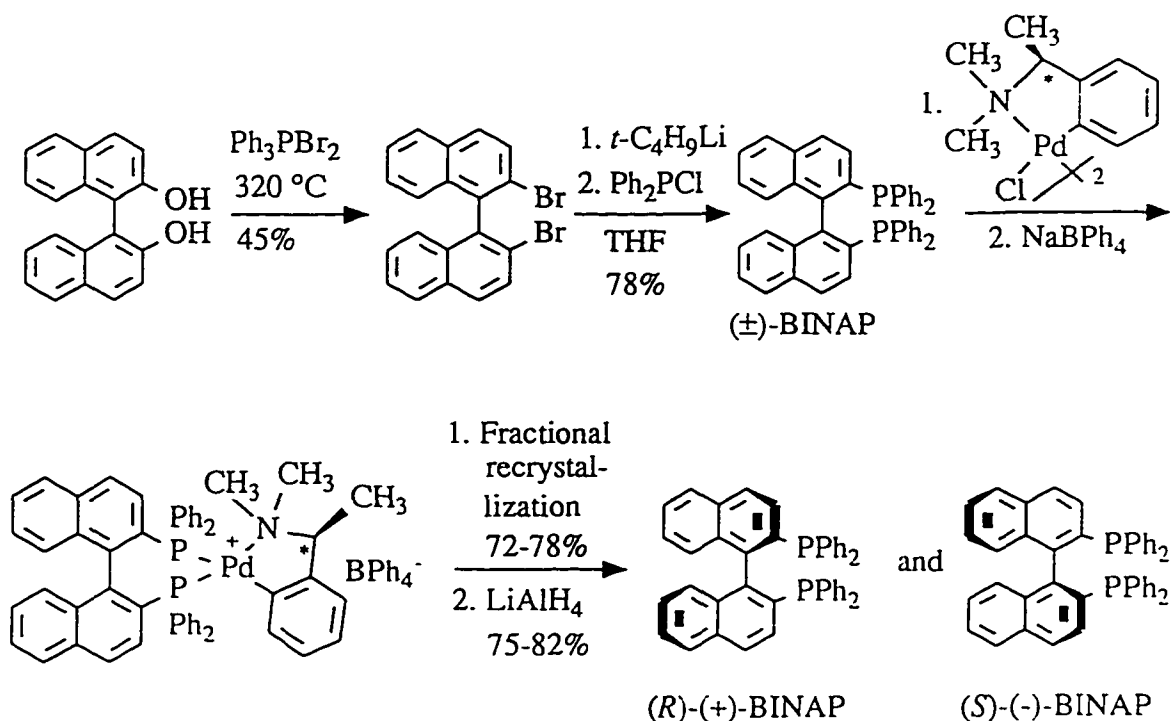
Scheme 1-4. Synthesis of BINAP.

of not requiring resolution of the enantiomers, since the starting materials that form the chiral backbones in the final products are normally already resolved, as illustrated by the synthesis of Diop (Scheme 1-5).[27] Naturally occurring L(+)-tartaric acid was used as the starting material, and an optically pure final product is obtained since the stereogenic centres in the starting material retain their chirality during the reaction. However, the reaction yield is relatively low (the yield for the last step was reported as 48%), mainly due to the general low yields for reactions forming new C-P bonds.
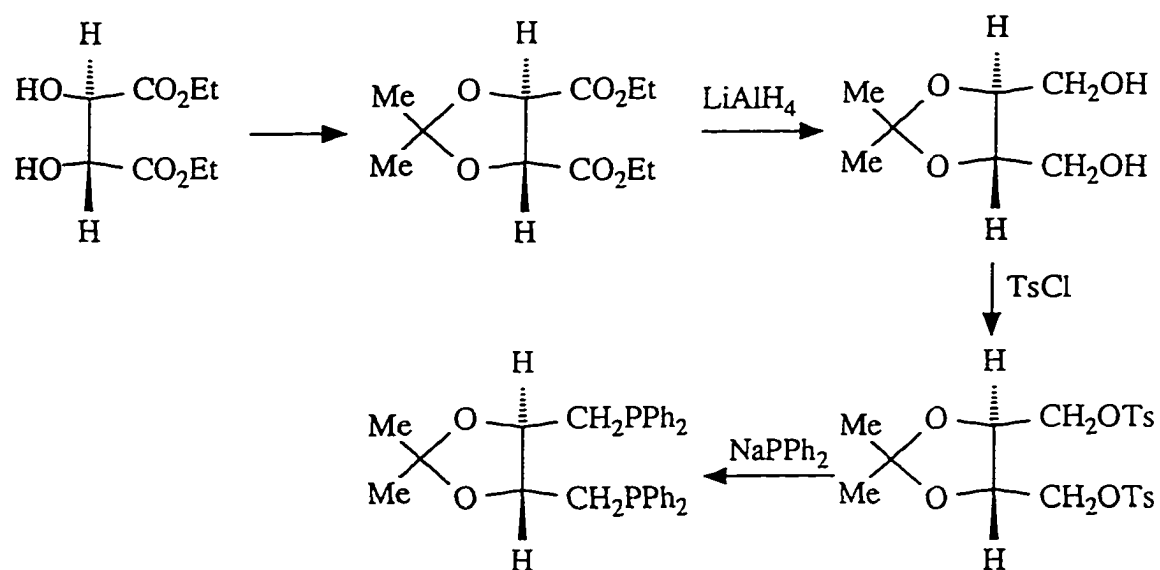
Scheme 1-5. Synthesis of Diop.

Because of the importance of chiral tertiary phosphorus ligands, and the difficulties involved in the synthesis of such compounds, the research described in this thesis has examined the synthesis and reactivity of a series of chiral phosphorus ligands derived from terpene alcohols. As is discussed in Chapter 2, high yields were achieved by avoiding constructing new C-P bonds. Instead, new O-P bonds, which are much easier to form, were generated. Terpene alcohols were chosen because several of them are cheap, naturally abundant, and they usually have bulky and rigid chiral frameworks

which are particularly important in asymmetric induction.[28]

Chapter 3 discusses the syntheses and characterization of some simple model complexes, synthesized by ligand replacement of CO in metal carbonyl complexes. In this way mono and di-substituted mononuclear iron carbonyl complexes and di-substituted cobalt carbonyl dimers were prepared in order to gain familiarity with the coordination properties of the ligands.

After these preliminary studies, ligands of the same type were used as stereo chemical probes in two different areas of chemistry that have been of major importance in this laboratory. In Chapter 4, the stereo chemistry and oxidative addition reactions of pyrazolyl bridged iridium(I) dimers containing such ligands are described. In Chapter five, the synthesis of a related ligand is reported. The tridentate ligand containing two phosphorus donors and one potential silyl donor was also derived from terpene alcohol. The syntheses of complexes of Group VIII transition metals, including platinum and iridium, containing this ligand were also reported. The reactivity of the iridium complex is discussed.

Chapter 2

SYNTHESIS AND CHARACTERIZATION OF THE LIGANDS

2.A. Introduction

The chiral tertiary phosphorus ligands reported in this chapter were derived from three readily available terpene alcohols. Terpenes are a class of natural products that consist of two or more isoprene (2-methyl-1,3-butadiene) units. Their oxygen containing derivatives are called terpenoids, of which terpene alcohols are one type. Because they are constructed from isoprene units, which are prochiral, terpene alcohols are chiral compounds, many examples of which can be isolated from plants and are optically pure. This provides a useful pool of readily accessible chiral building blocks for use in asymmetric synthesis.

The terpene alcohols that were chosen for use in ligand synthesis are (-)-menthol ((1R,2S,5R)-5-methyl-2-(1-methylethyl)cyclohexanol), (-)-borneol ((1S,2R,4S)-1,7,7-trimethylbicyclo[2.2.1]heptan-2-ol), and (+)-isopinocampheol ((1S,2S,3S,5R)-2,6,6-trimethylbicyclo[3.1.1]heptan-3-ol) (Figure 2-1). The common structural features among these three molecules are: (a) they are all optically active; (b) they are all based on a six-membered ring arrangement, which make their structures rigid, especially for the two in which bicyclic frameworks are present; (c) they are variously substituted with methyl or isopropyl groups on the ring structures, which makes them potentially bulky as ligand substituents; (d) each of them contains ten carbon atoms, the smallest number possible for terpenoids; (e) none of the hydroxyl groups in any of the three molecules is blocked

by other substituents. While features (a), (b), and (c) are essential for stereo and enantio control of the ligands, feature (d) makes the NMR spectroscopic data relatively easy to interpret, and feature (e) provides clear access for incoming phosphorus atoms to form P-O bonds.

(-)-Menthol   (-)-Borneol   (+)-Isopinocampheol
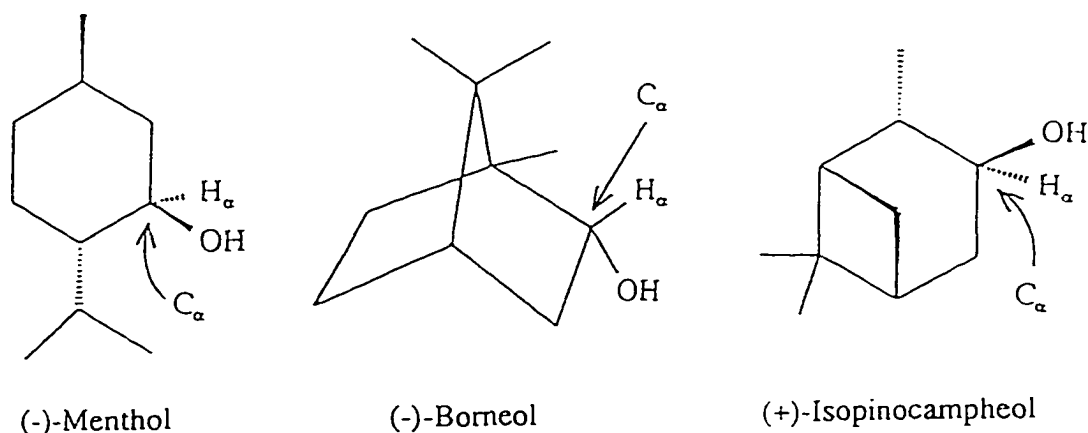
Figure 2-1. Structures of selected terpene alcohols.

Through out the text, abbreviations, Men, Bor, and Pin[i], are used in the molecular formulae to respectively. represent menthyl, bornyl, and isopinocamphyl groups (groups formed by removing OH groups from the original molecules). The carbon atoms directly attached to the oxygen atoms are referred to as α-carbons, and the hydrogen atoms directly bonded to the α-carbon atoms are referred to as α-hydrogens (or α-protons).

The tertiary phosphorus compounds reported in this chapter can be divided into three groups: (a) diphenylphosphinous acid alkyl esters (ROPPh$_2$, R = Men (1), Bor (2), or Pin[i] (3)); (b) phenylphosphonous acid bisalkyl esters ((RO)$_2$PPh, R = Men (4), Bor (5), or Pin[i] (6)); and (c) alkyl phosphites ((RO)$_3$P, R = Men (7), Bor (8), or Pin[i] (9)). Through out the text, these three groups of compounds are referred to as the phosphinites, the phosphonites, and the phosphites, respectively. Several of these compounds (compounds 1,[29] 4,[30] 5,[31] 7,[32] and 8[33]) have been reported previously,

but none of them has been studied in a systematic way, in terms of comparisons among individual members in a series of structurally related compounds. The synthesis and characterization of these molecules and four new analogues (compounds 4, 7, 8, and 9) are reported in this chapter, and their coordination chemistry is discussed in Chapters three and four.

2.B. Results and Discussion

Synthesis of the phosphinites was readily accomplished through the reactions of each of the terpene alcohols with Ph_2PCl (Equation 2-1).

$$ROH + PPh_2Cl \xrightarrow{Et_2O} ROPPh_2 + HCl$$

$$\underline{1} - \underline{3} \tag{2-1}$$

Compound 1:   R = Men,

2:          Bor,

3:          Pin^i.
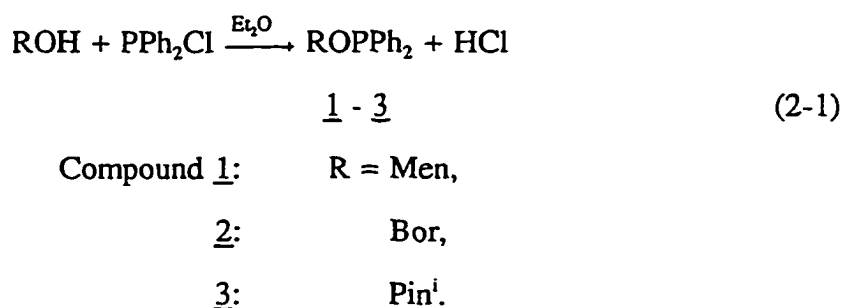
The difference between this method and that reported[29] earlier is that pyridine (or other bases) was not added during the reaction to remove HCl. HCl was removed along with the volatiles under vacuum. Compounds 1 - 3 were prepared by this method as either clear or pale yellow viscous liquids in very high yields.

The phosphonites can be synthesized through the reactions of the terpene alcohols with $PhPCl_2$ and excess Et_3N (Equation 2-2). In this chemistry, base (triethylamine) had to be used to absorb HCl generated during the reaction, because the resulting phosphonites were somewhat less stable than their phosphinite counterparts when HCl was present. To allow enough time for triethylamine to trap HCl, $PhPCl_2$ was added dropwise at 0 °C rather than all at once at room temperature as in the syntheses

of the phosphinites. Using this method, compounds $\underline{4}$ - $\underline{6}$ were synthesized as either pale yellow viscous liquid or white crystalline solid in high yields.

$$2ROH + PhPCl_2 + Et_3N \text{ (excess)} \xrightarrow{Et_2O} (RO)_2PPh + 2Et_3N \cdot HCl$$

$$\underline{4} - \underline{6} \qquad \qquad (2\text{-}2)$$
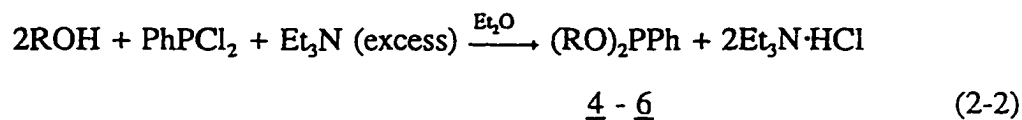
Compound $\underline{4}$:	R = Men,
$\underline{5}$:	Bor,
$\underline{6}$:	Pin^i.

Similarly, the phosphites were obtained through reactions of the terpene alcohols with PCl_3 in the presence of excess triethylamine (Equation 2-3). Differences versus phosphonite syntheses included a slower addition rate of PCl_3, a larger excess of triethylamine, and a lower reaction temperature (-70 °C). The reaction condition was modified because more HCl was generated during the reaction and the phosphites were much less stable than the phosphonites when HCl was present. Using this route, compounds $\underline{7}$ - $\underline{9}$ were synthesized in good yields. All compounds ($\underline{1}$ - $\underline{9}$) are soluble in most common organic solvents such as chloroform, dichloromethane, benzene, ether, *etc.*, and are stable under nitrogen but are slowly oxidized when exposed to air.

$$3ROH + PCl_3 + Et_3N \text{ (excess)} \xrightarrow{Et_2O} (RO)_3P + 3Et_3N \cdot HCl$$

$$\underline{7} - \underline{9} \qquad \qquad (2\text{-}3)$$
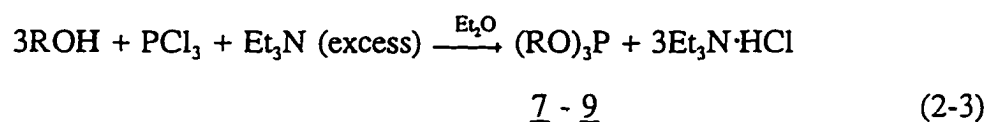
Compound $\underline{7}$:	R = Men,
$\underline{8}$:	Bor,
$\underline{9}$:	Pin^i.

The phosphite synthesis (Equation 2-3) was studied in further detail using menthol as a model. In deuterated chloroform, menthol was added to PCl_3 one mol.

equiv. at a time, until three mol. equiv. of menthol were present. After each successive addition, a $^{31}P\{^1H\}$ NMR spectrum was run to monitor the reaction. The results presented in Figure 2-2 show that typical Michaelis-Arbuzov rearrangement[34] occurs as illustrated in Scheme 2-1.

$$PCl_3 \xrightarrow[\text{(1)}]{\text{MenOH}} MenOPCl_2 \xrightarrow[\text{(2)}]{\text{MenOH}} (MenO)_2PCl \xrightarrow[\text{(3)}]{\text{MenOH}} (MenO)_3P$$

$$(MenO)_3P \xrightarrow[\text{(4)}]{\text{HCl}} (MenO)_2POH \xleftarrow[\text{(5)}]{} (MenO)_2P(O)H$$
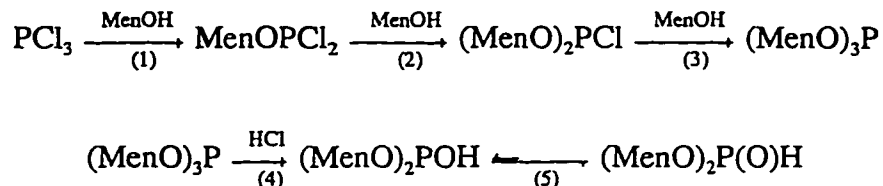
Scheme 2-1. Michaelis-Arbuzov rearrangement.

After the first addition, two products in addition to PCl_3 were evident in the $^{31}P\{^1H\}$ NMR spectrum: $MenOPCl_2$ (175.9 ppm), and $(MenO)_2P(O)H$ (5.2 ppm). The fact that a peak attributable to $(MenO)_2PCl$ was not observed indicated that as soon as $(MenO)_2PCl$ was formed, it reacted with another menthol molecule to form $(MenO)_3P$, which rapidly rearranges to yield $(MenO)_2P(O)H$. Similar behaviour was clear in the second spectrum; after the second addition, a peak at 169.2 ppm corresponding to $(MenO)_2PCl$ was barely detectable, all PCl_3 was consumed and the $(MenO)_2P(O)H$ peak had increased substantially in intensity. After the final addition, hardly any $MenOPCl_2$ was left and $(MenOP)_2PCl$ was undetectable.

During the whole process, $(MenO)_3P$ was never observed. This suggested that step four was very efficient. As soon as $(MenO)_3P$ was formed, it reacted with HCl to give $(MenO)_2P(O)H$. Therefore, in order to obtain $(MenO)_3P$, Et_3N was introduced to remove HCl as soon as it was generated, and the reaction was again monitored by $^{31}P\{^1H\}$ NMR spectroscopy. A spectrum was run after each addition of one mol. equiv. of menthol together with one mol. equiv. of triethylamine to PCl_3 in deuterated chloroform, until three mol. equiv. of menthol and triethylamine were added. As shown in Figure 2-3, with the presence of triethylamine, the formation of $(MenO)_2P(O)H$ was

a) One mol. equiv. of MenOH added

b) two mol. equiv. of MenOH added

c) three mol. equiv. of MenOH added
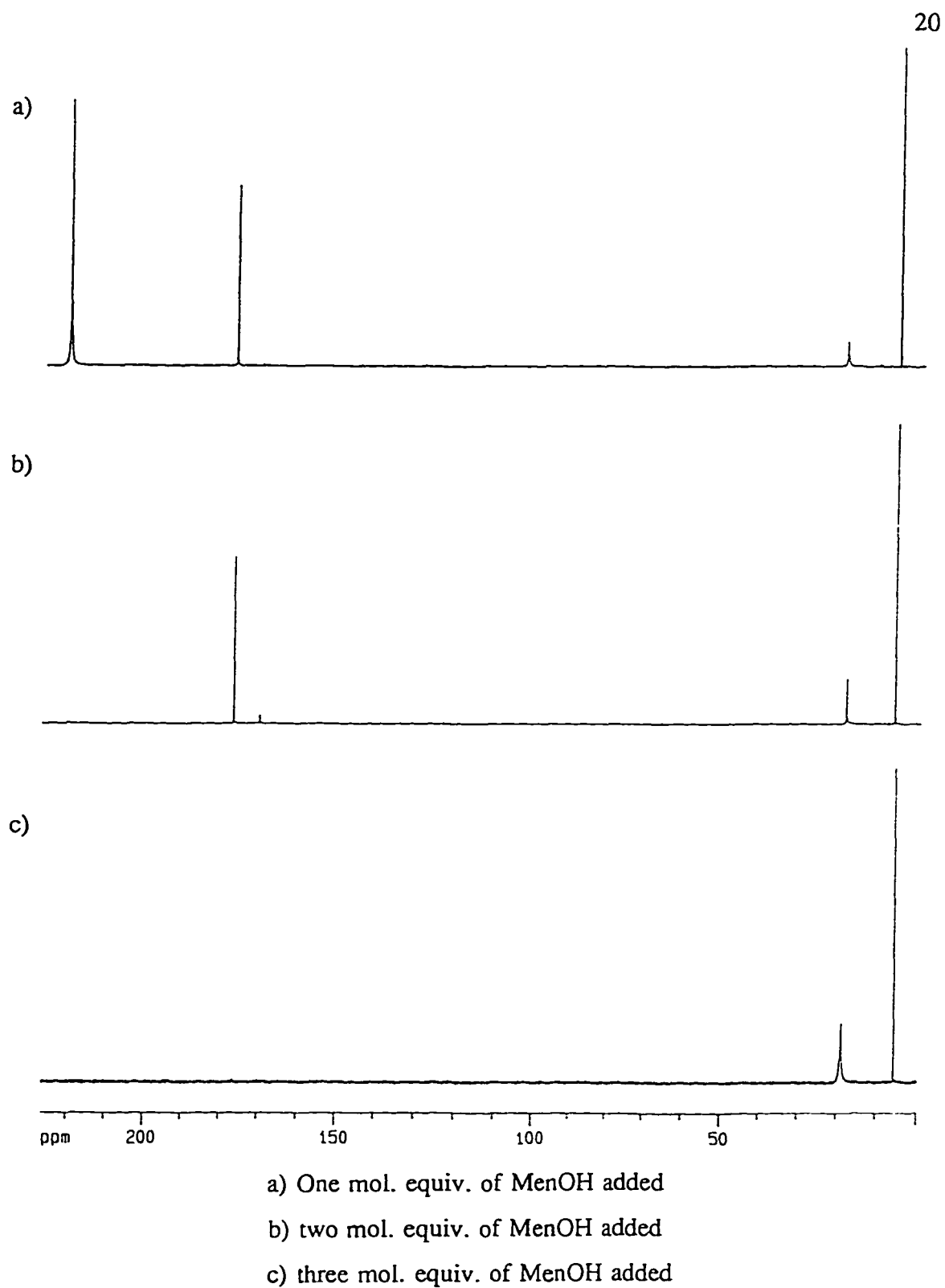
Figure 2-2. ^{31}P{^{1}H} NMR spectra of the reaction between MenOH and PCl$_3$.

a) One mol. equiv. of MenOH and Et₃N added

b) two mol. equiv. of MenOH and Et₃N added

c) three mol. equiv. of MenOH and Et₃N added
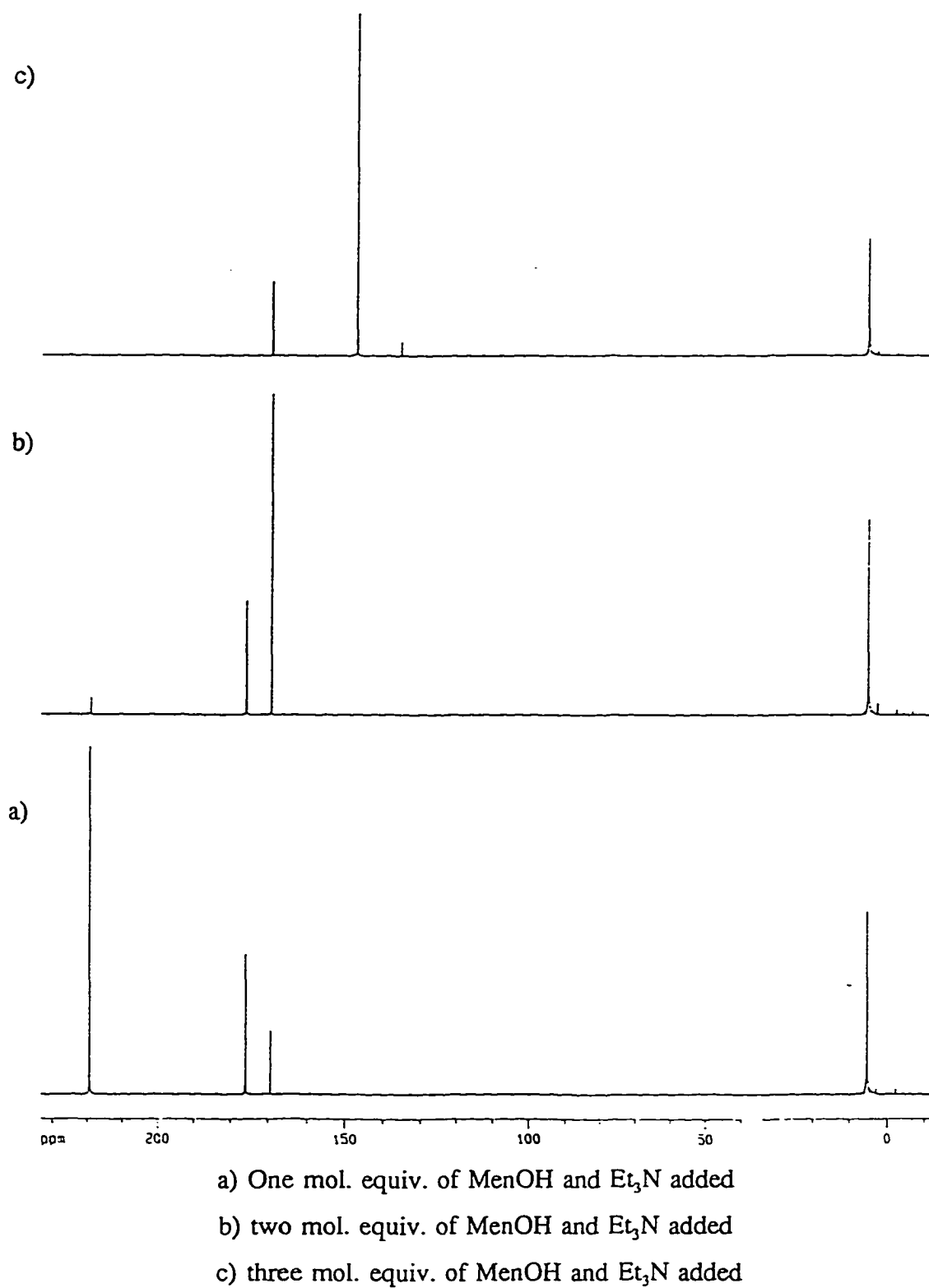
Figure 2-3. ^{31}P{^{1}H} NMR spectra of the reaction between MenOH, Et₃N, and PCl₃.

greatly suppressed. $MenOPCl_2$, $(MenO)_2PCl$, and $(MenO)_3P$ all showed up in an orderly fashion, with the phosphite as the main final product. Partial rearrangement to afford the side products resulted because the *in situ* reaction was carried out in an NMR tube at room temperature. In practice, pure phosphites were produced with optimized reaction conditions as mentioned before.

The $^{31}P\{^1H\}$ NMR spectra of compounds 1 - 9 all show single resonances as expected, at around 110 ppm, 160 ppm, and 145 ppm for the phosphinites, phosphonites, and phosphites, respectively. This is consistent with the chemical shifts of phosphorus in molecules with similar structures (Table 2-1).[35] Chemical shifts of the phosphonites are generally at lower frequency than those of phosphites, which means that the phosphorus atoms are more shielded in phosphites than those in phosphonites, although there are more oxygen atoms connected to phosphorus centre in phosphites and oxygen is more electronegative. This is due to the fact that the charge distribution about the phosphorus nucleus is not spherical, so the shielding constant depends not only on the electronegativity difference of the P-X bond, but also on the X-P-Y bond angles and the π-electron overlap.[36] Consequently, chemical shifts in ^{31}P NMR spectra are less easy to account for than those in ^1H or ^{13}C NMR spectra.

The $^{13}C\{^1H\}$ NMR spectra of the phosphinites (compounds 1 - 3) are much more complicated. The spectrum of $BorOPh_2$ is presented in Figure 2-4 as an example. The spectrum can be divided into two parts. The low field part above 120 ppm is the phenyl region. The two carbon atoms that are directly bonded to the phosphorus atom give two small doublets at 143.58 ppm ($^1J_{PC}$ = 18.2 Hz) and 142.88 ppm ($^1J_{PC}$ = 16.8 Hz), since they are not equivalent to each other due to the lack of symmetry in the molecule. Although there are another ten inequivalent carbon atoms in the two phenyl groups, there are only seven more lines shown in this region, presumably due to the overlap of some signals. There is no basis for specific assignment of any resonances to individual

Table 2-1. ^{31}P{^{1}H} NMR data of compounds $\underline{1}$ - $\underline{9}$.

Compound	Compound No.	δ P/ppm[a]
P(OMen)Ph$_2$	$\underline{1}$	107.3[b]
P(OBor)Ph$_2$	$\underline{2}$	110.6[b]
P(OPin^i)Ph$_2$	$\underline{3}$	109.9[b]
P(OMe)Ph$_2$		115.6[c]
P(OEt)Ph$_2$		109.8[c]
P(O-cHex)Ph$_2$		104.0[c]
P(OMen)$_2$Ph	$\underline{4}$	160.1[b]
P(OBor)$_2$Ph	$\underline{5}$	157.9[b]
P(OPin^i)$_2$Ph	$\underline{6}$	158.4[b]
P(OMe)$_2$Ph		159.0[c]
P(OEt)$_2$Ph		153.5[c]
P(OPh)$_2$Ph		164.9[c]
P(OMen)$_3$	$\underline{7}$	147.5[b]
P(OBor)$_3$	$\underline{8}$	143.4[b]
P(OPin^i)$_3$	$\underline{9}$	142.8[b]
P(OCHMe$_2$)$_3$		138.0-136.9[c]
P[OCHMe(CH$_2$CH$_2$CH$_3$)]$_3$		140.0[c]
P[OCHMe(CHMe$_2$)]$_3$		141.0[c]

[a] Chemical shifts are given in δ(ppm) relative to external 85% phosphoric acid solution.

[b] Recorded in CDCl$_3$ solution. [c] Data are taken from Ref. 35.

carbon atoms.

The high field part below 90 ppm is the alkyl region. The doublet occurred at 86.3 ppm ($^2J_{PC}$ = 19.3 Hz) can be assigned to the α-carbon atom in the bornyl group.
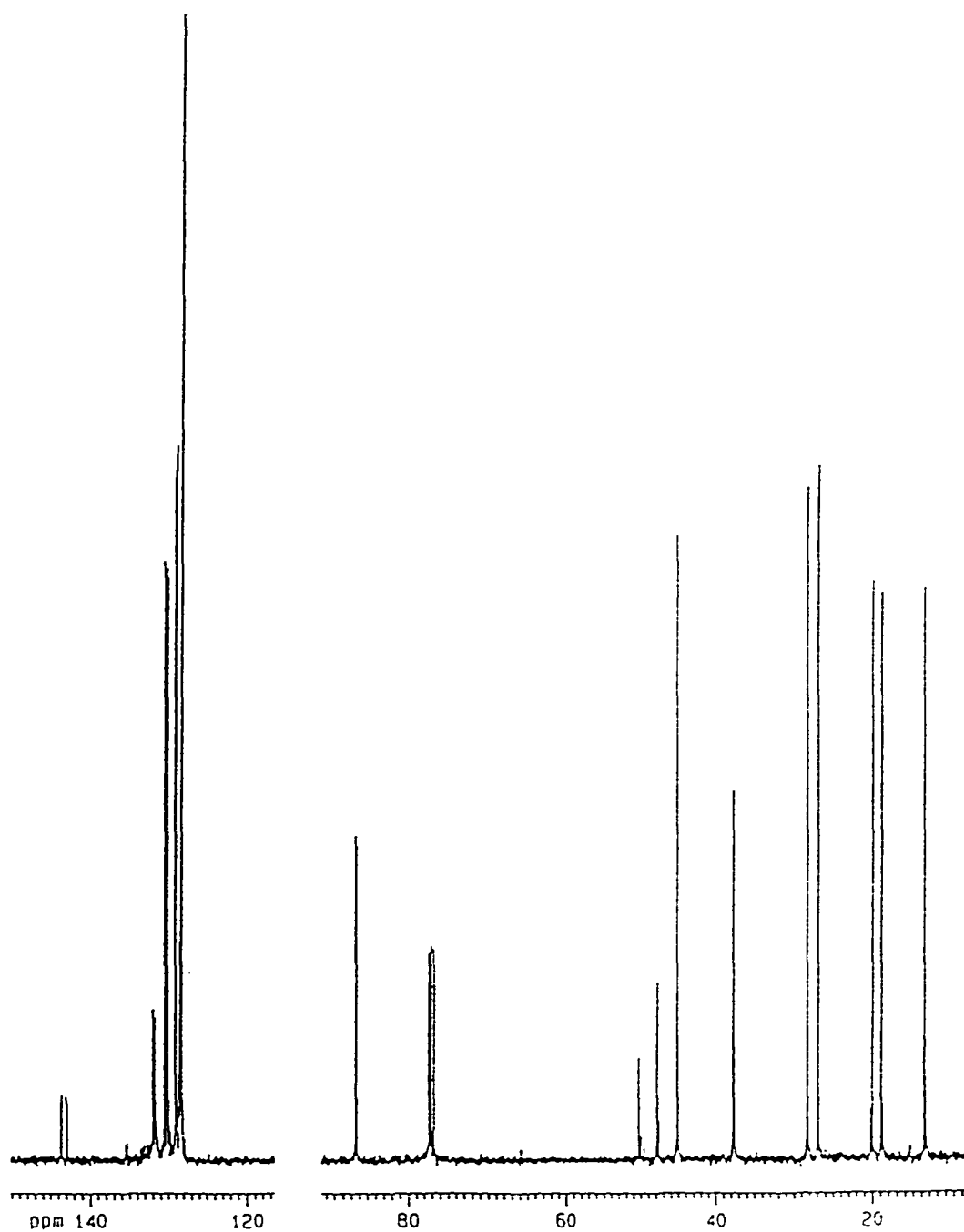
Figure 2-4. ^{13}C{^{1}H} NMR spectrum of BorOPPh$_2$, 2.

This peak is shifted down field by 9.14 ppm compared to that of the α-carbon atom in the free alcohol, which indicates that the electron density around the α-carbon is decreased upon substitution of the hydroxyl proton by the diphenylphosphino group. This is consistent with the fact that phosphorus atom is more electronegative than the hydrogen, so that the electron density around oxygen is shifted away from carbon towards phosphorus. The rest of the alkyl peaks are unaffected by coordination of the bornoxy group to phosphorus, although one of the peaks (at 50.2 ppm due to the quaternary carbon next to the α-carbon) shows what is a three-bond phosphorus carbon coupling ($^3J_{PC}$ = 3.7 Hz). The $^{13}C\{^1H\}$ NMR spectra of the other phosphinites are similar: in each case, the only alkyl peak significantly shifted upon the bonding between the alkoxy and diphenylphosphino groups is that due to the α-carbon atom in the alkoxy group (Table 2-2).

The ^1H NMR spectra of the phosphinites are also very complicated. A representative spectrum (spectrum of MenOPPh$_2$) is shown in Figure 2-5. It can be

Table 2-2. $^{31}C\{^1H\}$ NMR data[a] of the phosphinites and their corresponding free alcohols.

Compound		δ $\underline{C}$OP ppm	$^2J_{PC}$ Hz	δ $\underline{C}$OH[b] ppm
P(OMen)Ph$_2$,	<u>1</u>	81.3	18.6	71.4
P(OBor)Ph$_2$,	<u>2</u>	86.3	19.3	77.2
P(OPin^i)Ph$_2$,	<u>3</u>	81.3	18.6	71.6

[a] Chemical shifts are given in δ(ppm) relative to internal CDCl$_3$ with the middle branch of CDCl$_3$ signal set at 77.0 ppm. All spectra were recorded in CDCl$_3$ solution. [b] The chemical shift of the corresponding free alcohol.
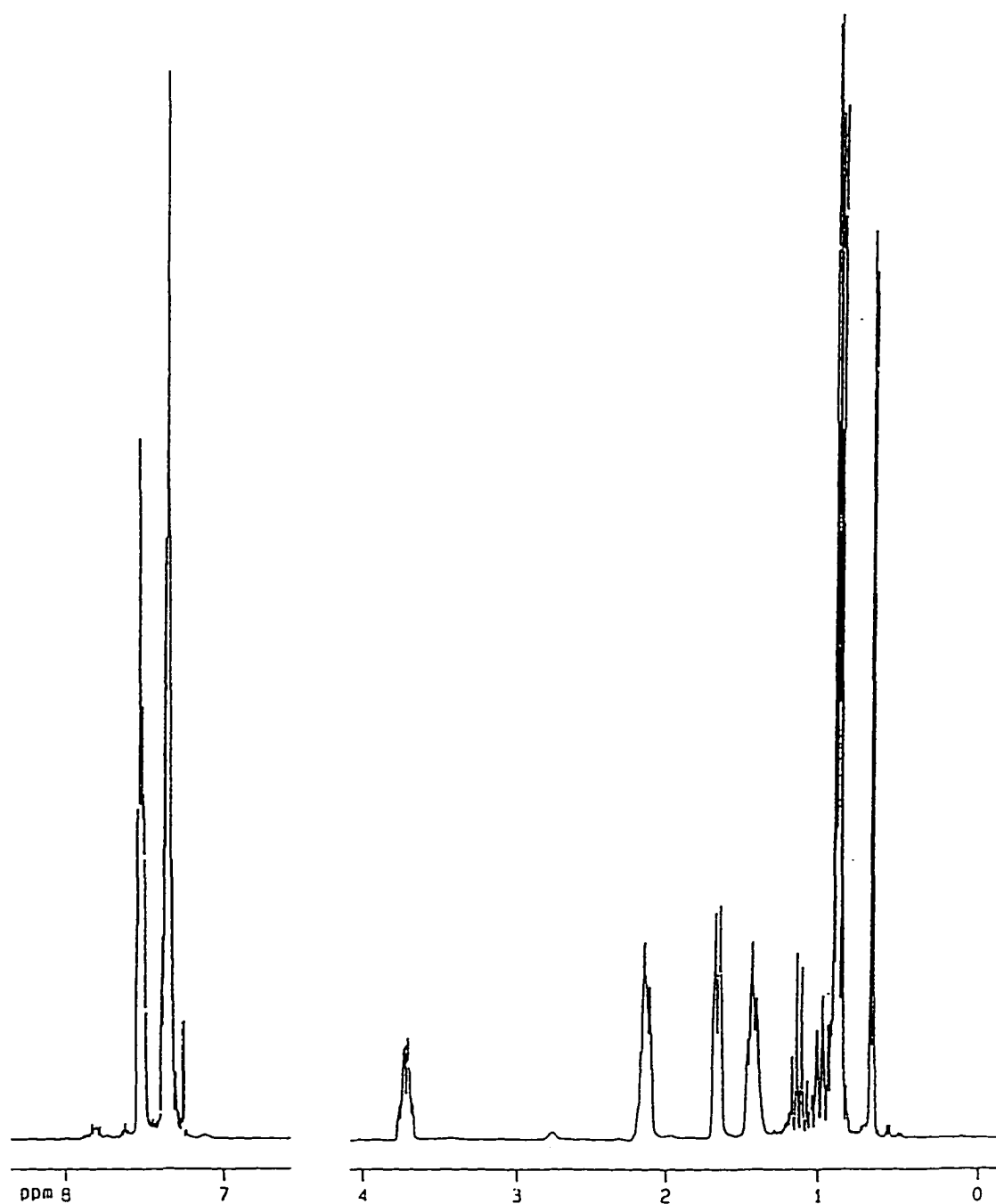
Figure 2-5. ^{1}H NMR spectrum of MenOPPh$_2$, $\underline{1}$.

divided into two parts, similar to the ^{13}C{^{1}H} NMR spectra. The phenyl region (7.2 -
7.6 ppm) is very complex because of the non-first order character of the aromatic proton
signals and the overlapping between the two sets of inequivalent phenyl peaks. The

chemical shifts and the patterns of the resonances in the alkyl region (0.6 - 3.8 ppm) show features comparable to those in the spectrum of (-)-menthol, except the peak due to the α-proton in the alkoxy group shifted downfield by 0.34 ppm to 3.70 ppm, again due to the decrease of electron density around this proton upon the coordination to the phosphorus atom, as explained for the $^{13}C\{H\}$ NMR spectra. This peak is also split into a triplet of doublets of doublets from the original triplet of doublets in the free menthol spectrum, due to the H-P coupling ($^3P_{HP}$ = 8.8 Hz). Similar characteristics are shown in the ^1H spectra of the other two chiral phosphinites (compounds 2 and 3): in each spectrum, the only signal notably shifted upon the diphenylphosphino substitution of the hydroxyl proton in the alcohol is that due to the α-proton in the alkoxy group (Table 2-3).

The $^{13}C\{^1H\}$ NMR spectra of (BorO)$_2$PPh (Figure 2-6) is typical for those of the phosphonites (compounds 4 - 6). The phenyl region (127 - 143 ppm) consists of 6 peaks due to the six inequivalent carbon atoms in the phenyl group. The peak at 142.58 ppm

Table 2-3. The ^1H NMR data[a] of the phosphinites and their corresponding alcohols.

Compound		δ $\underline{H}$COP	$^3J_{PH}$	δ $\underline{H}$COH[b]
		ppm	Hz	ppm
P(OMen)Ph$_2$,	1	3.70	8.8	3.36
P(OBor)Ph$_2$,	2	4.26	9.8	3.96
P(OPin^i)Ph$_2$,	3	4.31	4.9	4.07

[a] Chemical shifts are given in δ(ppm) relative to internal CDCl$_3$ with the CDCl$_3$ signal set at 7.24 ppm. All spectra were recorded in CDCl$_3$ solution. [b] Chemical shifts of the corresponding free alcohol.
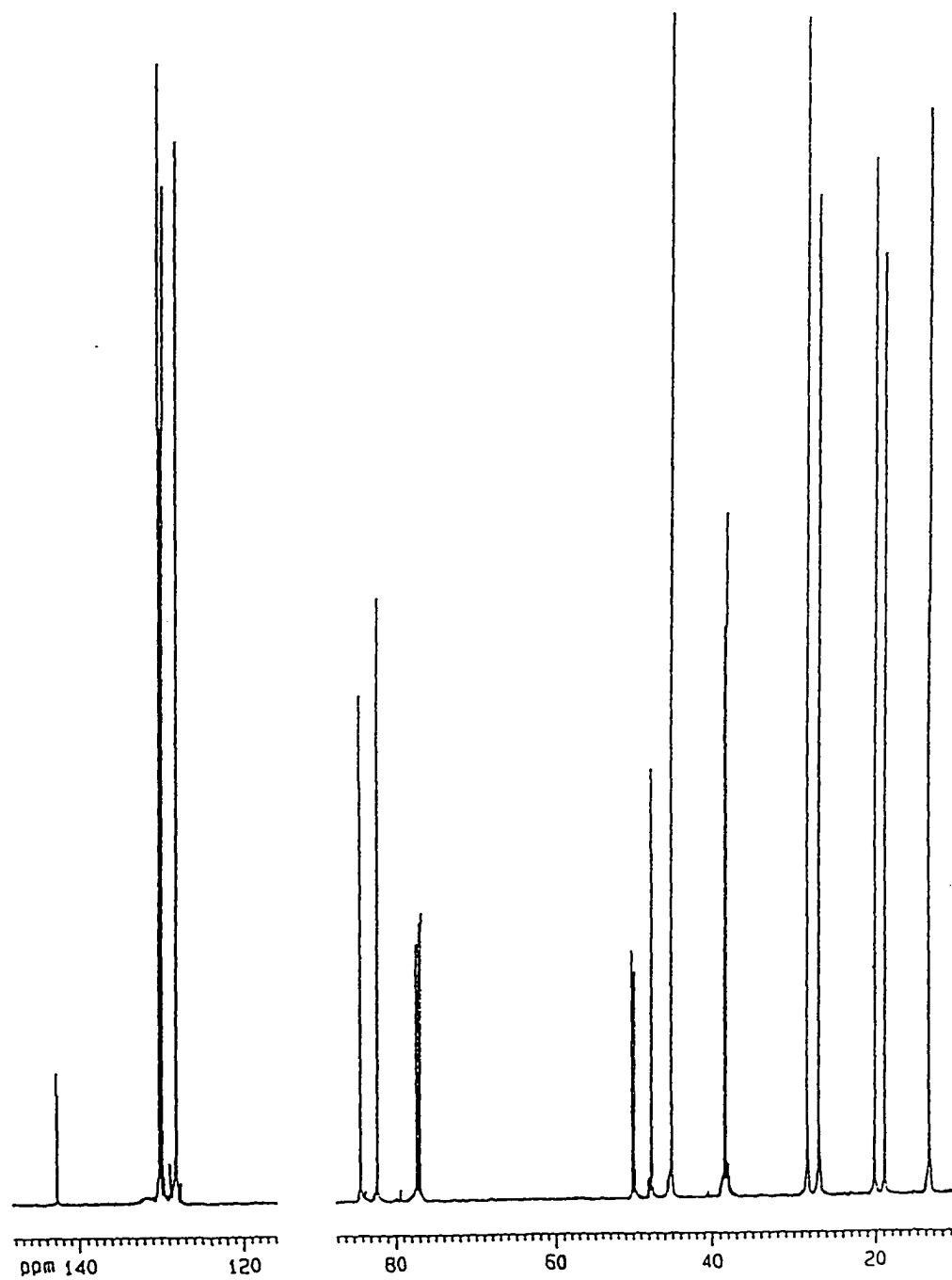
N.B. Each of the seven single lines between 10 - 50 ppm consists of two peaks, which can be observed when expanded. The two resonances at 84.1 and 82.1 ppm are doublets.

Figure 2-6. $^{13}C\{^1H\}$ NMR spectrum of $(BorO)_2PPh$, $\underline{5}$.

is a doublet ($^1J_{PC}$ = 16.2 Hz), and can be assigned to the carbon atom directly attached to the phosphorus centre. The alkyl region (13 - 85 ppm) appears much more complicated. Since the presence of the two optically active bornoxy groups removes all symmetry elements in the molecule, the two groups are not magnetically equivalent. Therefore the two sets of resonances, each consisting of 10 signals due to the 10 different carbons in each group, do not coincide with each other, so that a total of 20 peaks is observed. Except for those due to the α-carbons, this doubling of peaks gives pairs of signals that are very close to each other, the spacing ranging from 0.03 ppm to 0.4 ppm. The spacing of the peaks increases as the carbon pairs get closer to the phosphorus centre, to a maximum of 2.0 ppm for the α-carbon themselves. This may be because as it gets closer to the phosphorus centre, the local structure becomes more rigid, and the difference between the two inequivalent groups is more pronounced;

Table 2-4. $^{31}C\{^1H\}$ NMR Data[a] of the phosphonites and their corresponding free alcohols.

Compound		δ $\underline{C}_1O_1P$[b] ppm	$^2J_{PC1}$[b] Hz	δ $\underline{C}_2O_2P$[b] ppm	$^2J_{PC2}$[b] Hz	δ $\underline{C}OH$[c] ppm
P(OMen)$_2$Ph,	4	79.6	17.3	78.9	7.3	71.4
P(OBor)$_2$Ph,	5	84.1	15.7	82.1	8.2	77.2
P(OPin^i)$_2$Ph,	6	78.9	13.4	77.8	11.8	71.6

[a] Chemical shifts are given in δ(ppm) relative to internal CDCl$_3$ with the middle branch of the CDCl$_3$ signal set at 77.0 ppm. All spectra were recorded in CDCl$_3$ solution. [b] Subscript labels are used to distinguish the two carbon atoms and two oxygen atoms in the two alkoxy groups. The absolute assignment cannot be made. [c] Chemical shifts of the corresponding free alcohol.

whereas the carbon framework farther away from the phosphorus is more flexible, so the differences are smaller.

The chemical shifts that are affected most by the coordination of the bornoxy
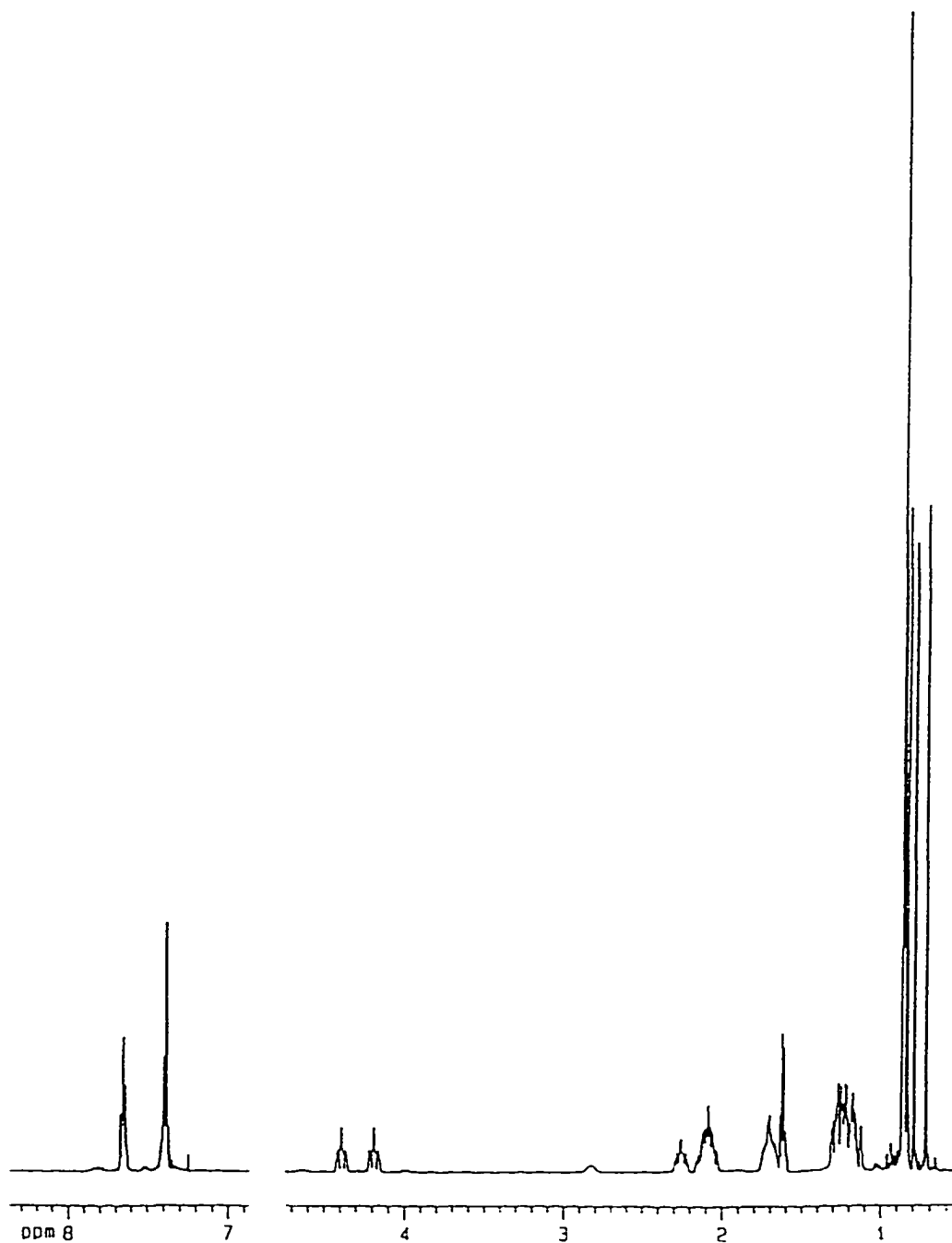
Figure 2-7. ^{1}H NMR spectrum of (BorO)$_2$PPh, 5.

group to phosphorus are the pair of peaks due to the two α-carbon atoms in the two bornoxy groups. They are shifted downfield from their original position in the free alcohol by 6.92 and 4.88 ppm to 82.1 and 84.1 ppm, respectively. because, again, the electron density around the α-carbons is shifted towards the phosphorus atom upon the bonding between oxygen and phosphorus. The rest of the bornoxy resonances are hardly affected except that several signals are split into doublets by the phosphorus atom ($^3J_{PC}$ = 4.6, and 3.8 Hz for the peaks at 50.0, and 49.6 ppm, respectively, due to the two quaternary carbons next to the α-carbons; $^3J_{PC}$ = 2.9 Hz for the peak at 38.4 ppm due to the secondary carbon next to the α-carbon in one of the two bornoxy groups. The same carbon in the other bornoxy group produced a singlet at 38.1 ppm). Similarly, in the $^{13}C\{^1H\}$ NMR spectra of the other phosphonites, the peaks of the α-carbon atoms in the alkoxy groups are shifted most (Table 2-4) while the chemical shifts of the remaining alkoxy resonances are very close to those in the corresponding free ligands.

Table 2-5. The ^{1}H NMR data* of the phosphonites and their corresponding free alcohols.

Compound	δ $\underline{H}_1C_1O_1$ ppm	$^3J_{PH1}$[b] Hz	δ $\underline{H}_2C_2O_2$ ppm	$^3J_{PH2}$[b] Hz	δ $\underline{H}COH$[c] ppm
P(OMen)₂Ph, <u>4</u>	3.80	8.89	3.71	7.74	3.36
P(OBor)₂Ph, <u>5</u>	4.38	10.0	4.18	9.86	3.96
P(OIpc)₂Ph, <u>6</u>	4.39	4.63	4.32	4.58	4.07

* Chemical shifts are given in δ(ppm) relative to internal $CDCl_3$ with the $CDCl_3$ signal set at 7.24 ppm. All spectra were recorded in $CDCl_3$ solution. [b] Subscript labels are used to distinguish the atoms in the two alkoxy groups. The absolute assignment cannot be made. [c] Chemical shifts of the corresponding free alcohol.

The ^{1}H NMR spectrum of (BorO)$_2$PPh shown in Figure 2-7 is typical for the phosphonites. In comparison with the ^{1}H NMR spectrum of BorOPPh$_2$, the phenyl region (7.2 - 7.9 ppm) is simplified while the alkyl region (0.7 - 4.5 ppm) is complicated. The peaks due to the two α-protons in the two bornoxy groups are shifted downfield by 0.42 and 0.22 ppm to 4.38 and 4.18 ppm, respectively, due to the deshielding effect of the phosphorus atom discussed previously. The multiplicity of these peaks is transformed from the original doublet of doublets of doublets in the free alcohol into a triplet of quintets, indicating a three-bond phosphorus proton coupling ($^3J_{PH}$ = 10.0, and 9.9 Hz for the peaks centred at 4.38, and 4.18 ppm, respectively). Table 2-5 shows characteristic ^{1}H NMR data of the chiral phosphonites and their corresponding free alcohols.

Because of the lack of aromatic groups and the existence of C_3 rotational molecular symmetry for the phosphites (compounds 7 - 9), the ^{13}C{^{1}H} NMR spectra of these compounds appear considerably simplified compared with those of the

Table 2-6. ^{31}C{^{1}H} NMR data^a of the phosphites and their corresponding free alcohols.

Compound		δ $\underline{C}$OP ppm	$^2J_{PC}$ Hz	δ $\underline{C}$OH^b ppm
P(OMen)$_3$,	7	73.5	12.3	71.4
P(OBor)$_3$,	8	77.9	10.4	77.2
P(OPin^i)$_3$,	9	72.9	11.5	71.6

^{a} Chemical shifts are given in δ(ppm) relative to internal CDCl$_3$ with the central resonance of the CDCl$_3$ signal set at 77.0 ppm. All spectra were recorded in CDCl$_3$ solution. ^{b} Chemical shifts of the corresponding free alcohol.

phosphinites and the phosphonites: one set of alkoxy resonances is to be expected. The spectrum of P(OPin^i)$_3$ shown in Figure 2-8 is chosen as an example. The peak due to the α-carbons in the isopinocamphoxy groups is located at 72.9 ppm with a downfield
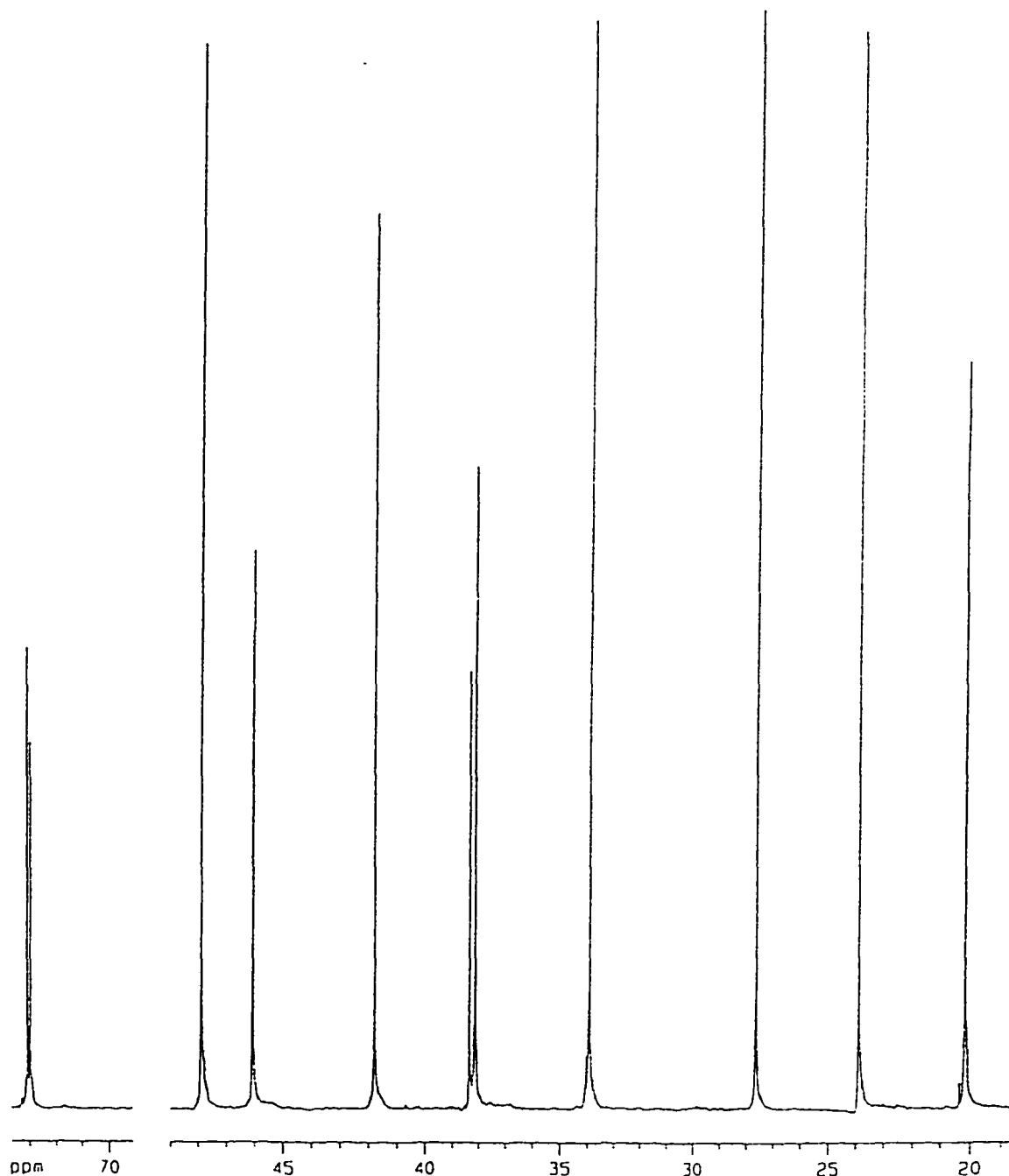
Figure 2-8. ^{13}C{^{1}H} NMR spectrum of (Pin^{i}O)$_3$P, 9.

shift of 1.3 ppm from the free alcohol. This chemical shift change is smaller than those of P(OPin^i)$_2$Ph (7.3, and 6.2 ppm), which in turn is smaller than that of P(OPin^i)Ph$_2$ (9.7 ppm). A reasonable explanation of this is that the electron deshielding effect of the phosphorus atom is shared among the alkoxy groups attached to it. The more alkoxy groups bonding to it, the less deshielding effect it has towards individual α-carbon atoms. Three-bond phosphorus carbon couplings are also observed in this spectrum ($^3J_{PC}$ = 3.3 and 2.0 Hz for the peaks at 46.0 and 38.1 ppm due to the tertiary and secondary carbon atoms next to the α-carbons, respectively). The ^{13}C{^{1}H} NMR spectra of other phosphites have similar features (Table 2-6).

The ^{1}H NMR spectra of the phosphites (compounds $\underline{7}$ - $\underline{9}$) are similar to their phosphinite counterparts (except that there are no resonances in the aromatic region), as can be seen in the spectrum of (BorO)$_3$P (compound $\underline{8}$) shown in Figure 2-9. The resonance due to the α-protons in the bornoxy groups is also shifted downfield to 4.32 ppm from its original position at 3.96 ppm in borneol. Unlike that observed in the

Table 2-7. ^{1}H NMR data^a of the phosphites and their corresponding free alcohols.

Compound	δ $\underline{H}$COP	$^3J_{PH}$	δ $\underline{H}$COH^b
	ppm	Hz	ppm
P(OMen)Ph$_2$, $\underline{7}$	3.79	8.9	3.36
P(OBor)Ph$_2$, $\underline{8}$	4.33	9.9	3.96
P(OPin^i)Ph$_2$, $\underline{9}$	4.45	4.9	4.07

^{a} Chemical shifts are given in δ(ppm) relative to internal CDCl$_3$ with the CDCl$_3$ signal set at 7.24 ppm. All spectra were recorded in CDCl$_3$ solution. ^{b} Chemical shifts of the corresponding free alcohol.

corresponding $^{13}C\{^1H\}$ NMR spectra, this chemical shift difference is not smaller than those in the spectra of $P(OBor)_2Ph$ or $P(OBor)Ph_2$. In fact, the chemical shifts of the peaks due to the α-protons in each series of compounds containing the same alkoxy groups (e.g. $BorOPPh_2$, $(BorO)_2PPh$, and $(BorO)_3P$) are within a range of 0.2 ppm. This is probably because the protons in question are farther away from the phosphorus atom
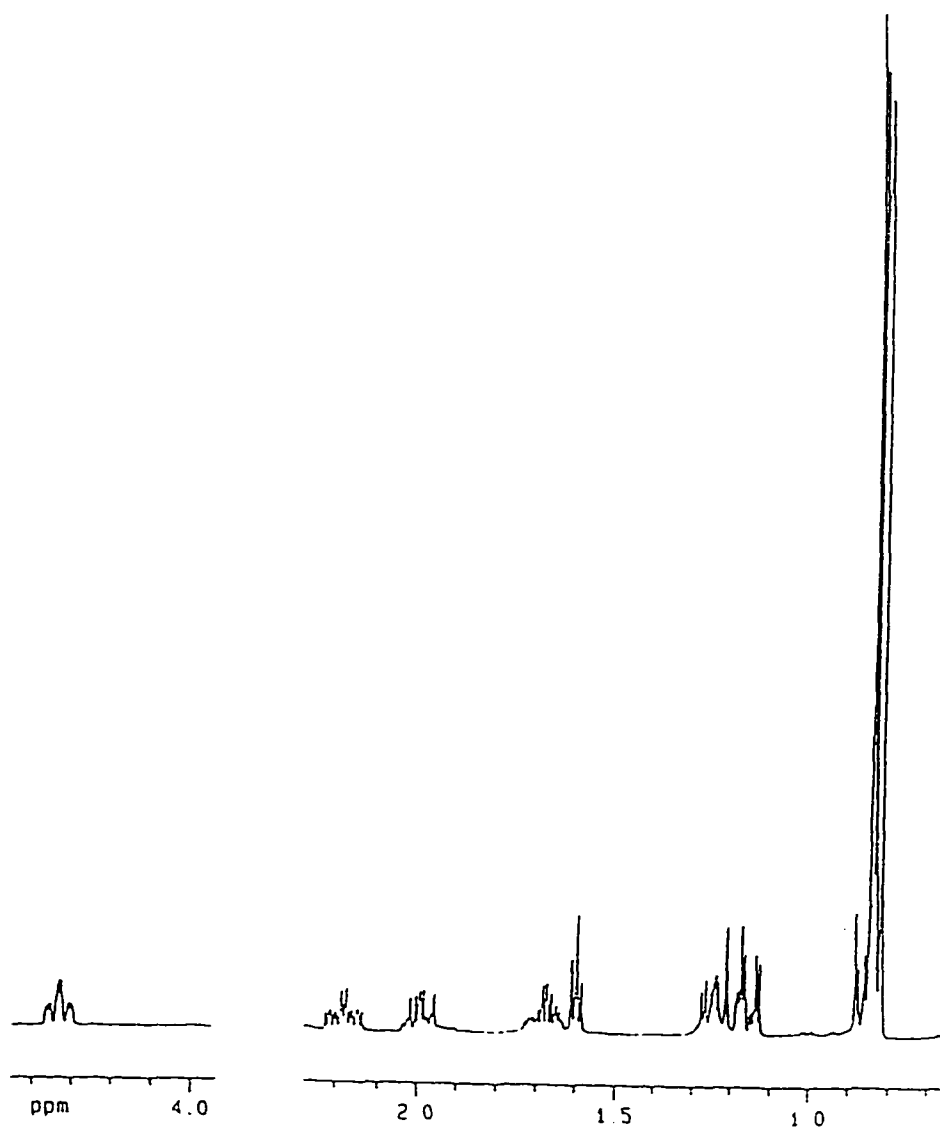
Figure 2-9. ^1H NMR spectrum of $(BorO)_3P$, 8.

than their carbon counterparts. Therefore, the electron deshielding effect is not strong enough to differentiate the chemical shift changes in each series. The multiplicity of the α-proton resonance in the spectrum of 8 signal changed from doublet of doublets of doublets in the free alcohol to triblet of doublets of doublets, indicating a coupling between phosphorus and the proton ($^3J_{PH}$ = 9.9 Hz). Similar features are observed for the other ^{1}H NMR spectra of the phosphites, (Table 2-7).

The IR spectra of compounds 1 - 9 were also recorded. The patterns are all very similar to each other with few structurally significant features. Absorptions at 2800 - 3100 cm^{-1} can be assigned to C-H stretching vibrations from hydrocarbon groups. The aromatic rings in the phosphinites and phosphonites show weak absorptions at about 1600 cm^{-1} and medium strong absorptions in the 1450 - 1500 cm^{-1} region, which contains a series of bands that could not be unambiguously assigned. These aromatic bands and the bands at about 3060 cm^{-1}, which can be also assigned to aromatic C-H stretching vibrations, are not present in the phosphite spectra, since there are no phenyl groups in the phosphites. The strong v(P-O-C) bands, which are expected at about 1000 cm^{-1}, are masked by other bands in the same region, so cannot be identified.

MenPPh₂   neo-MenPPh₂
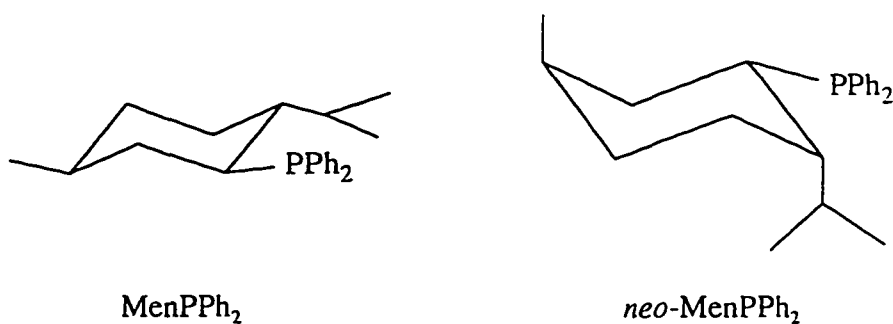
Diphenylmenthylphosphine (MenPPh₂) and its epimer, diphenylneomenthyl-phosphine (neo-MenPPh₂) are closely related to MenOPPh₂ (compound 1). The two epimers are frequently employed as optically active phosphorus ligands in the studies on asymmetric induction via transition metal catalysts.[37] They were first prepared by

Morrison and co-workers in the early 1970s,[38] using the reaction between lithium or sodium diphenylphosphide, obtained by treating chlorodiphenylphosphine with lithium[39] or reacting diphenylphosphine with sodium, respectively, and (+)-neomenthyl[40] or menthyl chloride,[41] derivatives of (-)-menthol (Equations 2-4 - 2-9).

$$PPh_2Cl + 2Li \longrightarrow Ph_2PLi + LiCl \qquad (2-4)$$

$$2PPh_2H + 2Na \longrightarrow 2Ph_2PNa + H_2 \qquad (2-5)$$

$$MenOH + HCl \xrightarrow{ZnCl_2} MenCl + H_2O \qquad (2-6)$$

$$MenOH + HCl \longrightarrow neo\text{-}MenCl + H_2O \qquad (2-7)$$

$$Ph_2PLi + MenCl \longrightarrow neo\text{-}MenPPh_2 + LiCl \qquad (2-8)$$

$$Ph_2PNa + neo\text{-}MenCl \longrightarrow MenPPh_2 + NaCl \qquad (2-9)$$
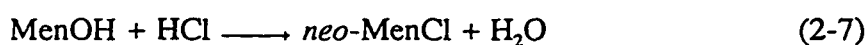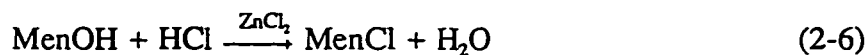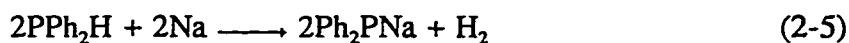
The yields of these two preparations are 34% for neo-MenPPh$_2$ from MenCl, and 25-30% for MenPPh$_2$ from MenCl, which are fairly low. The latter was later improved to 51% by Tanaka and co-workers using the Grignard reaction (Equations 2-10 and 2-11).[42]

$$MenCl + Mg \longrightarrow MenMgCl \qquad (2-10)$$

$$MenMgCl + ClPPh_2 \longrightarrow MenPPh_2 + MgCl_2 \qquad (2-11)$$

Although the Grignard reaction offers a notably higher yield, this method was not extended to the synthesis of neo-MenPPh$_2$, since the preparation of a Grignard reagent from an chiral alkyl halide where the halogen is attached to an asymmetric carbon often results in significant racemization.[43] The preparation of MenMgCl is a rare exception. The overall conversion yield for MenPPh$_2$ from MenOH (less than 45%) is still low, compared to that of the synthesis of MenOPPh$_2$. With proper care taken to prevent the Michaelis-Arbuzov rearrangement from occurring, compounds 1 - 9 can all be readily synthesized with high yields.

In surprising contrast, however, attempted parallel synthesis of chiral phosphinites, phosphonites, and phosphites starting from two other available terpene

alcohols, (+)-fenchyl alcohol ((1*R*,2*R*,4*S*)-1,3,3-trimethylbicyclo[2.2.1]heptan-2-ol) and

(+)-cedrol ((3*R*,3a*S*,6*R*,7*R*,8a*R*)-6-hydroxyl-1,2,4,5,8a-pentahydro-3,8,8-trimethyl-3a,7-

methanoazulene), was completely unsuccessful. In the first of these compounds, the

hydroxyl group is *endo* between two substituent methyl groups, which may block the

entering phosphorus centre, thus preventing the reaction. Cedrol differs from the other

terpene alcohols referred to in this chapter in that it is a tertiary alcohol, which could

easily lose the hydroxyl group to form a stable carbocation intermediate. The latter

could then lead to various products such as olefins or substituted cedrane compounds,

but not to any analogue of compounds 1 - 9.
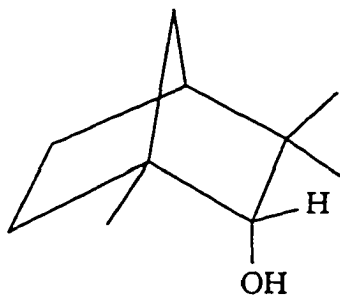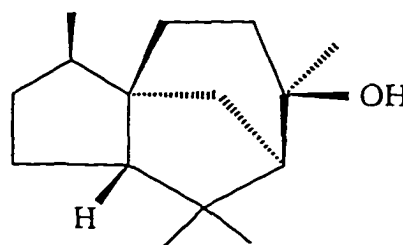
Fenchyl alcohol   Cedrol

Every compound in the series 1 - 9 exists as a single stereoisomer based on the

inherent natural property of the terpene fragment. These are so-called "backbone chiral"

molecules, where the stereogenic units are located within the substituting (backbone)

groups. Thus, the conventional optical resolution of these molecules can be avoided

when optically pure substituents are used, because the final product will have the same

enantiomeric excess if no racemization steps are involved during the synthesis. However,

most synthetic substituents are first obtained as a racemic mixture, which require usually

inefficient resolution steps to acquire high optical purity. In the cases where natural

available optically pure starting materials (such as the terpene alcohols discussed in this

chapter) are used, optical resolution is completely avoided, and the final products may be synthesized in high yields and optical purity.
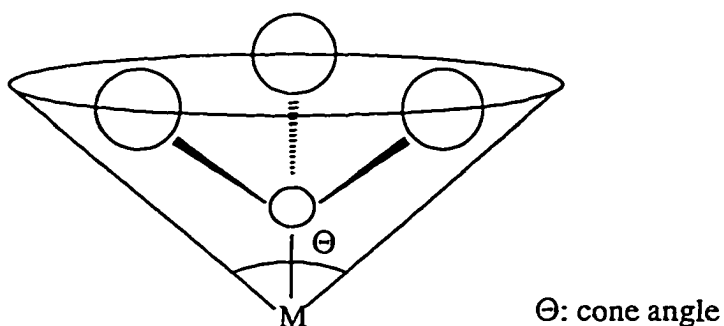
Θ: cone angle

Figure 2-10. Tolman's cone angle.

With one or more alkoxy groups (MenO, BorO, and Pin^{i}O), each possessing ten carbon atoms, compounds 1 - 9 may be viewed as bulky ligands. The steric bulk is a very important parameter for a ligand. To quantitatively describe the size of a ligand, the cone angle was introduced by Tolman as the apex angle of a cylindrical cone when all ligand substituents are arranged so as to occupy as little space as possible (Figure 2-10).[44] The cone angles of a series symmetrical phosphorus ligands are shown in Table

Table 2-8. Selected cone angles, Θ, for tertiary phosphorus ligands.

Ligand	Θ (°)	Ligand	Θ (°)
PH_3	87	P(cyclohexyl)$_3$	170
PMe_3	118	PBu$^t_3$	182
PEt_3	132	P(o-tol)$_3$	194
PPh_3	145	PEt$_2$Ph	136
PPr$^i_3$	160	PEtPh$_2$	140

2-8.[45] Although the size of $\underline{1}$ - $\underline{9}$ are comparable to that of cyclohexyl group or o-tolyl group, the steric tensions between the substituents in $\underline{1}$ - $\underline{9}$ are not as high as in their cyclohexyl or o-tolyl analogues, because the bulky alkyl fragments in the alkoxy groups are distant from the phosphorus centre as they are connected through an oxygen atom. Therefore, the cone angles of $\underline{1}$ - $\underline{9}$ are smaller than those of $P(cyclohexyl)_3$ or $P(o\text{-}tol)_3$, as suggested by the V.T. NMR spectra of iron and cobalt complexes of $\underline{1}$ - $\underline{9}$ (see Chapter 3). Nonetheless, the steric bulk of these compounds is estimated to be comparable to that of PPh_3, which is implied by the stereochemistry of the iron, cobalt, and iridium complexes of $\underline{1}$ - $\underline{9}$ (see Chapters 3 and 4).

Another important parameter for any ligand is its electronic property. The analysis of the IR and NMR spectra of the iron and cobalt complexes of $\underline{1}$ - $\underline{9}$ show small but consistent change the Lewis basicity of these ligands. Detailed discussion will be presented in Chapter 3.

Chapter 3

SYNTHESIS AND CHARACTERIZATION OF CARBONYL IRON AND COBALT COMPLEXES WITH CHIRAL PHOSPHORUS LIGANDS

3.A. Introduction

Following the synthesis of the first metal carbonyl complex, $(PtCl_2CO)_2$, by Schutzenberger in 1868,[46] carbonyl complexes of every transition metal element in the periodic table were discovered over the last 120 years. The first binary transition metal carbon monoxide complex, $Ni(CO)_4$, was reported by Mond *et al.* in 1890.[47] Following that, binary carbonyl complexes of Groups 6 - 9 elements and vanadium were all synthesized as either mononuclear, or multinuclear species, illustrating that carbon monoxide shows a strong tendency to form complexes with the middle elements (Groups 6 - 9). This is ascribed to the bonding mechanism between the carbonyl group and the metal. According to the synergic bonding theory originally developed by Dewar,[48] Chatt, and Duncanson,[49] carbon monoxide, which is a classic π-acid ligand, is believed to bond to a metal centre through two types of orbital interactions simultaneously: a) σ-donation of electrons from the HOMO of CO, a weakly bonding σ-orbital, into an empty σ type d orbital on the metal atom; b) π-back-donation from a filled π type d orbital on the metal to the LUMO of CO, an antibonding π-orbital. The σ-bond between carbon and the metal is strengthened by the back-donation of electrons from the metal centre, so that the CO bond order decreases as the electron density in the anti-bonding LUMO of CO increases. Because the back-donation of electrons from metal to CO requires the metal to have filled d orbitals, in order to form stable metal carbonyl complexes high electron density at d orbitals on the metal centre is needed. Thus, early transitions metals

and transition metals in high oxidation states will not readily form metal carbonyl complexes. For the last two triads, as the transition metal centre is approaching the *p* block of the periodic table, the energy difference between the valence *d* orbitals and the HOMO and LUMO of carbon monoxide becomes too big for there to be significant overlap, so that the carbonyl complexes of these elements are also rare.

Extensive investigation on transition metal carbonyl complexes has been carried out, partially due to their wide use as catalysts in numerous organic syntheses, especially those involving carbon monoxide as a reagent. For example: $Co_2(CO)_8$ and $Ni(CO)_4$ are used as catalyst in the oxo process[50] (Equation 3-1), and the Reppe synthesis[51] (Equation 3-2), respectively. In order to obtain higher efficiency under milder reaction conditions, or better regio and stereoselectivity, various modifications to the binary systems have been made. Among all substituents, tertiary phosphorus ligands are among those most commonly employed, as illustrated by the modified oxo process: when triethylphosphine is added to the $Co_2(CO)_8$ catalyst, fairly high yields can be obtained.[52]

$$RHC=CH_2 + CO + H_2 \xrightarrow{Co_2(CO)_8} RCH_2CH_2CHO \text{ or } R(CHO)CHCH_3 \quad (3\text{-}1)$$

$$HC\equiv CH + CO + H_2O \xrightarrow{Ni(CO)_4} CH_2=CHCOOH \quad (3\text{-}2)$$
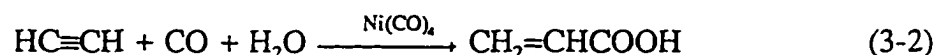
Because the stretching frequencies of the carbonyl groups range from 1700 to 2200 cm^{-1}, where few other functional groups exhibit vibrational bands, IR spectroscopy is the preeminent physical method for characterizing metal carbonyls, although ^{13}C NMR spectra have become increasingly available in recent years. A considerable amount of information, including the geometry of the molecule (with the aid of group theory), the oxidation state of the metal centre, *etc.*, may be deduced from the IR spectra of the metal carbonyl derivatives.

Metal carbon monoxide complexes were chosen to model the coordination behaviour of the chiral tertiary phosphorus ligands discussed in Chapter 2, because not only it is theoretically interesting to investigate their stereochemical properties and internal bonding scheme, but also because they are potentially important as asymmetric catalysts and are relatively easy to characterize by IR and NMR. Mononuclear mono- and di-substituted iron(0) carbonyls and dinuclear di-substituted cobalt(0) carbonyls were selected as specific target molecules.

CO

CO

OC ——— Fe

CO

CO
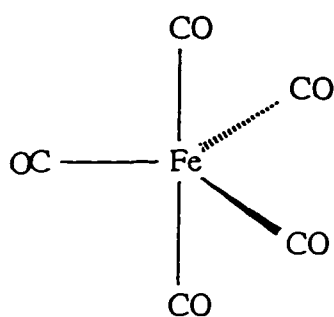
$Fe(CO)_5$.

Iron pentacarbonyl ($Fe[CO]_5$), discovered[53, 54] only one year after $Ni(CO)_4$, is not only a good catalyst for hydrosilation reactions,[55] but is also a common starting material for organoiron compounds.[56] The neutral five-coordinate complex satisfies the 18-electron rule and adopts a trigonal bipyramidal structure. The five CO groups undergo rapid interchange even at -170 °C.[57, 58] Stereochemical nonrigidity is a

L_1
L_4
L_3 —— Fe
L_5
L_2
⇌
L_1
L_4
L_3 —— Fe
L_5
L_2
⇌
L_4
L_1
L_3 —— Fe
L_2
L_5
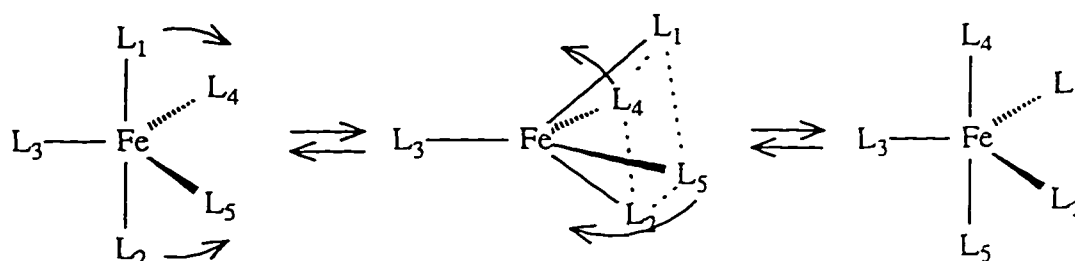
Scheme 3-1. Pseudo-rotation of the five-coordinate complexes.

common phenomenon with five-coordinate complexes, and it is accepted that the ligand interchange occurs via the pseudo-rotation mechanism originally proposed by Berry (Scheme 3-1).[59, 60] A series of mono- and di-substituted iron carbon monoxide complexes substituted with various alkyl and aryl phosphines has been prepared from $Fe(CO)_5$ and their stereochemistry has been extensively studied.[56] In general it has been observed that ligands occupy first the axial position and then di-substitution occurs to give the *trans* diaxial species (Scheme 3-2).

P: Tertiary phosphorus ligand
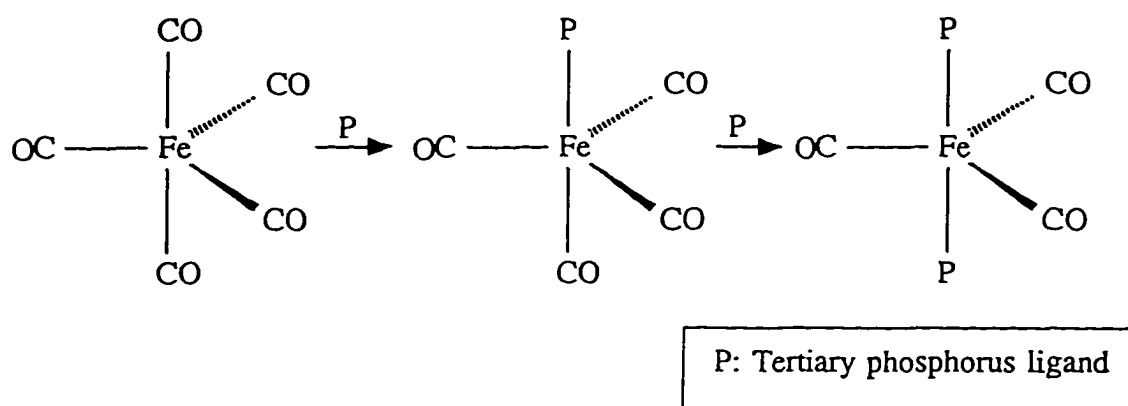
Scheme 3-2. Substitution of $Fe(CO)_5$

Because cobalt has an odd number (9) of valence electrons, its simplest binary carbon monoxide complex that satisfies the 18-electron rule is $Co_2(CO)_8$, which contains

(a)   (b)   (c)
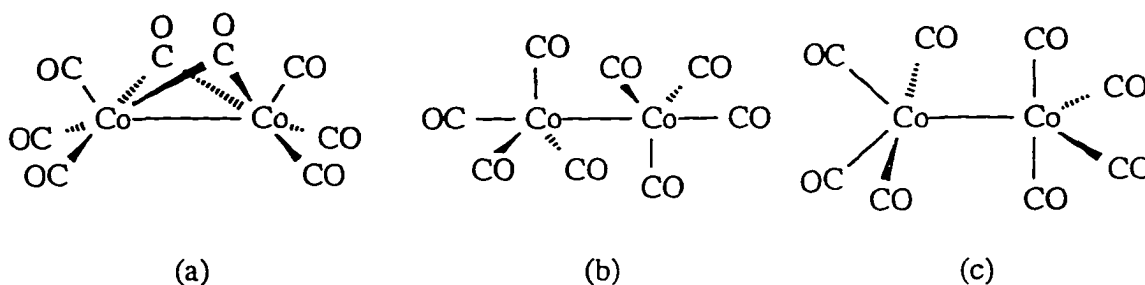
Figure 3-1. Molecular structures of $Co_2(CO)_8$.

a Co-Co bond. The molecular structure of $Co_2(CO)_8$ in the solid state is shown in Figure 3-1(a).[61] In solution, however, two other structures (Figure 3-1(b) and (c)) appear. At low temperature (77 K), structure (a) is most abundant, but the amount of the other two increases with temperature. At 298 K approximately 30% of $Co_2(CO)_8$ adopts structure (c), which predominates at higher temperatures.[62]

Various dimeric Co(0) carbonyl complexes containing other ligands can be derived from $Co_2(CO)_8$.[63] The number of substituting ligands can be up to eight (e.g. $Co_2[CNR]_8$),[64] although with Lewis base ligands (such as phosphines) di-substituted products appear to be most common. The crystal structures of several di-substituted dimeric cobalt carbonyl complexes, such as $Co_2(CO)_6(PBu_3)_2$,[65,66] $Co_2(CO)_6[P(OPh)_3]_2$,[67] and $Co_2(CO)_6[PPh_2(C_4F_4)AsMe_2]_2$,[68] have been determined, showing the two phosphorus ligands occupying the two axial positions, without any bridging CO ligands. However, IR studies in solution show evidence for CO-bridged isomeric forms, although non-bridged isomers are favoured by higher temperatures, polar solvents, and bulky ligands.[69]
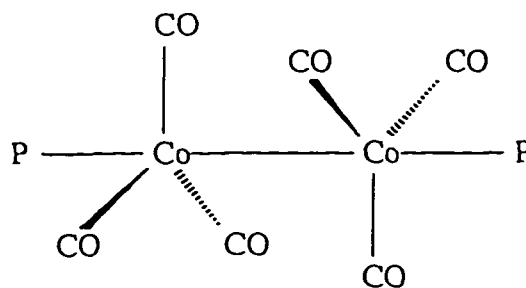
Di-substituted cobalt carbonyl complexes.

In this Chapter, the syntheses and characterization of mono- and di-substituted monomeric iron(0) and di-substituted dimeric cobalt(0) complexes containing ligands from Chapter 2 are reported; the structural analysis of these complexes by IR and variable temperature NMR spectrometry are discussed; and preliminary studies on hydroformylation reactions under oxo conditions using several cobalt complexes as

catalysts are presented.

3.B. Mono-substituted Iron Carbonyl Complexes

Tetracarbonyliron(0) complexes containing chiral phosphinite, phosphonite and phosphite ligands (compounds $\underline{1}$ - $\underline{9}$) were synthesized by $CoCl_2 \cdot 2H_2O$ catalyzed reaction of excess $Fe(CO)_5$ with the phosphorus ligands according to Equation 3-3.[70]

$$Fe(CO)_5 + PPh_{3-n}(OR)_n \xrightarrow[\text{toluene}]{CoCl_2 \cdot 2H_2O} Fe(CO)_4[PPh_{3-n}(OR)_n] + CO$$

<div align="center">Compounds <u>10</u> - <u>18</u>   (3-3)</div>
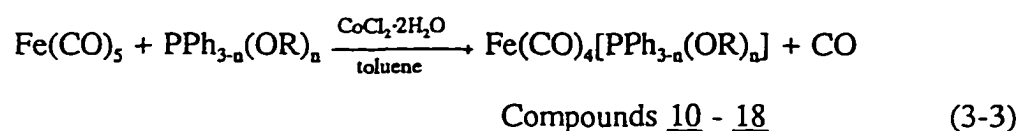
Compound <u>10</u>:	R = Men,	n = 1;	Compound <u>14</u>:	R = Bor,	n = 2;
<u>11</u>:	Bor,	1;	<u>15</u>:	Pin^i,	2;
<u>12</u>:	Pin^i,	1;	<u>16</u>:	Men,	3;
<u>13</u>:	Men,	2;	<u>17</u>:	Bor,	3;
			<u>18</u>:	Pin^i,	3.

Using this route, compounds <u>10</u> - <u>18</u> were obtained as either orange yellow crystals or very viscous deep orange liquids in relatively high yields. These compounds are soluble in most common organic solvents such as hexanes, dichloromethane, chloroform, benzene, *etc.*, showing increased solubility in the more polar solvents. Compounds <u>10</u> - <u>18</u> are stable in air in the solid state. In solution, however, these compounds decompose slowly when exposed to air.

Several other methods for preparing $Fe(CO)_4L$ complexes including both direct procedures, which are promoted either thermally[71] or photochemically,[72] and indirect procedures, such as the reaction between the ligand and triiron dodecacarbonyl,[73] or the reduction of iron(II) carbonyl halide complexes with phenyllithium in the presence

of the ligand,[74] have been reported. However, mixtures of the mono- and di-substituted species are usually generated, and separation processes are required. The use of $CoCl_2 \cdot 2H_2O$ as a catalyst sufficiently suppressed the formation of the di-substituted products, that the separation step could be avoided. The function of the catalyst in this reaction is not clear, but it is believed that a $CoCl_2L_2$ complex is formed first and the interaction between this species and $Fe(CO)_5$ facilitates the nucleophilic replacement of coordinated CO by the phosphorus ligands.[75]

The IR spectra of the mono-substituted iron complexes were all recorded in hexane solutions. The stretching frequencies of the carbonyl groups are listed in Table 6-6. As shown in a typical IR spectrum (that of $(CO)_4Fe[P(OPin^i)_3]$) in Figure 3-2, each spectrum consists of four carbonyl stretching bands, at around 2055, 1985, 1950 and 1942 cm^{-1}. As mentioned in the Introduction, the most common structure for mono-phosphorus tetracarbonyl iron complexes is trigonal bipyramid with the ligand occupying one of the axial positions (Scheme 3-2), and it belongs to either strict or approximate
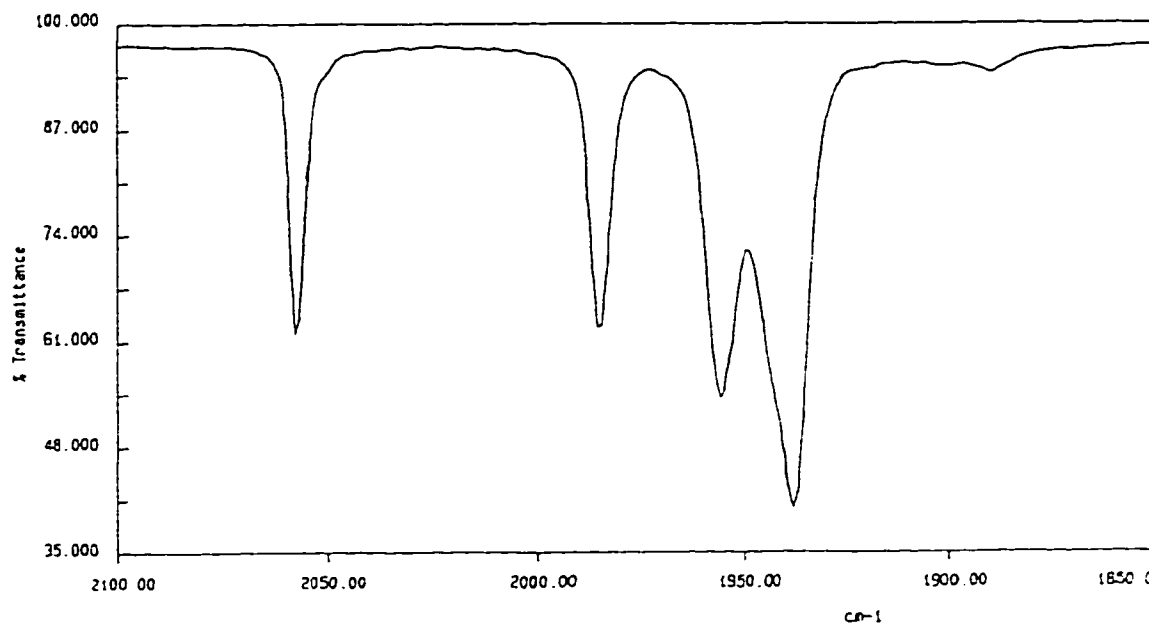
Figure 3-2. IR spectrum of $(CO)_4Fe[P(OPin^i)_3]$, **18**.

C_{3v} point group, depending on the symmetry of the ligand. According to the group theory, tetracarbonyl complexes with strict C_{3v} symmetry possesses three bands in the v_{CO} stretching region ($2A_1 + E$). However, when the substituting ligand has a lower symmetry, which is the case for compounds 10 - 18, the doubly degenerate (E) band will be split into two adjacent absorptions. This is consistent with the four-band pattern observed in the IR spectra of 10 - 18. If the complex is equatorially substituted (Figure 3-3), which occurs when an π-ligand, such as an olefin, is used,[76] the molecule belongs to the C_{2v} point group, in which the four carbonyl groups should also display a four-band pattern ($2A_1 + B_1 + B_2$) in the v_{CO} region of the IR spectrum. To differentiate the IR spectra of the C_{3v} and C_{2v} species, detailed calculations of the intensities of each band have been reported by Darensbourg and co-workers, and the results show that the intensity ratios between the two A_1 bands (the two bands at higher energy) are about 1 and 0.5 for the C_{3v} and C_{2v} systems, respectively.[77] This further indicates that compounds 10 - 18 are axially substituted, as the ratio of the intensities of the two A_1 absorptions in the IR spectra of 10 - 18 are all about unity.
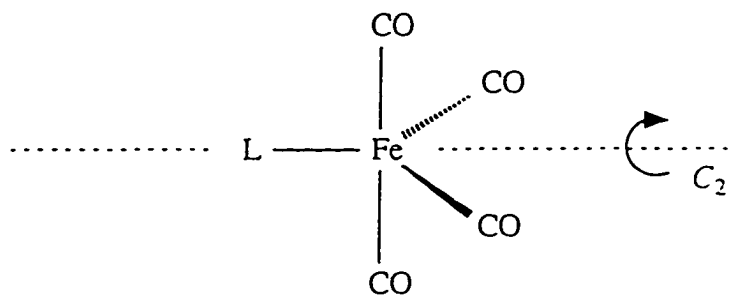
Figure 3-3. Equatorially substituted tetracarbonyliron.

Among the four CO stretching bands observed in each IR spectrum of 10 - 18, the frequencies of the three absorptions below 2000 cm^{-1} are shifted to lower energy in comparison with those in the IR spectrum of $Fe(CO)_5$, whose two CO stretching bands are located at 2022, 2000 cm^{-1}.[78] This is ascribed to the fact that the phosphorus

ligands used to replace the CO groups are better σ-donors and poorer π-acceptors than carbon monoxide. Therefore, electron density on the iron centre in compounds 10 - 18 is higher than that in $Fe(CO)_5$, so that excess electron density can be delocalized into the antibonding orbitals of the CO groups. Thus, the bond strength is weakened and the CO stretching frequencies are shifted to lower energy. By contrast, the A_1 band at highest energy in each IR spectrum (10 - 18) is shifted to a higher frequency than that of $Fe(CO)_5$. This may be due to the lack of *trans* CO vibrational coupling, which exists

Table 3-1. $^{31}P\{^1H\}$ NMR coordination shifts[a] (Δ δP_{c-l}) for compounds 10 - 18.

Compound		δ $P_{com.}$ ppm	δ $P_{lig.}$ ppm	Δ δP_{c-l} ppm
$(CO)_4Fe[P(OMen)Ph_2]$,	10	164.1	107.3	56.8
$(CO)_4Fe[P(OBor)Ph_2]$,	11	167.9	110.6	57.3
$(CO)_4Fe[P(OPin^i)Ph_2]$,	12	167.9	109.9	58.0
$(CO)_4Fe[P(OMen)_2Ph]$,	13	188.1	160.1	28.0
$(CO)_4Fe[P(OBor)_2Ph]$,	14	197.4	157.9	39.5
$(CO)_4Fe[P(OPin^i)_2Ph]$,	15	194.0	158.4	35.6
$(CO)_4Fe[P(OMen)_3]$,	16	163.7	147.5	16.2
$(CO)_4Fe[P(OBor)_3]$,	17	173.6	143.5	30.1
$(CO)_4Fe[P(OPin^i)_3]$,	18	169.4	142.8	26.6

[a] Chemical shifts are given in δ(ppm) relative to external 85% phosphoric acid solution. All spectra were recorded in $CDCl_3$ solution.

in Fe(CO)$_5$.[79]

Like those of the free ligands, the ^{31}P{^{1}H} NMR spectra of 10 - 18 are very simple. Each spectrum consists of one resonance, since there is only one phosphorus atom in each molecule. The coordination shift, $\Delta\delta$, which is the chemical shift difference between the coordinated and free ligands, is positive for each of 10 - 18, $i.e.$ the chemical shift of the resonance in each spectrum is shifted downfield from corresponding free ligand (Table 3-1), presumably due to an increase of electron occupation of the phosphorus d_π orbitals upon coordination.[80]

The ^{13}C{^{1}H} NMR spectra of the mono-substituted iron complexes (compounds 10 - 18) are quite complex. The spectrum of Fe(CO)$_4$[P(OBor)$_2$Ph] is presented as an example in Figure 3-4. A common feature for all ^{13}C{^{1}H} NMR spectra of 10 - 18 is that in the region above 200 ppm, every spectrum shows one doublet at about 213 ppm, due to the carbon nuclei in the carbonyl groups coupling to the phosphorus atom ($^2J_{CP}$ is about 20 Hz). Although the four carbonyl groups are not all symmetry-related, since in the axially substituted trigonal bipyramidal structure one carbonyl group occupies the remaining axial position and the other three hold the equatorial sites, only one averaged signal is observed due to the rapid interchange among the four carbonyl groups via the pseudo rotation mechanism for five-coordinate species, as mentioned earlier.

The ^{13}C{^{1}H} NMR spectra of the mono-substituted iron phosphinites complexes (compounds 10 - 12) can be divided into three distinct regions of interest: the carbonyl region, the aromatic region and the alkyl region. The carbonyl region consists of the doublet mentioned above. The aromatic region (120 - 145 ppm) is predicted to show 12 resonances due to the twelve different carbon atoms in the two phenyl groups. However, due to signal overlapping and coupling to the phosphorus nuclei, complicated patterns and different numbers of resonances are observed for each complex. The alkyl region (10 - 90 ppm) exhibits ten resonances, due to the chiral C$_{10}$ alkoxy groups. The most
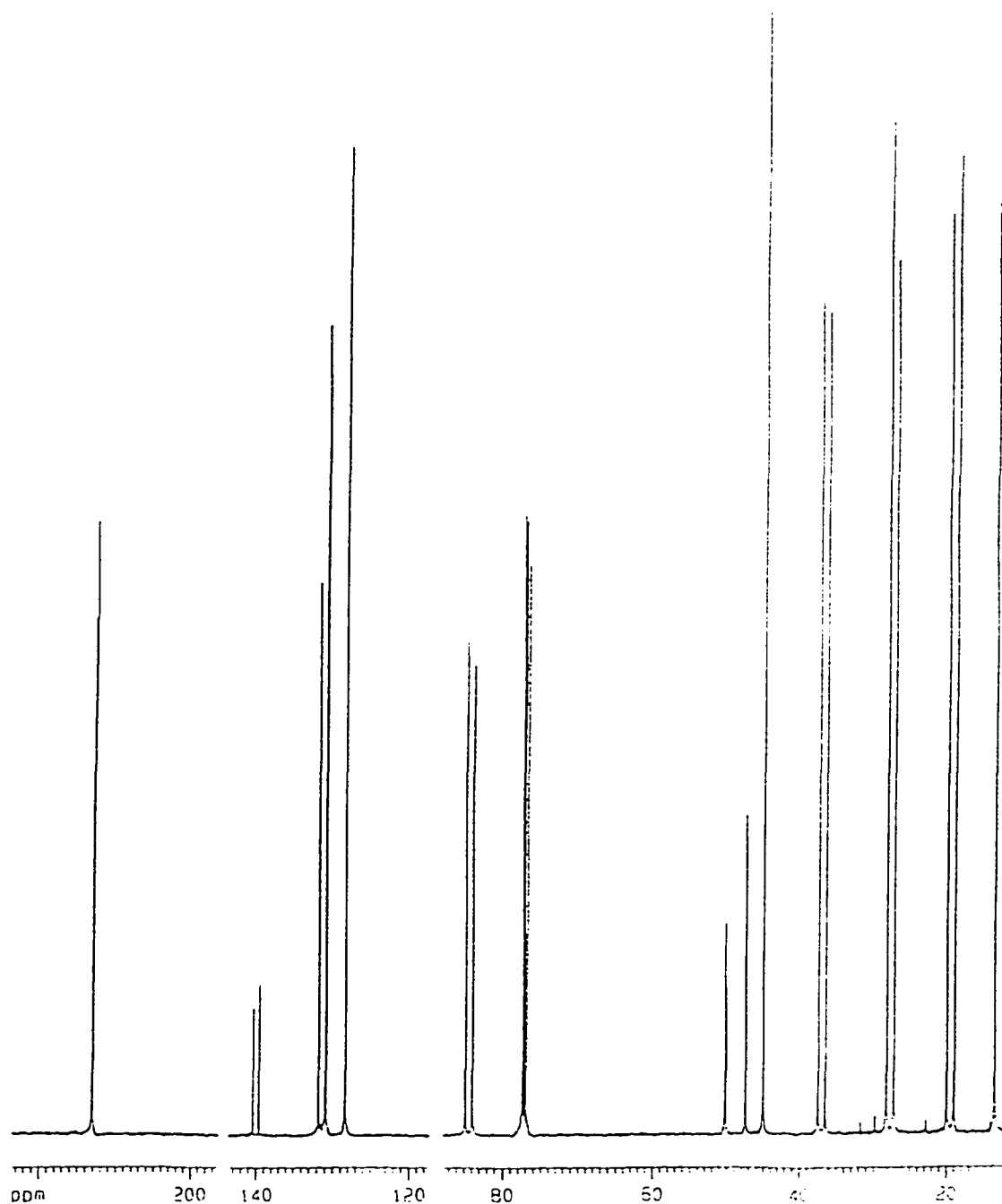
Figure 3-4. $^{13}C\{^1H\}$ NMR spectrum of $Fe(CO)_4[P(OBor)_2Ph]$, 14.

downfield peak in this region is a doublet at about 80 ppm due to the α-carbon atom, the splitting being caused by phosphorus coupling, with a two-bond coupling constant of about 4 Hz. This peak is shifted upfield by about 2 ppm relative to the free ligands

(Table 3-2). This small shift indicates that the coordination of the phosphorus atom to the iron centre has little effect on the electron density at the α-carbon atom in the alkoxy group.

The spectra of the phosphonite complexes (compounds 13 - 15) can be similarly divided into three regions. The carbonyl region again consists of only one averaged doublet at about 213 ppm. The aromatic region (120 - 145 ppm) is simplified because there is only one phenyl group in every phosphonite ligand. However, the alkyl region

Table 3-2. $^{13}C\{^1H\}$ NMR data[a] for mono-substituted iron complexes and their corresponding ligands.

Compound		$\delta~\underline{C}OP_{com.}$ ppm	$\delta~\underline{C}OP_{lig.}$ ppm	$\Delta~\delta\underline{C}OP_{c-l}$ ppm
$(CO)_4Fe[P(OMen)Ph_2]$,	10	79.3	81.3	-2.0
$(CO)_4Fe[P(OBor)Ph_2]$,	11	84.3	86.3	-2.0
$(CO)_4Fe[P(OPin^i)Ph_2]$,	12	78.8	81.3	-2.5
$(CO)_4Fe[P(OMen)_2Ph]$,	13	80.6, 80.4	79.6, 78.9	1.0, 1.5
$(CO)_4Fe[P(OBor)_2Ph]$,	14	84.7, 83.8	84.1, 82.1	0.6, 1.7
$(CO)_4Fe[P(OPin^i)_2Ph]$,	15	79.4, 78.8	78.9, 77.8	0.5, 1.0
$(CO)_4Fe[P(OMen)_3]$,	16	78.7	73.5	5.2
$(CO)_4Fe[P(OBor)_3]$,	17	83.2	77.9	5.3
$(CO)_4Fe[P(OPin^i)_3]$,	18	77.7	72.9	4.8

[a] Chemical shifts are given in δ(ppm) relative to internal $CDCl_3$ with the middle branch of $CDCl_3$ signal set at 77.0 ppm. All spectra were recorded in $CDCl_3$ solution.

(10 - 90 ppm) is much more complicated since there are two magnetically inequivalent alkyl groups in each phosphonite ligand: this arises because the intrinsic chirality of the alkyl groups lowers the symmetry of the molecule. There are therefore twenty signals due to the twenty different carbon atoms. The only peaks that can be easily identified are the two doublets due to the two α-carbon atoms in the two alkoxy groups. They are around 80 ppm and split by the phosphorus atom ($^2J_{PC}$ ranges from 5.4 to 13.3 Hz). These peaks are hardly shifted (Table 3-2) upon coordination, which again implies a very small effect on the electronic environment of the α-carbon atoms.

The spectra of the phosphite complexes (compounds 16 - 18) are less complex. Besides the doublet at around 213 ppm as the common feature discussed above, there are only ten other peaks in each spectrum in the alkyl region (10 - 85 ppm) due to the three equivalent alkoxy groups, which are rotationally related by the C_3 axis of the molecule. Again, the most easily identified peak is the doublet around 80 ppm due to the α-carbon atom in the alkoxy group coupling to the phosphorus atom ($^2J_{PC}$ is about 7 Hz). These peaks are shifted downfield by about 5 ppm on average upon coordination.

The ^1H NMR spectrum of $Fe(CO)_4[P(OBor)_2Ph]$ is shown in Figure 3-5 as an example for compounds 10 - 18. The resolution of these spectra is lower than that of the ^1H NMR spectra of the free ligands. Therefore, the fine coupling patterns are not always resolved. Generally, the spectra of the complexes are similar to those of their corresponding free ligands. The only significant difference is the chemical shifts of the signals due to the α-protons in the alkoxy groups. These peaks are on average shifted downfield by about 0.4 ppm (Table 3-3). This may be because upon coordination, the electron density in the ligand is shifted towards the metal centre, so that the α-protons are deshielded.

Variable temperature $^{31}P\{^1H\}$ and ^1H NMR spectra of 10 - 18 were acquired from -90 °C to ambient temperature to investigate the stereochemistry of these
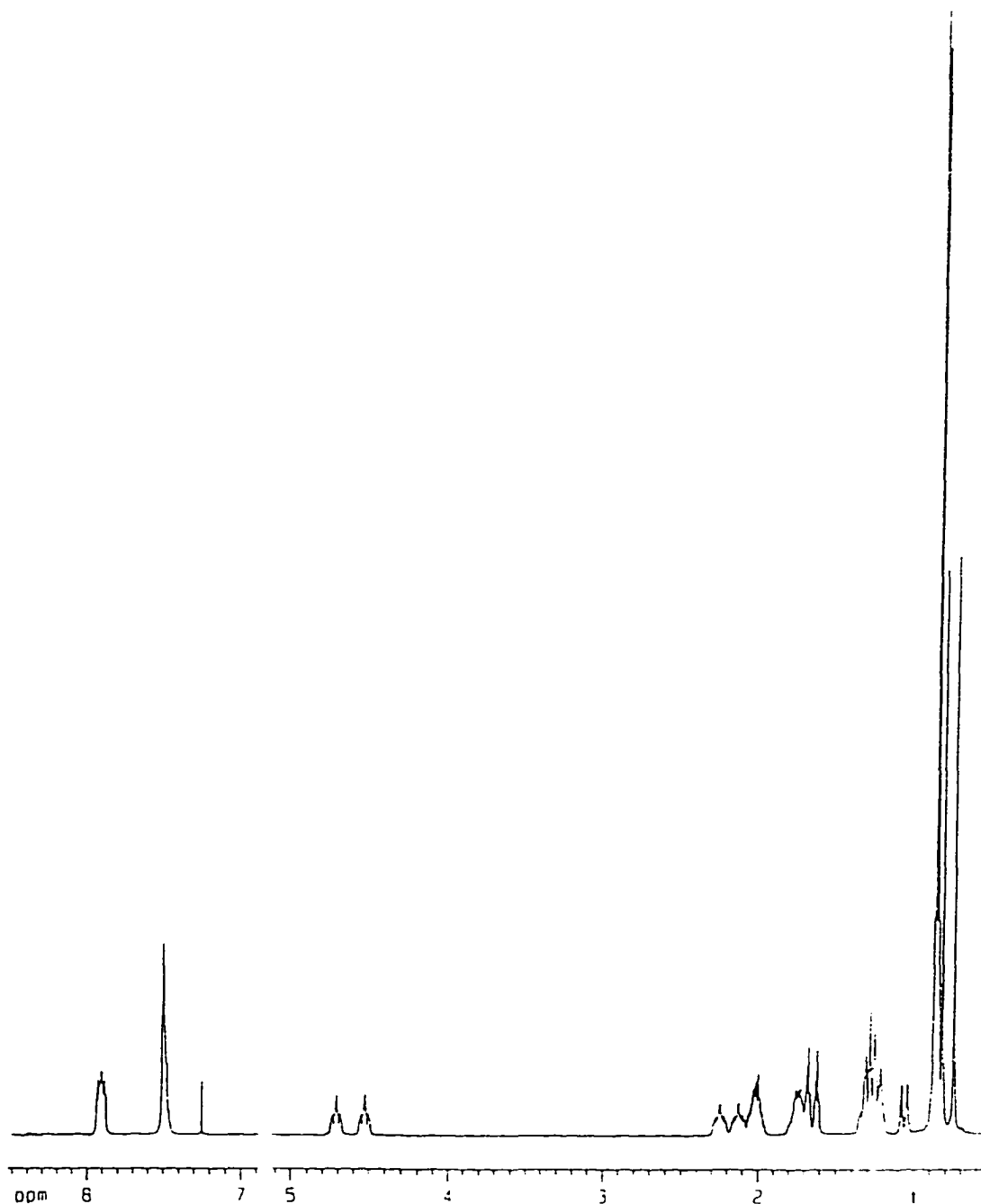
Figure 3-5. ^{1}H NMR spectrum of Fe(CO)$_4$[P(OBor)$_2$Ph], <u>14</u>.

complexes. All spectra show little variation as the temperature decreases except for slight chemical shift displacement (Figure 3-6, V.T. NMR spectra of Fe(CO)$_4$[P(OMen)$_3$]). When the temperature is approaching -90 °C, line broadening is

Table 3-3. ¹H NMR data[a] for mono-substituted iron complexes and their corresponding ligands.

Compound		δ $\underline{H}CO_{com.}$ ppm	δ $\underline{H}CO_{lig.}$ ppm	Δ δ$\underline{H}CO_{c-l}$ ppm
$(CO)_4Fe[P(OMen)Ph_2]$,	10	4.21	3.73	0.48
$(CO)_4Fe[P(OBor)Ph_2]$,	11	4.62	4.26	0.36
$(CO)_4Fe[P(OPin^i)Ph_2]$,	12	4.77	4.31	0.46
$(CO)_4Fe[P(OMen)_2Ph]$,	13	4.37, 3.69	3.80, 3.71	0.57, -0.02
$(CO)_4Fe[P(OBor)_2Ph]$,	14	4.71, 4.52	4.38, 4.18	0.33, 0.34
$(CO)_4Fe[P(OPin^i)_2Ph]$,	15	4.70, 4.66	4.39, 4.31	0.31, 0.35
$(CO)_4Fe[P(OMen)_3]$,	16	4.14	3.72	0.42
$(CO)_4Fe[P(OBor)_3]$,	17	4.61	4.33	0.28
$(CO)_4Fe[P(OPin^i)_3]$,	18	4.74	4.45	0.29

[a] Chemical shifts are given in δ(ppm) relative to internal $CDCl_3$ with residual $CHCl_3$ signal set at 7.24 ppm. All spectra were recorded in $CDCl_3$ solution.

observed, primarily caused by poor resolution due to sample precipitation and increased solvent viscosity induced by the low temperature.

It is well known that even at very low temperatures, the five CO groups in pentacarbonyliron undergo rapid internal exchange (*vide supra*). Similarly, for $Fe(CO)_4L$ complexes, the four carbonyl groups can not be distinguished in the low temperature ¹³C{¹H} NMR spectrum; the only exceptions occur when very bulky ligands are employed. Howell and co-works reported that at -75 °C, the averaged resonances for
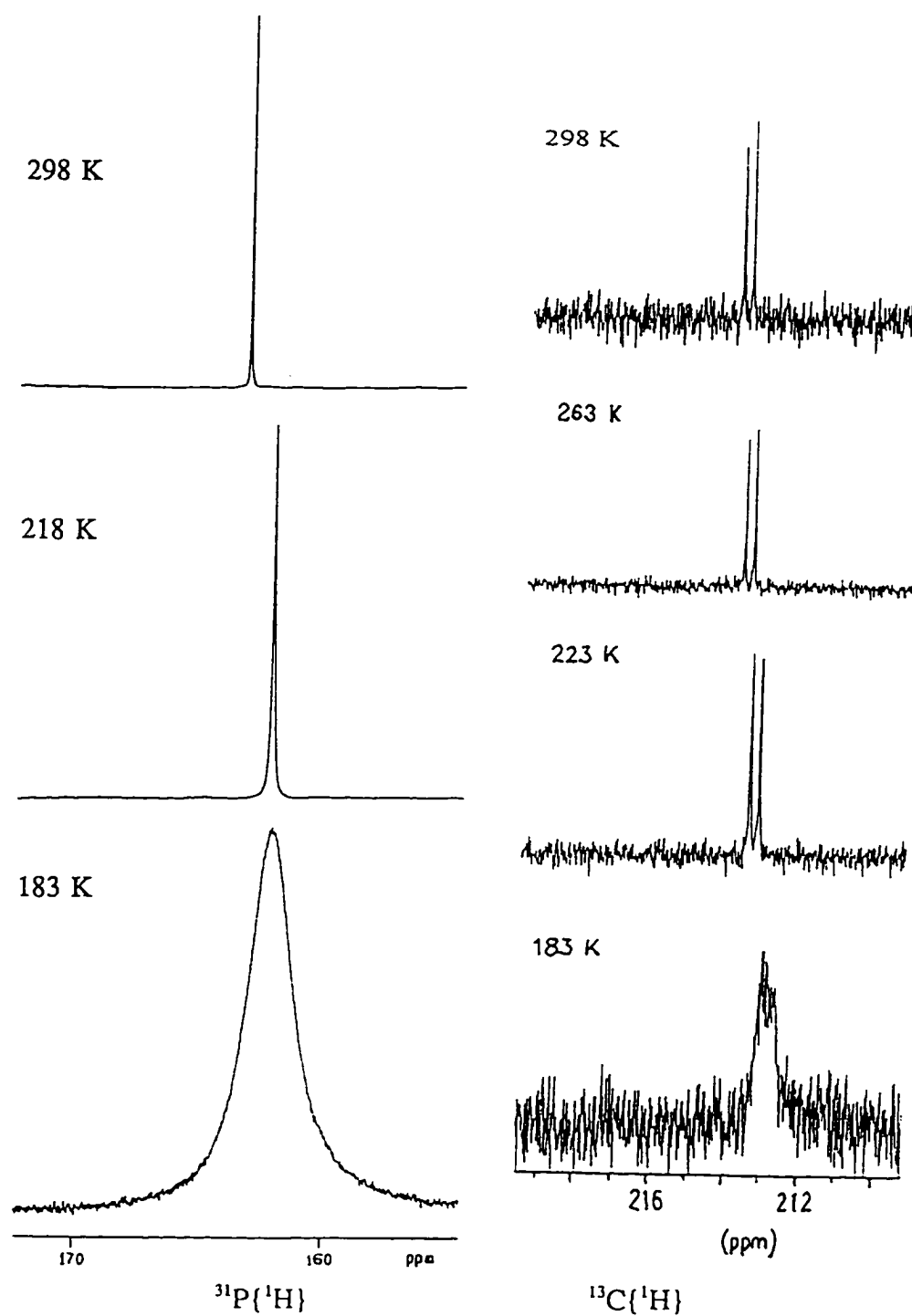
Figure 3-6. V.T. NMR spectra of Fe(CO)$_4$[P(OMen)$_3$], 16.

the carbons in the carbonyls in the $^{13}C\{^1H\}$ NMR spectra of Fe(CO)$_4$[P(o-tolyl)$_3$] and Fe(CO)$_4$[As(o-tolyl)$_3$] are resolved into two doublets, in 1:3 ratio, indicating that pseudo-rotation among the carbonyl groups has been "frozen out".[81] However, a similar limiting low-temperature $^{13}C\{^1H\}$ spectrum for Fe(CO)$_4$[P(o-tolyl)$_2$CH$_2$Ph], where P(o-tolyl)$_2$CH$_2$Ph is only slightly less bulky than P(o-tolyl)$_3$ or As(o-tolyl)$_3$, was not observed. The $^{13}C\{^1H\}$ NMR spectra of compounds 10 - 18 show no sign of resolution at -90 °C, suggesting that the cone angles of ligands 1 - 9 are smaller than those of P(o-tolyl)$_3$ and As(o-tolyl)$_3$ as expected, because (a) phenyl groups are considerably smaller than o-tolyl groups in terms of their contribution to the cone angles of the ligands, and (b) although the alkoxy groups are bulkier than the tolyl groups, the oxygen atom that connects the phosphorus centre and the alkyl groups extend the distance between them and relax the steric tension among the groups attached to the phosphorus centre. Due to the latter reason, it can be predicted that the cone angles of the phosphinites are larger than those of the phosphonites, which in turn are larger than those of the phosphites.

For five-coordinate iron carbonyl complexes, the molecules seldom adopt structures other than trigonal bipyramid unless chelating substituting ligands are involved. The site preference of the substituting ligands in compounds of the type Fe(CO)$_4$(L) has been extensively studied, and the results show that both steric and electronic properties of the ligands should be taken into consideration. For steric reasons, the substituting ligands will occupy the site that generates the least intramolecular repulsion. Although the equatorial positions are believed to be more hindered than the axial positions in five-coordinate complexes for ER$_3$ ligands because they can adopt a configuration that is completely staggered with respect to the carbonyls,[82] the fact that extremely bulky ligands, such as PPh(PPh$_2$)$_2$,[83] or P[C(SiMe$_3$)$_2$][N(SiMe$_3$)$_2$],[84] prefer the equatorial sites indicates otherwise. However, the steric control of the ligands is

effective only for exceptionally large ligands. Even P(t-Bu)$_3$, which has a cone angle[45] of 182°, adopts an axial position in Fe(CO)$_4$ in the solid state,[85] as a result of the electronic effect (*vide infra*). Therefore, the stereochemistry of Fe(CO)$_4$L complexes depends more on the electronic properties of the substituting ligands, when they are of normal bulk (*i.e.* with smaller cone angles than that of P(t-Bu)$_3$, which is true for the majority of tertiary phosphorus ligands, including compounds 1 - 9). Electronically, it is usually assumed that in five-coordinate complexes, the ligand (such as the olefins, or PF$_3$) with better π-accepting abilities than CO adopts the equatorial position.[86] While this is proven true in many cases, the σ-donor properties of the ligands should also be taken into consideration. Theoretical calculations show that for d^8 species such as these iron(0) complexes, the stronger σ-donor would prefer the axial position, or conversely, the weaker σ-donor would favour the equatorial site.[87] This provides the basis for rationalization of the existence of equatorially substituted Ru(CO)$_4$(SbPh$_3$)[88] and Os(CO)$_4$(SbPh$_3$)[89], where SbPh$_3$ is considered as a poorer σ-donor than carbon monoxide.

As evidenced by the IR and NMR spectra of 10 - 18, the common axially substituted trigonal bipyramidal structure is adopted by these complexes, which indicates that compounds 1 - 9 are good ligands with comparable steric and electronic properties to most of the tertiary phosphorus ligands, such as PPh$_3$.

3.C. Di-substituted Iron Carbonyl Complexes

The Di-substituted tricarbonyliron(0) complexes containing chiral phosphinite, phosphonite and phosphite ligands (compounds 1 - 9) were synthesized by the reaction of phosphorus ligands with K[FeH(CO)$_4$], which was generated by the reaction of Fe(CO)$_5$ with KOH and reacted *in situ* (Equations 3-4, and 3-5).[90]

$$Fe(CO)_5 + 2KOH \xrightarrow{EtOH} K[FeH(CO)_4] + KHCO_3 \qquad (3-4)$$

$$K[FeH(CO)_4] + 2PPh_{3-n}(OR)_n + EtOH \xrightarrow{EtOH} Fe(CO)_3[PPh_{3-n}(OR)_n]_2 + CO + H_2 + KOEt$$

$$\text{Compounds } \underline{19} - \underline{27} \qquad (3-5)$$
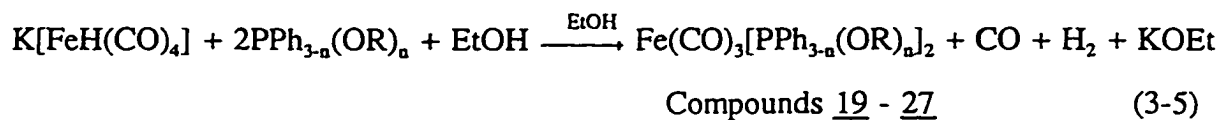
Compound $\underline{19}$:	R = Men,	n = 1;	Compound $\underline{23}$:	R = Bor,	n = 2;
$\underline{20}$:	Bor,	1;	$\underline{24}$:	Pin^i,	2;
$\underline{21}$:	Pin^i,	1;	$\underline{25}$:	Men,	3;
$\underline{22}$:	Men,	2;	$\underline{26}$:	Bor,	3;
			$\underline{27}$:	Pin^i,	3.

Direct one-step synthetic methods for $Fe(CO)_3L_2$, where L is a phosphine ligand, have also been previously reported. However, these methods, including both thermal[91] or photochemical[92] reactions, not only produce the desired products in fairly low yields, but also are accompanied with separation difficulties of the unreacted phosphines and the mono-substituted complexes from the di-substituted products. Two other methods using reducing agents $Li(AlH_4)$[93] or $Na(BH_4)$[94] afford fair to high yields, but they demand either long reaction time or excess phosphines. The present preparative method generates the di-substituted complexes via $K[FeH(CO)_4]$, from which several other important organoiron complexes such as $FeH_2(CO)_2[P(OR)_3]_2$, where R = Me, Et, or Ph, can be obtained.[95] The advantages of this route is that only stoichiometric amounts of phosphorus ligands are required, the reaction rate is relatively fast, and the product is free from mono-substituted analogues.

Compounds $\underline{19}$ - $\underline{27}$ are yellow or orange solids. The yields for these compounds vary from 50% to 90% depending on the ligand. These products can be dissolved in most common organic solvents, with better solubility in polar solvents. In the solid state, they are stable in air. In solution, however, they decompose slowly when exposed to
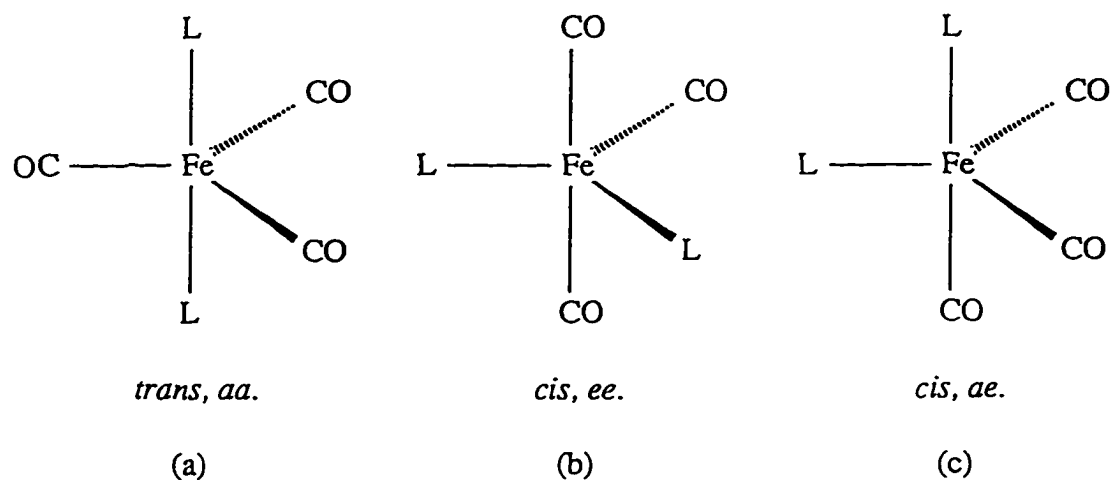
Figure 3-7. Structures of di-substituted iron carbonyls.

atmospheric oxygen.

For di-substituted five-coordinate carbonyl complexes, there are three possible structures, *i.e.* diaxial (*trans, aa.*), diequatorial (*cis, ee.*), and axial equatorial (*cis, ae.*), which belong to D_{3h}, C_{2v}, and C_s point groups, respectively (Figure 3-7). For the two *cis*
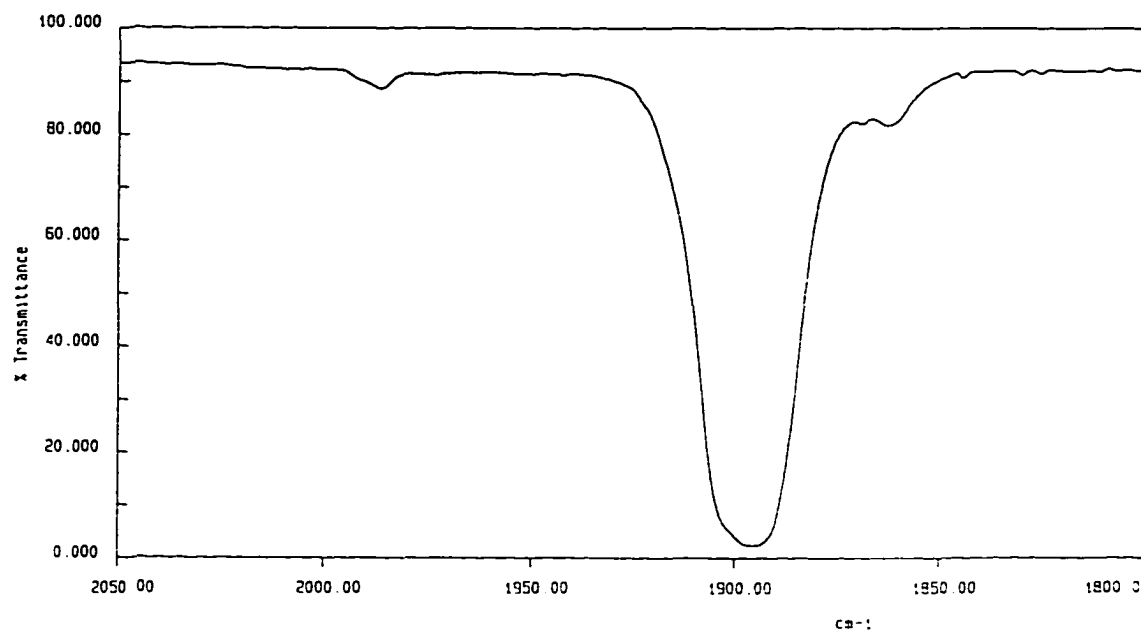
Figure 3-8. IR spectrum of $Fe(CO)_3[P(OBor)_3]_2$, 26.

conformations, three v_{CO} bands ($[2A_1 + B_2]$ for *ee*., and $[2A' + A']$ for *ae*.) are predicted in each IR spectrum, whereas for the *trans* conformation, only one band ($[A' + E']$, but the A' mode is IR inactive) will be generated in the same region. Each IR spectrum of 19 - 27 recorded in hexane solutions has only one strong v_{CO} band, at about 1900 cm^{-1}, as shown in Figure 3-8 for $Fe(CO)_3[P(OBor)_3]_2$. This confirms that compounds 19 - 27 are *trans* di-substituted trigonal bipyramids, which is the expected geometry as discussed in the introduction. The CO stretching frequencies of compounds 19 - 27 are listed in Table 6-10.

The vibrational frequencies of the CO stretching mode of the di-substituted iron complexes are shifted to lower energy compared with those of the mono-substituted compounds. This is accounted for by the increased electron density on the metal center due to further replacement of CO group by another phosphorus ligand. Thus, more electron density is back donated to the anti-bonding orbitals of the carbonyl groups, causing the CO bonds to be further weakened and the CO stretching bands to occur at a lower frequency.

Each $^{31}P\{^1H\}$ NMR spectrum of the di-substituted iron complexes (compounds 19 - 27) consists of one line, indicating the two phosphorus atoms in each complex are equivalent. This is consistent with the results obtained from the IR analysis, since in the *trans* structure identified by IR spectrometry the two phosphorus atoms are equivalent.

Compared with their mono-substituted counterparts, the chemical shifts of 19 - 27 are shifted further downfield (Table 3-4). This may be explained by the increase of electron occupation of the phosphorus d_{π} orbitals because of more electron back donation to phosphorus from the metal centre caused by the increase of electron density at the metal center when the carbonyl group is replaced by the phosphorus ligand, since phosphorus ligands are better σ-donors and worse π-acceptors than carbonyl groups.

Analogous to those of the mono-substituted iron complexes, each $^{13}C\{^1H\}$ NMR

Table 3-4. $^{31}P\{^1H\}$ NMR coordination shifts[a] ($\Delta \delta P_{c-l}$) for compounds 19 - 27.

Compound		$\delta P_{com.}$ ppm	$\delta P_{lig.}$ ppm	$\Delta \delta P_{c-l}$ ppm
$(CO)_3Fe[P(OMen)Ph_2]_2$,	19	171.2	107.3	63.9
$(CO)_3Fe[P(OBor)Ph_2]_2$,	20	175.1	110.6	64.5
$(CO)_3Fe[P(OPin^i)Ph_2]_2$,	21	175.3	109.9	65.4
$(CO)_3Fe[P(OMen)_2Ph]_2$,	22	199.9	160.1	39.8
$(CO)_3Fe[P(OBor)_2Ph]_2$,	23	210.4	157.9	52.5
$(CO)_3Fe[P(OPin^i)_2Ph]_2$,	24	207.4	158.4	49.0
$(CO)_3Fe[P(OMen)_3]_2$,	25	177.9	147.5	30.4
$(CO)_3Fe[P(OBor)_3]_2$,	26	188.9	143.5	45.4
$(CO)_3Fe[P(OPin^i)_3]_2$,	27	184.7	142.8	41.9

[a] Chemical shifts are given in δ(ppm) relative to external 85% phosphoric acid solution. All spectra were recorded in $CDCl_3$ solution.

spectrum of the di-substituted iron complexes (compounds 19 - 27), as represented by the spectrum of $Fe(CO)_3[P(OMen)_2Ph]_2$ in Figure 3-9, can be divided into three parts (two for the phosphite complexes since they do not possess any phenyl groups). The low field part (above 200 ppm) consists of a triplet at about 213 ppm indicating that the three carbonyl groups are equivalent and coupling to two equivalent phosphorus atoms. The coupling constants ($^2J_{PC}$) are about 30, 34, and 39 Hz for the complexes containing the phosphinite, phosphonite, and phosphite ligands, respectively.
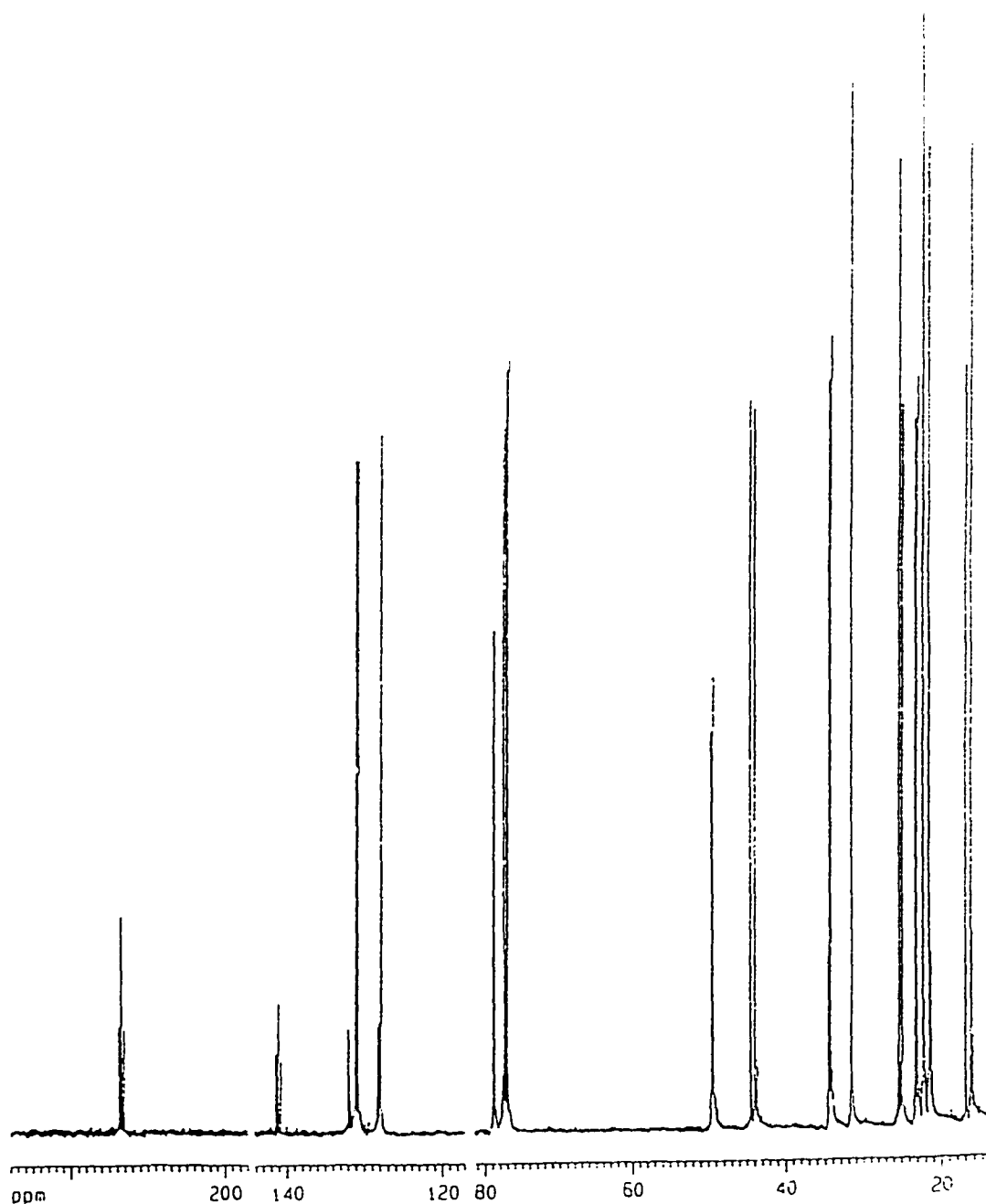
Figure 3-9. $^{13}C\{^1H\}$ NMR spectrum of $Fe(CO)_3[P(OMen)_2Ph]_2$, 22.

The middle part (125 - 145 ppm) of the $^{13}C\{^1H\}$ NMR spectra of the phosphinite

and phosphonite complexes (compounds 19 - 24) is the aromatic region. This region

bears strong resemblance to that in the mono-substituted complexes and is quite complex

since the twelve carbons in the two phenyl groups of the phosphinite ligands or the six carbons in the phenyl group of the phosphonite ligands are all inequivalent. This is further complicated by signal overlapping and the splitting of some of the resonances caused by phosphorus coupling. The resonances cannot be individually assigned due to this complexity.

The high field part of the spectra is the alkyl region between 10 to 85 ppm. This region also shows strong similarity to its counterpart in the mono-substituted complexes.

Table 3-5. $^{13}C\{^1H\}$ NMR data[a] for di-substituted iron complexes and their corresponding ligands.

Compound		$\delta \underline{C}OP_{com.}$ ppm	$\delta \underline{C}OP_{lig.}$ ppm	$\Delta \delta\underline{C}OP_{c-l}$ ppm
$(CO)_3Fe[P(OMen)Ph_2]_2$,	19	77.7	81.3	-3.6
$(CO)_3Fe[P(OBor)Ph_2]_2$,	20	82.9	86.3	-3.4
$(CO)_3Fe[P(OPin^i)Ph_2]_2$,	21	77.4	81.3	-3.9
$(CO)_3Fe[P(OMen)_2Ph]_2$,	22	78.8, 78.7	79.6, 78.9	-0.8, -0.2
$(CO)_3Fe[P(OBor)_2Ph]_2$,	23	83.1, 82.1	84.1, 82.1	-1.0, 0.0
$(CO)_3Fe[P(OPin^i)_2Ph]_2$,	24	77.8, 77.2	78.9, 77.8	-1.1, -0.6
$(CO)_3Fe[P(OMen)_3]_2$,	25	77.3	73.5	3.8
$(CO)_3Fe[P(OBor)_3]_2$,	26	81.6	77.9	3.7
$(CO)_3Fe[P(OPin^i)_3]_2$,	27	76.4	72.9	3.5

[a] Chemical shifts are given in δ(ppm) relative to internal $CDCl_3$ with the middle branch of $CDCl_3$ signal set at 77.0 ppm. All spectra were recorded in $CDCl_3$ solution.

For the phosphinite and phosphite complexes, ten peaks are observed, since the phosphinite ligand has one chiral alkoxy group with ten different carbon atoms while in the phosphite ligand the three alkoxy groups are equivalent due to the C_3 symmetry. The equivalence of the three chiral alkoxy groups in the phosphite complexes provides further evidence to the *trans* structure, because the two *cis* structures in Figure 3-7 do not possess C_3 axes. The peak furthest downfield in this region is, unlike those in the spectra of the mono-substituted complexes, a singlet at about 80 ppm, showing no sign of coupling to the phosphorus atom. This singlet is again assigned to the α-carbon atoms in the alkoxy groups. For the phosphonite complexes, there are twenty peaks in this region, since the twenty carbon atoms in the two alkoxy groups are all inequivalent. Again, the only peaks that can be easily assigned are the two peaks around 80 ppm due to the two α-carbon atoms in the two alkoxy groups. In all di-substituted iron complexes, the α-carbon peaks are hardly shifted upon coordination (Table 3-5), indicating again, that the coordination of the phosphorus to the iron centre has little effect on the electronic environment of the α-carbon atom.

The ^{1}H NMR spectra of the di-substituted iron complexes are analogues to those of the mono-substituted iron complexes as shown by the spectrum of $Fe(CO)_3[P(OPin^i)Ph_2]_2$ in Figure 3-10. Due to rather poor resolution, the lines in these spectra are broadened, and the fine coupling patterns are lost in most cases. The general features of these spectra are similar to those of their corresponding ligands. The signals due to the α-protons in the alkoxy groups are again shifted downfield by about 0.5 ppm from those in the free ligands (Table 3-6), which is a downfield shift by about 0.1 ppm from those of the mono-substituted species.

Each of the variable temperature ^{31}P{^{1}H} NMR spectra of the phosphinite and phosphonite complexes (19 - 24) is resolved into two resonances at -90 °C while those of the phosphite complexes (25 - 27) are not (Figure 3-11, V.T. ^{31}P{^{1}H} NMR spectra
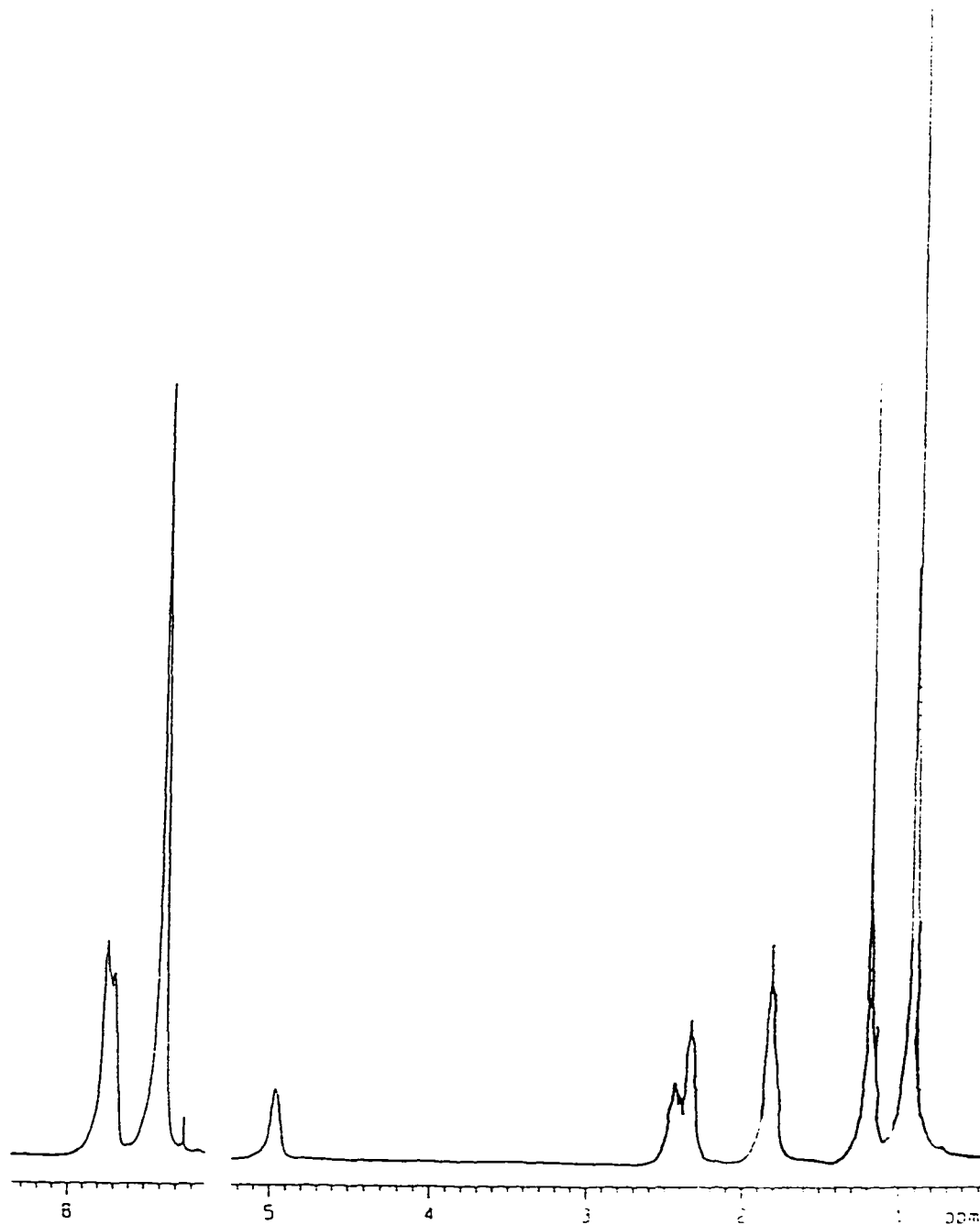
Figure 3-10. ^{1}H NMR spectrum of Fe(CO)$_3$[P(OPin^i)Ph$_2$]$_2$, <u>21</u>.

of Fe(CO)$_3$[P(OBor)$_2$Ph]$_2$ and Fe(CO)$_3$[P(OBor)$_3$]$_2$). The V.T. ^{1}H NMR spectra of these complexes do not show any meaningful features due to the poor resolution at low temperature.

Table 3-6. ^{1}H NMR data[a] for di-substituted iron complexes and their corresponding ligands.

Compound	δ $\underline{H}CO_{com.}$ ppm	δ $\underline{H}CO_{lig.}$ ppm	Δ $\delta\underline{H}CO_{c-l}$ ppm
$(CO)_3Fe[P(OMen)Ph_2]_2$, 19	4.36	3.73	0.63
$(CO)_3Fe[P(OBor)Ph_2]_2$, 20	4.82	4.26	0.56
$(CO)_3Fe[P(OPin^i)Ph_2]_2$, 21	4.96	4.31	0.65
$(CO)_3Fe[P(OMen)_2Ph]_2$, 22	4.46, 3.84	3.80, 3.71	0.66, 0.13
$(CO)_3Fe[P(OBor)_2Ph]_2$, 23	4.83, 4.66	4.38, 4.18	0.45, 0.48
$(CO)_3Fe[P(OPin^i)_2Ph]_2$, 24	4.93, 4.74	4.39, 4.31	0.54, 0.43
$(CO)_3Fe[P(OMen)_3]_2$, 25	4.18	3.72	0.46
$(CO)_3Fe[P(OBor)_3]_2$, 26	4.62	4.33	0.29
$(CO)_3Fe[P(OPin^i)_3]_2$, 27	4.81	4.45	0.36

[a] Chemical shifts are given in δ(ppm) relative to internal $CDCl_3$ with $CHCl_3$ signal set at 7.24 ppm. All spectra were recorded in $CDCl_3$ solution.

For complexes $Fe(CO)_4L$, where L = $P(o\text{-tolyl})_3$, $As(o\text{-tolyl})_3$, or $P(o\text{-tolyl})_2CH_2Ph$, the two resolved resonances in each of their $^{31}P\{^1H\}$ NMR spectra at low temperatures were assigned to the exo_3 and exo_2 isomers, respectively (Figure 3-12).[81] The resolution of the conformational isomers of the ligands, however, are not likely to be the reason for the limiting low-temperature spectra for complexes 19 - 24, since no similar resolution was observed for their corresponding mono-substituted complexes (10 - 15). Thus, the two resonances in each of the low-temperature $^{31}P\{^1H\}$ NMR spectrum

298 K

233 K

183 K

Fe(CO)$_3$[P(OBor)$_2$Ph]$_2$, <u>23</u>   Fe(CO)$_3$[P(OBor)$_3$]$_2$, <u>26</u>
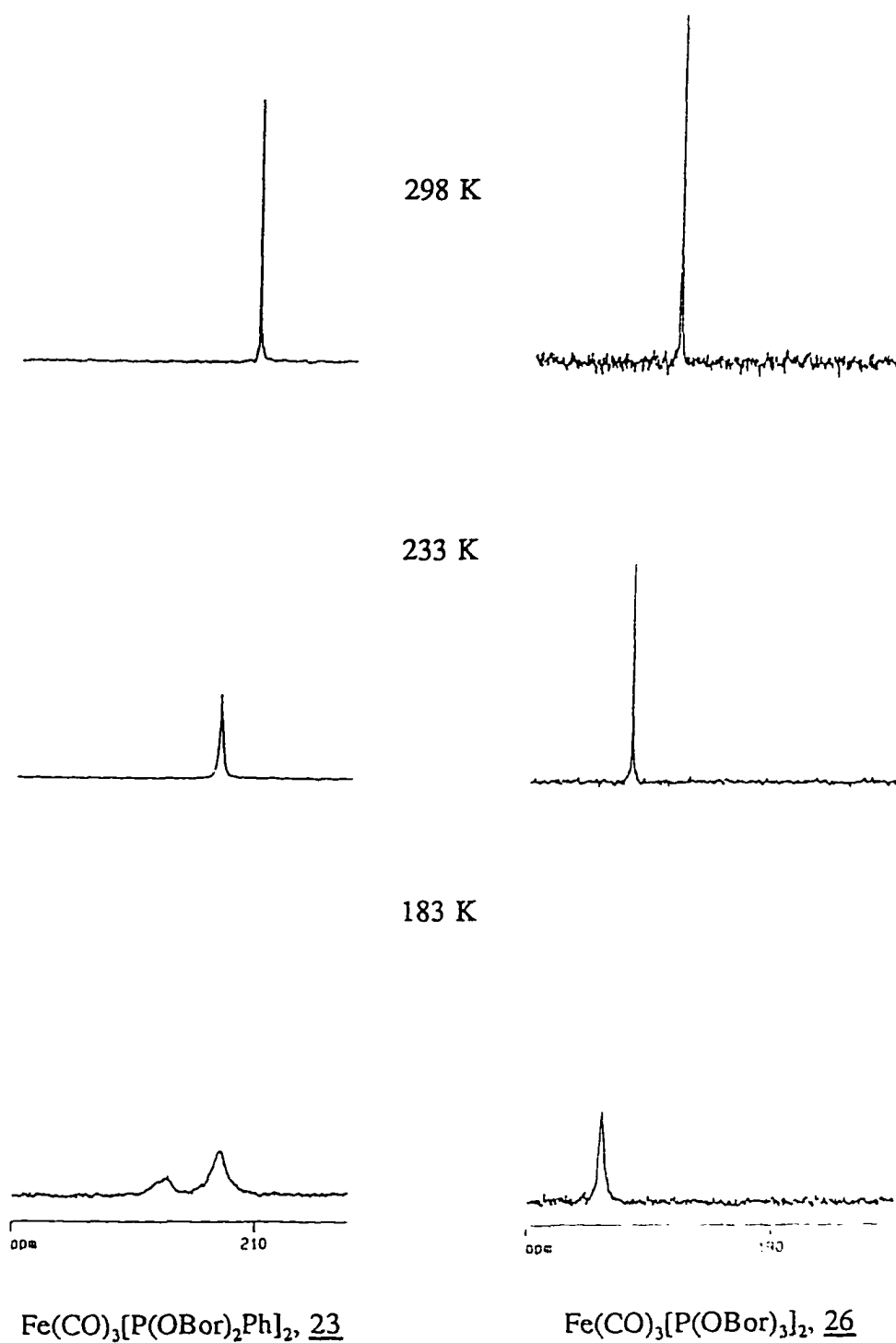
Figure 3-11. V.T. ^{31}P{^{1}H} NMR spectra of compounds <u>23</u> and <u>26</u>.

of 19 - 24 are assigned to the staggered (major) and eclipsed (minor) isomers, respectively (Figure 3-13).

exo₃   exo₂
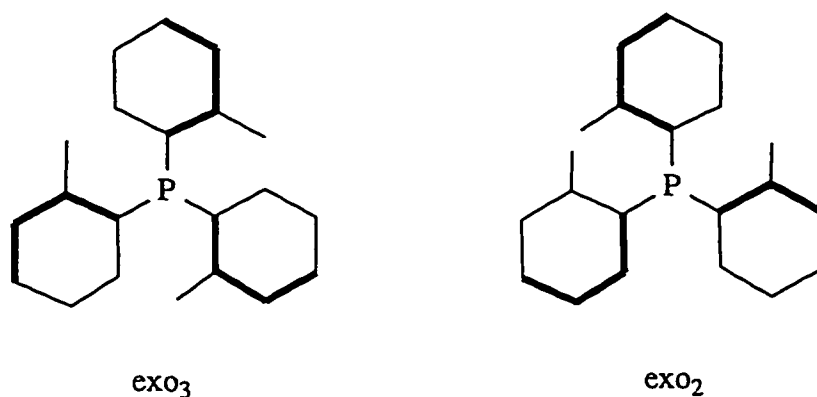
Figure 3-12. Conformational isomers of P(o-tolyl)$_3$.

staggered   eclipsed
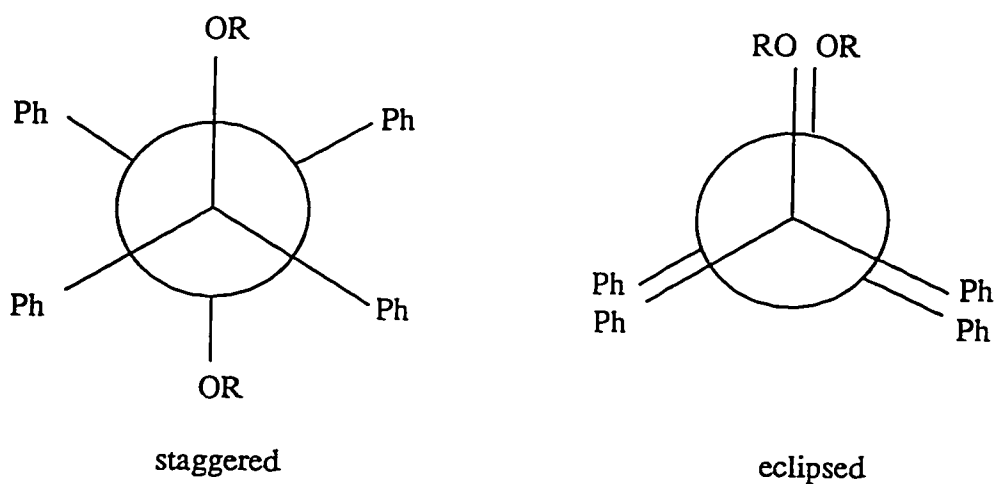
R = Men, Bor, or Pin^i

Figure 3-13. Conformational isomers of compounds 19 - 21.

The fact that the $^{31}P\{^1H\}$ NMR spectra of the phosphite complexes are not resolved at -90 °C indicate that the cone angles of the phosphite ligands are smaller than those of the phosphonite and phosphinite ligands. This is as expected for the

reasons discussed in the previous section.

The site preference of the ligands in $Fe(CO)_3L_2$ species also depends on the electronic and steric properties of the ligands. The arguments applied to the mono-substituted systems are still valid for the di-substituted species. Since they are weaker π-acceptors and stronger σ-donors than CO, normal tertiary phosphorus ligands prefer the axial positions. Thus, most structurally characterized di-substituted tricarbonyliron complexes have a *trans* geometry. Even when the two phosphorus donors are part of the same chelating ligand, they would still occupy the axial position if the spacing between the two phosphorus atoms is large enough.[96] Only when the two phosphorus donors are restrained within a short distance in a chelating ligand, would a *cis* isomer be formed as the stable product, whose trigonal bipyramidal structures are usually very distorted.[97,98]

3.D. Cobalt Carbonyl Dimers

Synthetic methods for di-substituted cobalt(0) carbonyl dimers containing phosphorus ligands include the direct reaction between the ligands and $Co_2(CO)_8$ in

$$Co_2(CO)_8 + 2PPh_{3-n}(OR)_n \xrightarrow{\text{benzene}} Co_2(CO)_6[PPh_{3-n}(OR)_n]_2 + 2CO$$

Compounds <u>28</u> - <u>36</u>   (3-6)
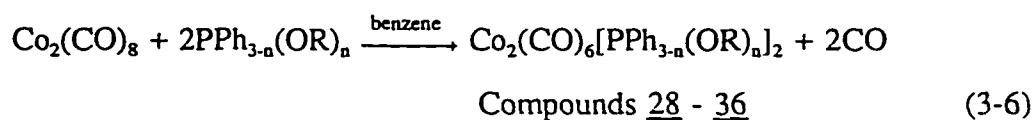
Compound <u>28</u>:	R = Men,	n = 1;	Compound <u>32</u>:	R = Bor,	n = 2;
<u>29</u>:	Bor,	1;	<u>33</u>:	Pin^i,	2;
<u>30</u>:	Pin^i,	1;	<u>34</u>:	Men,	3;
<u>31</u>:	Men,	2;	<u>35</u>:	Bor,	3;
			<u>36</u>:	Pin^i,	3.

nonpolar solvents at elevated temperature,[99] the high pressure reaction using cobalt metal, the ligands, and carbon monoxide gas,[100] and the reverse reaction of the disproportionated products, $[Co(CO)_{5-x}L_x][Co(CO)_4]$, under heat, among which the first route is most convenient, and it is the procedure used to synthesize hexacarbonyldicobalt(0) complexes with the chiral phosphorus ligands (ligands 1 - 9) (Equation 3-6).

Complexes 28 - 36 were prepared as deep orange solids in 50% to 90% yields. These compounds are soluble in most common organic solvents, exhibiting increased solubility in polar solvents. The solid products showed no indication of decomposition in air over a few months, while in solution, they decompose slowly when exposed to air.

Each of the IR spectra of 28 - 36 in hexane solutions shows four carbonyl stretching bands, at around 1935 (w.), 1965 (st.), 1982 (m. st., sh.), and 2042 (w,) cm^{-1}, as shown in the spectrum of $Co_2(CO)_6[P(OMen)Ph_2]_2$ in Figure 3-14. No absorptions in the range of bridging CO stretching frequencies (1700 - 1900 cm^{-1}) are observed, which
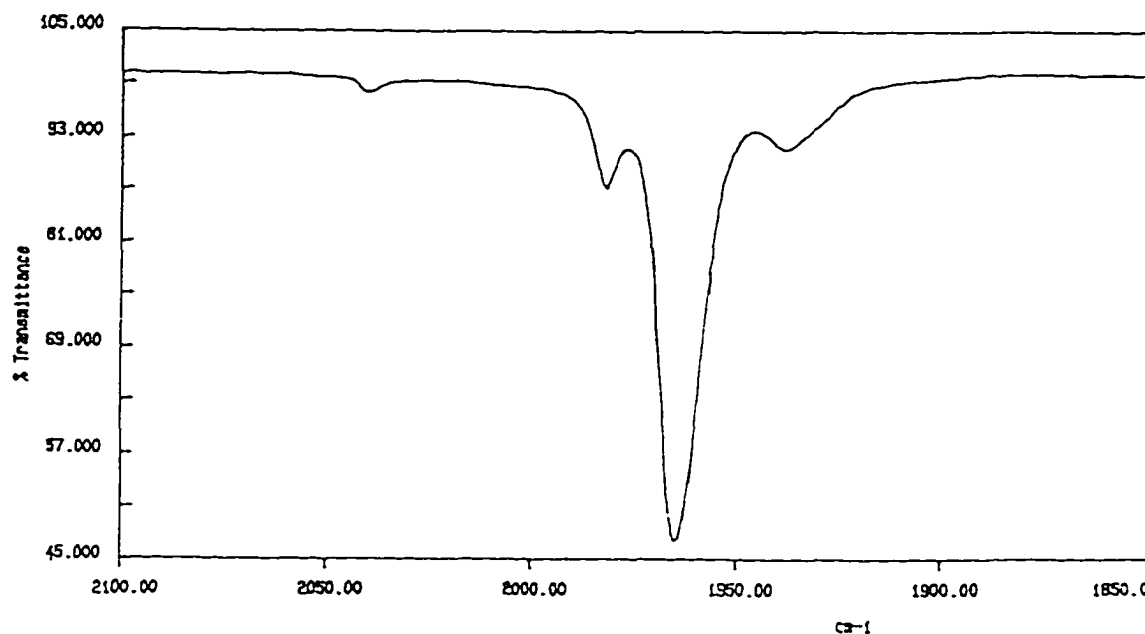
Figure 3-14. IR spectrum of $Co_2(CO)_6[P(OMen)Ph_2]_2$, 28.

indicates that no isomers with bridging carbonyl groups are present in solution at ambient temperature. As mentioned in the introduction, the expected structure for bis-phosphorus substituted cobalt carbonyl dimers is the one in which the local geometry of each cobalt centre is trigonal bipyramidal, and the P-Co-Co-P array is coincidental with the C_3 axis of the molecule. There are two possible forms of this structure, *i.e.* staggered and eclipsed (Figure 3-15, (a) and (b)), belonging to the D_{3d} and D_{3h} point groups, respectively. Either of the two structures will produce two CO stretching bands. For the staggered structure, they are $A_{2u} + E_u$, with the other two stretching modes, $A_{1g} + E_g$, being IR inactive, while for the eclipsed one, $A_2'' + E'$ are the IR active modes, and the $A_1' + E''$ are IR inactive. Due to the similarity, the two conformations cannot be distinguished by their IR spectra, although the staggered one is considered as more probable since steric interactions between the two sets of radial carbonyl groups in this structure would be reduced to a minimum.[101] The IR spectra of 28 - 36 are compatible with this conformation because the two stronger bands, at around 1965 and 1982 cm⁻¹, can be assigned to E_g and A_{1g} modes, respectively;[102] the other two weak bands at about 2042 and 1935 cm⁻¹ may be caused by A_{1g} and E_g modes. Although forbidden by the selection rules, the latter two absorptions are visible probably because the chiral

Staggered, D_{3d} Eclipsed, D_{3h}

(a)   (b)
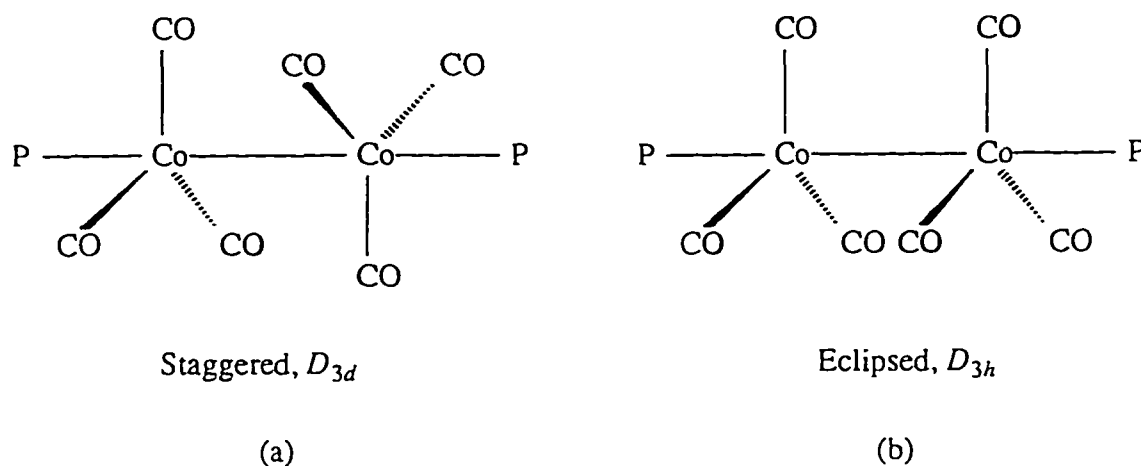
Figure 3-15. The staggered and eclipsed conformations of $Co_2(CO)_6P_2$.

ligands in these complexes violate perfect D_{3d} symmetry in these molecules.

The frequencies of v_{CO} bands in the IR spectra of 28 - 36 are lower than those of $Co_2(CO)_8$ (2069, 2031, and 2022 cm^{-1}),[103] again due to increased electron back donation from cobalt to the CO antibonding molecular orbital, caused by phosphorus substitution of CO group since phosphorus is a stronger σ-donor and poorer π-acceptor than CO.

Only one peak is found in each $^{31}P\{^1H\}$ NMR spectrum of compounds 28 - 36,

Table 3-7. $^{31}P\{^1H\}$ NMR coordination shifts[a] (Δ δP$_{c-l}$) for cobalt dimers.

Compound	δ P$_{com.}$ ppm	δ P$_{lig.}$ ppm	Δ δP$_{c-l}$ ppm
{(CO)$_3$Co[P(OMen)Ph$_2$]}$_2$, 28	160.8	107.3	53.5
{(CO)$_3$Co[P(OBor)Ph$_2$]}$_2$, 29	164.8	110.6	54.2
{(CO)$_3$Co[P(OPin^i)Ph$_2$]}$_2$, 30	165.2	109.9	55.3
{(CO)$_3$Co[P(OMen)$_2$Ph]}$_2$, 31	187.4	160.1	27.3
{(CO)$_3$Co[P(OBor)$_2$Ph]}$_2$, 32	196.1	157.9	38.2
{(CO)$_3$Co[P(OPin^i)$_2$Ph]}$_2$, 33	193.5	158.4	35.1
{(CO)$_3$Co[P(OMen)$_3$]}$_2$, 34	159.8	147.5	12.3
{(CO)$_3$Co[P(OBor)$_3$]}$_2$, 35	171.1	143.5	41.0
{(CO)$_3$Co[P(OPin^i)$_3$]}$_2$, 36	167.7	142.8	24.9

[a] Chemical shifts are given in δ(ppm) relative to external 85% phosphoric acid solution. All spectra were recorded in CDCl$_3$ solution.

since the two phosphorus atoms in each molecule are related with each other by C_2 symmetry. The chemical shifts of all resonances are shifted downfield from corresponding free ligands (Table 3-7). The coordination shifts are comparable to those
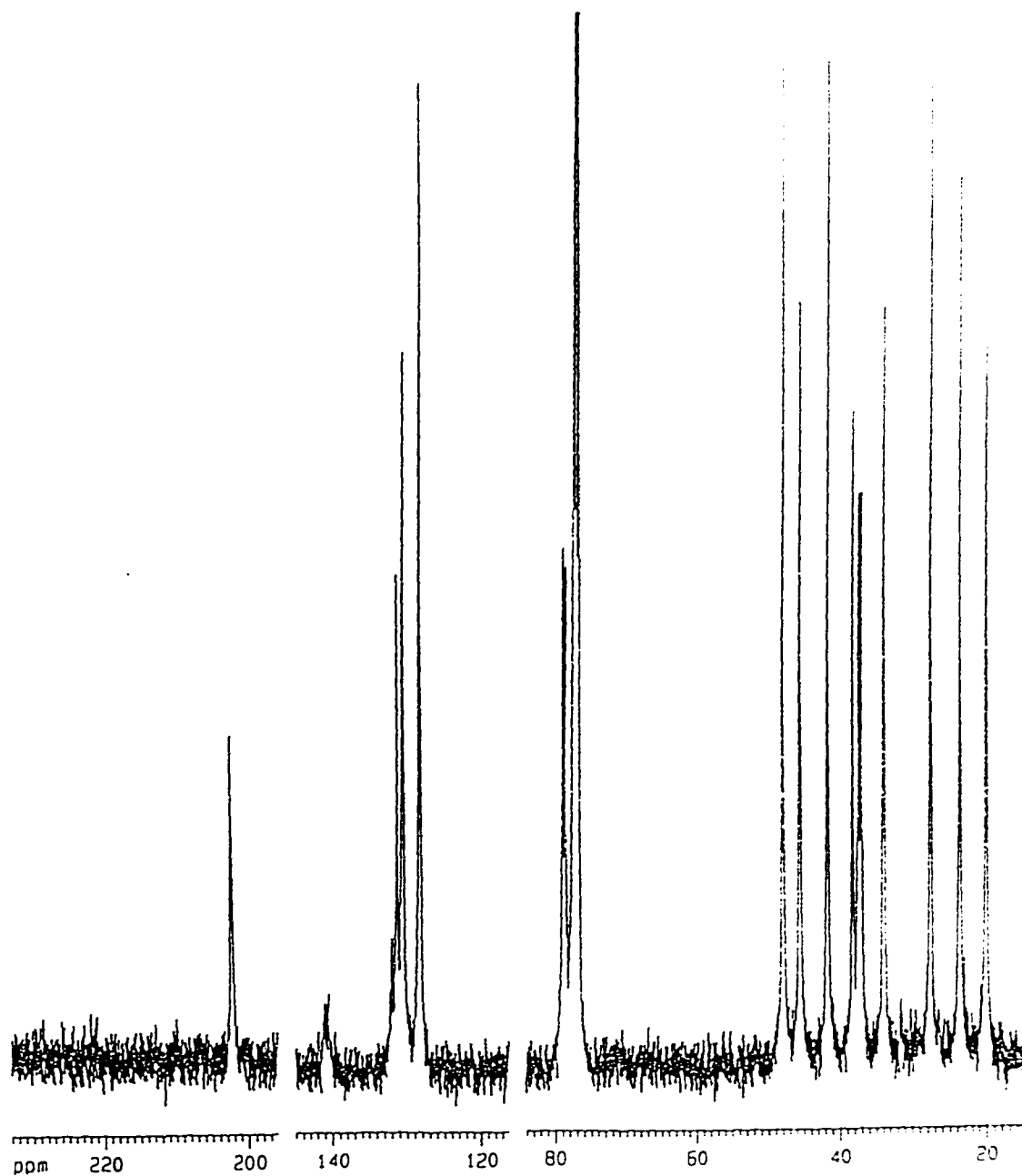
Figure 3-16. $^{13}C\{^1H\}$ NMR spectrum of $\{Co(CO)_3[P(OPin')_2Ph]\}_2$, 33.

for compounds 10 - 18, which suggests that the reason of the downfield shifts is same as those for the substituted iron carbonyl compounds (10 - 27) discussed before.

The $^{13}C\{^1H\}$ NMR spectra of 28 - 36 are rather similar to those of the di-substituted iron carbonyl complexes. The spectrum of $\{Co(CO)_3[P(OPin^i)_2Ph]\}_2$ is presented as an example in Figure 3-16. Once more, the spectra can be divided into three parts, i.e., the carbonyl region (above 200 ppm), the aromatic region (125 - 145 ppm), and the alkyl region (10 - 85 ppm).

Table 3-8. $^{13}C\{^1H\}$ NMR data[a] for cobalt dimers and their corresponding ligands.

Compound	$\delta\ \underline{C}OP_{com.}$ ppm	$\delta\ \underline{C}OP_{lig.}$ ppm	$\Delta\ \delta\underline{C}OP_{c\text{-}l}$ ppm
$\{(CO)_3Co[P(OMen)Ph_2]\}_2$ 28	79.3	81.3	-2.0
$\{(CO)_3Co[P(OBor)Ph_2]\}_2$ 29	84.5	86.3	-1.8
$\{(CO)_3Co[P(OPin^i)Ph_2]\}_2$ 30	79.1	81.3	-2.2
$\{(CO)_3Co[P(OMen)_2Ph]\}_2$ 31	79.9, 79.6	79.6, 78.9	0.3, 0.7
$\{(CO)_3Co[P(OBor)_2Ph]\}_2$ 32	84.3, 83.0	84.1, 82.1	0.2, 0.9
$\{(CO)_3Co[P(OPin^i)_2Ph]\}_2$ 33	78.9, 78.5	78.9, 77.8	0.0, 1.7
$\{(CO)_3Co[P(OMen)_3]\}_2$, 34	77.6	73.5	4.1
$\{(CO)_3Co[P(OBor)_3]\}_2$, 35	82.4	77.9	4.5
$\{(CO)_3Co[P(OPin^i)_3]\}_2$, 36	78.2	72.9	5.3

[a] Chemical shifts are given in δ(ppm) relative to internal $CDCl_3$ with the middle branch of $CDCl_3$ signal set at 77.0 ppm. All spectra were recorded in $CDCl_3$ solution.

In the carbonyl region, there is a triplet at about 202 ppm in each spectrum. The triplet is a result of "virtual coupling" of the two phosphorus atoms at the two axial positions of the dimer. Although the three carbon atoms on each cobalt centre are only directly coupling to the single phosphorus atom on the same cobalt centre, the fact that the two phosphorus atoms are coupling to each other generates a non-first order pattern appearing as a triplet. Such three-bond P-P coupling is indicative of a linear geometry for the P-Co-Co-P fragment in each dimer.[104] The coupling constants $^2J_{PC}$ range from 19 to 30 Hz (Table 6-15). In the aromatic region, except those of the phosphite substituted dimers (compounds 34 - 36), which do not contain phenyl groups, complicated patterns analogous to those found in the spectra of the carbonyl iron complexes are exhibited. Likewise, in the alkyl region, all spectra of 28 - 36 show very similar feature to the corresponding carbonyl iron complexes. The peaks due to the α-carbon atoms in the alkoxy groups are only slightly shifted upon coordination, and the coordination shifts are very comparable to those of mono-substituted iron complexes (Table 3-8).

The ^{1}H NMR spectra of compounds 28 - 36 are also very similar to those of the iron carbonyl complexes, as exemplified by the spectrum of {Co(CO)$_3$[P(OBor)Ph$_2$]}$_2$ in Figure 3-17. These spectra have very similar features to those of their corresponding free ligands, except that the fine coupling patterns are not observed due to poor resolution, and the signals due to α-protons in the alkoxy groups are shifted downfield by about 0.4 ppm (Table 3-9).

Variable temperature ^{31}P{^{1}H} and ^{1}H NMR spectra of 28 - 36 were obtained in CD$_2$Cl$_2$ solutions. The ^{1}H V.T. NMR spectra show little of significance as the signals are very broad. The ^{31}P{^{1}H} V.T. NMR spectra do not show any changes from ambient temperature to - 90 °C except slight displacement in chemical shifts and considerable line broadening at low temperatures (Figure 3-18, ^{31}P{^{1}H} V.T. NMR spectra of
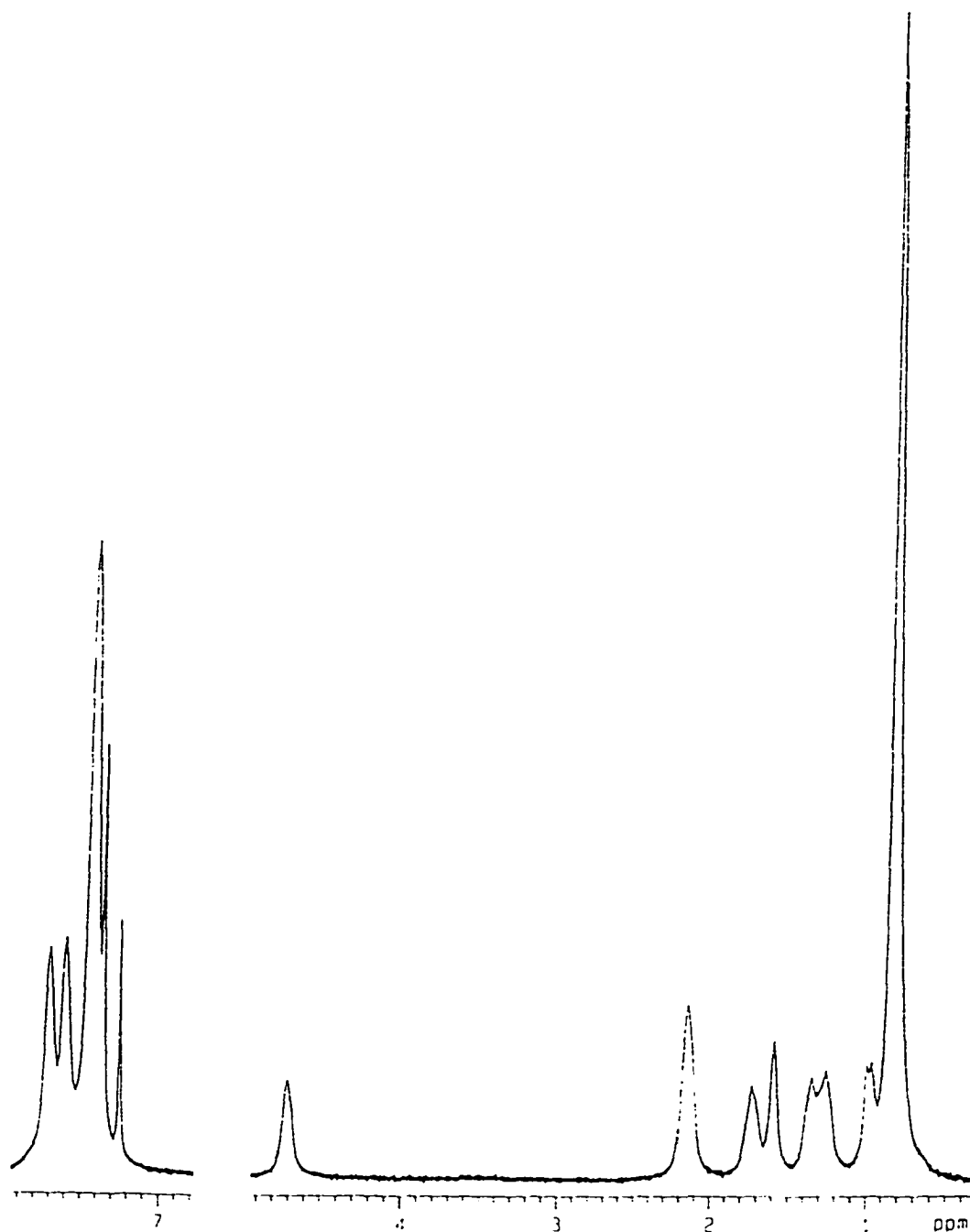
Figure 3-17. ^{1}H NMR spectrum of $\{Co(CO)_3[P(OBor)Ph_2]\}_2$, 29.

$\{Co(CO)_3[P(OMen)Ph_2]\}_2$). The staggered and eclipsed conformational isomerism for

the two *trans* phosphorus ligands, such as observed for di-substituted iron complexes (19

- 24), were not observed for 28 - 36, presumably due to the longer distance between the

Table 3-9. ^{1}H NMR data[a] for cobalt dimers and their corresponding ligands.

Compound	δ $\underline{H}CO_{com.}$ ppm	δ $\underline{H}CO_{lig.}$ ppm	Δ $\delta\underline{H}CO_{c-l}$ ppm
{(CO)$_3$Co[P(OMen)Ph$_2$]}$_2$,28	4.21	3.73	0.48
{(CO)$_3$Co[P(OBor)Ph$_2$]}$_2$,29	4.70	4.26	0.44
{(CO)$_3$Co[P(OPin^i)Ph$_2$]}$_2$,30	4.85	4.31	0.54
{(CO)$_3$Co[P(OMen)$_2$Ph]}$_2$,31	4.27, 3.81	3.80, 3.71	0.47, 0.10
{(CO)$_3$Co[P(OBor)$_2$Ph]}$_2$,32	4.70, 4.59	4.38, 4.18	0.32, 0.41
{(CO)$_3$Co[P(OPin^i)$_2$Ph]}$_2$,33	4.82, 4.70	4.39, 4.31	0.43, 0.39
{(CO)$_3$Co[P(OMen)$_3$]}$_2$, 34	4.11	3.72	0.39
{(CO)$_3$Co[P(OBor)$_3$]}$_2$, 35	4.61	4.33	0.28
{(CO)$_3$Co[P(OPin^i)$_3$]}$_2$, 36	4.78	4.45	0.33

[a] Chemical shifts are given in δ(ppm) relative to internal CDCl$_3$ with CHCl$_3$ signal set at 7.24 ppm. All spectra were recorded in CDCl$_3$ solution.

two phosphorus ligands in the cobalt dimers since they are separated by two cobalt atoms, rather than the single iron atom in the di-substituted iron monomers. Although it is believed that more carbonyl bridged isomers will be formed at low temperatures, the isomers with or without bridged carbonyl groups are not resolved in the NMR spectra within the temperature range for the V.T. NMR experiment, even if the bridged isomers were generated.
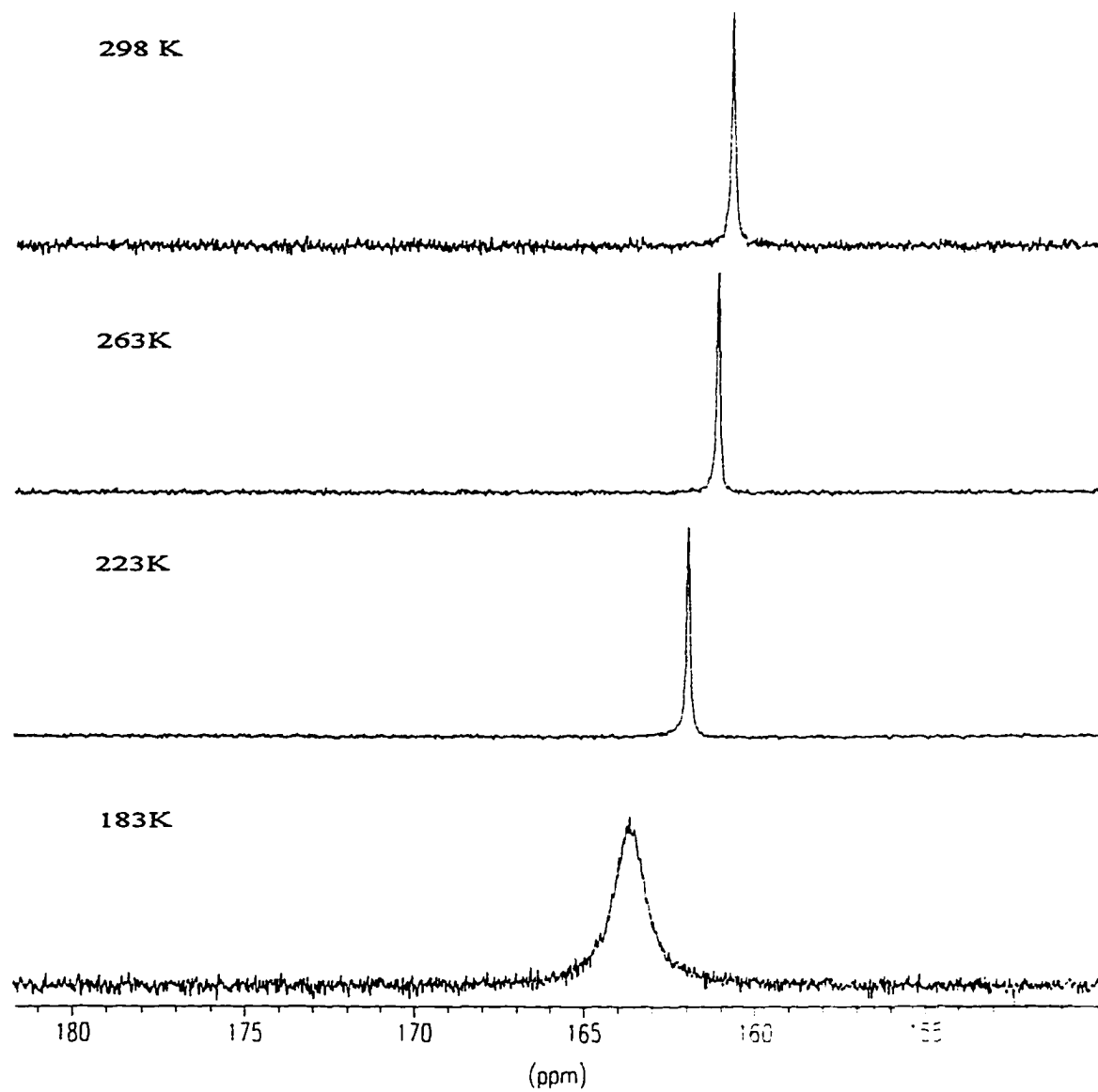
Figure 3-18. ^{31}P{^{1}H} V.T. NMR spectra of {Co(CO)$_3$[P(OMen)Ph$_2$]}$_2$, $\underline{28}$.

The cobalt carbonyl complexes, as mentioned in the introduction, are well known catalysts for hydroformylation reactions under oxo condition (Equation 3-1), chemistry that was discovered by Roelen in 1938.[105] In view of its versatility in the functionalization of C=C bonds, hydroformylation became the world's largest industrial homogeneous catalytic process.[106] In this process alkenes react with hydrogen and carbon monoxide to give either linear or branched aldehydes (Scheme 3-3).

The reaction proceeds only in the presence of a catalyst. In general, two other reactions compete with hydroformylation:

(a) Hydrogenation

$$RCH=CH_2 + H_2 \longrightarrow RCH_2CH_3$$

$$RCH_2CH_2CHO + H_2 \longrightarrow RCH_2CH_2CH_2OH$$

(b) Isomerization

$$RCH_2CH=CH_2 \longrightarrow RCH=CHCH_3$$
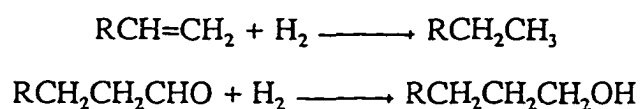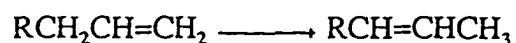
Therefore, in order to minimize the formation of the hydrogenation and isomerization products, the catalyst has to be chemoselective, *i.e.*, able to selectively catalyze the
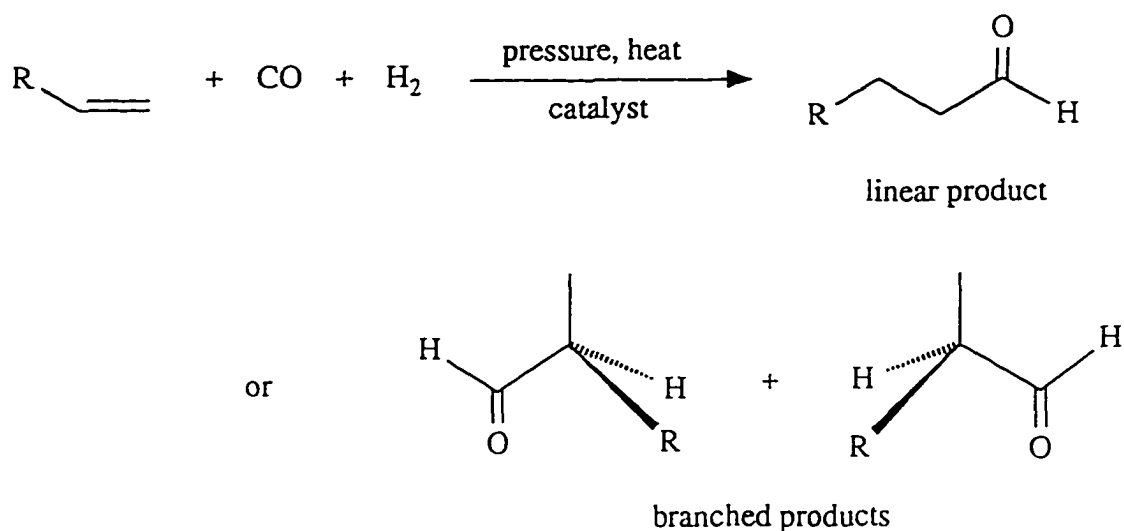
Scheme 3-3. Hydroformylation of olefins.

generation of one functional group over others. Meanwhile, depending whether the linear or branched aldehyde is desired, the catalyst must also be able to selectively maximize the yield of the product in demand, *i.e.*, be regioselective. Since most of the starting olefins, such as 1-hexene, or styrene, are prochiral, when branched aldehydes are produced, the products will be chiral. Therefore, in order to obtain products with high enantiomeric excess, which is often required, catalysts that can preferentially induce the formation of one enantiomer of the product over the other are desired. As discussed in the Introduction, such enantioselective catalysts must be optically active, and asymmetric transition metal complexes are potential candidates for this function. As the demand for optically pure chiral aldehydes, a class of very important building blocks, is increasing rapidly, much research has been devoted to asymmetric hydroformylation, using various chiral ligands, such as DIOP, BINAP, *etc.*, on different metal centres, such as Rh, Pt, or Co.[107] In order to examine the potential for asymmetric induction of ligands $\underline{1}$ - $\underline{9}$, hydroformylation of 1-hexene under oxo conditions, using $\{Co(CO)_3[P(OBor)Ph_2]\}_2$ ($\underline{29}$), $\{Co(CO)_3[P(OPin^i)Ph_2]\}_2$ ($\underline{30}$), $\{Co(CO)_3[P(OBor)_2Ph]\}_2$ ($\underline{32}$), or $\{Co(CO)_3[P(OPin^i)_2Ph]\}_2$ ($\underline{33}$) as catalyst was investigated. The results are shown in Table 3-10. Low to zero conversion rates were observed for these catalysts, probably due to relatively low pressure (CO : H_2 = 600 : 600 psi) and low temperature (70 °C) applied to these reactions (for oxo reactions using cobalt catalysts, the pressure is usually above 1500 psi and the temperature over 100 °C).[105] Experiments under normal oxo conditions were not attempted due to the limitation of the equipment available. Although the conversion rate was low, the catalyst did show some chemo and regioselectivity, since virtually no hydrogenation and isomerization products were formed and the linear product was formed preferentially. The enantioselectivity was not investigated due to the low conversion rate. Better results may be obtained with more suitable reaction conditions or substrates.

Table 3-10. Results for hydroformylation of 1-hexene catalyzed by cobalt dimers.

Catalyst	Conversion (%)[a]	ROH (%)[b]	n : b[c]
$\{Co(CO)_3[P(OBor)Ph_2]\}_2$, <u>29</u>	7	0	2.1 : 1
$\{Co(CO)_3[P(OPin^i)Ph_2]\}_2$, <u>30</u>	3	< 0.5	-
$\{Co(CO)_3[P(OBor)_2Ph]\}_2$, <u>32</u>	< 1	0	-
$\{Co(CO)_3[P(OPin^i)_2Ph]\}_2$, <u>33</u>	< 1	0	-

[a] Total conversion to oxygenated products (principally aldehydes and alcohols). [b] Percentage of heptanol in total hydrocarbons. [c] Ratio of linear to branched products.

In conclusion, chiral tertiary phosphorus ligands <u>1</u> - <u>9</u> can be reacted with transition metals to form complexes as expected. These ligands are bulky (although not extraordinarily so) and may have potential for asymmetric induction. The mono- and di-substituted iron carbonyl complexes containing these ligands (<u>10</u> - <u>18</u>) possess the predicted trigonal bipyramidal structure, with the phosphorus ligands at one or both axial positions. The structures of the di-substituted cobalt complexes are also analogous to those of the known compounds in the same class, with the two phosphorus ligands occupying the two axial sites. The coordination shifts from multinuclear NMR experiments show small but consistent differences for the three classes of ligands (i.e. the phosphinites, phosphonites, and phosphites), suggesting differences in the electronic properties among these ligands. Since alkoxy groups have stronger conjugative effects than phenyl or alkyl groups, phosphites are believed to be more basic than phosphines.[108] When the mixed ligands such as the phosphinites or the phosphonites are also taken into consideration, the order of the basicity of these ligands would be: phosphite > phosphonite > phosphinite > phosphine. Together with the steric bulk trend

among these ligands being: phosphite < phosphonite < phosphinite, as evidenced by the results from the V.T. NMR experiments, the orderly changes in the electronic and the steric properties for these three classes of ligands may provide basis for designing desired ligands in a systematic way.
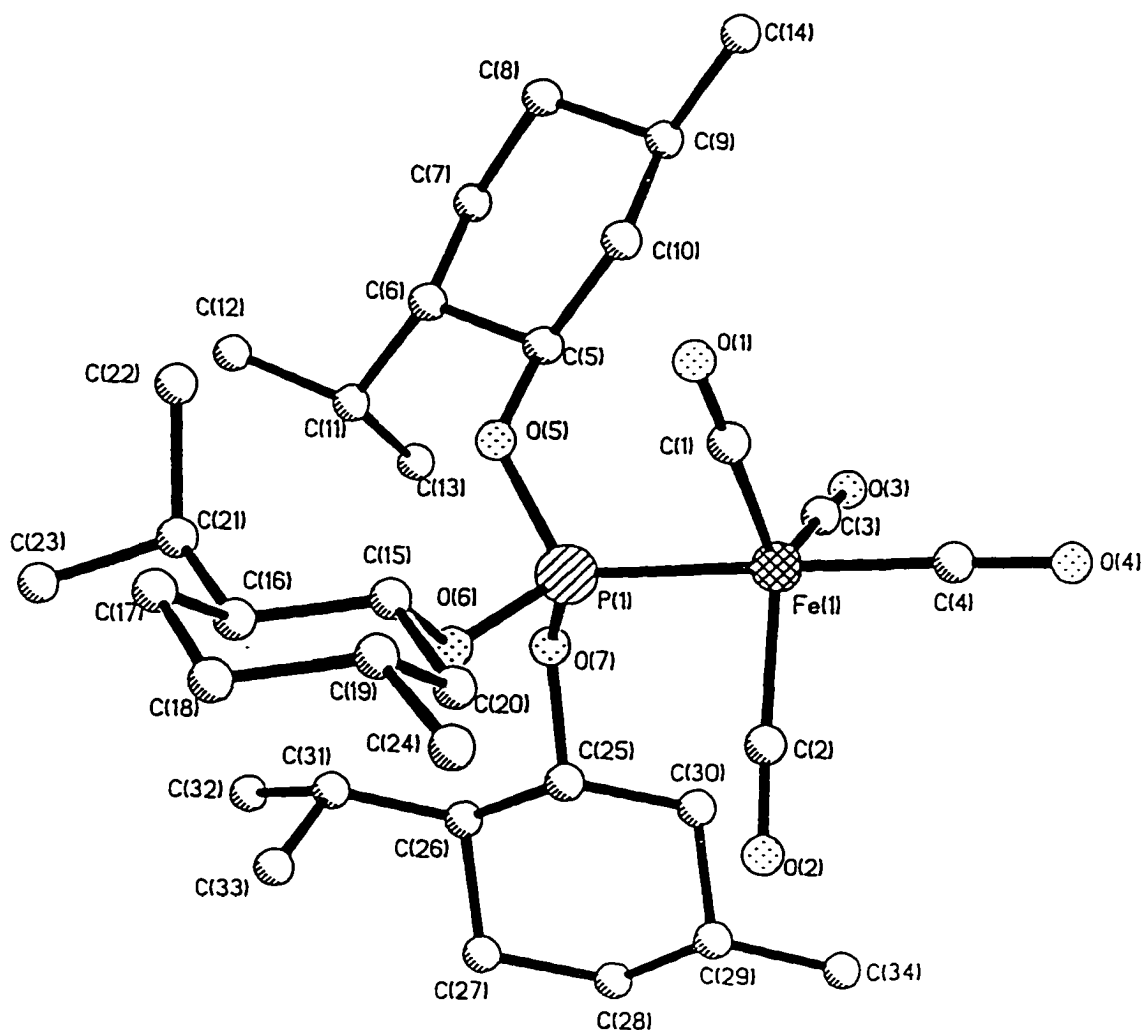
Figure 3-19. Molecular structure of $(CO)_4Fe[P(OMen)_3]$, 16.

The first solid state structural profile of $P(OMen)_3$ was recently provided by Dr. Tuscano, *et al.*, along with the crystallographic analysis of $(CO)_4Fe[P(OMen)_3]$ (16).

Table 3-11. Important interatomic distances and bond angles in compound 16.[a]

(a) Bond distances: Atoms	Distance (Å)	Atoms	Distance (Å)
Fe(1)-P(1)	2.189(3)	Fe(1)-C(1)	1.796(14)
Fe(1)-C(4)	1.771(14)	O(2)-C(2)	1.122(18)
O(4)-C(4)	1.140(17)	P(1)-O(6)	1.573(8)
(b) Bond angles: Atoms	Angle (°)	Atoms	Angle (°)
C(1)-Fe(1)-P(1)	89.9(4)	C(4)-Fe(1)-P(1)	175.9(5)
C(1)-Fe(1)-C(2)	117.1(6)	C(1)-Fe(1)-C(4)	93.6(6)
Fe(1)-C(1)-O(1)	178.1(13)	Fe(1)-P(1)-O(5)	117.4(3)
O(5)-P(1)-O(6)	100.9(4)	P(1)-O(5)-C(5)	126.5(7)

[a] Estimated standard deviations are given in parentheses.

There are four molecules in each orthorhombic unit cell. As inferred from the IR and NMR spectra, the five-coordinate complex adopts a trigonal-bipyramidal structure, with the phosphorus ligand occupying the axial position (Figure 3-19). The ligand is indeed very bulky, with the methyl groups in two of three menthoxy ligands appearing on the other side of the equatorial plane. All bond lengths and bond angles are within expected range (important bond lengths and bond angles are listed in Table 3-11). Detailed crystallography data are listed in the appendix.

Chapter 4

PYRAZOLYL-BRIDGED IRIDIUM DIMERS

WITH CHIRAL PHOSPHORUS LIGANDS

4.A. Introduction

Oxidative addition is a reaction of a metal complex with a substrate that causes an increase in both the coordination number and formal oxidation state of the metal centre. This and its reverse process, reductive elimination, are two very important types of reactions in transition metal chemistry, since they have been widely recognized as pivotal steps in many transition metal catalyzed cycles.[109] Generally, there are two types of oxidative addition reactions, *i.e.* one-centre and two-centre oxidative addition. The former refers to those reactions involving only monomeric metal complexes, and obviously, the latter is referring to those involving dinuclear metal complexes.

Scheme 4-1 outlines some typical one-centre oxidative addition reactions. The most common one is the first reaction (Equation 4-1), during which X-Y adds to a single metal centre to give a product whose oxidation state and coordination number have increased by two. Reactions resulting in two-electron oxidation of the metal and

$$L_m M^n + X—Y \longrightarrow Y—L_m M^{n+2}—X \qquad (4\text{-}1)$$

$$L_m M^n + X—Y \longrightarrow [L_m M^{n+2}—X]^+[Y]^- \qquad (4\text{-}2)$$

$$2L_m M^n + X—Y \longrightarrow L_m M^{n+1}—X + L_m M^{n+1}—Y \qquad (4\text{-}3)$$

$$2L_m M^n + X—Y \longrightarrow X—L_m M^{n+1}—M^{n+1}L_m—Y \qquad (4\text{-}4)$$
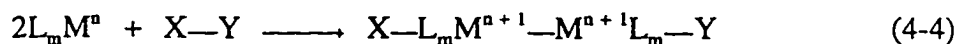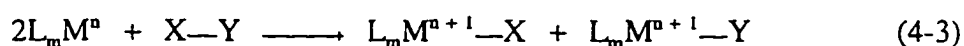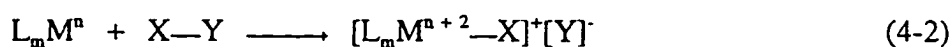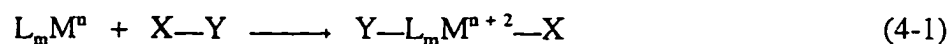
Scheme 4-1. One centre oxidative addition.

only unit increase of the coordination number (Equation 4-2), or only unit increases in both oxidation state and coordination number (Equations 4-3, and 4-4) are also known. The last reaction (Equation 4-4) is classified into the one-centre oxidative addition reactions, because the starting metal complex is a mononuclear species, although a metal-metal bond is formed in the product.

One-centre oxidative addition reactions, especially those of Vaska's complex, *trans*-[Ir(CO)(Cl)(PPh$_3$)$_2$], and [Pt(PPh$_3$)$_3$] have been extensively studied.[108-110] The main effort has been focused on the elucidation of the mechanism. The results show that the mechanism for these reactions varies considerably, depending on several factors, including the properties of the substrates, the metal centres, and the auxiliary ligands. At least three different reaction mechanisms have been identified: (a) nucleophilic addition (S$_N$2 addition), observed with only small primary alkyl halides (*e.g.*: methyl iodide); (b) radical addition, usually responsible for the oxidative addition of ethyl or higher alkyl halides; (c) concerted three-centre addition, identified for reactions of dihydrogen and silicon hydrides with electron-rich complexes.

Two-centre oxidative addition reactions can be classified into three types (Scheme 4-2): (a) two-centre addition causing single-electron oxidation at each metal centre and formation of metal-metal bond (Equation 4-5); (b) two-centre addition

$$M^n \quad M^n + X—Y \longrightarrow X—M^{n+1}—M^{n+1}—Y \qquad (4\text{-}5)$$

$$M^n—M^n + X—Y \longrightarrow X—M^{n+1} \quad M^{n+1}—Y \qquad (4\text{-}6)$$

$$M^n \quad M^n + X—Y \longrightarrow M^n \quad M^{n+2}—X \qquad (4\text{-}7)$$
$$\underset{\displaystyle Y}{|}$$
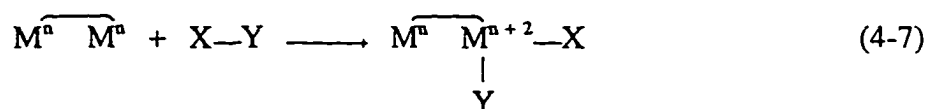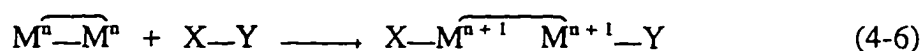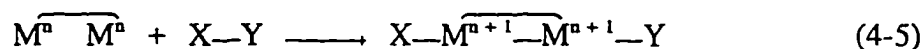
Scheme 4-2. Two centre oxidative addition.

causing single-electron oxidation at each metal centre and cleavage of metal-metal bond (Equation 4-6); (c) single-centre two-electron oxidative addition producing a heterovalent complex (Equation 4-7). Since the first report of a type (a) reaction by Schmidbauer and co-workers[111] in the middle of 1970s, numerous other similar reactions have been reported,[112 - 115] most of which involve late transition metal complexes. Reactions of type (b) are typical for early transition metal dimers containing a metal-metal bond.[116] Type (c) amounts to a one-centre oxidative addition similar to Equation 4-1. This type is not common, but has been shown as an intermediate step in two-centre oxidative addition reactions.[117, 118]

Compared to reactions involving mononuclear species, the mechanistic details of the oxidative addition reactions of dimeric complexes are not as well understood, despite the importance of such chemistry as a basis for understanding cooperative intermetallic effects, especially in relation to reactivity at metal-metal bonds[119] and cooperative catalytic action. The principles established from these dimeric complexes may be translated into the context of polynuclear species and ultimately to substantiate a "cluster/surface" analogy.[120]

A number of pyrazolyl bridged iridium(I) dimers and their oxidative addition reactions with various substrates including alkyl halides, dihalides, and dihydrogen have been reported by Stobart and coworkers.[121 - 136] The pyrazolyl anion is derived from pyrazole when the proton on one of the two nitrogen atoms is removed by a base. The
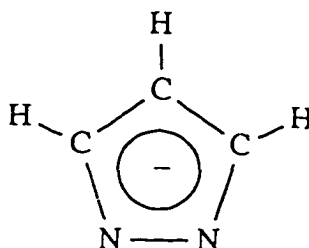
Pyrazolyl anion.

negative charge makes the anion aromatic and the two nitrogens equivalent. The anion normally functions as a bridging ligand in transition metal complexes with the two nitrogen atoms bonding to two metal centres. This bridging ligand is a particularly good choice for the studies on two-centre oxidative addition reactions of dimeric complexes because it possesses some useful properties, such as: (a) it can accommodate a wide range of metal-metal separations (from 2.623 Å in $Ir_2(COD)_2(\mu\text{-}pz)_2(\mu\text{-}CF_3CF_3)$[121] to 4.339 Å in $[TiCp_2(\mu\text{-}pz)]_2)$[137], which often arise within a binuclear system when it is subjected to redox changes, especially when the changes cause metal-metal bond formation or cleavage (Equations 4-5, and 4-6 on page 86); (b) it is resistant to bridge cleavage, hence enhances the stability of the dimeric system; (c) it can bind to a metal in a number of oxidation states; and (d) it is unreactive to many reagents which add to the metal centres, thus makes the oxidative addition using a variety of substrates possible.

The focus of the research on the chemistry of pyrazolyl bridged iridium dimers has been the oxidative addition reactions of $[Ir(COD)(\mu\text{-}pz)]_2$ (37), $[Ir(CO)_2(\mu\text{-}pz)]_2$ (38), and $[Ir(CO)(PPh_3)(\mu\text{-}pz)]_2$ (39), among which exist some common structural features: (a) Each iridium atom is in a +1 oxidation state with 8 d electrons and a local square planar geometry. A facile oxidative addition to these unsaturated electron rich iridium centres is expected, as evidenced by the chemistry of Vaska's complex, $[Ir(CO)(Cl)(PPh_3)_2]$. (b) The two iridium atoms and the four nitrogen atoms in the two pyrazolyl bridges in each molecule form a six-membered ring with a boat conformation (Figure 4-1). The boat conformation is also adopted by many other bis-pyrazolyl bridged dimers, but complexes with other conformations do exist. For example, the central core in $[Ni(NO)(\mu\text{-}3,5\text{-}Me_2pz)]_2$[138] is planar while those in $[Ti(Cp)_2(\mu\text{-}pz)]_2$[137] and $[Rh(C_5Me_5)Cl(\mu\text{-}pz)]_2$[139] adopt a chair conformation (Figure 4-2).

In spite of the similarities among the structures of compounds 37 - 39, the

[Ir(CO)(COD)(μ-pz)]$_2$, __37__

[Ir(CO)$_2$(μ-pz)]$_2$, __38__
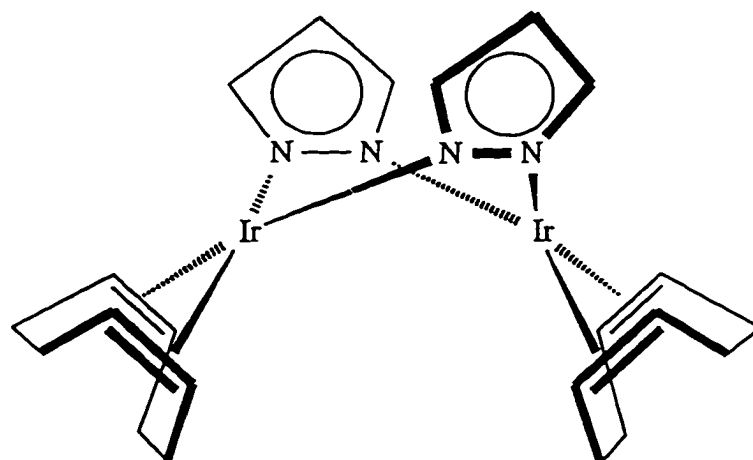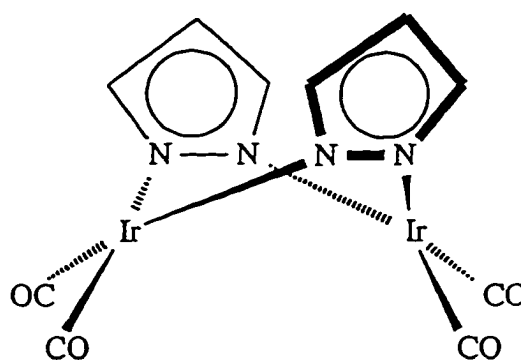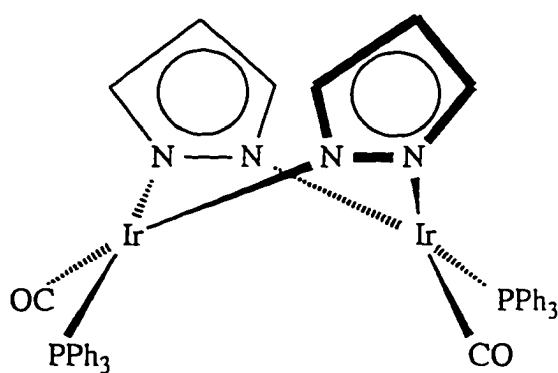
[Ir(CO)(PPh$_3$)(μ-pz)]$_2$, __39__

Figure 4-1. Molecular structures of compounds __37__ - __39__.

[Ni(NO)(μ-3,5-Me₂pz)]₂

[Ti(Cp)₂(μ-pz)]₂   [Rh(C₅Me₅)Cl(μ-pz)]₂
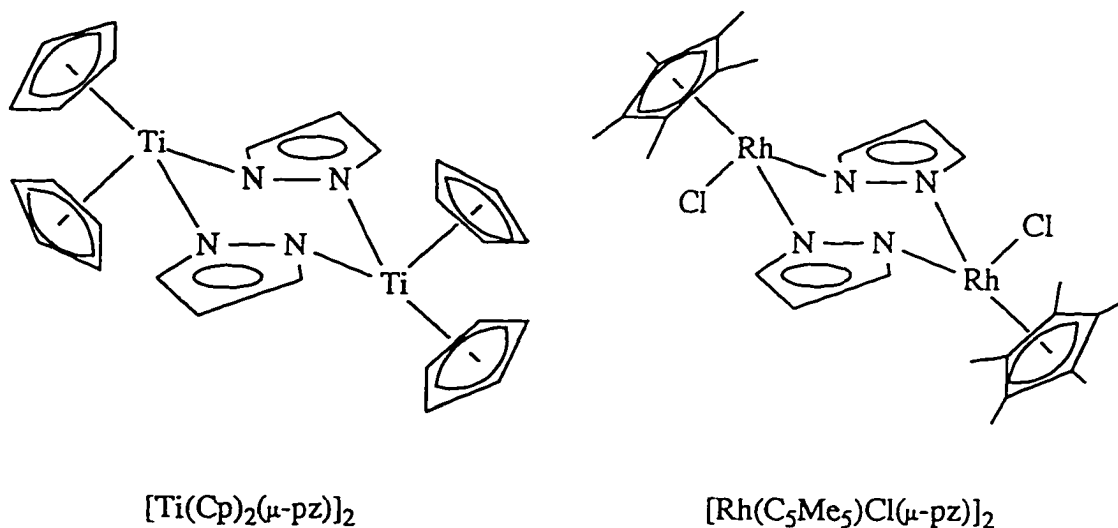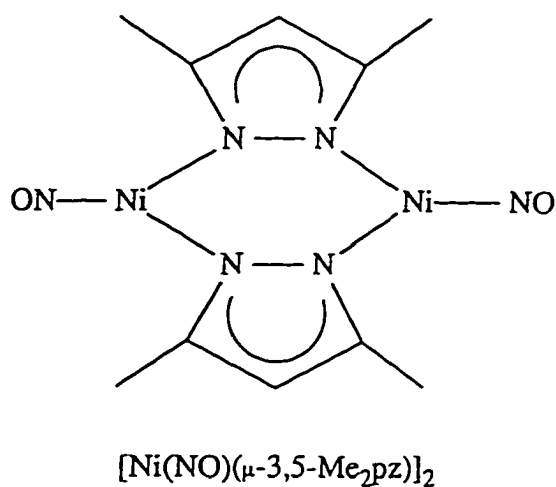
Figure 4-2. Molecular structures of selected pyrazolyl bridged dimers.

structure of 39 is different than the other two in terms of the symmetry considerations.

Each of the molecules of 37 and 38 possesses one C_2 axis and two symmetry planes.

Therefore, both 37 and 38 belong to the C_{2v} point group. In compound 39, however, two

different terminal ligands, CO and PPh_3, are coordinated to each iridium centre, and

either pair of CO groups or PPh_3 groups in each dimer are *trans* to each other, resulting

in the loss of the planar symmetry which exists in 37 and 38, leaving only one

symmetry operation other than the identity E: a C_2 rotational axis. The complex,

therefore, belongs to the C_2 point group, and is inherently left- or right-handed, *i.e.* is atropisomeric and is chiral.

Thus, compound **39** is interesting due to its potential capacity for asymmetric induction if it can be made to function as a homogeneous catalyst, as discussed in the Introduction. However, this is achievable only if the complex is not only chiral, but is also separable into its enantiomers, (*i.e.* is resolvable): a racemic mixture would catalyze a reaction with opposite stereochemistry and so produce a racemic product. It is questionable whether **39** can be isolated as enantiomers under normal conditions, since it is a conformationally chiral compound, in which the enantiomers can in theory be interconverted without breaking any covalent bonds. As shown in Scheme 4-3, the interconversion between the two enantiomers (atropisomers in this case) of **39** is effected
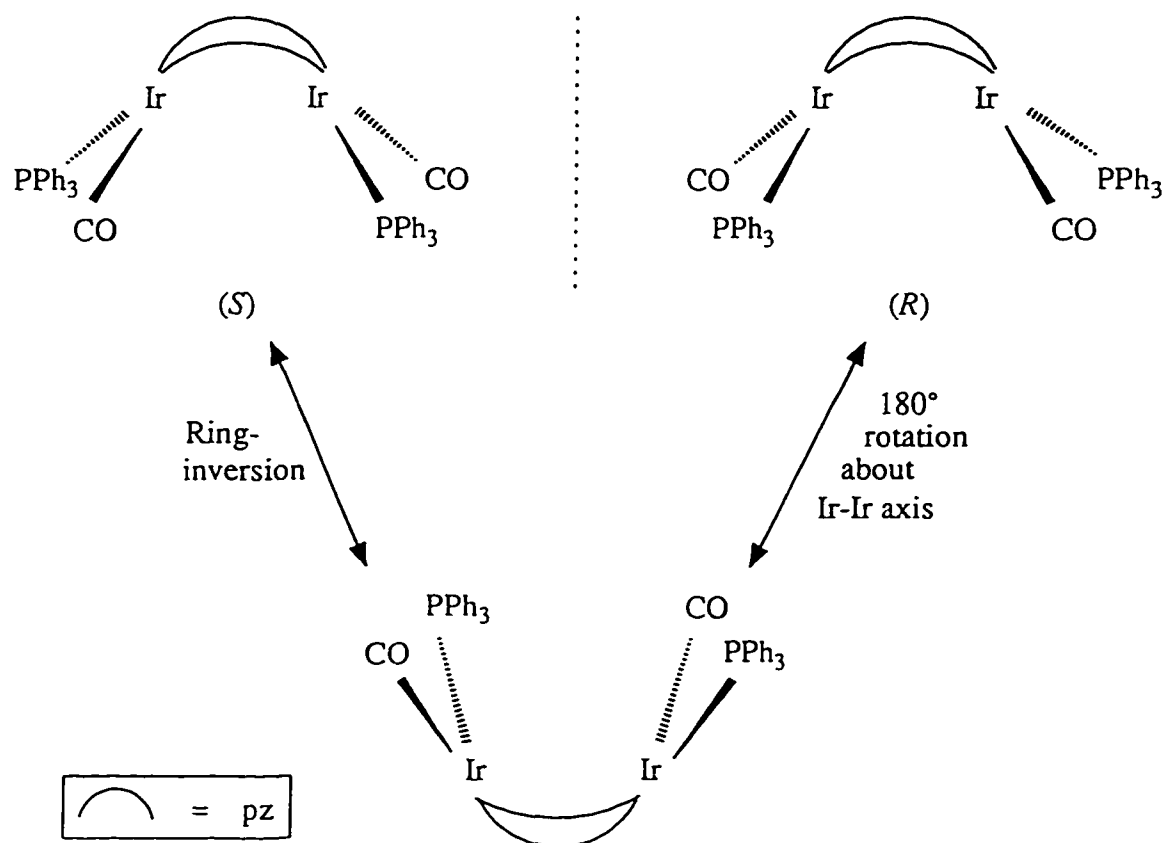
Scheme 4-3. The ring-inversion of compound **39**.

by inversion of the six-membered central bimetallocycle, a process that is conceptually related to the well-known ring inversion of cyclohexane. Ring inversion is thus important in relation to compound 39 since it will dictate whether or not this complex is useful in the context of asymmetric catalysis: the existence of the planar and the chair conformations in other $M_2(\mu\text{-pz})_2$ systems[137-139] suggests that the ring-inversion may be feasible.

Since enantiomers are indistinguishable by spectroscopy, the ring inversion process in 39 cannot be investigated by NMR spectroscopy, so that to use the latter as a probe it is necessary to modify the structure of the complex. This can be achieved by introducing an optically pure chiral centre into compound 39, so that diastereomers will be generated that are distinguishable by NMR spectroscopy. In addition, such modification could lead to separation of the two diastereomers, since the latter will have different physical properties. To investigate this, new diiridium(I) complexes were prepared using several of the optically active tertiary phosphines described in Chapter 2. The central ring inversion process of $\{Ir(CO)[PPh_2(OBor)](\mu\text{-pz})\}_2$ is also discussed.
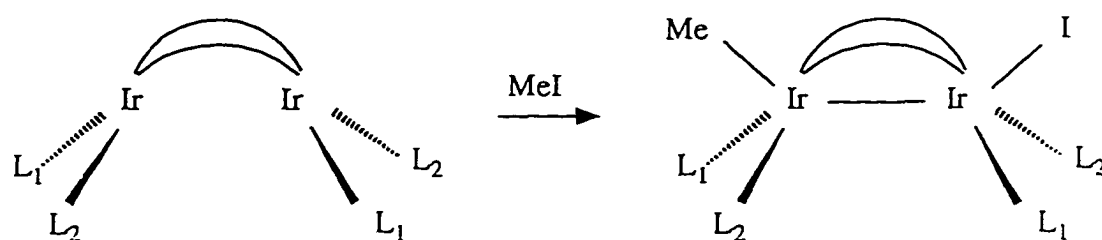
Compounds 37 to 39

Compounds 37: L_1L_2 = COD

38: L_1 = L_2 = CO

39: L_1 = CO; L_2 = PPh$_3$

$\fbox{$\frown$ = pz}$
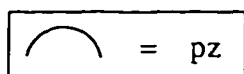
Scheme 4-4. Oxidative addition to the diiridium(I) systems.

Oxidative additions of alkyl halides to the iridium(I) dimers 37 - 39 belong to the first type of two-centre oxidative addition reactions (Equation 4-5 on page 86), with the alkyl group and the halide anion bonding to different iridium centres accompanied by the formation of iridium-iridium bond (Scheme 4-4). The resulting adducts were the first examples of d^7 iridium(II) species. Detailed kinetic studies on the oxidative addition of methyl iodide to 37 and 38 have been carried out, showing evidence for different mechanisms for these two dimers. When methyl iodide is added to 38, the reaction is believed to proceed irreversibly via a S_N2 mechanism (Scheme 4-5). By contrast, based on measured activation parameters a concerted four-centre transition state is proposed for the oxidative addition of MeI to 37 (Scheme 4-6), which establishes an equilibrium.
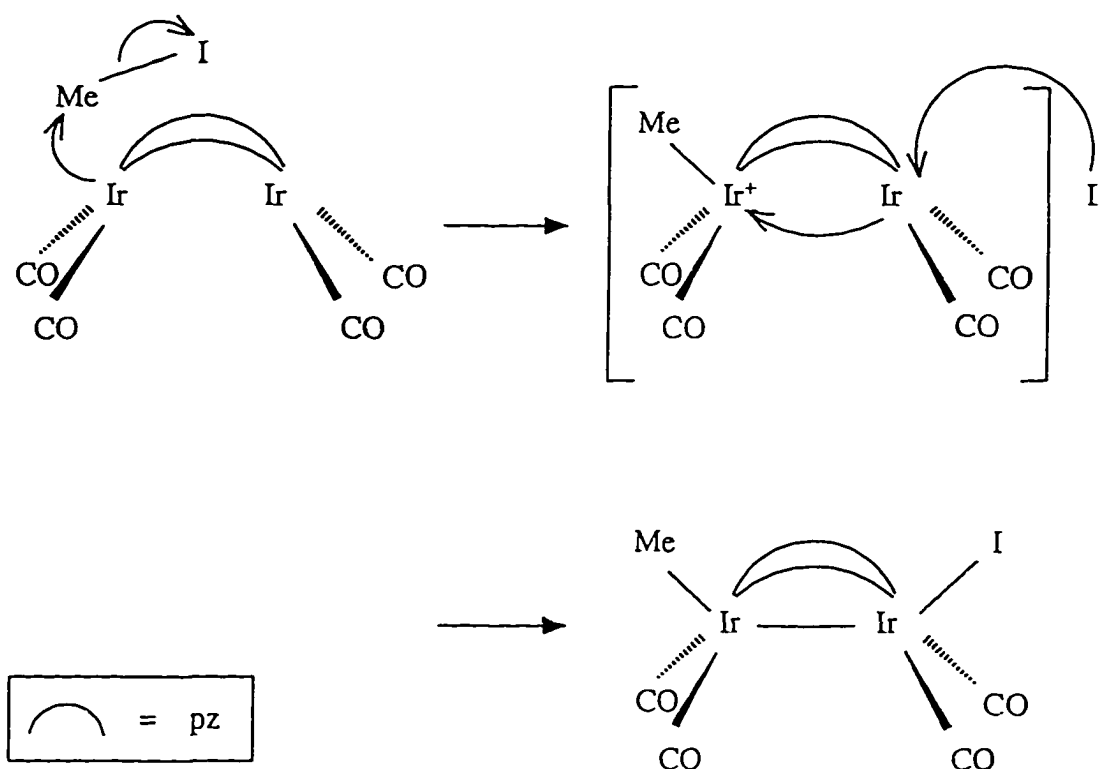
Scheme 4-5. S_N2 mechanism for oxidative addition of MeI to 38.

The kinetics of the reaction between MeI and 39 have not been investigated in detail. Although preliminary results from the kinetic studies support a S_N2 type reaction,
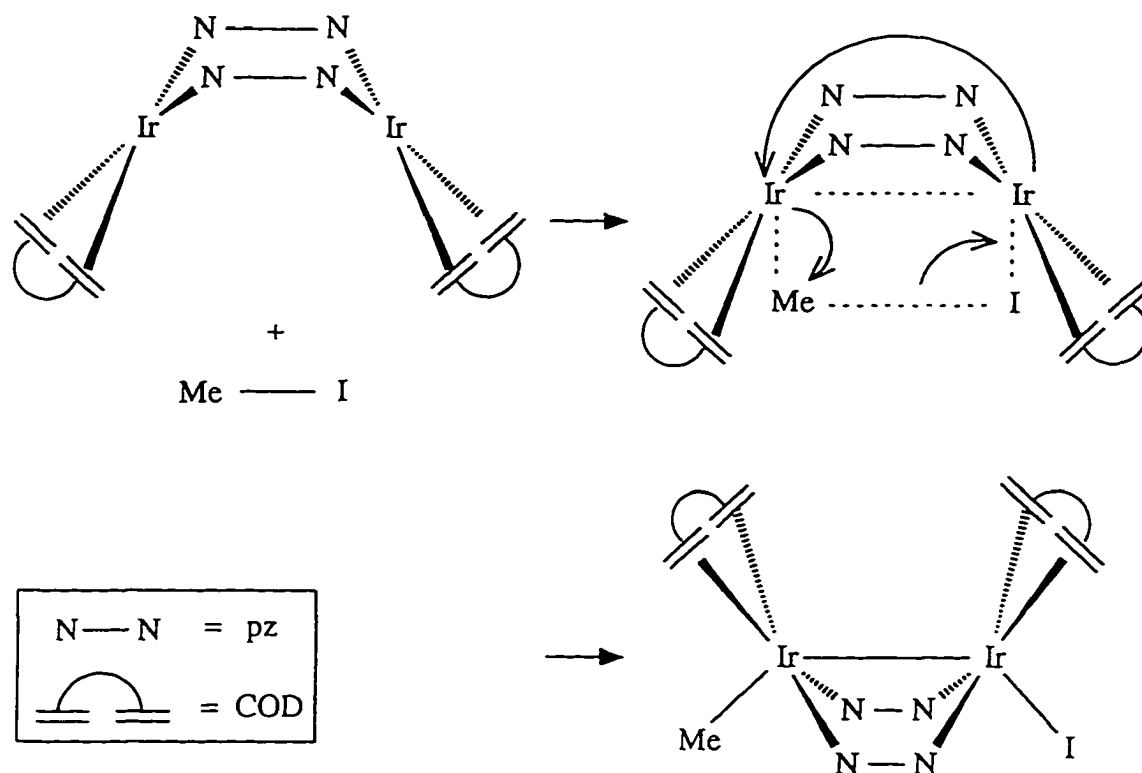
Scheme 4-6. Concerted mechanism for oxidative addition of MeI to <u>37</u>.

other reaction pathways cannot be entirely eliminated. In this chapter, oxidative addition of MeI to {Ir(CO)[PPh$_2$(OBor)](μ-pz)}$_2$, which is structurally related to <u>39</u>, is discussed in relation to the ring inversion process. Oxidative additions of bulky chiral alkyl iodides (*exo*- and *endo*-norbornyl iodide) to [Ir(CO)$_2$(μ-pz)]$_2$ (<u>38</u>) are also examined. The results show evidence for a mechanism that is different from that of the MeI addition.

4.B. Pyrazolyl-bridged Iridium(I) Dimers With Chiral Phosphorus Ligands

Pyrazolyl-bridged iridium(I) dimers containing chiral phosphorus ligands are synthesized using an analogous route to [Ir(CO)(PPh$_3$)(μ-pz)]$_2$. First, [Ir(CO)$_2$(μ-pz)]$_2$ (<u>38</u>) is generated by replacement of cyclooctadiene ligands in [Ir(COD)(μ-pz)]$_2$ (<u>37</u>) by

CO. This is followed by the substitution of the carbonyl groups in $\underline{38}$, which is reacted *in situ* with one of the phosphorus ligands, as shown in Scheme 4-7.

$$2IrCl_3 \cdot 3H_2O + 2COD + 2CH_3CH_2OH \xrightarrow{\text{EtOH}} [Ir(COD)(\mu\text{-Cl})]_2 + 4HCl + 2CH_3CHO + 6H_2O$$

$$[Ir(COD)(\mu\text{-Cl})]_2 + 2pzH + Et_3N \xrightarrow{\text{THF}} [Ir(COD)(\mu\text{-pz})]_2 + 2Et_3N \cdot HCl$$

$$[Ir(COD)(\mu\text{-pz})]_2 + 4CO \xrightarrow{\text{THF}} [Ir(CO)_2(\mu\text{-pz})]_2 + 2COD$$

(S) (R)
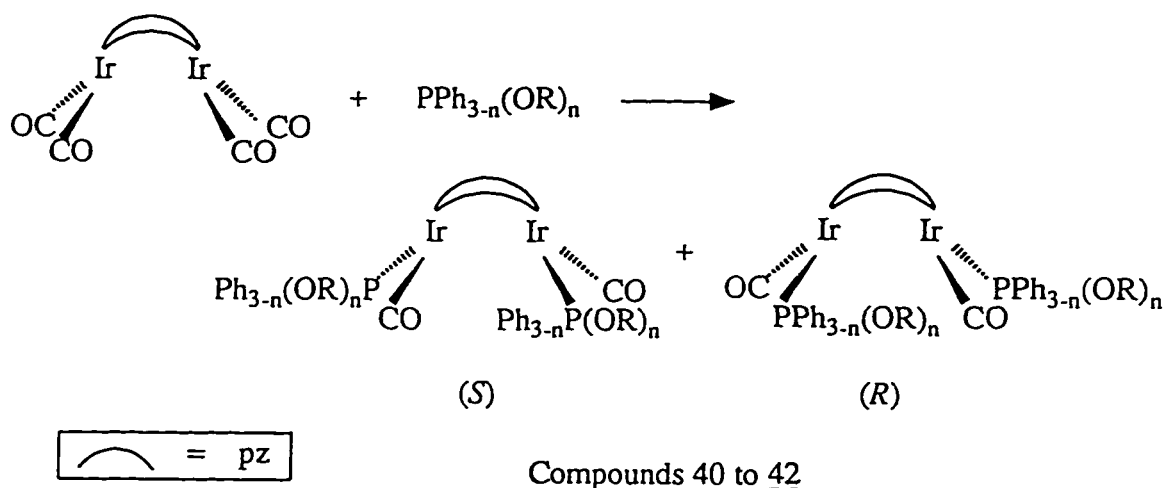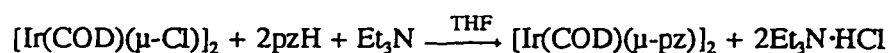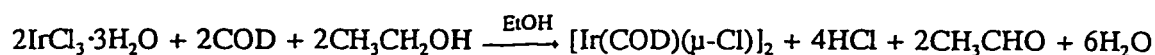
Compounds $\underline{40}$ to $\underline{42}$

Compound $\underline{40}$: R = Men, n = 1;

$\underline{41}$: Bor, 1;

$\underline{42}$: Men, 2.

Scheme 4-7. Syntheses of compounds $\underline{40}$ - $\underline{42}$.

All products are orange crystalline solids, and are stable in the solid state when protected by an inert atmosphere. The compounds are soluble in dichloromethane, chloroform, THF, benzene, and toluene, whereas in saturated hydrocarbon solvents, such as hexanes, the solubility is low.

After purification, the $^{31}P\{^1H\}$ NMR spectrum of each of compounds $\underline{40}$ - $\underline{42}$ exhibits two resonances of unequal ratio (Figure 4-6, see page), indicating that each

product consists of a pair of diastereomers, as predicted in Scheme 4-7; only one resonance will be generated by each diastereomer since in each isomer the two phosphorus atoms are related by C_2 rotation. The ratios are 33:67, 40:60, and 26:74 for 40, 41, and 42, respectively, as determined by the integration of ^1H NMR spectra. This suggests that the ligand containing more chiral alkoxy ligands leads to a more significant free energy difference between the two diastereomers, so that one is favoured more strongly over the other in the thermodynamic distribution.

The signals are shifted upfield from those of the corresponding free ligands (Table 4-1). This is opposite to what was found for the coordination shifts of the iron and cobalt carbonyl complexes. In the latter (compounds 9 - 36), the three or more carbonyl groups at each metal centre delocalize a significant amount of electron density into the CO π^* orbitals, making the central atom relatively electron deficient. Therefore, the phosphorus ligands in these compounds can act as strong σ donors with little π back donation, showing large electron deshielding effects in the NMR spectra. In compounds 40 - 42, however, the electron density at the iridium centre, at each of which there is

Table 4-1. $^{31}P\{^1H\}$ NMR coordination shifts[a] ($\Delta \, \delta P_{c-l}$) for compounds 40 to 42.

Compound		$\delta \, P_{com.}$ ppm	$\delta \, P_{lig.}$ ppm	$\Delta \, \delta P_{c-l}$ ppm
{Ir(CO)[P(OMen)Ph$_2$](μ-pz)}$_2$,	40	94.2, 92.6	107.3	-13.1, -14.7
{Ir(CO)[P(OBor)Ph$_2$](μ-pz)}$_2$,	41	96.8, 95.8	110.6	-13.8, -14.8
{Ir(CO)[P(OMen)$_2$Ph](μ-pz)}$_2$,	42	115.3, 111.8	160.1	-44.8, -48.3

[a] Chemical shifts are given in δ(ppm) relative to external 85% phosphoric acid solution. All spectra were recorded in C_6D_6 solution.

only one carbonyl group present, is considerably higher. Because of this, the phosphorus ligands in these compounds function not only as σ donors, but also as π acceptors, leading to electronic shielding effects in the NMR spectra.
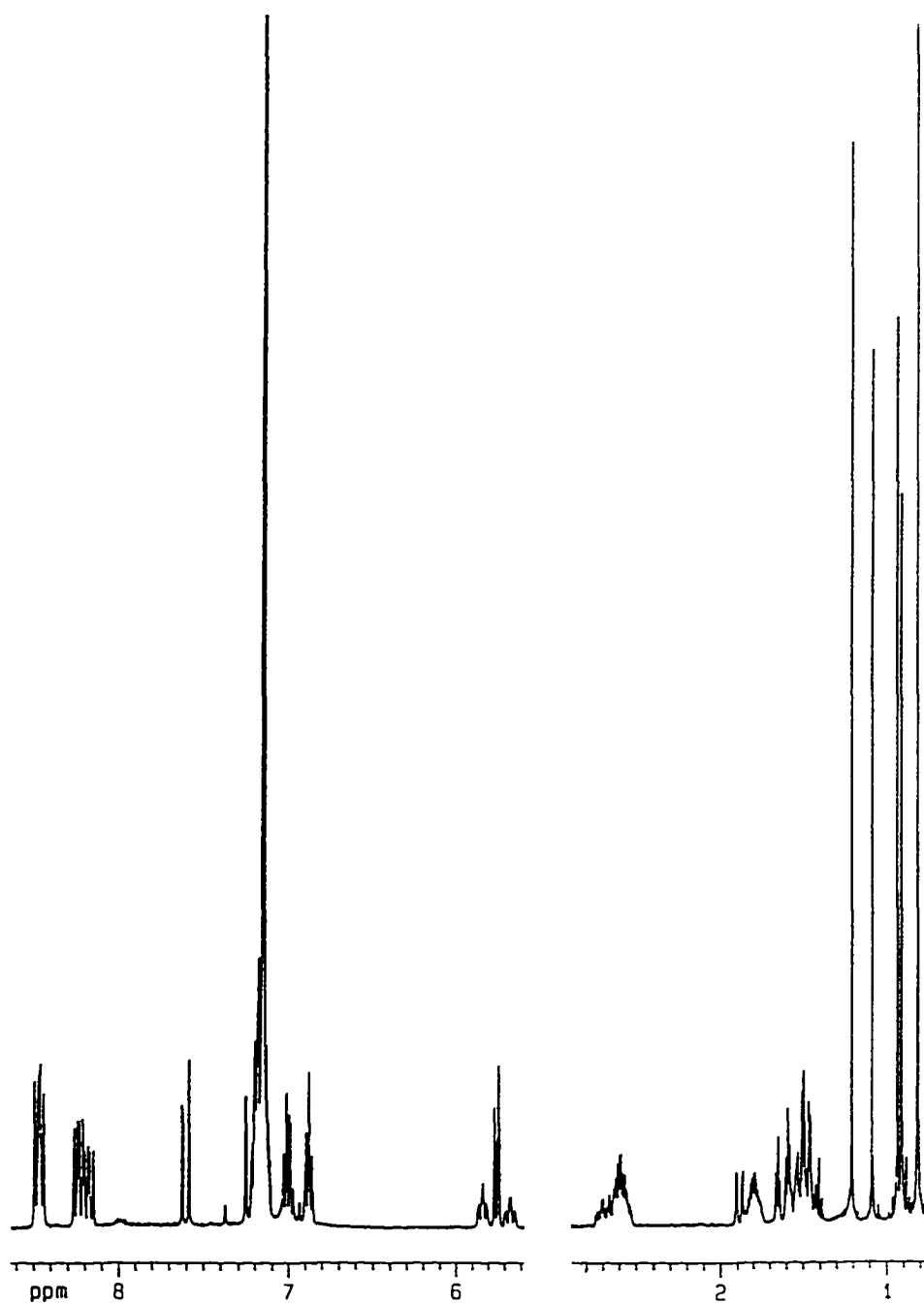
Figure 4-3. ^{1}H NMR spectrum of {Ir(CO)[P(OBor)Ph$_2$](μ-pz)}$_2$.

The ^{1}H NMR spectrum of compound 41 is shown in Figure 4-3. Since each complex exists as two diastereomers in solution, up to double the number of peaks anticipated for a single configuration may be observed in each spectrum. The pyrazolyl bridge proton signals are assigned by analogy with the triphenylphosphine analogue [Ir(CO)(PPh$_3$)(μ-pz)]$_2$, 39.[140] For 39, the peaks due to H$^{3,3'}$, H$^{4,4'}$, and H$^{5,5'}$ (the labelling scheme of the bridge protons is shown in Figure 4-4) are located at 7.58, 5.84, and 6.52 ppm, respectively (in CD$_2$Cl$_2$ solution). The assignment is based on the following arguments: a) H$^{4,4'}$ protons are expected to be deshielded the least among the pyrazolyl protons as they are farther away from the nitrogen atoms. b) Using a comparison to [Ir(CO)$_2$(μ-pz)]$_2$, where H^{3,5} protons exhibit signals at 7.70 ppm, the resonances at 7.58 and 6.52 ppm in the ^{1}H NMR spectrum of 39 are respectively assigned to H$^{3,3'}$ and H$^{5,5'}$, since the former is *cis* to the phosphorus ligand, experiencing less shielding effect than the latter, which is *trans* to the phosphorus. For the same reason, for compound 40, the multiplets at 5.73 and 5.76 ppm are due to H$^{4,4'}$ nuclei in the two diastereoisomers and the peaks at 7.62 and 7.58 ppm are assigned to H$^{3,3'}$ atoms. The H$^{5,5'}$ peaks are buried under the phenyl multiplets from 6.8 to 7.3 ppm. Each of the two peaks of H$^{4,4'}$ is made up of two triplets overlapping each other showing an apparent sextet. The triplet is due
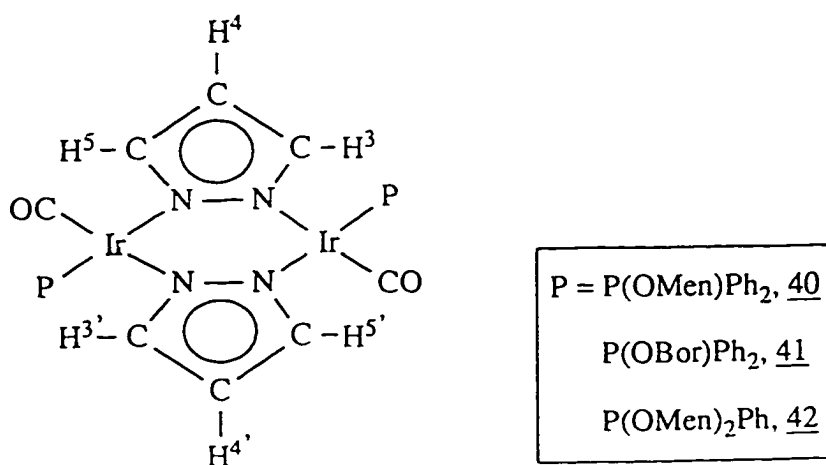
Figure 4-4. Labelling scheme for bridge protons in compounds 40 - 42.

to proton-proton coupling within the pyrazolyl ring ($^3J_{HH}$ = 2.2 Hz), while the doublet splitting is caused by the *trans* phosphorus coupling ($^4J_{HP}$ = 1.2 Hz). The H$^{3,3'}$ resonances are doublets ($^3J_{HH}$ = 2.1 Hz) due to the coupling to H$^{4,4'}$.

The peaks due to the coordinated tertiary phosphine (BorOPPh$_2$) are difficult to identify individually, with the exception of the peaks due to the α-protons in the chiral alkoxy groups; these protons appear at 5.83 and 5.66 ppm for the two diastereomers. The ^{1}H NMR spectra for compounds 41 and 42 are assigned similarly. The data are shown in Table 4-2.

Only one broad absorption is observed in the CO stretching region of each of the compounds 40 - 42. This implies that any difference in v_{CO} frequencies between the two diastereomers is too small to be detected (Table 6-18). The frequencies of the v_{CO} bands for compounds 40 - 42 (about 1900 cm^{-1}) are comparable to that for 39 (1970 cm^{-1}), and are considerably lower than those for [Ir(CO)$_2$(μ-pz)]$_2$, which possesses three

Table 4-2. Selected ^{1}H NMR data[a] for compounds 40 to 42.

Compound	δ H$^{3,3'}$ ppm	δ H$^{4,4'}$ ppm	δ α-H$_{com.}$ ppm	δ α-H$_{lig.}$ ppm
{Ir(CO)[P(OMen)Ph$_2$](μ-pz)}$_2$	7.73, 7.66	5.84, 5.76	5.47, 5.29	3.70
{Ir(CO)[P(OBor)Ph$_2$](μ-pz)}$_2$	7.62, 7.58	5.76, 5.73	5.83, 5.66	4.26
{Ir(CO)[P(OMen)$_2$Ph](μ-pz)}$_2$	7.86, 7.81	5.97, 5.93	(5.35, 4.26), (4.92, 3.91)[b]	(3.80, 3.71)

[a] Chemical shifts are given in δ(ppm) relative to internal C$_6$D$_6$ with the C$_6$H$_6$ signal set at 7.24 ppm. All spectra were recorded in C$_6$D$_6$ solution. [b] Each pair of chemical shifts in the bracket are for the protons in the same molecule.

bands (2084, 2070, 2001 cm^{-1}) in the CO stretching region. This shift to low energy may be ascribed to the better σ donating and poorer π accepting abilities of the phosphorus ligands in comparison with the CO ligand.

Compound 41 was recrystallized from THF solution to yield lustrous, bright orange, regular bar-shaped crystals. The X-ray crystal structure determination (Ms. K.A. Beveridge and Dr. G.W. Bushnell), of compound 41 revealed a very surprising phenomenon: the two diastereomers of compound 41 cocrystallized in the same unit cell. Although it is well known for enantiomers, the cocrystallization of other stereoisomers is extremely rare. There are four dimers in each unit cell. Each asymmetric unit contains half of both diastereomers, which are about 12 Å away from one another with the two Ir-Ir axes roughly parallel to each other. The molecular structures of these diastereomers are shown in Figure 4-5. Important bond angles and bond distances are shown in Table 4-3. It can be seen that these structures are similar to that of their triphenylphosphine analogue[141]. The six-membered bimetallocycle is folded into a boat conformation. The Ir-Ir distances of 3.296(3) and 3.323(3) Å (for two diastereomers) are within normal range for non-bonding Ir$_2$ separations. Both dimers possess rigorous C_2 symmetry. Each pair of terminal ligands (either CO or [(BorO)PPh$_2$]) are mutually *trans* across the metal-metal axis. However, the sense of rotation about the C_2 axis is reversed in the (*R*)-isomer *vs.* the (*S*)-isomer (*i.e.* C(1)-O(1) is forward with P(1) back in the (*S*)-isomer *vs.* P(2) forward, C(2)-O(2) back in the (*R*)-isomer). Since the bornoxy groups in both isomers possess the same stereochemistry, the reversed arrangement of the terminal ligands in the two molecules effects the diastereoisomerism between them. The geometry about each Ir(I) is approximately square planar as is common for four-coordinate mononuclear complexes of d^8 transition metal species, such as Rh(I), Pd(II), or Pt(II).

As discussed earlier, the boat-shaped six-membered central ring in compounds

(R)

(S)

Figure 4-5. Molecular structures of the two diastereomers of Compound 41

Table 4-3. Important interatomic distances and bond angles in compound 41.[a]

(a) Bond distances:

Atoms	Distance (Å)	Atoms	Distance (Å)
Ir(1)-Ir(1')	3.296(3)	Ir(2)-Ir(2')	3.323(3)
Ir(1)-P(1)	2.227(6)	Ir(2)-P(2)	2.231(5)
Ir(1)-C(1)	1.888(17)	Ir(2)-C(2)	1.792(19)
Ir(1)-N(1')	1.952(12)	Ir(2)-N(4')	2.130(12)
C(1)-O(1)	1.103(22)	C(2)-O(2)	1.216(28)
P(1)-O(5)	1.626(19)	P(2)-O(6)	1.617(14)
P(1)-C(11)	1.816(10)	P(2)-C(31)	1.816(10)

(b) Bond angles:

Atoms	Angle (°)	Atoms	Angle (°)
C(1)-Ir(1)-P(1)	89.4(7)	C(2)-Ir(2)-P(2)	93.6(8)
N(2)-Ir(1)-P(1)	93.9(4)	N(5)-Ir(2)-P(2)	92.4(4)
N(1')-Ir(1)-C(1)	88.8(9)	N(4')-Ir(2)-C(2)	89.2(9)
N(1')-Ir(1)-N(2)	87.7(9)	N(4')-Ir(2)-N(5)	85.1(9)
Ir(1)-C(1)-O(1)	162.3(25)	Ir(2)-C(2)-O(2)	163.6(25)
P(1)-O(5)-C(52)	120.1(13)	P(2)-O(6)-C(62)	117.8(11)
Ir(1)-N(2)-N(1)	115.4(6)	Ir(2)-N(5)-N(4)	117.0(3)

[a] Estimated standard deviations are given in parentheses.

<u>40</u> - <u>42</u> (see *e.g.* Scheme 4-3 at page) may undergo ring inversion, a process that is directly related to the rigidity of the bridging framework and to racemization of the inherent chirality generated by the C_2 symmetry of compound <u>39</u>. To investigate the inversion process of the six-membered bimetallocycle, variable temperature $^{31}P\{^1H\}$ NMR spectra of the equilibrium diastereomeric mixtures of compounds <u>40</u> - <u>42</u> were recorded (Figure 4-6). The spectra show that the diastereomeric ratio in each compound changes with temperature, indicating that the ring inversion does occur. However, no coalescence was observed at up to 90 °C, suggesting that the inversion is too slow to average magnetic environments in an accessible temperature range.

The cocrystallization of the two diastereomers of compound <u>41</u> made it possible to study the shift from the kinetic distribution to the thermodynamic distribution of the pair. Each unit cell of the crystals of compound <u>41</u> contains half of each diastereomer, which means the ratio of the two in the crystals is 1:1 (*i.e.* kinetic distribution). Monitoring of a solution of crystalline <u>41</u> using ^1H NMR spectroscopy (Figure 4-7) at ambient temperature showed that the ratio of the two stereoisomers changed over time, indicating that ring inversion does occur, although at a relatively slow rate. The equilibrium constant K and the rate constants k_1 and k_{-1} were determined by curve fitting (Figure 4-8). The results are: $K = 1.47 \pm 0.02$, $k_1 = (8.7 \pm 0.6) \times 10^{-4}$ s^{-1}, $k_{-1} = (6.0 \pm 0.4) \times 10^{-4}$ s^{-1}. ΔG^0_{298} was obtained from the following calculation: $\Delta G^0_{298} = -RT\ln K = 0.96 \pm 0.01$ kJmol^{-1}.

A very familiar example of dynamic change in ring conformation is provided by cyclohexane, although the latter consists of only saturated hydrocarbon groups without any substitution. Thus the conversion rate between the chair conformations in cyclohexane is extremely fast ($\sim 10^6$ s^{-1} at room temperature)[142], in comparison with the ring inversion in <u>41</u>. This is ascribed to the substitutions and the presence of heteroatoms (Ir and N), since it is well known that heteroatoms and substitutions can
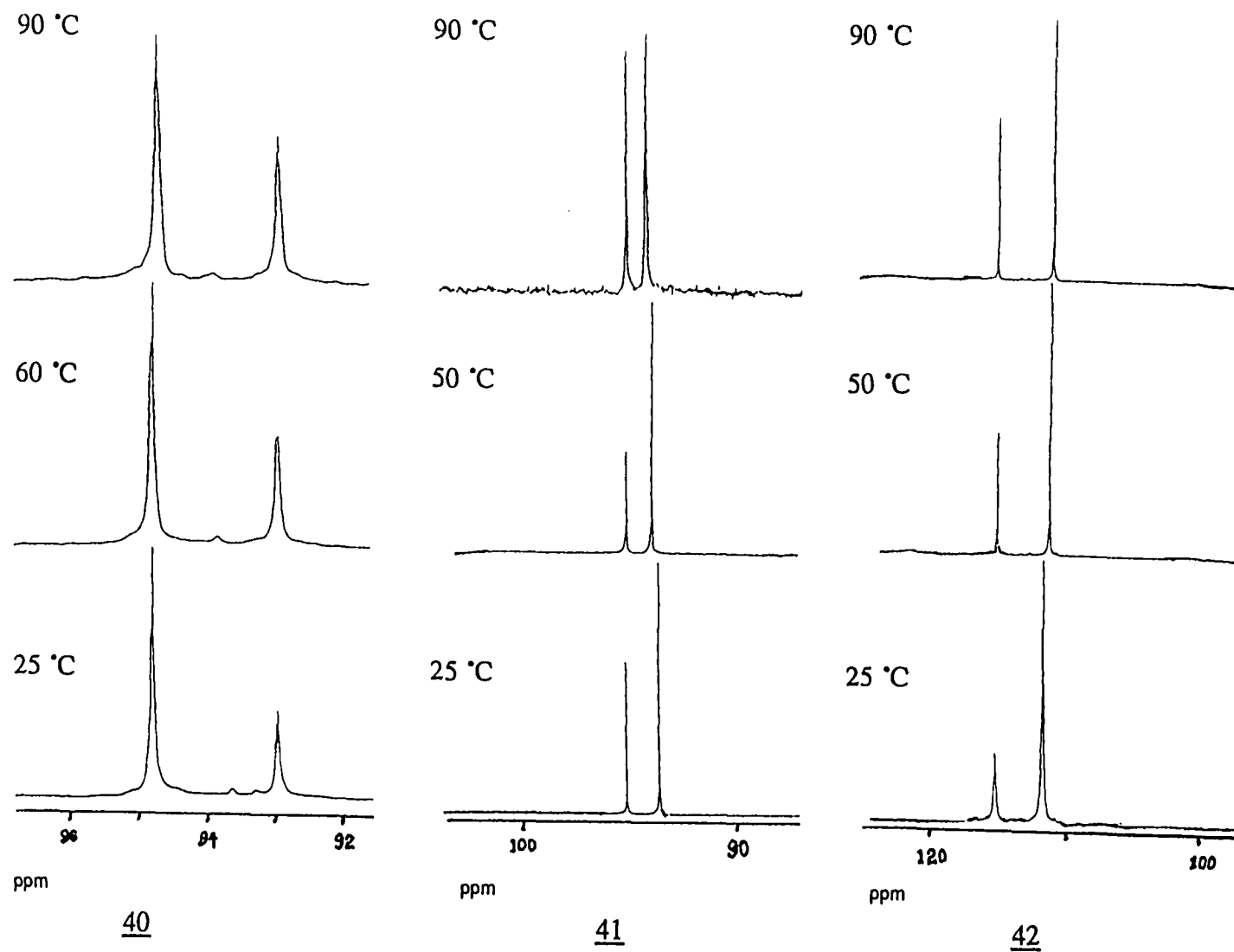
Figure 4-6. Variable temperature $^{31}P\{^1H\}$ NMR spectra of compounds 40 - 42.
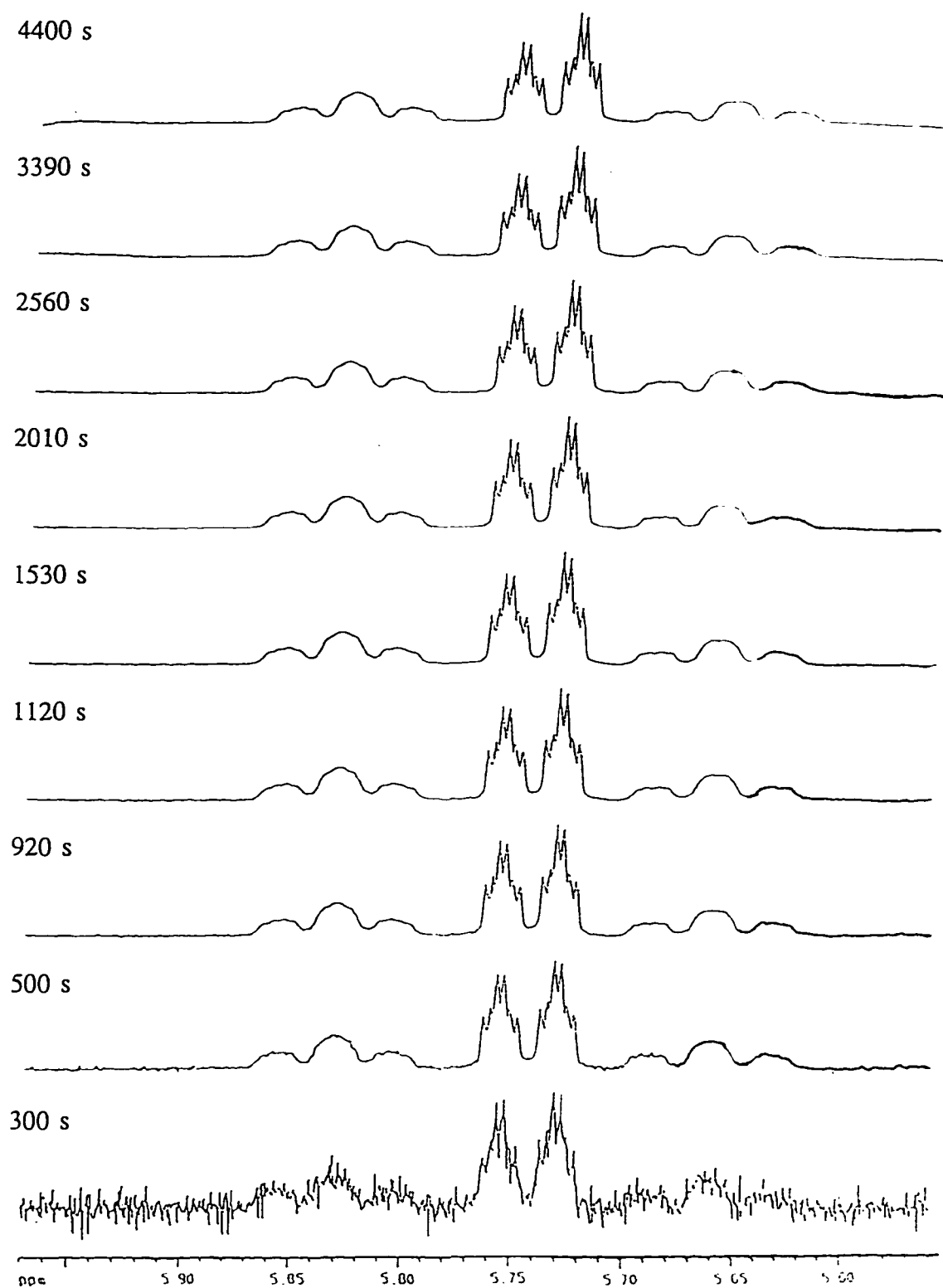
Figure 4-7. Diastereoisomerization monitored by ^{1}H NMR spectroscopy.

dramatically slow down the ring inversion process, as is evidenced by the duplodithioacetone molecule, whose inversion rate is in the order of 10^1 s^{-1} at room temperature.[143]
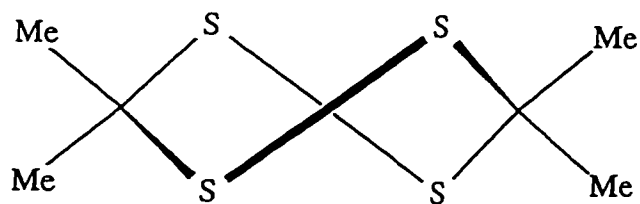
Structure of duplodithioacetone.

$$\underline{\mathbf{41a}} \xrightarrow[k_{-1}]{k_1} \underline{\mathbf{41b}}$$

$K = 1.47 \pm 0.02$

$k_1 = (8.7 \pm 0.6) \times 10^{-4}$ s^{-1}

$k_{-1} = (6.0 \pm 0.4) \times 10^{-4}$ s^{-1}.
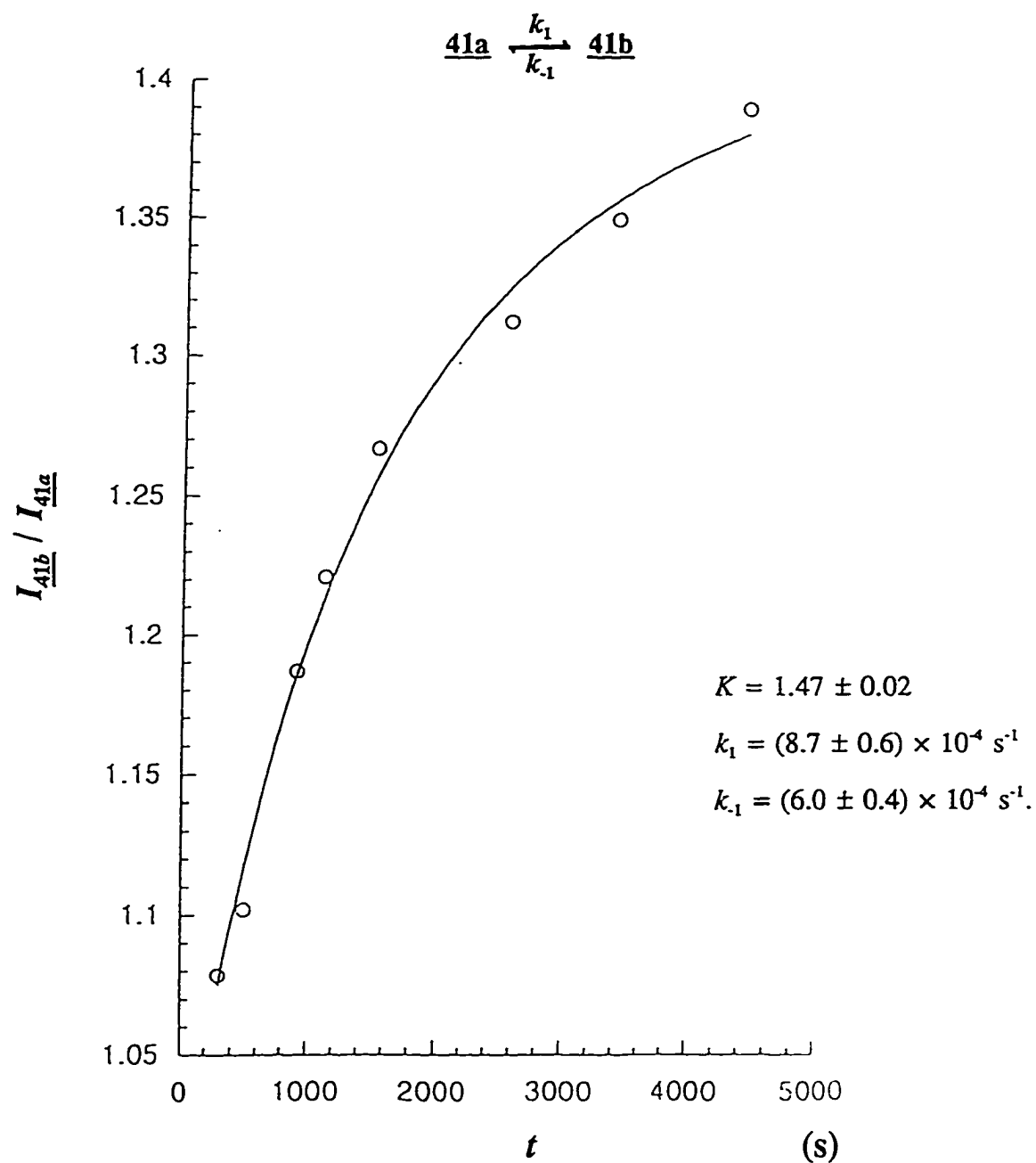
Figure 4-8. Plot of the integration ratio of the two diastereoisomers in $\underline{41}$ vs. time. $\underline{41a}$ and $\underline{41b}$: minor and major diastereomers in compound $\underline{41}$, respectively. I: integration. Equation used for curve-fitting:

$$\frac{I_{\underline{41b}}}{I_{\underline{41a}}} = \frac{2K(1+K)k_1 t - K(1-K)(e^{-\frac{1+K}{K}k_1 t} - 1)}{2(1+K)k_1 t + K(1-K)(e^{-\frac{1+K}{K}k_1 t} - 1)} \tag{4-8}$$

4.C. Methyl Iodide Addition Reaction

Because it is a C_1 unit and is one of the most reactive alkyl halides, methyl iodide is often used as a model addendum in oxidative addition reactions of both mono and dinuclear transition metal complexes, such as *trans*-IrCl(CO)(PPh$_3$)$_2$[144], Pt(PPh$_3$)$_3$[145], [(C$_5$Me$_5$)Rh(μ-PMe$_2$)$_2$Mo(CO)$_4$][146], or [Pt$_2$(dpm)$_3$][147]. Different mechanisms, including S_N2 and radical pathways, have been proposed for various complexes. As mentioned earlier, kinetics studies show that MeI addition to 37 proceeds via a concerted four-centre transition state, and MeI addition to 38 occurs through an S_N2 type reaction. In addition, qualitative kinetics data suggest that the oxidative addition of MeI to 39 is similar to that to 38, *i.e.*, an S_N2 type reaction. To investigate the corresponding reaction between 40 - 42 and MeI, especially in relation to the ring inversion process discussed in the previous section, compound 41 was used because it was available in non-equilibrium as well as equilibrium distribution.

$$\{Ir(CO)[P(OBor)Ph_2](\mu\text{-pz})\}_2 + MeI \xrightarrow{\text{THF}} Ir_2(CO)_2[P(OBor)Ph_2]_2(\mu\text{-pz})_2(Me)(I)$$

Compound 41 Compound 43 (4-9)
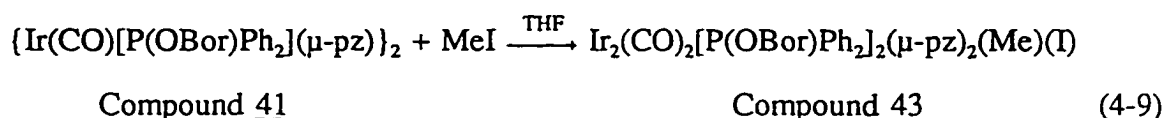
The ^{1}H NMR spectrum run within 5 minutes after the initiation of the reaction showed that the latter was essentially complete. A slight but immediate change in colour of the solution also indicates a fast reaction. The product, Ir$_2$(CO)$_2$[P(OBor)Ph$_2$]$_2$(μ-pz)$_2$(Me)(I) (compound 43, Equation 4-9), is a orange-yellow solid, stable under a N$_2$ atmosphere. The solubility of 43 in completely non-polar solvents, such as hexanes, is considerably lower than in other common organic solvents, such as CCl$_2$H$_2$, THF, or benzene. Analytical data were consistent with formulation of this product as a diiridium(II) adduct resembling those format by the analogue 39.

The mass spectrum of 43 exhibits an M + 1 peak with seven branches centred

at 1394.2 (M for $\underline{43}$ = 1393.40 g/mol). The relative intensity of the peak is 24%. The seven-lined pattern is expected since each of Ir and C has two natural isotopes: ^{191}Ir, ^{193}Ir, ^{12}C and ^{13}C. The combinations of the isotopes generate seven different detectable isotopomers of $\underline{43}$. The intensity ratio among individual fragment ions is consistent with the calculated distribution. The fragmentation peaks are also observed, two of which are most significant: the seven-lined patterns centred at 1266.2 (100%) and 1378.2 (18%), corresponding to $Ir_2[P(OBor)Ph_2]_2(CO)_2(\mu\text{-}pz)_2Me$ ($\underline{43}$ - I) and $Ir_2[P(OBor)Ph_2]_2(CO)_2(\mu\text{-}pz)_2I$ ($\underline{43}$ - Me), respectively.

The $^{31}P\{^1H\}$ NMR spectrum of compound $\underline{43}$ consists of four signals at 82.0, 81.9, 81.0, and 80.4 ppm, indicating that the two phosphorus nuclei in each diastereoisomer of compound $\underline{43}$ are differentiated since one is closer to the methyl group and the other to the iodide. By intensity relationships, the four peaks can be divided into two pairs (82.0, 81.0 ppm and 81.9, 80.4 ppm), each belonging to one diastereoisomer. The peaks are moved upfield by over 10 ppm comparing to those in compound $\underline{41}$, suggesting an increased electron shielding effect around the phosphorus nuclei. This is probably because oxidative addition to $\underline{41}$ reduces the electron density at the iridium centres with a change in formal oxidation state from +1 to +2. This results in less π back-donation to the phosphorus atom, hence less shielding.

Because the two entering groups, Me and I, create different chemical environments around the two iridium centres in each of the two diastereoisomeric dimers (*i.e.* the symmetry is reduced from C_2 to C_1), the ^1H NMR spectrum of $\underline{43}$ (Figure 4-9) is much more complicated than that of unoxidized $\underline{41}$. The resonances due to the four $H^{4,4'}$ protons (the labelling scheme of the bridge protons is shown in Figure 4-10) in the two diastereoisomers are shifted slightly upfield from the iridium(I) dimers to 5.65, 5.49, 5.42, and 5.37 ppm. All signals are quartets (J = 2.12, 2.16, 2.11, and 2.13 Hz, respectively), indicating coincidentally equal coupling constants between $H^{4,4'}$ and $H^{5,5'}$,
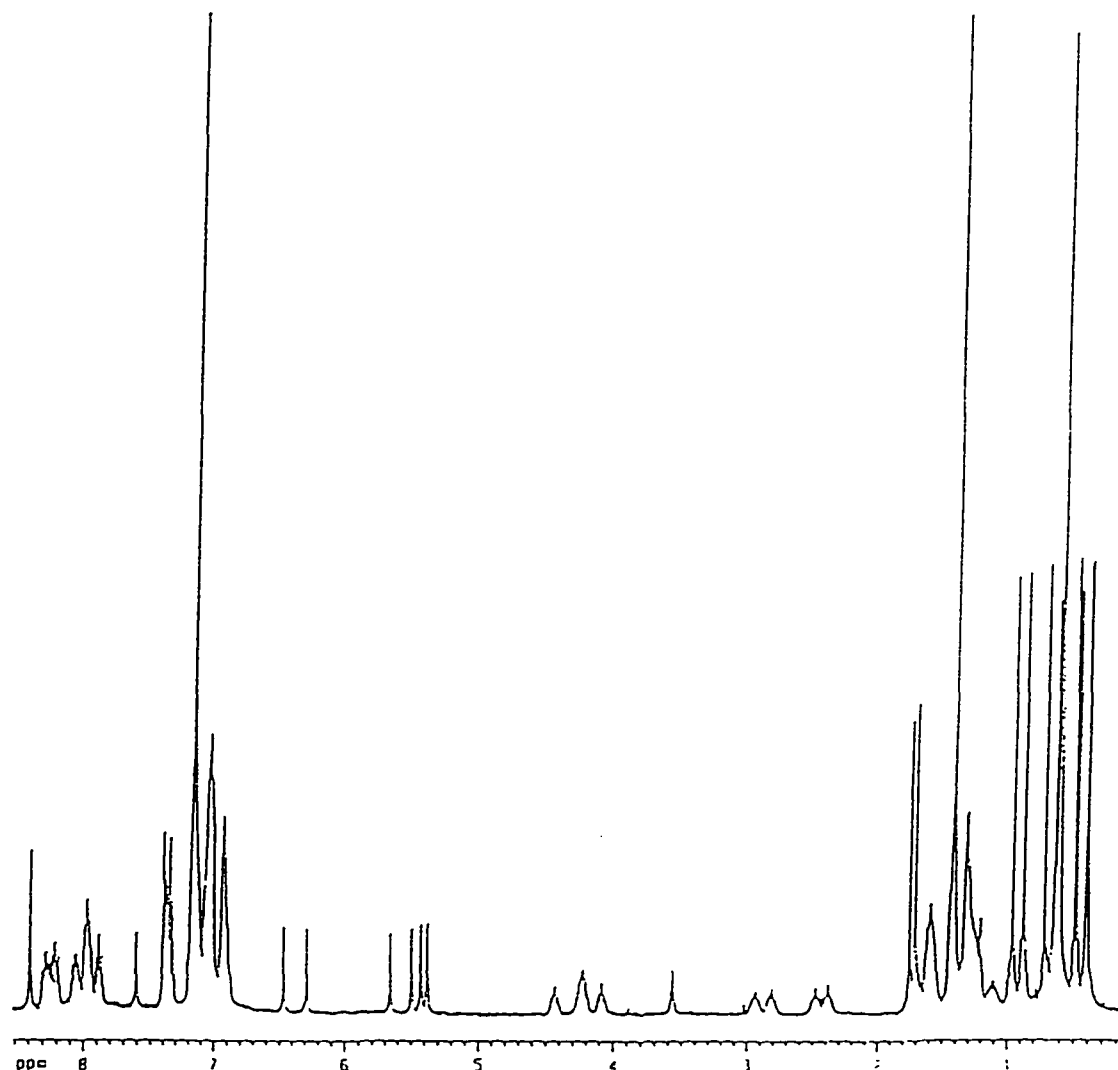
Figure 4-9. ^{1}H NMR spectrum of compound $\underline{43}$.

H$^{3,3'}$, and the *trans*-phosphorus atoms. The H$^{5,5'}$ peaks are also repositioned at a higher field, giving two broad singlets at 6.46, and 6.28 ppm, while the H$^{3,3'}$ peaks shifted to 7.39 (J = 2.20 Hz), 7.37 (broad singlet), 7.34 (broad singlet) and 7.31 (J = 2.15 Hz) ppm. The peaks due to the α-protons in the bornoxy groups are found as three multiplets at 4.42, 4.22, and 4.07 ppm, with the middle peak integrating for two protons and showing a more complicated pattern than the other two. The changes in chemical shift are in the same sense as those in the ^{31}P{^{1}H} NMR spectrum, and are probably due

$P = P(OBor)Ph_2$, 43
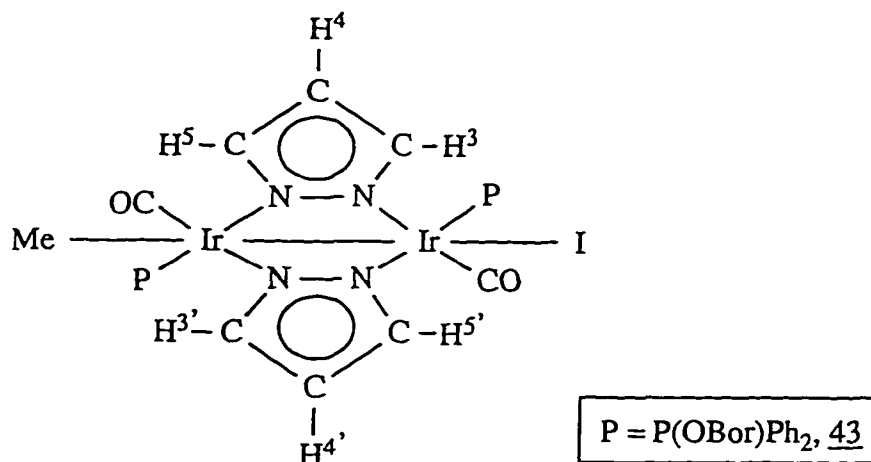
Figure 4-10. Labelling scheme of the bridge protons in compound 43.

to the same effect (*vide supra*). The peaks due to the methyl groups bonded to the iridium centres are found at 1.75, and 1.70 ppm as doublets ($^3J_{HP}$ = 1.73, and 1.89 Hz, respectively).

The ^{1}H NMR spectrum of 43 shown in Figure 4-9 was obtained by dissolving crystalline 41 in a 5% C_6D_6 solution of MeI in a NMR tube. The kinetic distribution (1:1) between the two atropisomers in 41 was found to be unchanged after reaction with MeI, *i.e.* showing a 1:1 ratio between the two diastereomers in 43. When 41 in thermodynamic distribution (40:60) was reacted with MeI, the same ratio (40:60) was also observed in the product (43).

The C_2 symmetry in 41 is eliminated when the methyl group and the iodide anion add to two different iridium centres to form 43. This is reflected in the IR spectrum of compound 43, which shows two v_{CO} bands at 2017 and 1983 cm^{-1}. Compared to the single broad v_{CO} band at 1971 cm^{-1} in 41, those in 43 are shifted to high frequency as expected because of the reduced electron density at the iridium centre. As in the IR spectrum of 41, the difference in the carbonyl stretching frequencies between the two diastereoisomers in 43 is too small to be detected.

A very interesting observation is made when 43 is left in solution over a long

period of time: the ratio of the two diastereoisomers in 43 shifts very slowly away from the distribution observed initially. At room temperature, this diastereoisomerization process goes to completion in about 10 days, giving a thermodynamic distribution of about 60:40 (Figure 4-11). The equilibrium constant ($K = 1.5 \pm 0.2$) and observed rate constants ($k_1 = (2.1 \pm 0.2) \times 10^{-6}$ s^{-1}, $k_{-1} = (1.4 \pm 0.2) \times 10^{-6}$ s^{-1}) are obtained by curve fitting (Figure 4-12). When a substantial excess (about 10 fold) of methyl iodide is present in the solution, the reaction is slowed down so much that the ratio does not change within six days, indicating that the interconversion of the two diastereomers in 43 involves dissociation of methyl iodide. The overall reaction pathway will therefore follow Scheme 4-8: From one diastereoisomer in 43 (*e.g.* 43a), reductive elimination of methyl iodide will regenerate 41a. The ring-inversion of the latter leads to the other isomer of 41 (41b), oxidative addition of methyl iodide to which affords 43b, completing the stereomutation. All steps are in equilibrium. Since the overall reaction is about 400 times slower than the rate of interconversion between 41a and 41b ($k_1 = (8.7 \pm 0.6) \times 10^{-4}$ s^{-1}, $k_{-1} = (6.0 \pm 0.4) \times 10^{-4}$ s^{-1}, see page 107), the reductive elimination of methyl iodide must be the rate determining step.

41a   ⇌   41b

\+   \+

MeI   MeI

43a   43b
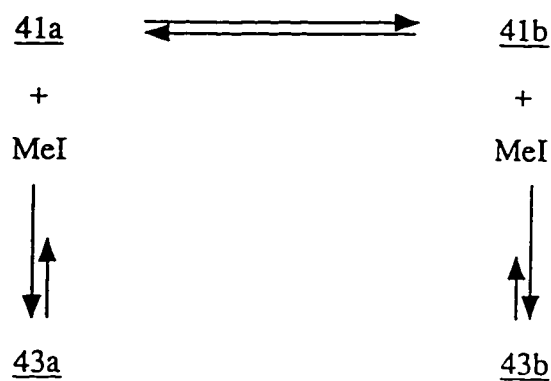
Scheme 4-8. Proposed mechanism for interconversion of the two diastereomers in 43.

0 min.

864 min.

1213 min.

3003 min.

4384 min.

5575 min.

7015 min.

11501 min.

ppm   6.4   6.2   5.6   5.4
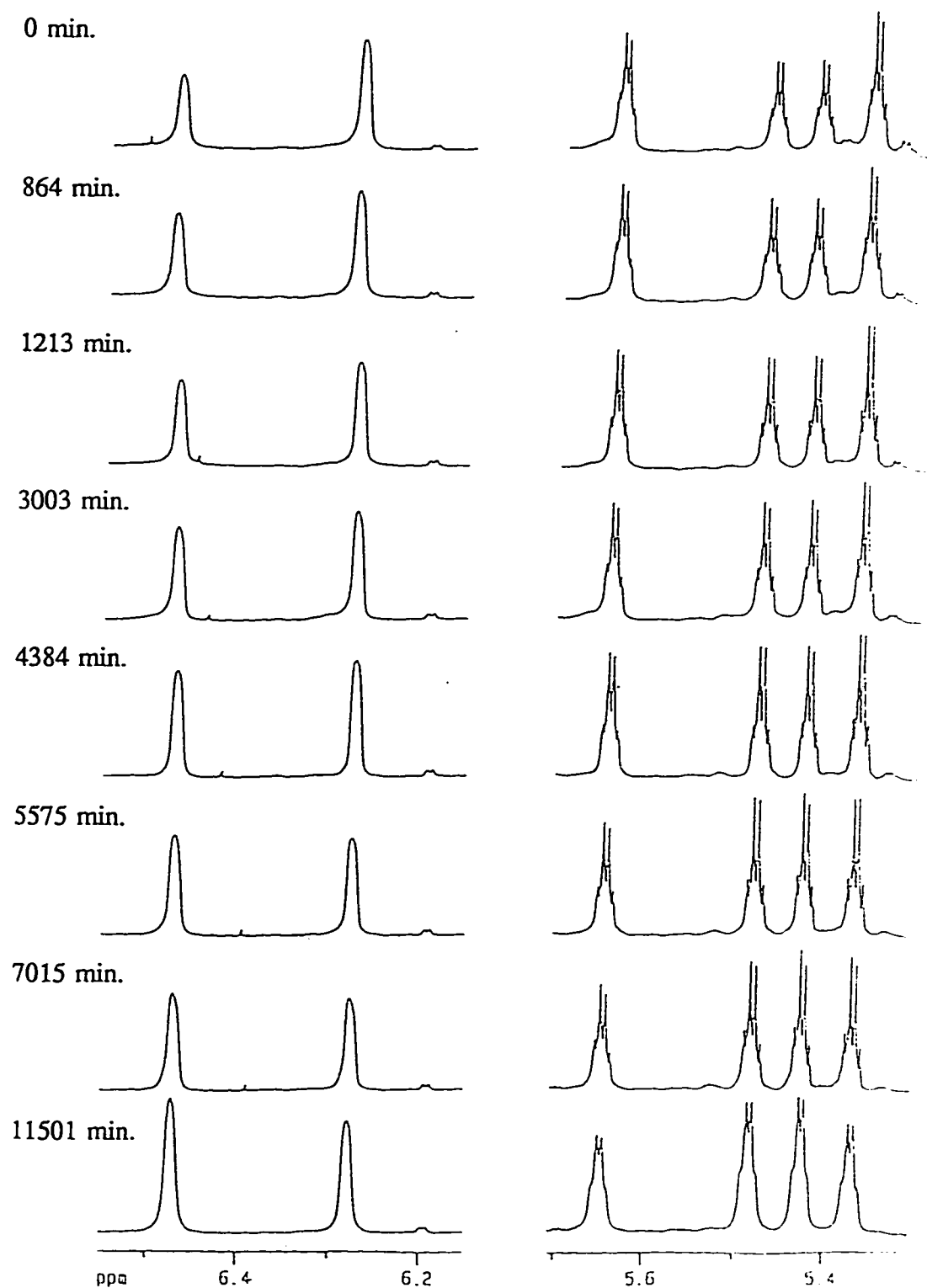
Figure 4-11. ^{1}H NMR of the interconversion process of the two diastereomers in 43.

$$\underline{43a} \xrightarrow[k_{-1}]{k_1} \underline{43b}$$

$K = 1.5 \pm 0.2$

$k_1 = (2.1 \pm 0.2) \times 10^{-6} \text{ s}^{-1}$

$k_{-1} = (1.4 \pm 0.2) \times 10^{-6} \text{ s}^{-1}.$
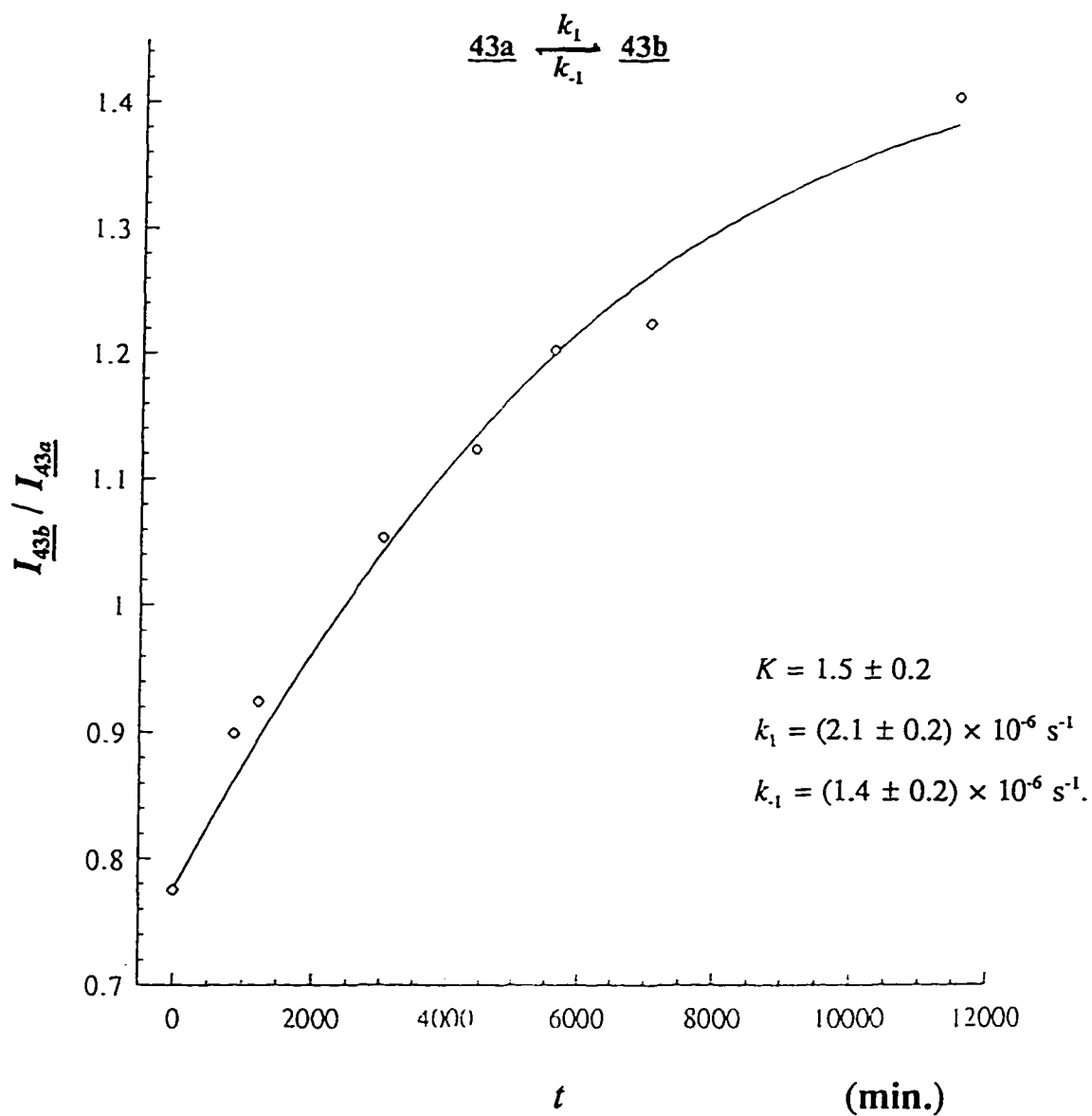
Figure 4-12. Plot of the integration ratio of the two diastereoisomers in $\underline{43}$ vs. time. $\underline{43a}$ and $\underline{43b}$: minor and major diastereomers in compound $\underline{43}$ at equilibrium, respectively. I: integration. Equation used for curve-fitting:

$$\frac{I_{\underline{43b}}}{I_{\underline{43a}}} = \frac{k_1 - [k_1 - (k_1 + k_{-1}) \frac{1}{[I_{\underline{43a}}/I_{\underline{43b}}]_0 + 1}] e^{-(k_1 + k_{-1})t}}{k_{-1} - [k_{-1} - (k_1 + k_{-1}) \frac{1}{[I_{\underline{43b}}/I_{\underline{43a}}]_0 + 1}] e^{-(k_1 + k_{-1})t}} \qquad (4-10)$$

where $[I_{\underline{43a}}/I_{\underline{43b}}]_0$ is the initial integration ratio.

The rate of the addition reaction of MeI to $\underline{41}$, which is too fast to be monitored by using NMR, is clearly much faster than that of the ring inversion, implying that the latter is not part of addition mechanism. Previous studies postulated that the mechanism of the methyl iodide addition to $\underline{39}$, the triphenylphosphine analogue of $\underline{41}$, is of S_N2 type (Scheme 4-5, page 93), based on the fact that the kinetic profiles of MeI addition to $\underline{38}$ and $\underline{39}$ resemble each other and are very different to that with $\underline{37}$.[148] Thus the equilibrium constants for the reactions with $\underline{38}$ and $\underline{39}$ are obviously much bigger than that of $\underline{37}$, although they have not been measured. Products are formed irreversibly from $\underline{38}$ or $\underline{39}$, while the adduct of $\underline{37}$ can be isolated from solution only when large excess (100 fold) of MeI is present. Significantly, therefore, the behaviour of the diastereomeric adducts $\underline{43a}$ and $\underline{43b}$ supports the earlier assumption that the back-reaction (*i.e.* reductive elimination of MeI) is slow from $\underline{38}$ to $\underline{39}$.

This evidence strongly suggests that adduct formation from diastereomeric $\underline{41}$ resembles the behaviour of $\underline{38}$ and $\underline{39}$ although other reaction pathways (*e.g.* radical) have not been specifically excluded. Although the S_N2 mechanism appears to be dominant in the MeI addition to Vaska's complex, there is evidence that for $Pd(PPh_3)_3$, both S_N2 and radical pathways can operate.[109] A more detailed kinetic investigation of the reaction of $\underline{41}$ with MeI would include examination of the solvent effect on reaction rates, and the effect of radical initiators or scavengers. This would constitute a major task because each of two separate diastereomeric manifolds (from $\underline{43a}$ to $\underline{41a}$ and from $\underline{43b}$ to $\underline{41b}$, Scheme 4-8) are operating simultaneously. Since the addition reaction proceeds rapidly, "fast techniques", such as stopped flow may prove to be useful. The rate constant may also be acquired by determining the rate constants for the equilibrium between $\underline{43a}$ and $\underline{43b}$ (Scheme 4-8) under pseudo first order conditions, *i.e.* with the presence of large excess of MeI.

Because of the stereomutation between the two isomers of $\underline{41}$ in solution, and

the fortuitous cocrystallization of the two in the solid state, the isolation of a pure diastereomer was not achieved in this system. However, in spite of the ring-inversion process, the much more rapid rate of addition of MeI to $\underline{41}$ suggests that asymmetric induction would be possible using a complex of this type in a catalytic process occurring at a suitable rate.

4.D. Addition of Norbornyl Iodide to $[Ir(CO)_2(\mu\text{-}pz)]_2$

Several alkyl halides adducts of $[Ir(CO)_2(\mu\text{-}pz)]_2$ $(\underline{38})$, including $[Ir_2(CO)_4(\mu\text{-}pz)_2(Me)(I)]$, $[Ir_2(CO)_4(\mu\text{-}pz)_2(Me)(Br)]$, $[Ir_2(CO)_4(\mu\text{-}pz)_2(Et)(I)]$, $[Ir_2(CO)_4(\mu\text{-}pz)_2(Pr)(I)]$, $[Ir_2(CO)_4(\mu\text{-}pz)_2(octyl)(I)]$, and $[Ir_2(CO)_4(\mu\text{-}pz)_2(octadecyl)(I)]$, have been synthesized by oxidative addition of corresponding alkyl halides to $\underline{38}$.[140] The kinetic investigation of MeI addition to $\underline{38}$ showed evidence for a S_N2 type mechanism.[148] However, the addition rates were found to increase with increasing chain length when longer chain alkyl halides were used. This is contrary to that expected on steric grounds for an S_N2-type reaction, where the increased steric bulk of the alkyl chain would encumber the transition state.[149] Also, the rate difference observed in primary *vs.* secondary alkyl addition to $\underline{38}$ is consistent with a mechanism involving either a carbocation or a radical intermediate. Since the stereochemistry of the addition process is directly related to its mechanism, this area has been extended as part of the present study to examine the reaction of the tetracarbonyl dimer $\underline{38}$ with bulky alkyl halides based on a chiral framework like those referred to in earlier chapter. *Exo-* and *endo*-norbornyl iodides (*exo-* and *endo*-2-iodobicyclo[2.2.1]heptane; for convenience these two compounds will be abbreviated as *exo-* and *endo*-R˙I, respectively, Figure 4-13) were selected as model substrates because each of them is relatively easy to prepare, because their NMR spectra can be readily interpreted, and because they are closely related to the bornyl group

J

which is the chiral focus of the phosphine ligand in the crystallographically characterized diastereomeric pair, 41a and 41b (see Figure 4-5 at page 101). The behaviour of these diastereomeric iodides towards dimer 38 was conceived as a preliminary to studying their addition to either 41a or 41b.

exo-norbornyl iodide   *endo*-norbornyl iodide
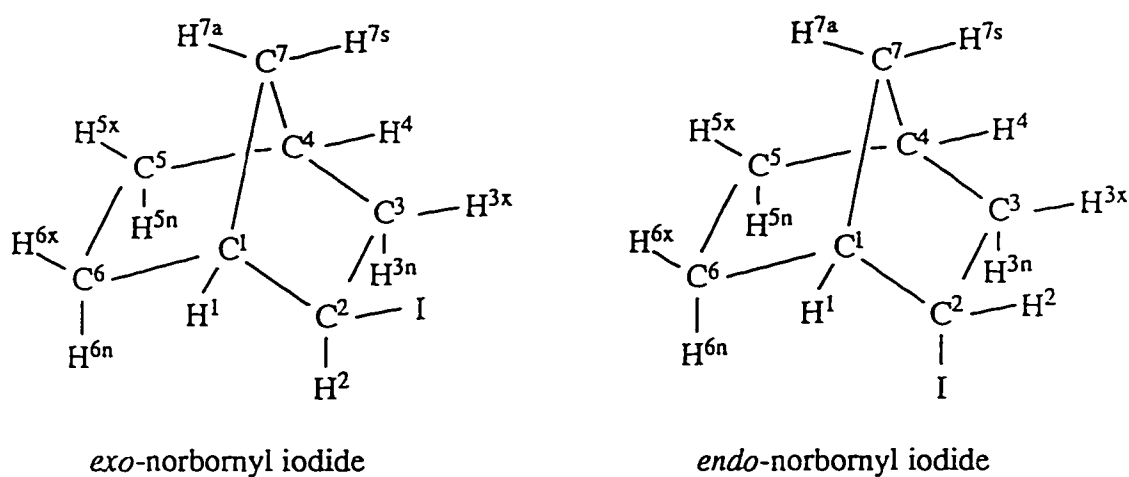
Figure 4-13. Molecular structures of *exo*- and *endo*-norbornyl iodide.

Exo-norbornyl iodide was synthesized through the addition reaction of HI to norbornene (bicyclo[2.2.1]hept-2-ene, Scheme 4-9); the product is an analogue of *exo*-norbornyl chloride reported by Brown *et al.*.[150] *Endo*-norbornyl iodide was prepared
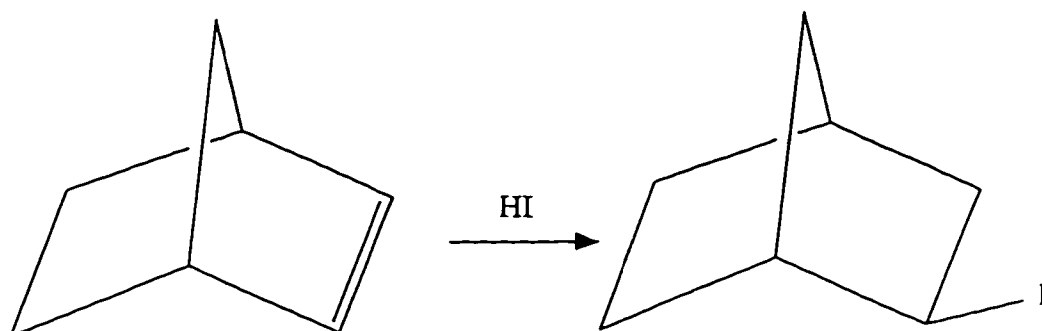
Scheme 4-9. Synthesis of *exo*-norbornyl iodide.

using a procedure that was also first reported by Brown *et al.*[151] (Scheme 4-10): this produces the *endo* isomer as the major product via a hydroboration step. Both iodides are colourless liquids that are thermally stable in the dark, but gradually decompose when exposed to light.
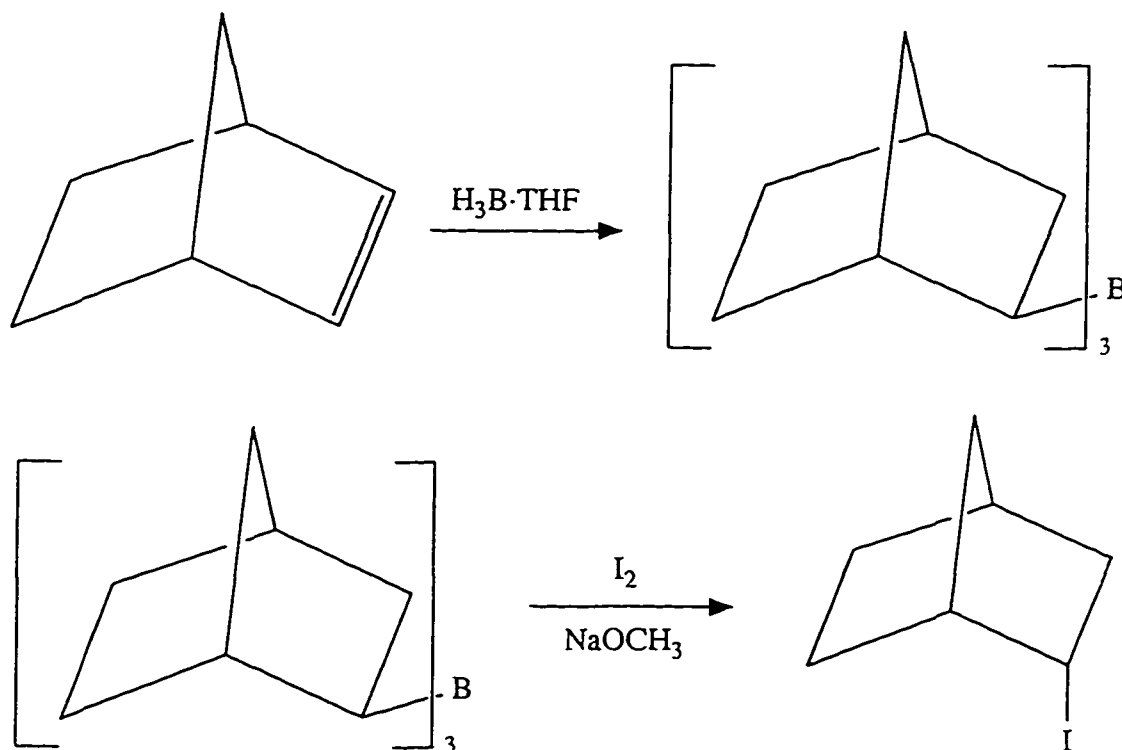
Scheme 4-10. Synthesis of *endo*-norbomyl iodide.

The chemical shifts of the resonances in the $^{13}C\{^1H\}$ NMR spectrum of *exo*-R*I recorded in C_6D_6 solution are comparable with the values obtained from $CDCl_3$ solution[152], with the largest deviation being less than 0.4 ppm. The assignment of individual resonances is listed in Table 4-4. The ^1H NMR spectrum of *exo*-R*I in C_6D_6 solution, however, shows considerable difference from that in $CDCl_3$.[153] Chemical shift differences of up to 0.36 ppm (for H^{2n}: for labelling schemes for *exo*- and *endo*-R*I, see Figure 4-13) were observed between these two solvents. The relative positions of some

of the resonances also appear to be altered: *e.g.* in C_6D_6, the H^{3x} resonance is well separated to low field of the H^4 resonance whereas in $CDCl_3$, these two signals overlap with H^{3x} centred at slightly higher field. To clarify the interpretation of this complicated spectrum, $^1H/^1H$ homonuclear and $^{13}C/^1H$ heteronuclear COSY (COrrelation SpectroscopY) NMR spectra of *exo*-R˙I were recorded. These two routines are extremely useful in revealing the spin coupling relationships between individual pairs of nuclei in a molecule, so helping to interpret the 1-D NMR spectrum. Further use was made of COSY spectra in analyzing the NMR spectra of products formed from the iridium dimer (38). Based on the $^{13}C/^1H$ and $^1H/^1H$ COSY NMR spectra of *exo*-R˙I in C_6D_6 (Figures 4-14 and 4-15, respectively), and the peak assignment for the spectrum from the $CDCl_3$ solution, the resonances in the ^1H NMR spectrum of *exo*-R˙I in C_6D_6 are reassigned as shown in Figure 4-15.

The resonances in the $^{13}C\{^1H\}$ NMR spectrum of *endo*-R˙I can be readily

Table 4-4. $^{13}C\{^1H\}$ NMR data[a] for *exo*-, *endo*-R˙I, and compound 44.

Compound	$\delta\ C^1$ ppm	$\delta\ C^2$ ppm	$\delta\ C^3$ ppm	$\delta\ C^4$ ppm	$\delta\ C^5$ ppm	$\delta\ C^6$ ppm	$\delta\ C^7$ ppm
exo-norbornyl iodide	47.9	29.5	45.0	37.9	28.2	28.3	36.1
endo-norbornyl iodide	44.6	31.7	43.1	36.8	28.4	29.5	35.9
$Ir_2(CO)_4(\mu\text{-pz})_2(\text{norbornyl})(I)$,[b] 44	50.0	32.7	46.8	39.2	29.9	32.1	38.1

[a] Chemical shifts are given in δ (ppm) relative to internal C_6D_6 with the middle branch of C_6D_6 signal set at 128.0 ppm. All spectra were recorded in C_6D_6 solution. [b] Only the chemical shifts for the carbons in the norbornyl groups are listed. See text for the rest of peak assignment.
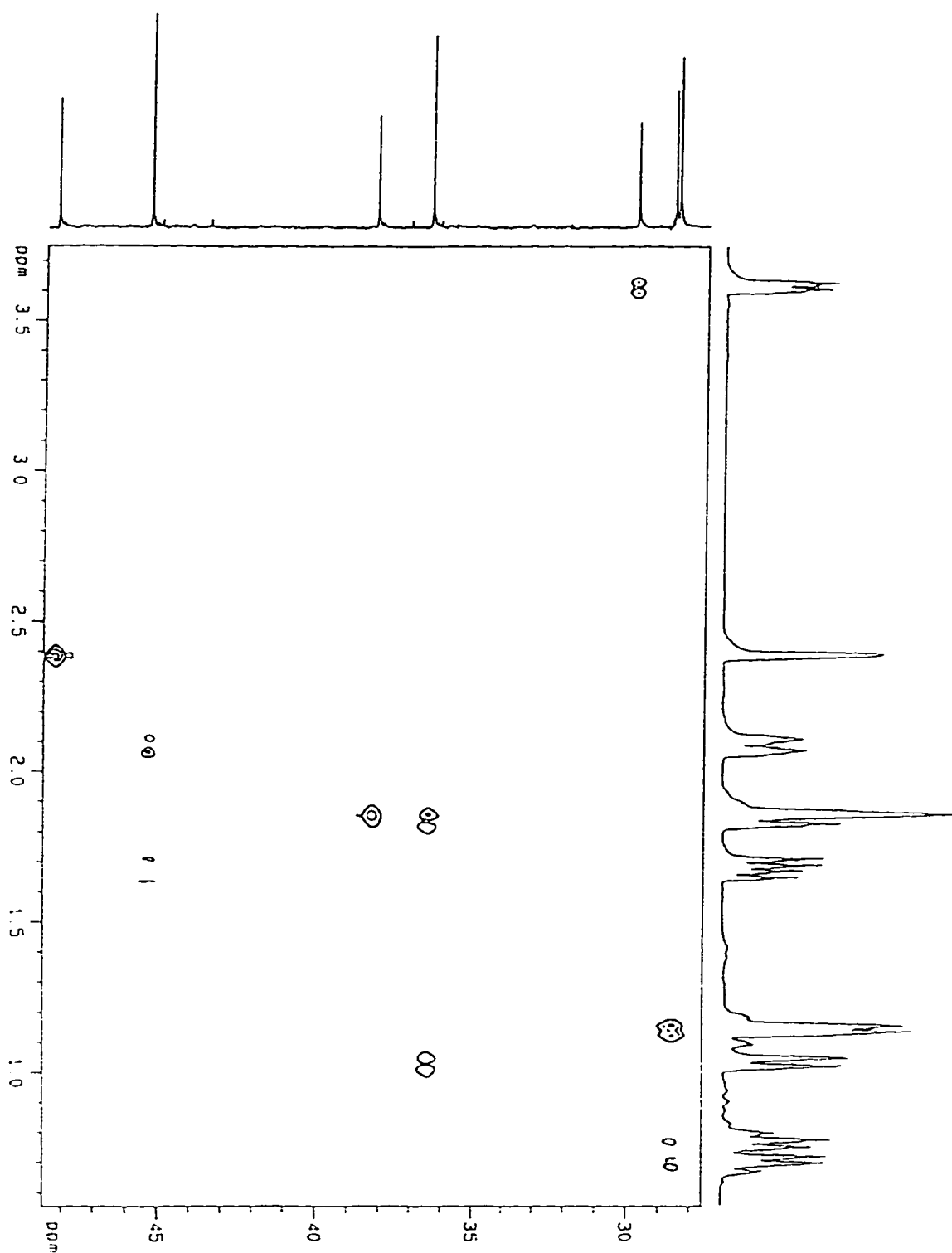
Figure 4-14. $^{13}C/^1H$ cosy NMR spectrum of *exo*-norbornyl iodide.
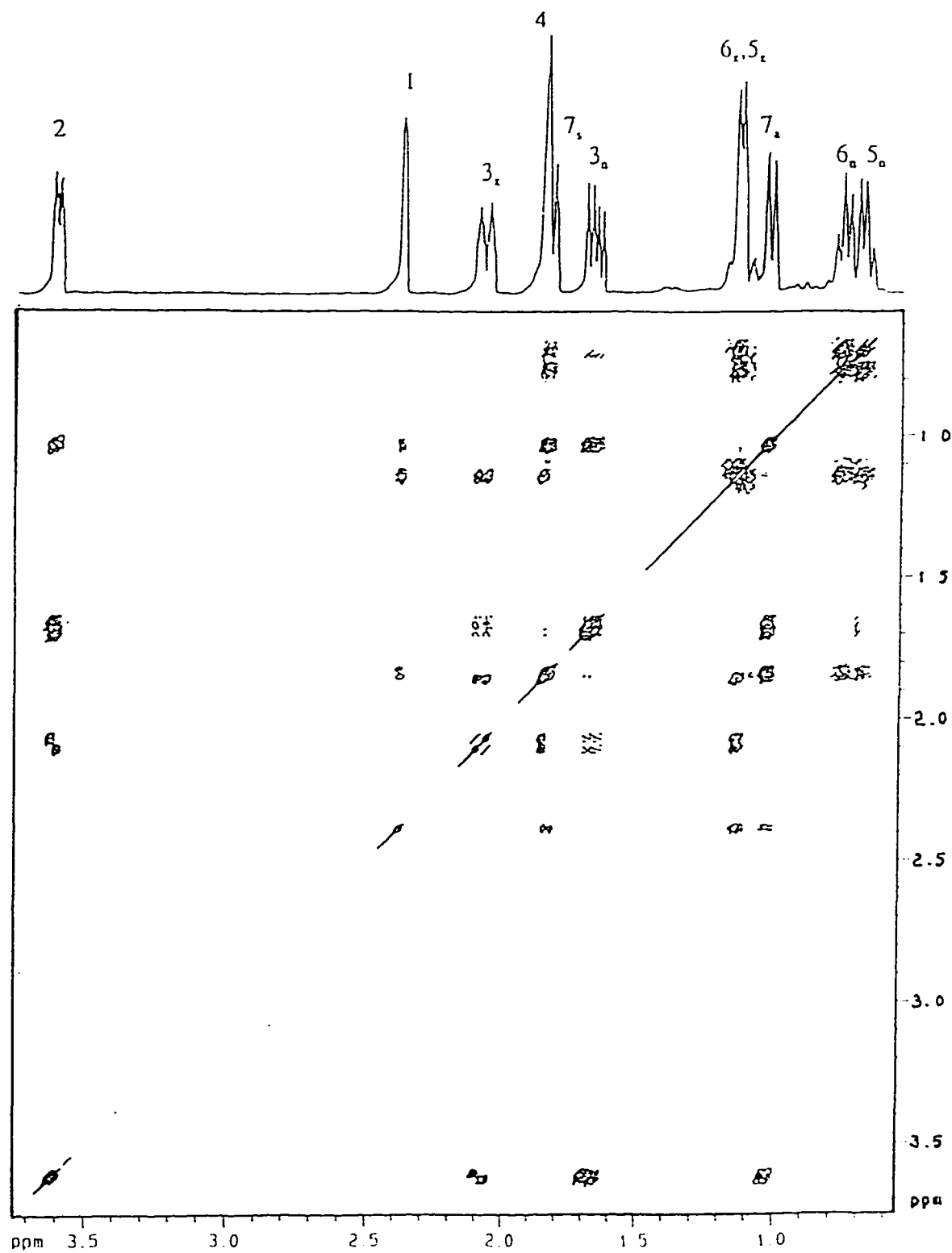
Figure 4-15. The ^{1}H/^{1}H cosy NMR spectrum of *exo*-norbornyl iodide.

assigned (Table 4-4), by making appropriate comparisons with the spectrum of *exo*-R˙I. The $^{13}C\{^1H\}$ NMR spectra of the two isomers are very similar, with only small variations in chemical shifts in corresponding resonances. The largest chemical shift difference is that for the C^1 resonance, which is shifted upfield by 3.3 ppm (to 44.6 ppm) for the *endo* diastereomer compared with that of the *exo*-R˙I. This is because in the *endo* structure, the iodine atom is bent farther away from C^1 due to increased sterical hinderance on the *endo*- norbornyl face.

The resonances in the ^1H NMR spectrum of *endo*-R˙I were assigned (Figure 4-16) by analyzing the $^1H/^1H$ and $^{13}C/^1H$ COSY NMR spectra (Figures 4-16 and 4-17, respectively). Significant variation is found between the spectra of *endo*- and *exo*-R˙I because of the structural differences between the isomers: the *endo* iodine atom is distant from the H^{7s} and H^{7a} protons, so that its interactions with the H^7 protons are minimal. This results in a non-first order AB pattern centred at 0.88 ppm for the two H^7 protons in the ^1H NMR spectrum of *endo*-R˙I. However, in the ^1H NMR spectrum of the *exo* isomer, H^{7a} and H^{7s} are well separated (1.04 and 1.83 ppm, respectively), because of relative proximity effects to the iodine atom; the latter is much closer to the H^{7s} than to H^{7a}. Similarly, while the resonances for the H^6 protons are located at 1.16 and 0.79 ppm in the ^1H NMR spectrum of the *exo* isomer, the peaks for the same protons are found at 1.89 ppm as one multiplet showing possible AB character in the ^1H NMR spectrum of the *endo* isomer.

In both *exo*- and *endo*-R˙I, the H^2 protons are coupled with $H^{3x,n}$ protons. However, in the *exo* isomer, H^2 is also coupled with H^{7a} due to the long range coupling often observed for protons separated by three carbons in a "W" conformation (in this case, H^{7a}, C^7, C^1, C^2, and H^2 are in a "W" shape)[154]; while in the *endo* isomer, additional splitting of the H^2 resonance is caused by H^{6x}, also due to the "W" coupling, and H^1. The coupling between H^1 and H^2 is not observed in the *exo* isomer, since the
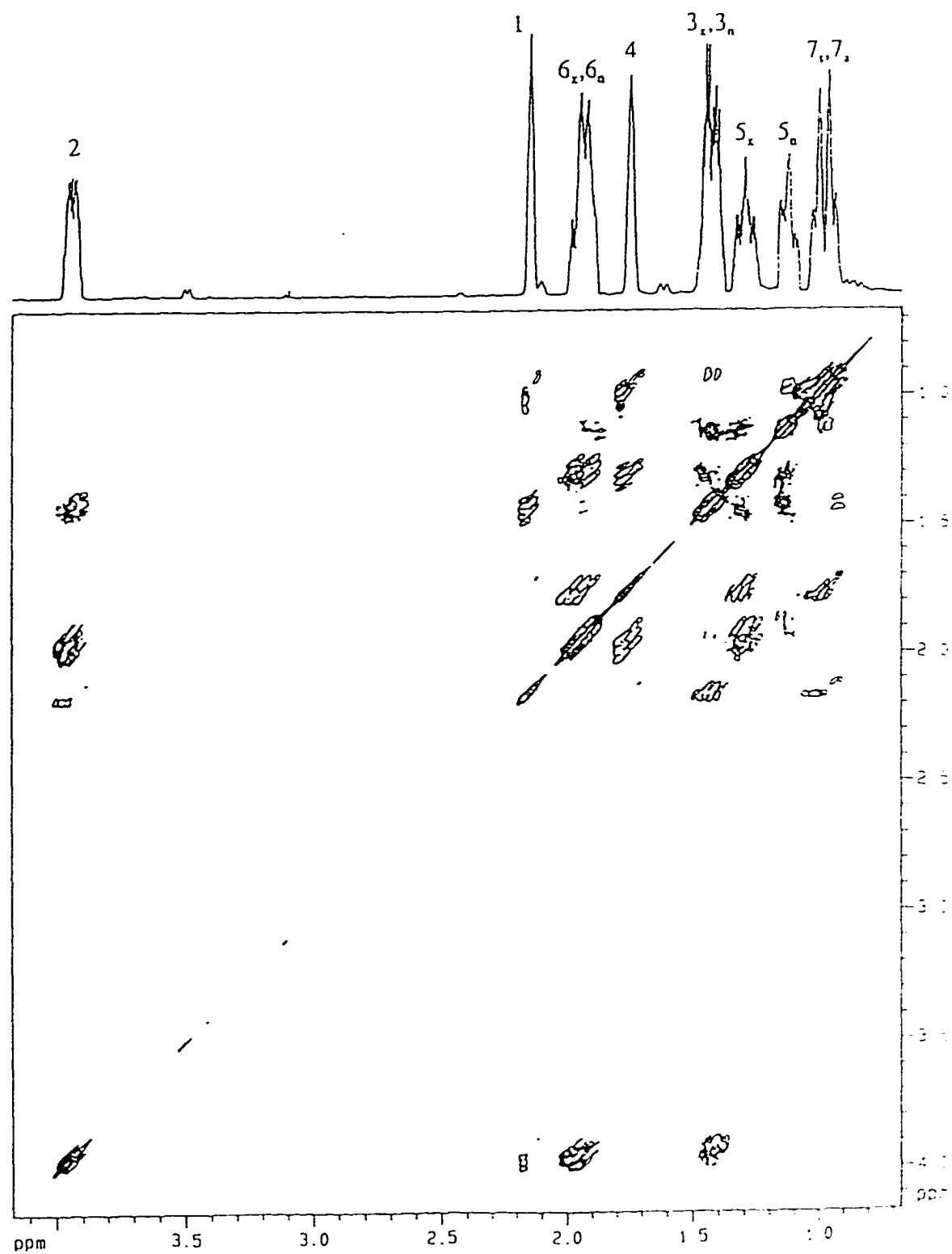
Figure 4-16. ^{1}H/^{1}H cosy NMR spectrum of *endo*-norbornyl iodide.
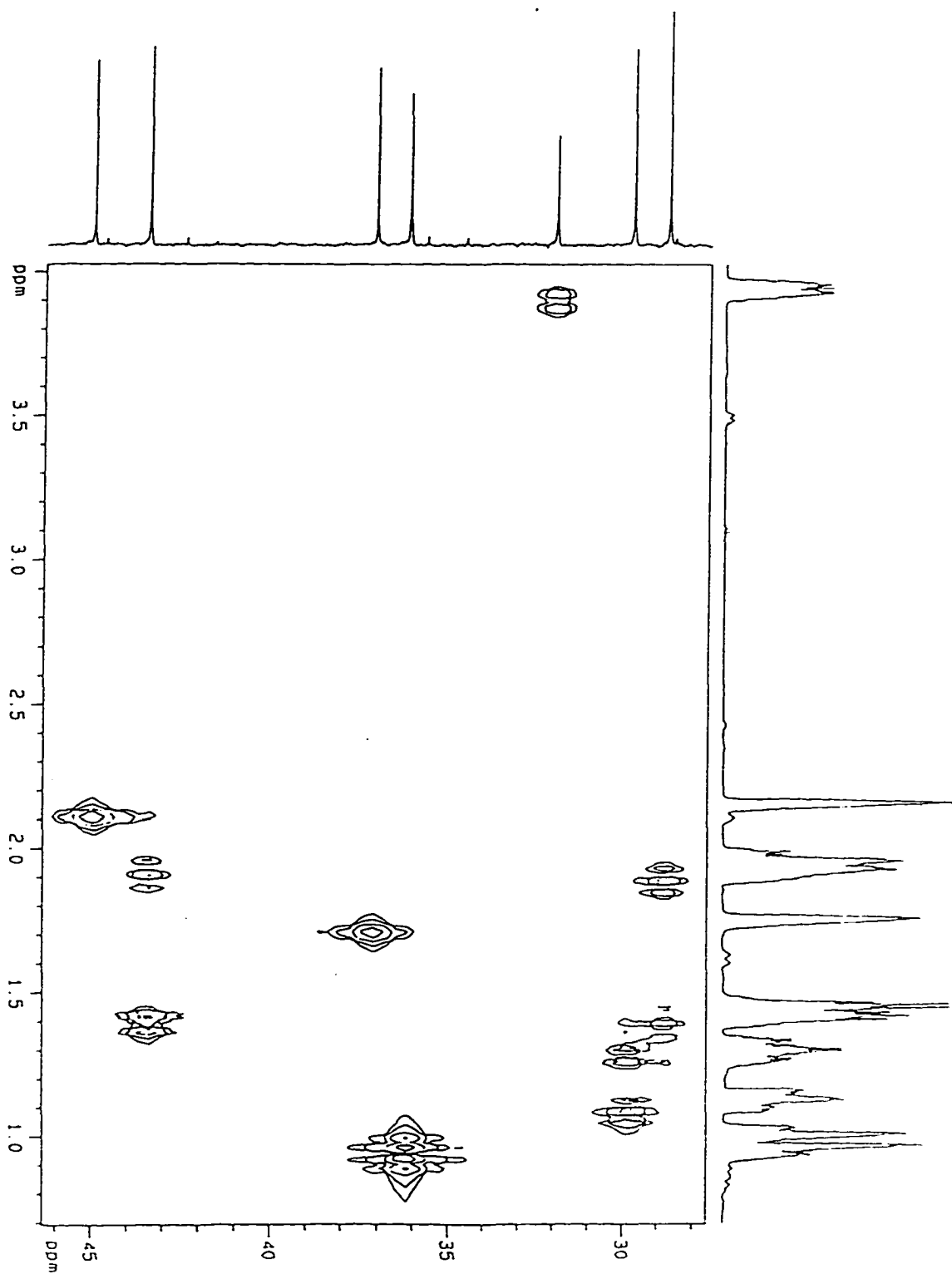
Figure 4-17. $^{13}C/^{1}H$ cosy NMR spectrum of *endo*-norbornyl iodide.

dihedral angle between the H^1-C^1 and C^2-H^2 bonds is approaching 90°, at which angle, $^3J_{H(1),H(2)}$ will be too small to be detected; whereas in the *endo* isomer, the same angle is close to 0°, at which, $^3J_{H(1),H(2)}$ will be at its maximum.[155]

Both *exo-* and *endo-*R*I were found to undergo oxidative addition with $[Ir(CO)_2(\mu\text{-pz})]_2$ (compound 38, Equation 4-9). Compound 38 was generated by the reaction between $[Ir(COD)(\mu\text{-pz})]_2$ and CO, and thereafter used *in situ*. The reactions in THF are complete within 5 min as evidenced by the IR spectra. Instant colour change of the solution from bright yellow to orange is observed. The adducts are fine orange yellow crystalline powders, soluble in THF, benzene, or dichloromethane, but not in hexanes or pentane.

$$\{Ir(CO)_2](\mu\text{-pz})\}_2 + \textit{exo-} \text{ or } \textit{endo-}R^{\bullet}I \xrightarrow{\text{THF}} Ir_2(CO)_4(\mu\text{-pz})_2(\text{norbornyl})(I)$$

Compound 38   Compound 44   (4-11)
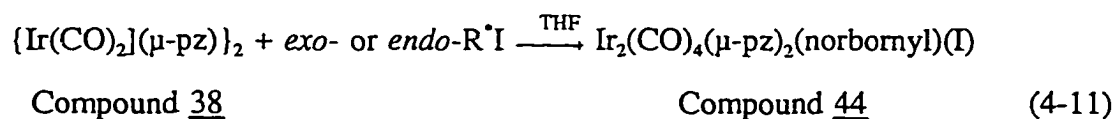
Analysis of the reaction products by IR, $^{13}C\{^1H\}$ NMR, and ^1H NMR spectra showed that use of either *exo-* or *endo-*R*I afforded an identical adduct: $Ir_2(CO)_4(\mu\text{-pz})_2(\text{norbornyl})(I)$, 44. In the IR, four bands were found at the same frequencies (2105, 2072, 2048, and 2029 cm^{-1}, Figure 4-18), *i.e.* to higher wavenumber than those in the IR spectrum of $[Ir(CO)_2(\mu\text{-pz})]_2$ (2080, 2065, and 2004 cm^{-1}), and consistent with oxidation to Ir(II). Attachment of the norbornyl group, which is chiral, at one of the iridium atoms in adduct 44 reduces the binuclear system to an asymmetric structure so that all four CO vibrations are IR active (C_1 symmetry).

The $^{13}C\{^1H\}$ NMR spectrum of 44 is shown in Figure 4-19. The four weak signals at very high frequency (above 160 ppm) are due to the carbonyl carbon atoms (Figure 4-20), two of which (169.0 and 168.9 ppm) can be assigned to CO groups adjacent to I on Ir with the other pair (167.4 and 167.1 ppm) due to CO groups that are close to the alkyl group. Also, the former two resonances (0.06 ppm apart) are more
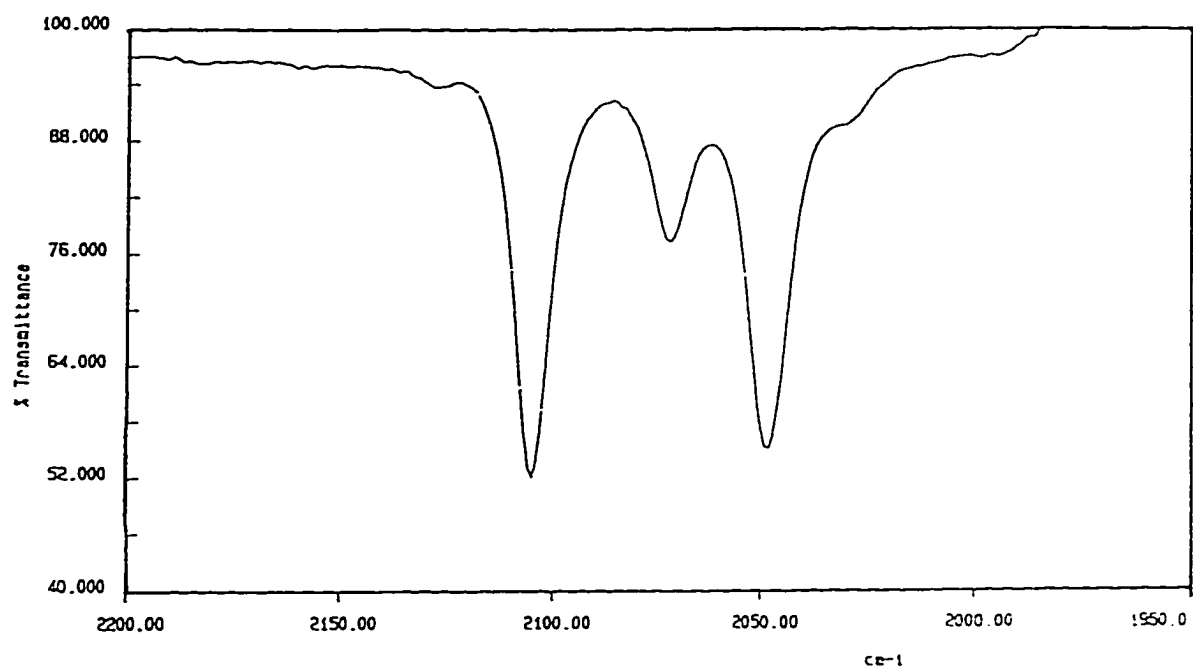
(b) Compound 46 from the reaction of 38 and 44
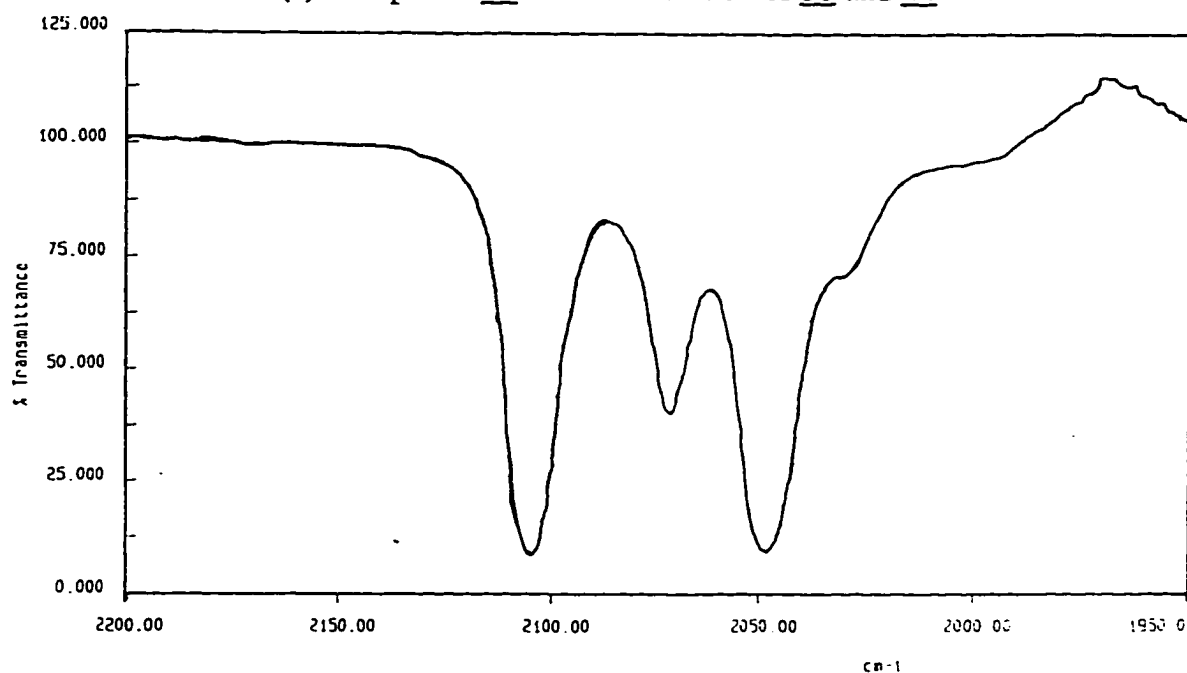
(a) Compound 46 from the reaction of 38 and 45

Figure 4-18. IR spectra of $Ir_2(CO)_4(\mu\text{-}pz)_2(norbornyl)(I)$, 44.
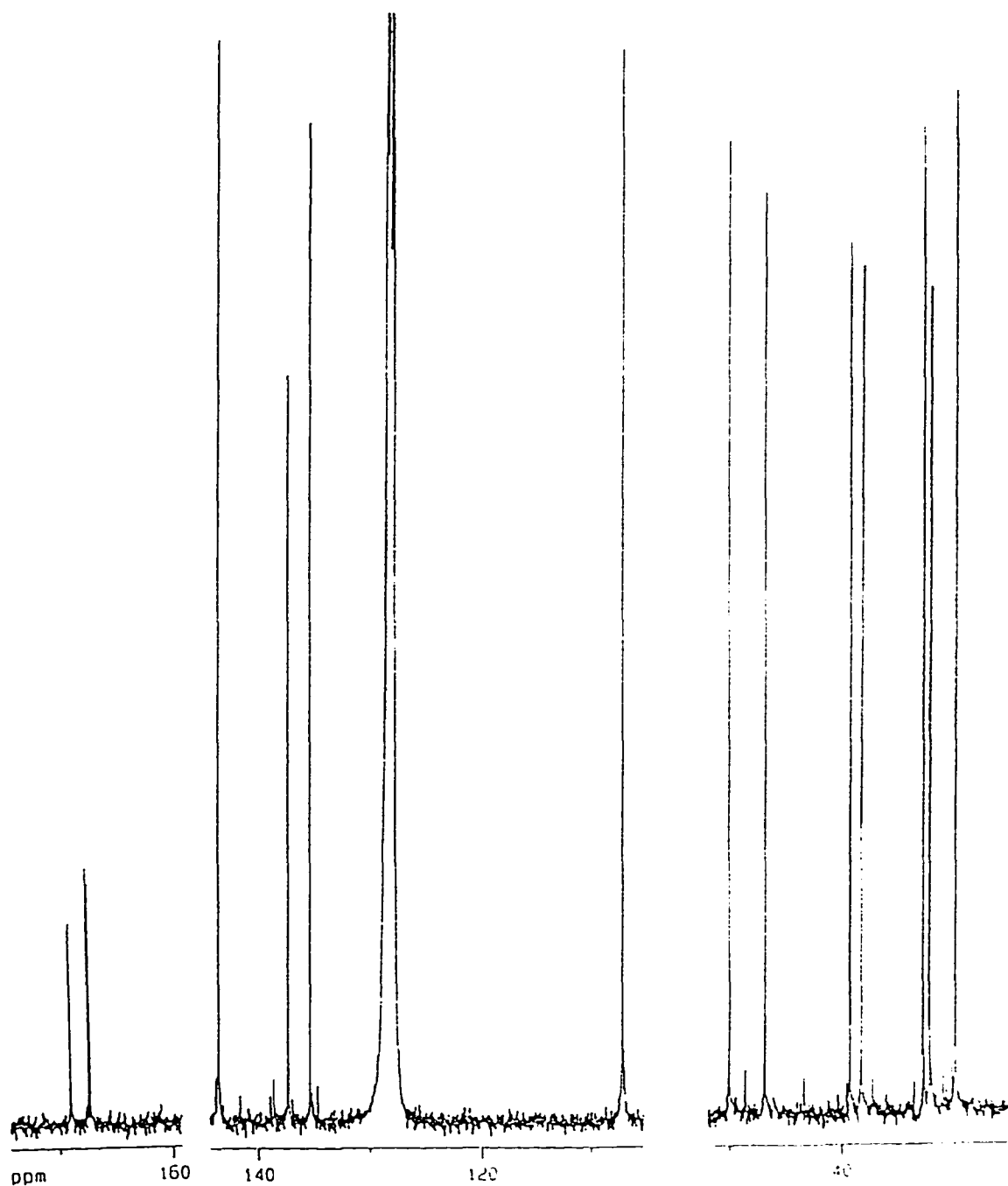
Figure 4-19. The $^{13}C\{^1H\}$ NMR spectrum of **44**.

closely spaced than the latter (0.23 ppm apart), indicating that the two carbons that cause the former resonances are farther away from the asymmetric norbornyl group, and their environments are less affected. The six resonances in the aromatic region (100 -

150 ppm) are due to pyrazolyl carbons and based on similar arguments to those used above and elsewhere, the pair at 143.4 ppm (only 0.03 ppm apart) are assigned to C^5 and $C^{5'}$, those at 137.3 and 135.3 ppm (well separated by 1.9 ppm) to C^3 and $C^{3'}$, and the remaining pair at highest field (107.1 and 107.0 ppm) to C^4 and $C^{4'}$. The seven resonances in the high field region (25 - 50 ppm) are due to the alkyl carbons in the norbornyl groups, and were assigned by analogy to the $^{13}C\{^1H\}$ NMR spectra of *endo*- and *exo*-norbornyl iodide (Table 4-4).
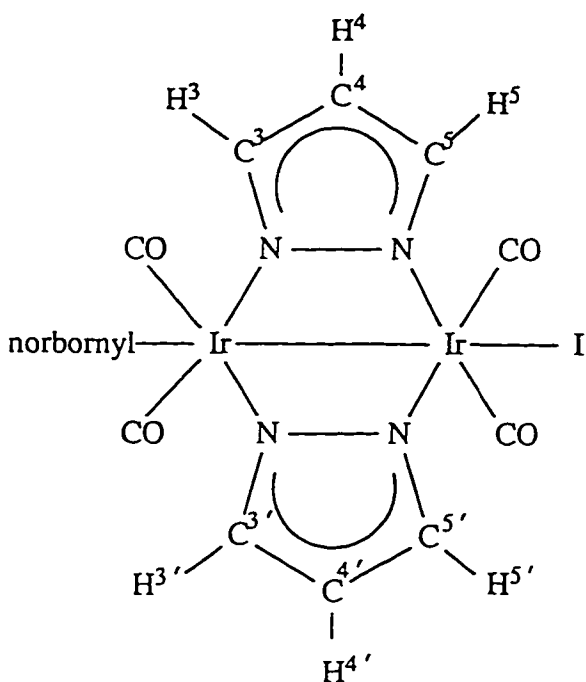
Figure 4-20. Molecular structure and the labelling scheme for 44.

The ^{1}H NMR spectrum of 44 was analyzed by using the relationships discussed above in the $^{13}C\{^1H\}$ NMR spectrum, together with correlation data from the $^{13}C/^1H$ and $^1H/^1H$ COSY NMR spectra (Figures 4-21 and 4-22, respectively). The two doublets both centred at 7.97 ppm with a chemical shift difference of only 0.2 Hz (operating frequency: 360.1 MHz) are due to H^5 and $H^{5'}$, coupling to H^4 and $H^{4'}$, respectively (for both doublets, $^3J_{HH}$ = 2.2 Hz). Another pair of doublets, located at 7.14 and 7.09 ppm,
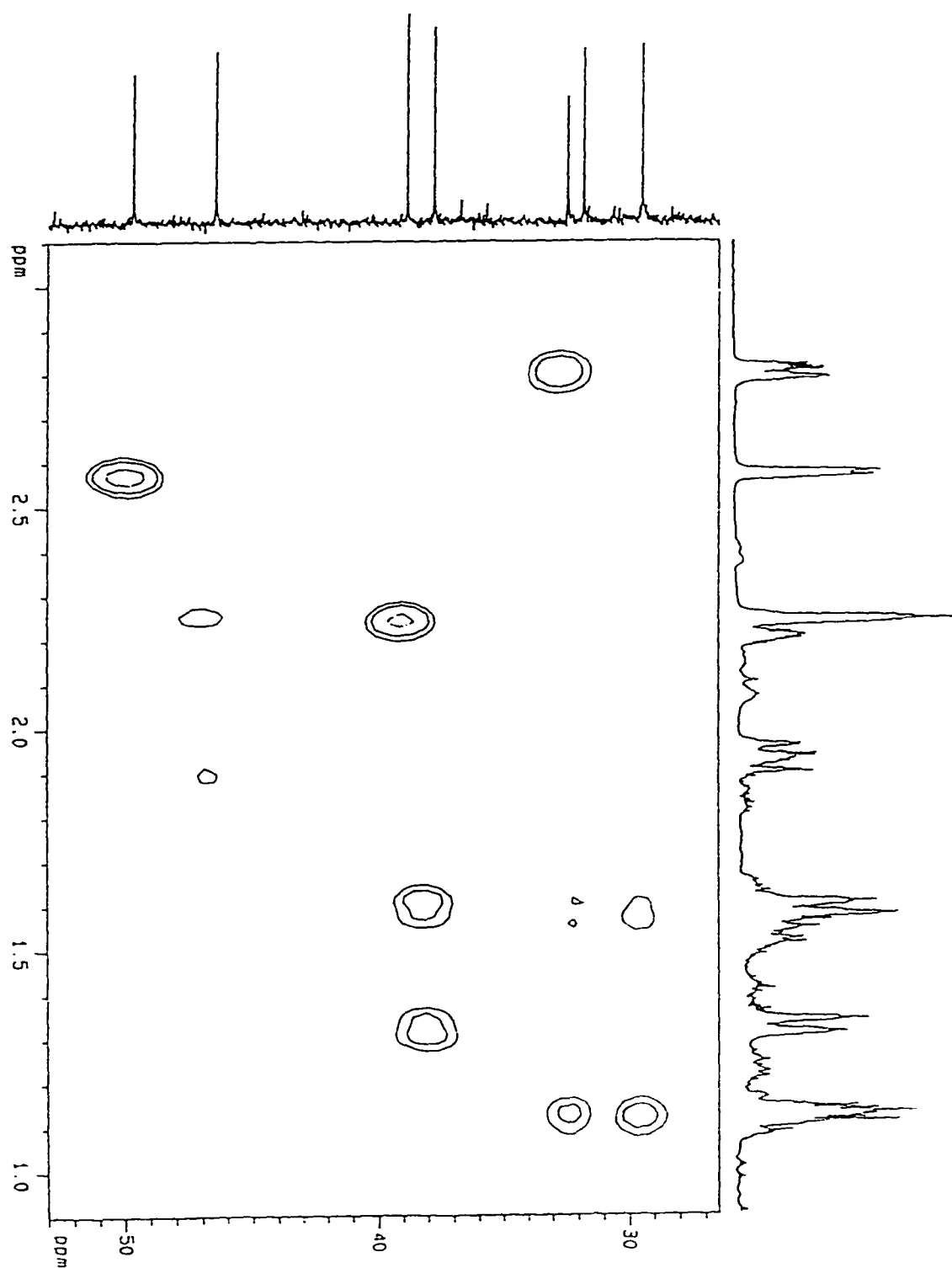
Figure 4-21. The $^{13}C/^1H$ cosy NMR spectrum of $Ir_2(CO)_4(\mu\text{-pz})_2(norbornyl)(I)$, __44__.
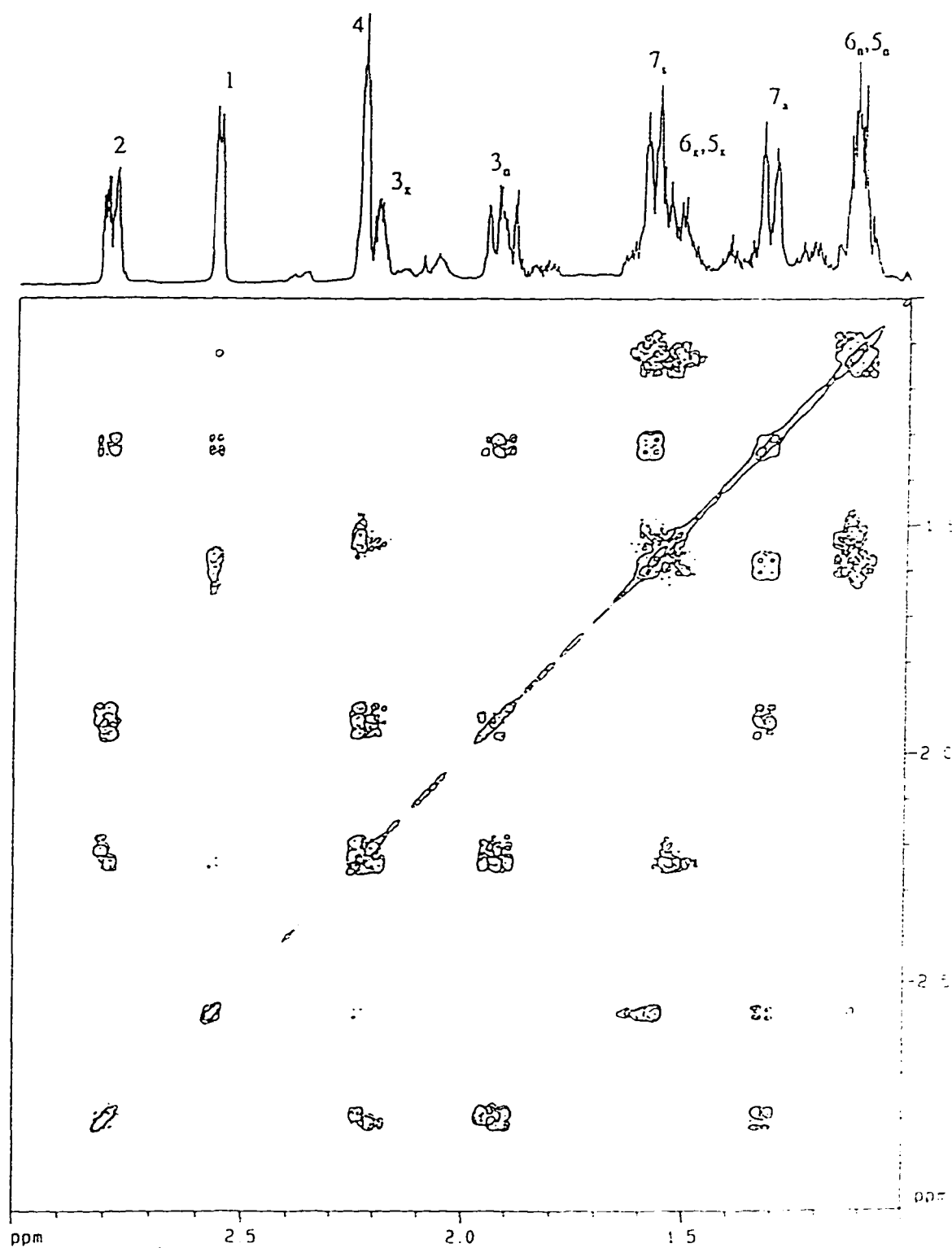
Figure 4-22. The ^{1}H/^{1}H cosy NMR spectrum of Ir$_2$(CO)$_4$(μ-pz)$_2$(norbornyl)(I), 44.

is assigned to H^3 and $H^{3'}$, also coupling to H^4 and $H^{4'}$ ($^3J_{HH}$ = 2.4 and 2.3 Hz, respectively). Signals due to the latter appear as an apparent quartet formed by overlapping triplets. These two triplets are centred at 5.593 and 5.589 ppm, with a averaged coupling constant of 2.0 Hz. The complete assignment for the norbornyl protons is shown in Figure 4-22.

There are several characteristic features in the alkyl region of the ^1H NMR spectrum of 44: a) The low field multiplet centred at 2.78 ppm is apparently due to H^2. This resonance is shifted to considerably higher field compared with the corresponding resonances in the ^1H NMR spectra of the iodides (3.62 and 3.86 ppm for *exo-* and *endo-*R˙I, respectively), because iridium is less electronegative than iodine, and has less electronic deshielding effect on the nuclei at its vicinity. The multiple splitting of the H^2 resonance arises from the couplings with $H^{3x,n}$ and H^{7a}, as shown in the $^1H/^1H$ COSY NMR spectrum of 44 (Figure 4-22). This coupling relationship is identical to that shown in the ^1H NMR spectrum of *exo*-R˙I. b) The two resonances at 1.58 and 1.31 ppm, which are due to H^{7s} and H^{7a}, respectively, are well separated. The similar phenomenon was also found in the ^1H NMR spectrum of *exo*-R˙I. By contrast, in the ^1H NMR spectrum of *endo*-R˙I, the spacing between the H^7 resonances is very small and leads to an AB pattern. c) The resonances due to the H^6 protons, located at 1.54 and 1.13 ppm, are also well separated. Similar arrangement of H^6 resonances was also observed in the ^1H NMR spectrum of *exo*-R˙I, but not *endo*-R˙I. In the latter, the resonances due to the H^6 protons overlap each other. Because the chemical shift values and the coupling patterns in NMR spectroscopy are directly related to the geometry of the molecule, all these features lead to one conclusion: the norbornyl group in compound 44 adopts a conformation similar to that of *exo*-R˙I, *i.e.* the diiridium fragment in 44 bonds to the norbornyl group through the *exo* site.

The results of the stereochemical analysis of norbornyl iodide addition to

$[Ir(CO)_2(\mu\text{-}pz)]_2$ (38) indicate that the reaction does not proceed via S_N2 or concerted mechanisms, either of which should lead to inversion of the configuration (in this case, *exo-* and *endo-*norbornyl diiridium adducts would be generated by *endo-* and *exo-*R·I, respectively, the second of which was not observed). This effectively rules out an S_N2 reaction pathway for the reaction of 38 with R·I because it is unlikely that *endo-* or *exo-*R·I would add by different mechanisms. A radical mechanism, which has been proposed for the oxidative additions of higher alkyl halides (*i.e.* other than methyl halides) to mononuclear Ir species including Vaska's complex, is also unlikely to be the major reaction pathway in this reaction, because no cross products (*i.e.* $[Ir(CO)_2(\mu\text{-}pz)(I)]_2$ or $[Ir(CO)_2(\mu\text{-}pz)(norbornyl)]_2$) were observed. The S_N1 mechanism, however, can explain the stereochemical results of this reaction very well (Scheme 4-11), in which both norbornyl iodides dissociate via ejection of iodide to form norbornyl carbocation. One of the iridium centres in the dimer then attack the carbocation through the less sterically crowded *exo* site to form the norbornyl diiridium cation, which then picks up the iodide at the other iridium centre to give the observed product. Since both norbornyl iodides generate the same carbocation, the final product will naturally be same, and the oxidative addition of norbornyl iodides to 38 seems likely to follow this route.

Since both MeI addition to $\{Ir[P(OBor)Ph_2](CO)(\mu\text{-}pz)\}_2$ (41) and norbornyl iodide addition to $[Ir(CO)_2(\mu\text{-}pz)]_2$ (38) have provided new information concerning the stereochemistries and mechanism of oxidative addition to diiridium systems, an effort has also been made to investigate the reaction between 41 and norbornyl iodide, where both participants are chiral. The reaction was carried out in THF solution. After removal of volatiles, the NMR spectra of the reaction mixture was recorded. The $^{31}P\{^1H\}$ NMR spectrum of the products exhibits 11 signals in the region between 70 - 80 ppm, where resonances due to the phosphorus ligands in the Ir(II) dimers are expected. If this reaction proceeds similarly to that of 38, four products are predicted: (*R*)-
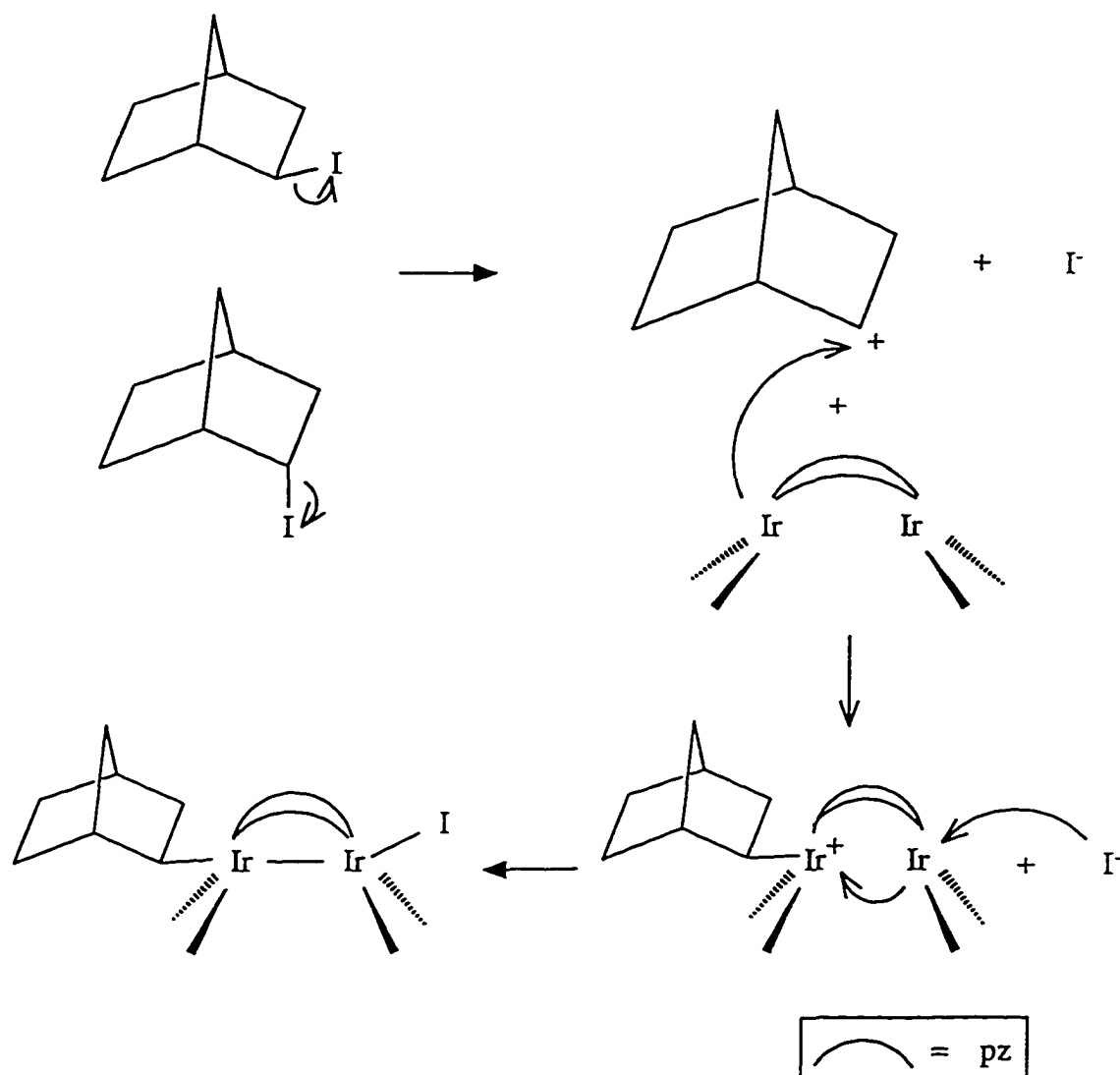
Scheme 4-11. S_N1 mechanism for the oxidative addition of norbornyl iodides to <u>38</u>.

{Ir[P(OBor)Ph$_2$](CO)(µ-pz)}$_2$[(R)-norbornyl](I), (R)-{Ir[P(OBor)Ph$_2$](CO)(µ-pz)}$_2$[(S)-norbornyl](I), (S)-{Ir[P(OBor)Ph$_2$](CO)(µ-pz)}$_2$[(R)-norbornyl](I), and (S)-{Ir[P(OBor)Ph$_2$](CO)(µ-pz)}$_2$[(S)-norbornyl](I). Each of these independent adducts will give two phosphorus resonances, i.e. a total of eight signals is expected in the ^{31}P{^{1}H} NMR spectrum of the mixture. The observed spectrum contains more than eight

resonances in the region, and the scale of this reaction led to poor quality of the NMR spectra. The products are expected to be difficult to separate, so that further investigation of this reaction will be required. Although the oxidative addition of norbornyl iodide to $\underline{41}$ clearly takes place, to give a family of adducts, the detail of how the latter are formed along diastereomeric pathways has yet to be determined.

Chapter 5

SYNTHESIS AND REACTIVITY OF METAL COMPLEXES
WITH CHIRAL PHOSPHINOALKYLSILYL LIGANDS

Organophosphinoalkylsilanes are bifunctional ligand precursors in which a reactive silane centre is connected to one or more phosphorus donors through a backbone hydrocarbon framework. The derived silyl ligands and their transition metal complexes have attracted much interest in recent decade mainly because they are good homogeneous catalysts in organic processes, such as hydroformylation,[156] and provide models for metal-support interactions in silica-derived systems for heterogeneous catalysis.[157,158] Unusual stereochemistry has also been exhibited by these compounds, as best illustrated by the iridium complex of bis(diphenylphosphinopropyl)methylsilane ([$Ph_2P(CH_2)_3]_2MeSiH$, abbreviated as biPSiH, $\underline{45}$), Ir(biPSi)HCl (structure on page 151), in which the axial-equatorial-axial conformation of the biPSiH ligand creates two inequivalent faces due to the tetrahedral geometry around the silicon atom.[159] This face-discriminating feature affects the orientation of external substrates approaching the metal centre, influencing in stereoisomerization.

Various organophosphinoalkylsilanes have been synthesized,[160-164] among which an extensive family of mono-(organophosphinoalkyl)silanes (PSi) with the general formula of $SiR_2P(CH_2)_nXYZ$ (R = Ph or Me; n = 1, 2, or 3; X, Y, or Z = H, Cl, Me, or Ph, 33 in total) and a series of poly-(organophosphinoalkyl)silanes with the general formula of $SiH[R_2P(CH_2)_m][R'_2P(CH_2)_m]_n(R'')_{2-n}$ (R or R' = Ph or cyclohexyl; m = 2, 3, or 4; n = 1 [biPSi] or 2 [triPSi]; R'' = Me or Ph, 13 in total) have been reported by Stobart and co-workers. The coordination chemistry of the late transition metals, such as platinum,[165,166] iridium,[167,168] rhodium,[169-171] ruthenium,[172-174] or osmium[175], with these

ligands has been intensively investigated, resulting in a variety of complexes containing such ligands, which are not only structurally interesting but also are useful as catalysts for homogeneous hydroformylation reactions.[156]

An analogue of biPSiH, (45), bis(2-diphenylphosphinobenzyl)methylsilane ([*o*-Ph$_2$PC$_6$H$_4$CH$_2$]$_2$MeSiH, abbreviated as mcbiPSiH, 46), was prepared and characterized recently in this laboratory.[176] Since the benzyl groups in 46 are less flexible than the polymethylene groups in 45, ligand 46 shows increased rigidity. This was reflected in the coordination chemistry of these ligands in their Pt and Ir model complexes (*vide infra*).[159,177]

The observed regioselectivity of biPSiH and mcbiPSiH systems in homogeneous catalysis suggests that they are good candidates for further modification so that enantioselectivity may be achieved. Naturally, this modification would involve the introduction of an asymmetric unit into the existing ligands. This may be realized using the same principles that were successful in obtaining chirality for the iron, cobalt and di-iridium systems discussed in the previous chapters, *i.e.* attaching optically active alkoxy groups onto the phosphorus or silicon centre.

Investigation of the platinum and iridium complexes of 45 and 46 revealed interesting coordination chemistry of these tri-dentate ligands. Thus, the synthesis and characterization of corresponding compounds formed from a chiral version of 45 and 46 may provide guidelines in the context of ligand development. A five-coordinate iridium system is a particularly attractive model as the unsaturated metal centre is essential for studying substrate coordination. The synthesis of the chiral ligand was first attempted with bis(2-dimenthoxyphosphinobenzyl)methylsilane ([*o*-(MenO)$_2$PC$_6$H$_4$CH$_2$]$_2$MeSiH, abbreviated as mcbiP*SiH) as the target, where the asymmetric units, the menthoxy groups, are bonded to the phosphorus atoms, because the dimenthoxyphosphino fragment is directly related to the ligands discussed in the

previous chapters. However, attempted synthesis *via* both lithiation and Grignard reactions (Scheme 5-1), were unsuccessful. The difficulty with the first approach appeared to be caused by the attack of lithium reagent on the O-P bonds rather than the Cl-P bond in $(MenO)_2PCl$; while generation of the "double" Grignard reagent in the second route proves to be troublesome. Also, the Grignard reagent may cause the cleavage of O-P bonds in $(MenO)_2PCl$.[178]
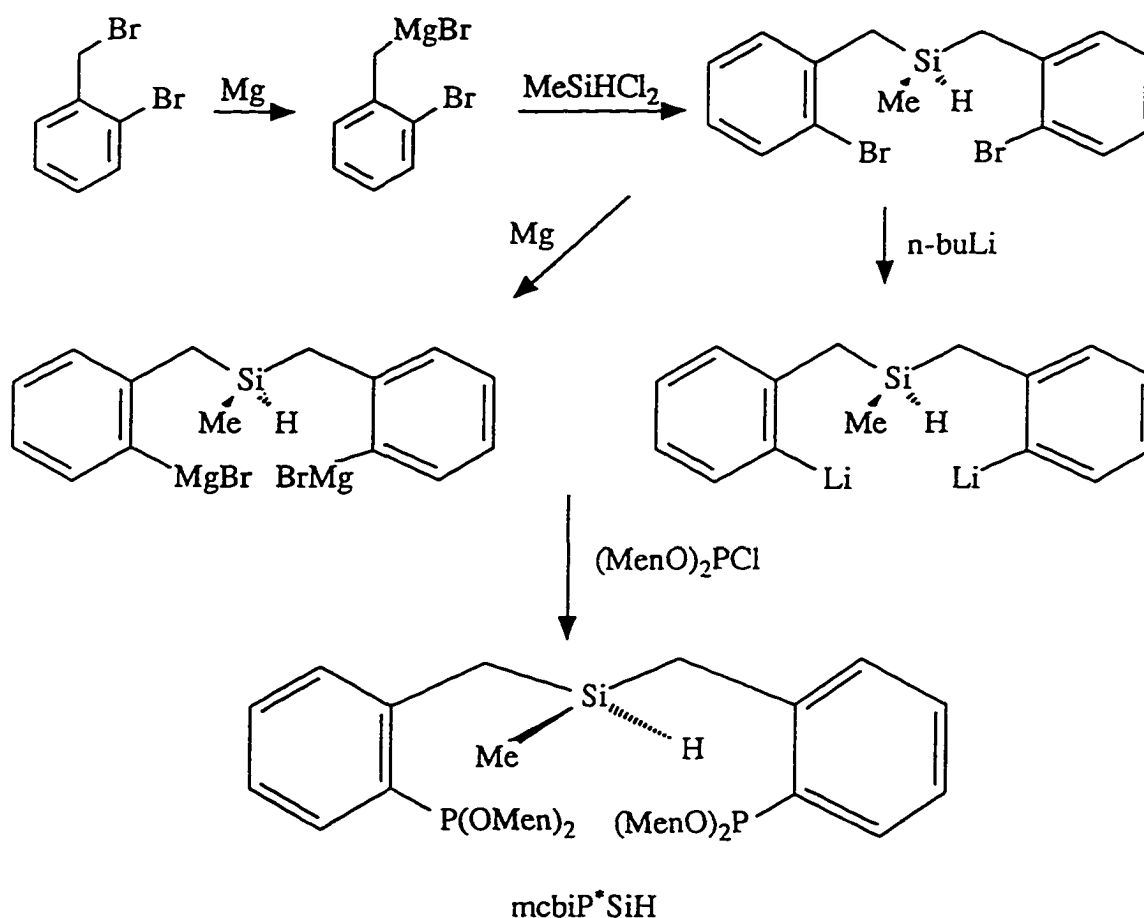
Scheme 5-1. Attempted synthesis of mcbiP*SiH.

Because of the obstacles in synthesizing mcbiP*SiH, another functional site in the mcbiPSiH framework, the silicon atom, was targeted for substitution by the chiral

menthoxy fragment. Synthesis of bis(2-diphenylphosphinobenzyl)menthoxysilane ([o-Ph$_2$PC$_6$H$_4$CH$_2$]$_2$(MenO)SiH, abbreviated as mcbiPSi*H, 47) was successful using a multi-step synthetic route (Scheme 5-2). TMEDA (N,N,N',N'-tetramethylethylenediamine) was employed to stabilize the 2-(diphenylphosphino)benzyl lithium salt. This salt can be isolated as a yellow orange solid and must be stored under argon because it is extremely sensitive towards water and oxygen. The final product is a colourless wax-like solid. It is thermally stable, and can be briefly handled in air. The solubility of 47 is good in most common organic solvents such as hexanes, benzene, ether, or chloroform. The silane precursor, MenOSiHCl$_2$, is readily prepared by the direct reaction between excess HSiCl$_3$ and MenOH. The colourless liquid product is thermally stable, but is hydrolysed rapidly when exposed to air.
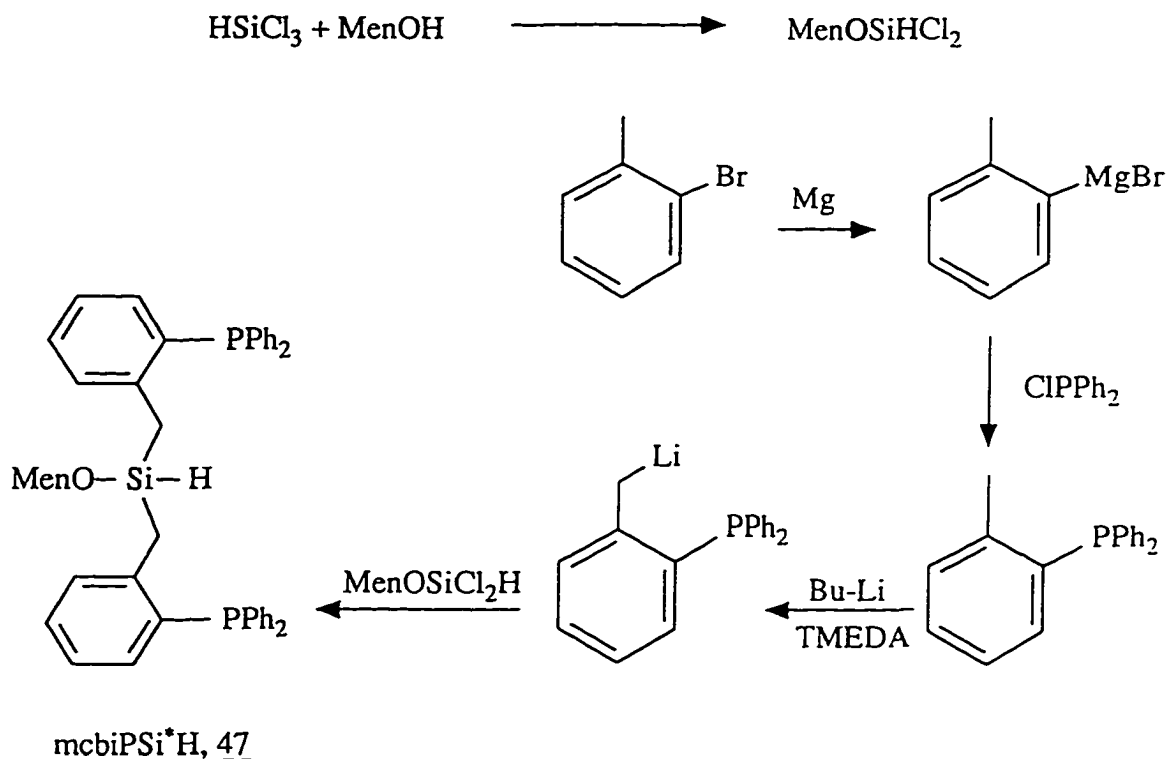
mcbiPSi*H, 47

Seheme 5-2. Synthesis of mcbiPSi*H, 47.

Two major preparative methods for PSi compounds have been reported. One involves the radical addition of a P-H bond of secondary phosphines to the terminal

double bond of unsaturated alkylsilanes (*e.g.* vinyl or allyl silanes) induced by UV[162-164] (Equation 5-1) or catalyzed by LiPMe$_2$[160,161] (Equation 5-2).

$$nR_2PH + (H_2C{=}CH(CH_2)_m)_nSiR'_{4-n} \xrightarrow{\ hv\ } (R_2PCH_2CH_2(CH_2)_m)_nSiR'_{4-n}$$

$$(m = 0, 1, \text{ or } 2; n = 1, 2, \text{ or } 3) \qquad (5\text{-}1)$$

$$Me_2PH + H_2C{=}CHSiMe_3 \xrightarrow{\ LiPMe_2\ } Me_2PCH_2CH_2SiMe_3 \qquad (5\text{-}2)$$
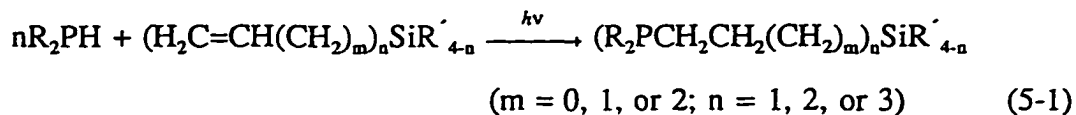
In spite of its wide use in the synthesis of PSi compounds, the photochemical reaction can be very time consuming (especially for m = 1) and is obviously unsuitable for the preparation of phosphinomethylsilanes or mcbiPSi*H (47) and its analogues, for which, no silane precursors with terminal double bonds are conceivable.

The other method employs either lithium or Grignard reagents to form a link between the silyl and phosphino groups. Phosphinomethylsilanes were synthesized using diphenylphosphinomethyllithium[179] (Equation 5-3),[163,180] and a mono-phosphino analogue of mcbiPSiH (46) has been prepared using a Grignard reagent (Equation 5-4).[181]

$$Ph_2PCH_2Li{\cdot}TMEDA + Me_2SiCl_2 \xrightarrow{\ -78\ °C\ } (Ph_2PCH_2)_2SiMe_2 + Ph_2PCH_2SiMe_2Cl)$$

$$(5\text{-}3)$$

$$o\text{-}BrMgC_6H_4CH_2SiMe_{3-n}H_n + Ph_2PCl \longrightarrow o\text{-}Ph_2PC_6H_4CH_2SiMe_{3-n}H_n$$

$$+ o\text{-}H_nMe_{3-n}SiC_6H_4CH_2PPh_2 \quad (n = 1 \text{ or } 2) \qquad (5\text{-}4)$$
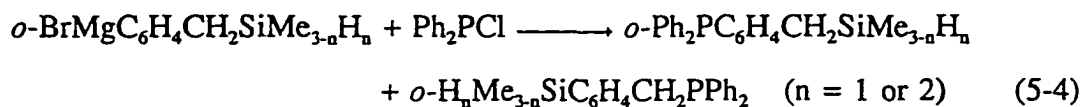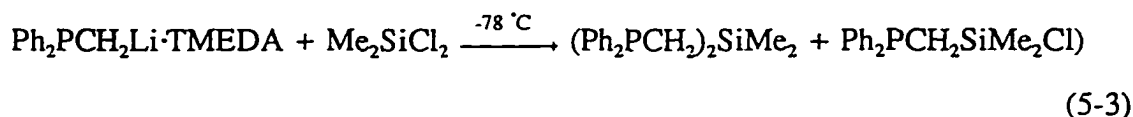
As shown in Equation 5-4, the Grignard reaction produces two isomers, which require a subsequent separation step. This was avoided in the synthesis of mcbiPSi*H (47) presumably because the diphenylphosphinobenzyllithium salt is stabilized by the interaction between the lithium and phosphorus atoms, leading to a sterically favourable five-membered metallocycle (Figure 5-1).

A new route to polyphosphinoalkylsilanes or polysilylalkylphosphines is currently being developed in this laboratory. The reaction of allylsilanes with Schwartz's
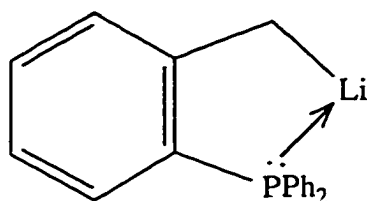
Figure 5-1. Interaction between lithium and phosphorus in o-$Ph_2PC_6H_4CH_2Li$.

reagent[182], Cp_2ZrHCl, generates anti-Markovnikov hydrozirconation products that can further react with halophosphines to give the target phosphinosilanes (Equations 5-5 and 5-6).[183]

$$Me_{3-n}HSi(CH_2CH=CH_2)_n + nCp_2ZrClH \longrightarrow Me_{3-n}HSi(CH_2CH_2CH_2ZrCp_2Cl)_n$$

$$Me_{3-n}HSi(CH_2CH_2CH_2ZrCp_2Cl)_n + nPh_2PCl \longrightarrow Me_{3-n}HSi(CH_2CH_2CH_2PPh_2)_n$$

$$+ nCp_2ZrCl_2 \quad (n = 1, 2, \text{ or } 3) \qquad (5\text{-}5)$$

$$nMe_2HSiCH_2CH_2CH_2ZrCp_2Cl + Ph_{3-n}PX_n \longrightarrow (Me_2HSiCH_2CH_2CH_2)_nPPh_2$$

$$+ nCp_2ZrX_2 \quad (n = 2, X = Cl; \text{ or } n = 3, X = Br) \qquad (5\text{-}6)$$
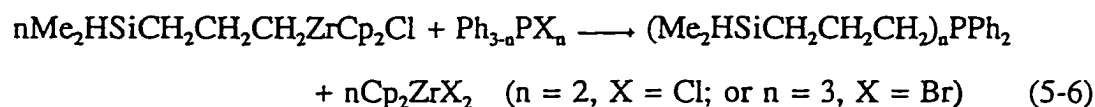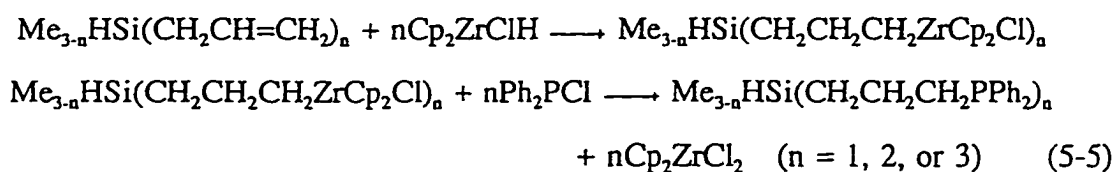
These thermal reactions are much faster than the corresponding photochemical processes and show great potential as a general method for the synthesis of polyphosphinoalkylsilanes or polysilylalkylphosphines, where the alkyl chains contain two carbon atoms or more.

The new chiral PSi precursor <u>47</u> (mcbiPSi·H) was characterized using various instrumental methods. The mass spectrum exhibits a molecular ion peak (M+1) spread over three mass units at 735(9%), 736(6%), 737(3%) (M.W. = 734 g/mol). The multiplet pattern results from combination of the minor isotopes of C and Si. The relative intensities of the three strongest lines are compatible with the theoretical values. The elemental analysis results of <u>47</u> also matched the expected atomic composition of $C_{48}H_{52}OP_2Si$.

The IR spectrum of <u>47</u> shows a medium strong band at 2117 cm^{-1} due to the Si-

H stretching vibration. The $^{31}P\{^1H\}$ NMR spectrum consists of two signals at -13.9 and -14.0 ppm due to the two phosphorus atoms. Unlike its achiral methyl analogue (mcbiPSiH, 46), which possesses planar symmetry that relates the two phosphinoalkyl arms attached to the silicon centre, compound 47 does not have any symmetry because it contains an optically active menthyl group. Therefore, the two phosphinoalkyl substituents are diastereotopic.

The $^{13}C\{^1H\}$ NMR spectrum is shown in Figure 5-2. The aromatic region of the spectrum is very complex because each of the 36 aromatic carbon atoms in the molecule is inequivalent to another, theoretically giving 36 resonances, resulting in significant overlapping. The menthoxy carbon peaks appear in the region from 10 to 80 ppm, and the chemical shifts are very close to those of menthol itself (Table 5-1), since hydrogen and silicon have similar electronegativities. The signals for the two benzylic carbons are found at 24.2 ($^3J_{PC}$ = 19.5 Hz) and 23.5 ($^3J_{PC}$ = 20.8 Hz) ppm. These two carbons atoms are inequivalent again due to the chirality introduced by the menthoxy group. The ^1H

Table 5-1. $^{13}C\{^1H\}$ NMR chemical shifts[a] for the menthoxy carbons in 47, in comparison with those in menthol.

Compound	δ C (ppm)				
$(Ph_2PC_6H_4CH_2)_2(MenO)SiH$, 49	71.4	50.0	44.9	34.4	31.5
	25.7	23.0	22.1	20.9	16.0
Menthol	71.4	50.1	45.0	34.5	31.6
	25.7	23.1	22.2	21.0	16.0

[a] Chemical shifts are given in δ(ppm) relative to internal $CDCl_3$ with the central resonance of the $CDCl_3$ signal set at 77.0 ppm. Spectra were recorded in $CDCl_3$ solution.
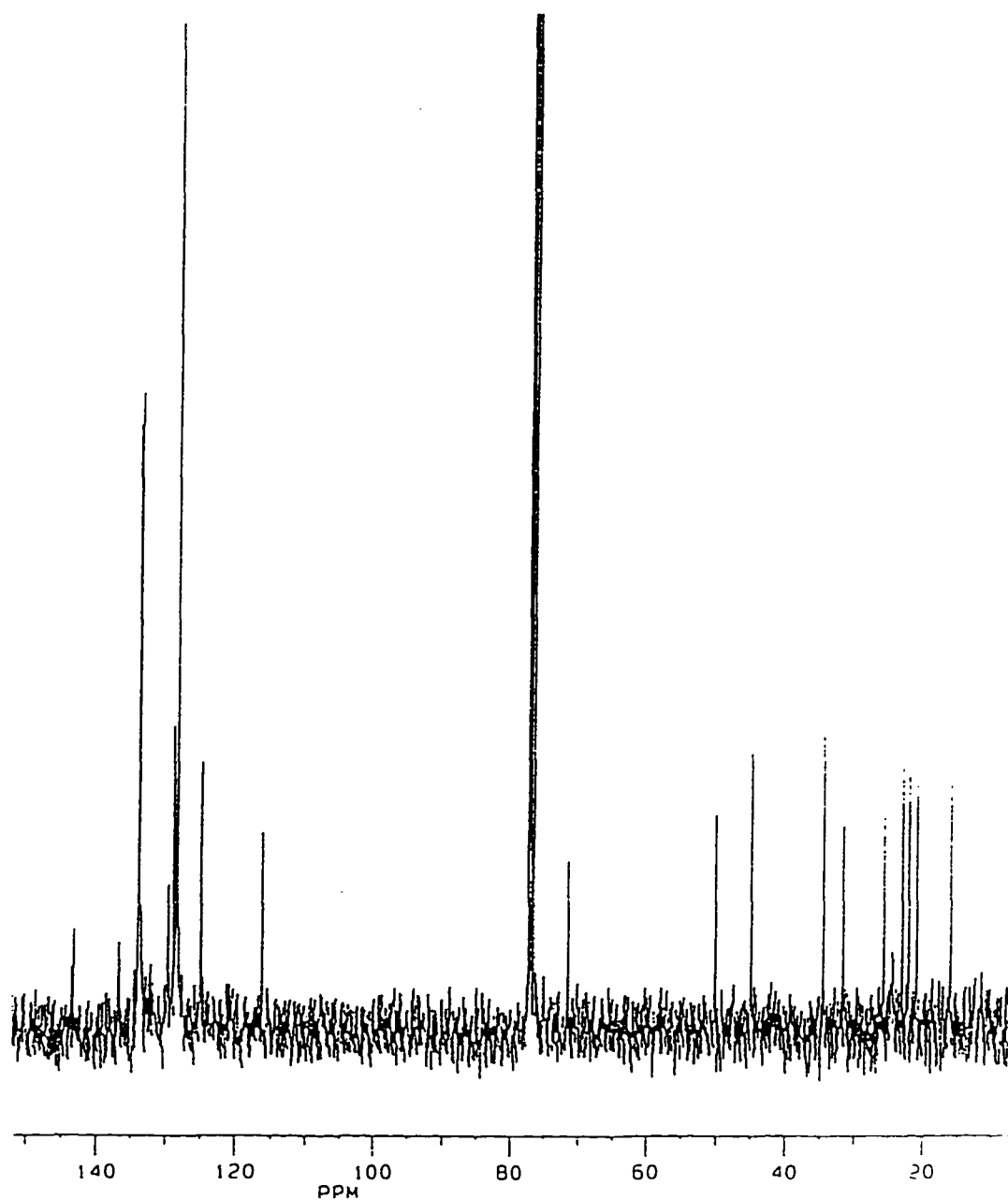
Figure 5-2. $^{13}C\{^1H\}$ NMR spectrum of mcbiPSi*H, 47.

NMR spectrum of 47 has similar features to those of the $^{13}C\{^1H\}$ NMR spectrum: there

is a very complicated aromatic region and the menthoxy protons show very close

chemical shifts and multiplicities to those of the parent alcohol (e.g. the resonance due

to the α-proton in the menthoxy group is located at 3.40 ppm, only shifted downfield by 0.04 ppm compared to that in the menthol). The multiplet centred at about 2.3 ppm is assigned to the four benzylic protons. The complicated pattern arises from the signal overlapping, coupling to the silicon hydride and possibly the two phosphorus atoms, and the non-first order splittings caused by the geminal coupling between the two protons bonded to the same benzylic carbon because they are magnetically inequivalent. The silicon hydride is detected at 4.62 ppm as a broad peak, indicating unresolved couplings to the benzylic protons.

In order to investigate the reactivity and coordination chemistry of the chiral tridentate ligand, mcbiPSi*H (47), a platinum complex containing 47 was synthesized. Platinum was chosen mainly because its characteristic NMR properties: the large ^{31}P-^{195}Pt couplings are easy to detect and often diagnostic of molecular structure. The
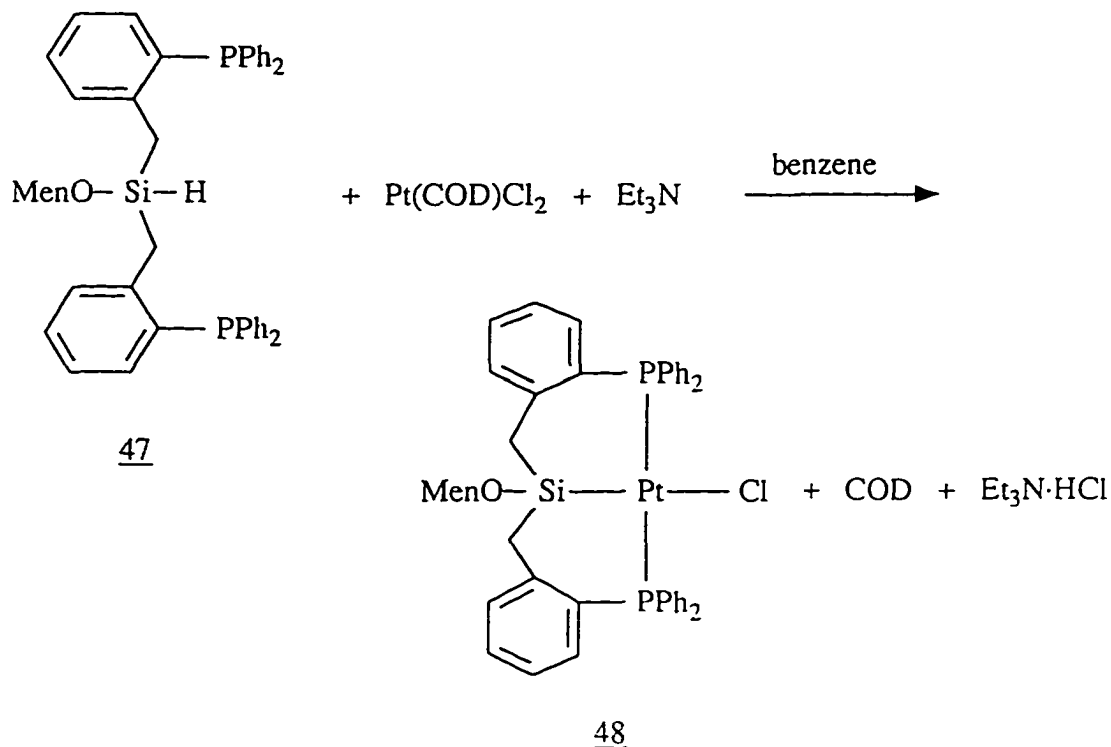
Scheme 5-3. Synthesis of complex Pt(mcbiPSi*)Cl. 48.

reaction of <u>47</u> with Pt(COD)Cl₂ in the presence of Et₃N gives PtCl[Si(OMen)(Ph₂PC₆H₄CH₂)₂] (Pt(mcbiPSi·)Cl, <u>48</u>, Scheme 5-3). The white crystalline product does not show signs of decomposition in the solid state when exposed to air for a short period of time. It is soluble in polar organic solvents such as benzene, ether, THF, or chloroform, but is insoluble in nonpolar solvents such as pentane or hexanes. Its isolation follows one of two main synthetic routes that have been employed to prepare organosilyl complexes: elimination reactions and oxidative addition reactions. The former, including the procedure used to prepare complex <u>48</u>, eliminate simple molecules, such as alkali halides, H_2, or HCl, while silicon metal bonds were formed, as shown in Equations 5-7 and 5-8:[184-187]

$$cis\text{-}[Pt(PR_3')_2Cl_2] + HSiR_3 + NEt_3 \longrightarrow trans\text{-}[Pt(PR_3')_2Cl(SiR_3)] + Et_3NHCl$$

$$(5\text{-}7)$$

$$cis\text{-}[Pt(PEt_3)_2Cl_2] + Hg(SiMe_3)_2 \longrightarrow trans\text{-}[Pt(PEt_3)_2Cl(SiMe_3)] + ClSiMe_3 + Hg$$

$$(5\text{-}8)$$
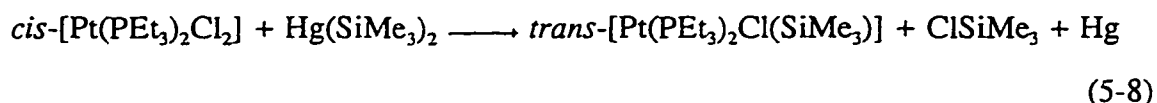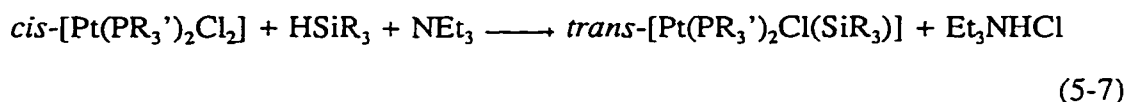
The oxidative addition route involves cleavage of the Si-H bond in the silane precursor and formation of M-Si and M-H bonds in the product. Equation 5-9 illustrates a typical example[188]. This method is also known as hydrosilation.

$$Rh(CO)_2Cp + HSiR_3 \longrightarrow Rh(CO)_2Cp(H)(SiR_3) \qquad (5\text{-}9)$$
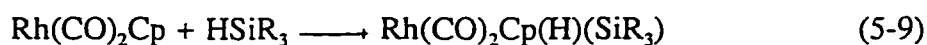
Because each of Pt, Cl, and C elements has two or more natural isotopes, polyisotopic molecular ion peaks are expected in the mass spectrum of mcbiPSi·PtCl (<u>48</u>, $PtC_{48}H_{51}ClOP_2Si$). This was confirmed by the observation of five-lined pattern at 963(4%), 964(7%), 965(8%), 966(5%), and 967(4%) in the actual spectrum. The measured values matched well with calculated distributions.

The $^{31}P\{^1H\}$ NMR spectrum of compound <u>48</u> is shown in Figure 5-3. The apparent triplet centred at 20.9 ppm with a 1:4:1 peak intensity ratio is typical for phosphorus nuclei coupling to platinum and arise because only 33.8% of platinum atoms
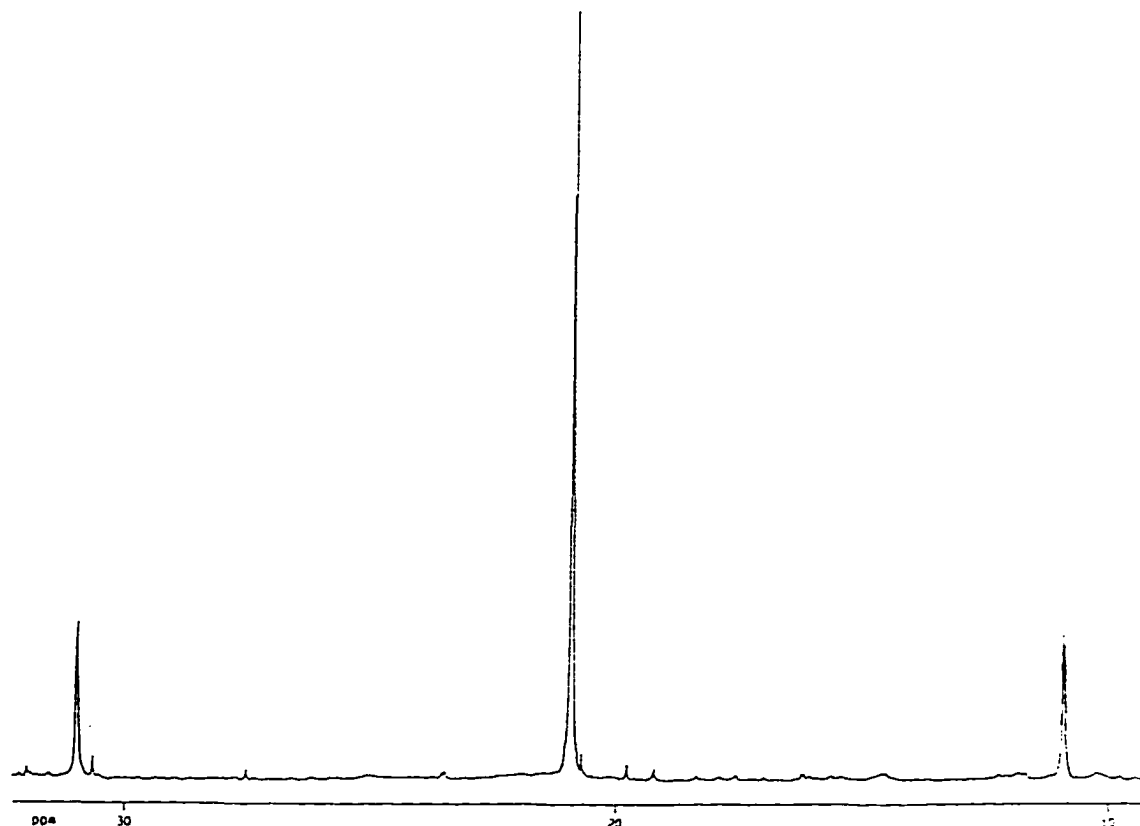
Figure 5-3. $^{31}P\{^1H\}$ NMR spectrum of Pt(mcbiPSi*)Cl, <u>48</u>.

are ^{195}Pt, I = 1/2. These ^{195}Pt atoms give rise to the satellite peaks in the spectrum with $^1J_{PtP}$ equal to 2921.4 Hz. Two barely discernible splittings in the centre and right branches of the spectrum are observed, measuring 5.7 and 4.1 Hz, respectively. These features are assigned to ABX splitting patterns caused by the coupling between the two inequivalent phosphorus atoms and the platinum nucleus. However, the difference in the chemical shifts caused by diastereotopicity between the two phosphorus nuclei is so small that the outer peaks of the ABX patterns are lost in the baseline noise, and the left branch of the spectrum remains as a broad singlet. The resonance of <u>48</u> is shifted downfield by 34.9 ppm compared to the free ligand, due to the electron donation from phosphorus atoms to the platinum centre, causing less shielding effect on the phosphorus nuclei.

In the $^{13}C\{^1H\}$ NMR spectrum of compound 48, the peak due to the α-carbon is found at 74.2 ppm as a pseudo triplet because of the platinum coupling ($^3J_{PtC}$ = 13.4 Hz). The two benzylic carbons are located at 28.8 and 28.4 ppm as multiplets, since they are coupled to both the phosphorus and the platinum nuclei.

Platinum complexes containing either mono- or bis-(phosphinoalkyl)silyl ligands have been reported.[163,172,183] In each case, the Pt(II) complexes adopt square planar geometry, as expected for sixteen electron Pt(II) species.[108] Analogues to Pt(mcbiPSi*)Cl (48), Pt(biPSi)Cl[159] and Pt(mcbiPSi)Cl[189] (Figure 5-4b) are formed with tridentate ligands, biPSi (45) and mcbiPSi (46), respectively, where the two phosphorus atoms are *trans* to each other. The $^1J_{PtP}$ values of Pt(biPSi)Cl and Pt(mcbiPSi)Cl are 2835 and 2908 Hz, respectively, *i.e.* very close to that reported above for Pt(mcbiPSi*)Cl (48).
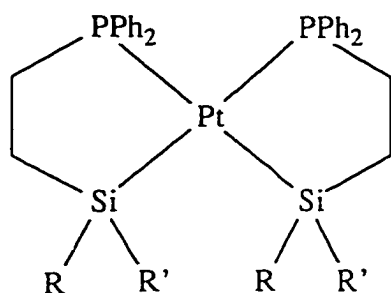
R = Me or Ph; R' = Me, Ph, or H   ⌢ = $(CH_2)_3$ or *o*-benzyl
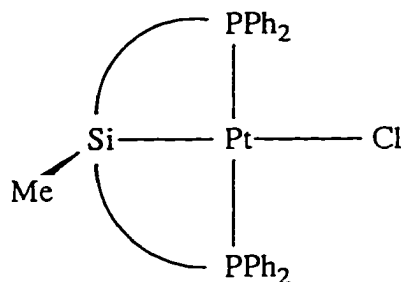
(a)   (b)

Figure 5-4. Structures of Pt-PSi complexes.

When Pt(COD)$_2$ reacts with bidentate PSi ligands, complexes of the formulae Pt(SiR'R''CH$_2$CH$_2$PPh$_2$)$_2$ (R', R'' = Me, Ph, or H, Figure 5-4a) are formed, where the two phosphorus donors are *cis* to each other. The coupling constants between the phosphorus nuclei and the platinum centre are in the range 1613-1838 Hz, which are

consistent with $^1J_{PtP}$ values for the phosphorus *trans* to silicon,[190] due to strong *trans* influence from the silyl groups. The *trans* influence is viewed as a thermodynamic phenomenon, where ligands can influence the ground state properties of groups to which they are *trans*.[191] These properties include the *trans* metal-to-ligand bond distance, the vibrational frequency or force constant, and the NMR coupling constant between the metal and the *trans* ligand donor atom. The larger $^1J_{PtP}$ values (2835 - 2921 Hz) obtained from the platinum complexes containing tridentate PSi ligands (45 - 47) indicate that the phosphorus donors are *trans* not to the silyl group but to the less strong *trans* influencing phosphorus atom.

The synthesis and characterization of the platinum complex 48 proved that the new chiral ligand precursor 47 functions similarly to its analogous, 45 and 46, in the context of its reactivity towards metal centres and showed asymmetric influence exerted
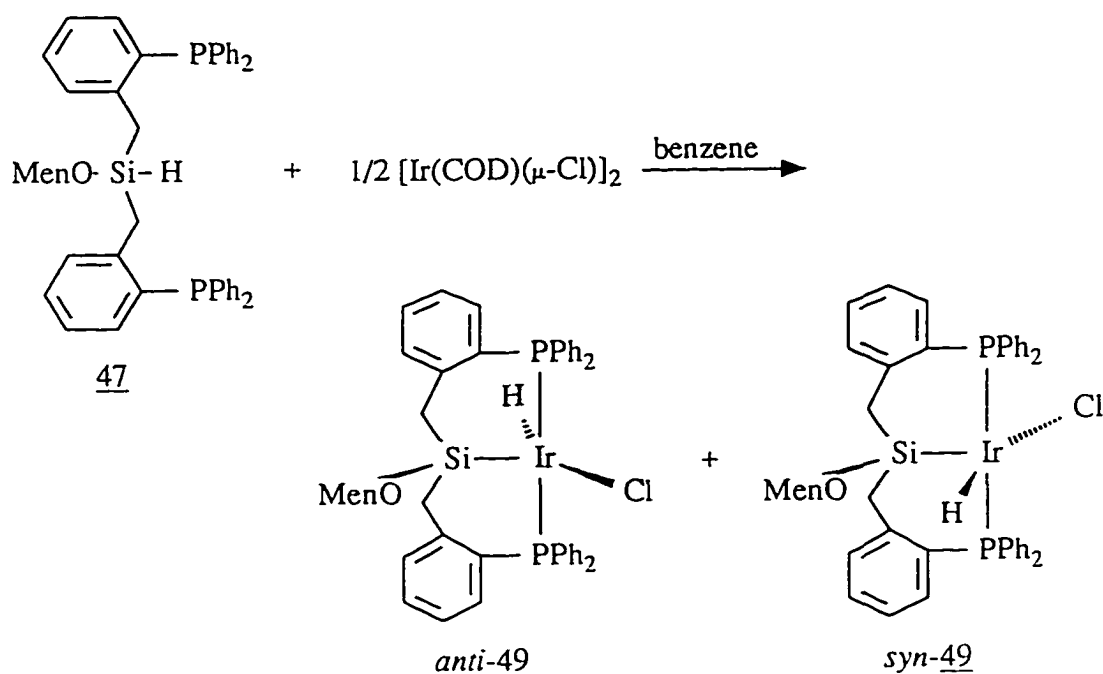
Scheme 5-4. Synthesis of IrH(mcbiPSi˙)Cl, 49.

by the optically active menthoxy fragment in the NMR spectra of the complex 48. However, because of the established stability of square planar d^8-Pt(II) system, further investigation of the chemistry of 48 was not pursued. Instead, the behaviour of mcbiPSi*H (47) towards iridium precursors was examined because coordinatively unsaturated five-coordinate species can be obtained in this manner, allowing the effect of the chiral framework on orientation of an incoming sixth ligand to be assessed.

A yellow crystalline solid was obtained from the reaction of [Ir(COD)(μ-Cl)]₂ with two mol. equiv. of 47 in benzene (Scheme 5-4). The product, 49, is soluble in $CHCl_3$, CH_2Cl_2, benzene, or THF, but can be precipitated out by the addition of non-polar solvents such as hexanes or pentane. The microanalysis results show that this compound contains 60.31% C, 5.58% H, consistent with the calculated values for IrH(mcbiPSi*)Cl (IrC₄₈H₅₂ClOP₂Si, C: 59.89%, H: 5.44%).

The ^{1}H NMR spectrum of 49 exhibits two hydride resonances at -19.52, -23.51 ppm in 8:1 ratio (Figure 5-5), indicating that there are two isomers in the product. The very high field chemical shifts of the hydride signals imply that the complexes are five-coordinate species, and the hydride is at the equatorial positions of a trigonal bipyramid or at the axial site of a square pyramid.[192] Both resonances are triplets due to the coupling to the two phosphorus atoms with coincidental equal coupling constants ($^2J_{PH}$ = 13.9 and 16.2 Hz, respectively). The low values of the coupling constants are suggestive of *cis* orientation between the hydride protons and the phosphorus atoms.[193] By analogy with the mcbiPSiH analogue of 49 (IrH(mcbiPSi)Cl, *vide infra*), the resonance at -19.52 ppm is assigned to the hydride in the *syn* isomer, while the signal at -23.51 ppm arises form the *anti* isomer (with *syn* and *anti* referring to the structural relationship between the Me-Si bond and the Ir-H bond throughout).[194]

The triplet of doublets centred at 3.07 ppm is characteristic of the resonance due to the α-proton in the menthoxy group. This signal is shifted upfield by 0.29 ppm from
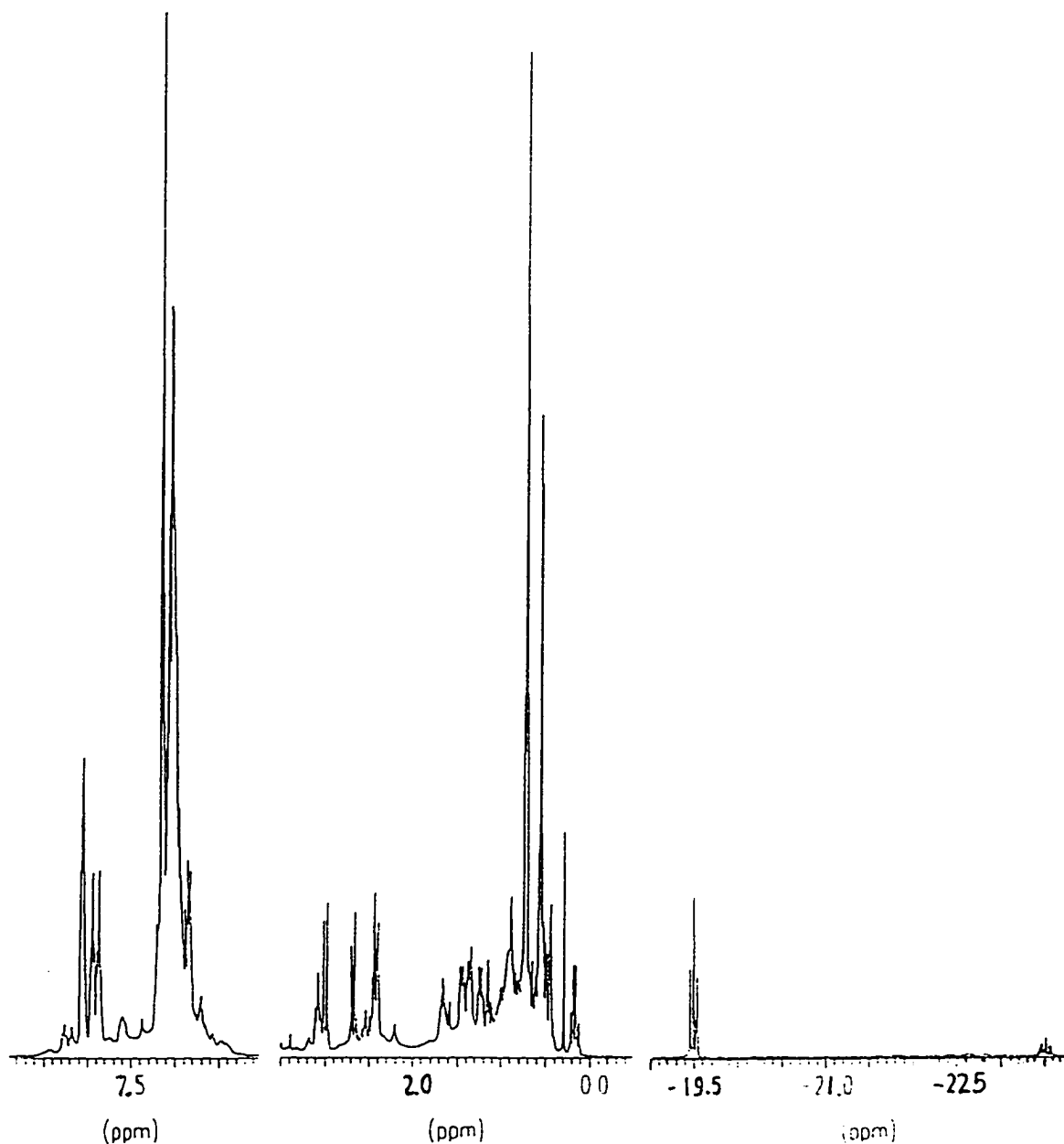
Figure 5-5. ^{1}H NMR spectrum of IrH(mcbiPSi*)Cl, <u>49</u>.

the free ligand, similar to that in the platinum complex <u>48</u>. The resonances due to the

four benzylic protons are observed as two pairs of doublets. One pair is located at 2.99

and 2.67 ppm ($^2J_{HH}$ = 14.4 Hz); the other at 2.44 and 2.40 ppm ($^2J_{HH}$ = 5.4 Hz). The

splitting pattern is due to the coupling between the two geminal protons in each

methylene group. The large differences in these chemical shifts and coupling constants suggests considerable rigidity in the two metallocyclic units of the molecule and substantial asymmetric influence from the optically active menthoxy group. Both the α-proton and the benzylic proton resonances discussed above arise from the *syn* isomer; the signals for the *anti* isomer in this region are not resolved due to its much lower concentration. However, in the thermodynamic distribution (*vide infra*), the *anti* isomer is dominant, and the relevant NMR data are obtained: the resonance due to the α-proton is found at 3.18 ppm as a triplet of doublets, and the two pairs of doublets due to the benzylic protons are located at 2.99, 2.56 ppm ($^2J_{HH} = 11.7$ Hz); and 2.56, 2.47 ppm ($^2J_{HH} = 16.2$ Hz). The rest of the proton resonances are not very informative and were not assigned individually.

The $^{31}P\{^1H\}$ NMR spectrum of <u>49</u> consists of two AB patterns centred at 26.9 and 18.2 ppm, corresponding to the two isomeric forms. The much more intense resonance at 26.9 is assigned to the *anti* isomer, with the other signal due to the *syn* isomer. The chemical shifts and coupling constants were obtained by computer simulations. For the *anti* isomer, $\delta P_A = 27.6$ ppm, $\delta P_B = 26.3$ ppm (A and B are arbitrarily assigned), $^2J_{PP} = 333.4$ Hz; whereas for the *syn* isomer, $\delta P_A = 19.0$ ppm, $\delta P_B = 17.5$ ppm, $^2J_{PP} = 336.3$ Hz. The P-P coupling constants are within the normal range for *trans* P-P coupling.[195]
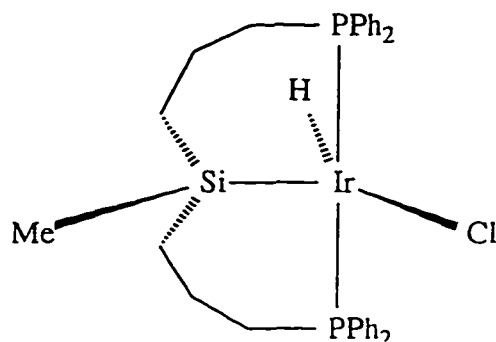
IrH(biPSi)Cl, <u>50</u>.

Similar iridium complexes containing organophosphinoalkylsilyl ligands have also been investigated in this group.[165-167,177,196] The reaction of [Ir(COD)(μ-Cl)]$_2$ with biPSiH (45) gives only one five-coordinate species (IrH(biPSi)Cl, 50), which has been characterized by NMR spectroscopy and X-ray crystallography. The crystal structure of 50 shows that the molecule adopts a trigonal bipyramidal structure, with the two phosphorus donors occupying the axial positions *trans* to each other, and the hydride being *anti* to the methyl groups attached to silicon. The hydride resonance in the ^{1}H NMR spectrum of 50 is located at -22.38 ppm as a triplet, due to the coupling to ($^2J_{PH}$ = 14.7 Hz) the two equivalent phosphorus nuclei. Unlike that of biPSiH (45), the reaction of mcbiPSi (46) with [Ir(COD)(μ-Cl)]$_2$ affords both *anti* and *syn* isomers, 10:1 ratio, in the product (IrH(mcbiPSi)Cl, 51). The hydride resonances located at -23.54 and -20.56 ppm in the ^{1}H NMR spectrum are assigned to the *anti* and the *syn* isomers, respectively. The solid state molecular structure of *anti*-51 was determined by X-ray crystallography, showing similar features to its biPSiH analogue, biPSiIrHCl (50).
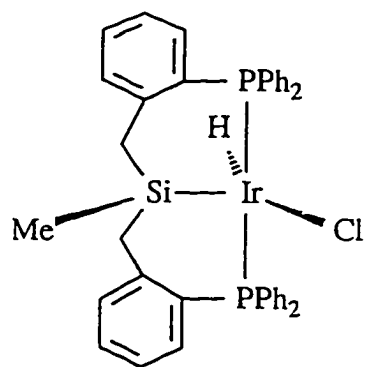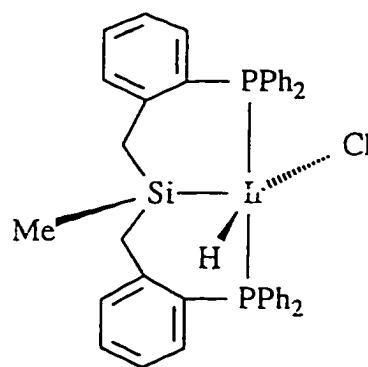
anti-51   *syn*-51

Five-coordinate complexes derived from tridentate ligand precursor mcbiPSi˙H (47) may have several possible structures depending on the orientation of the tridentate ligand and the geometry of the molecule (Figure 5-6). Among these possibilities, both
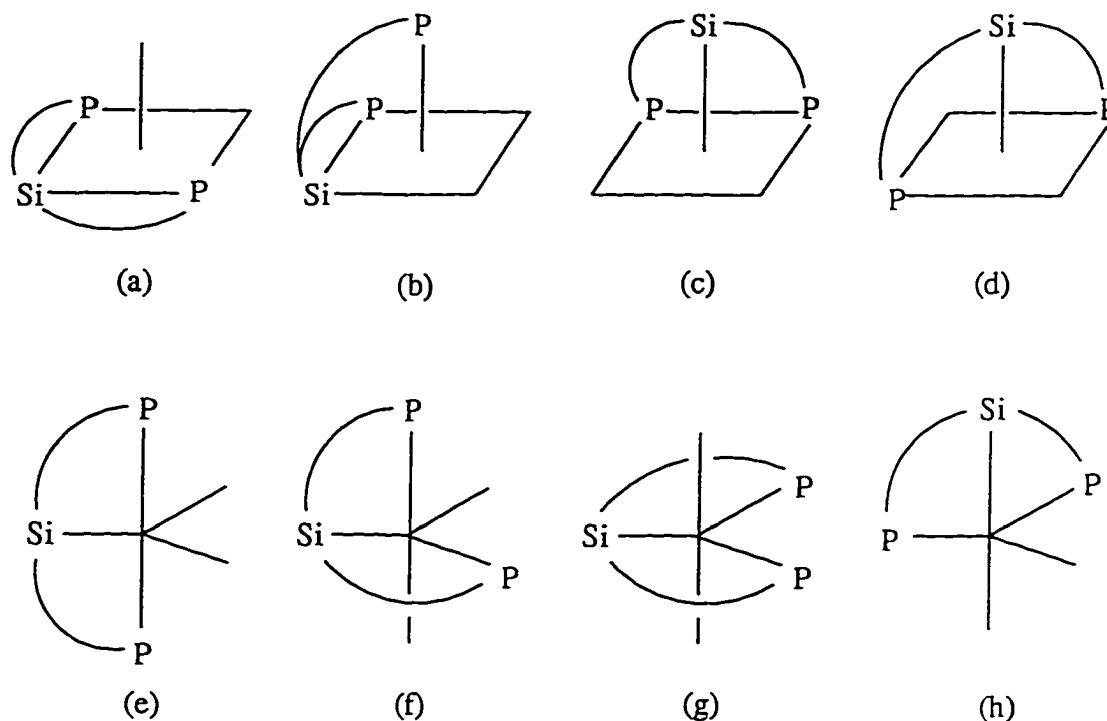
Figure 5-6. Possible structures for five-coordinate species containing mcbiPSi* ligands.

(a) and (e) in Figure 5-6 are compatible with all the available NMR data, and therefore cannot be distinguished without further analysis (*e.g.* X-ray structure determination). However, by making comparisons with those of its biPSiH and mcbiPSiH analogues (complexes 50 and 51), the structures of the two isomers in IrH(mcbiPSi*)Cl (49) are believed to be trigonal bipyramidal (Figure 5-6(e)), where the two phosphorus donors occupy the two axial sites and the silyl group, hydride and chloride are located at the equatorial positions. In the *anti* isomer, the hydride is *anti* to the menthoxy group, with H and OMen *syn* to each other in the *syn* isomer. These structures are also consistent with theoretical calculations, which have suggested that five-coordinate d^6 species containing four strong σ-donors and one single-faced π-donor would favour a distorted trigonal bipyramidal geometry, with the π-donor occupying an equatorial site. The angle formed by the two strong equatorial σ-donors and the metal centre is also

characteristically smaller than 120°, which is expected for a regular trigonal bipyramid.[197-199] Several complexes of this type have been reported, showing acute angles between two strong σ-donors in the equatorial plane ranging from 69° to 77.9°.[198,200] Similar features were also observed in five coordinate Ir-PSi complexes. In Ir(SiMe$_2$CH$_2$CH$_2$PPh$_2$)$_2$Cl, the Si-Ir-Si angle is 87°; in the single crystal structures of biPSiIrHCl (50)[159] and *anti*-mcbiPSiIrHCl (*anti*-51)[177], although the hydride atoms could not be located, the large Cl-Ir-Si angles (128° in 50, 131° in *anti*-51) imply small Si-Ir-H angles.
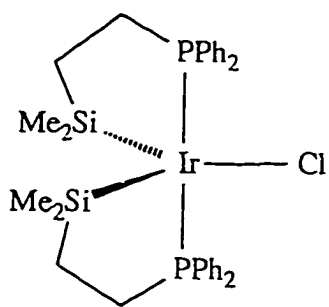
Ir(SiMe$_2$CH$_2$CH$_2$PPh$_2$)$_2$Cl

The ratio between the two isomers in the initial mixture of IrH(mcbiPSi*)Cl (49) is: *syn:anti* ≈ 8:1. This is in contrast with the results obtained from IrH(biPSi)Cl (50) and IrH(mcbiPSi)Cl (51). As mentioned earlier, only the *anti* isomer is observed in 50. In 51, although both isomers are present, the *anti*-51 is dominant. However, in the rhodium analogues of compounds 50 and 51, RhH(biPSi)Cl (52) and RhH(mcbiPSi)Cl (53), the percentage of the *syn* isomers in the kinetic products are considerably higher, with the *syn:anti* ratio being 40:60 in 52 and 7:1 in 53.[177] The rhodium analogue of 49, RhH(mcbiPSi*)Cl (54), was synthesized by Gossage of this research group. The kinetic product of 54 also consists of *syn* and *anti* diastereomers in 4:1 ratio.[177]

The formation of the *syn* or *anti* isomer is presumably influenced by steric

syn-<u>49</u>   *anti*-<u>49</u>

M = Ir,	R = MenO,	⌒⌒ = COD,	⌒ = *o*-benzyl
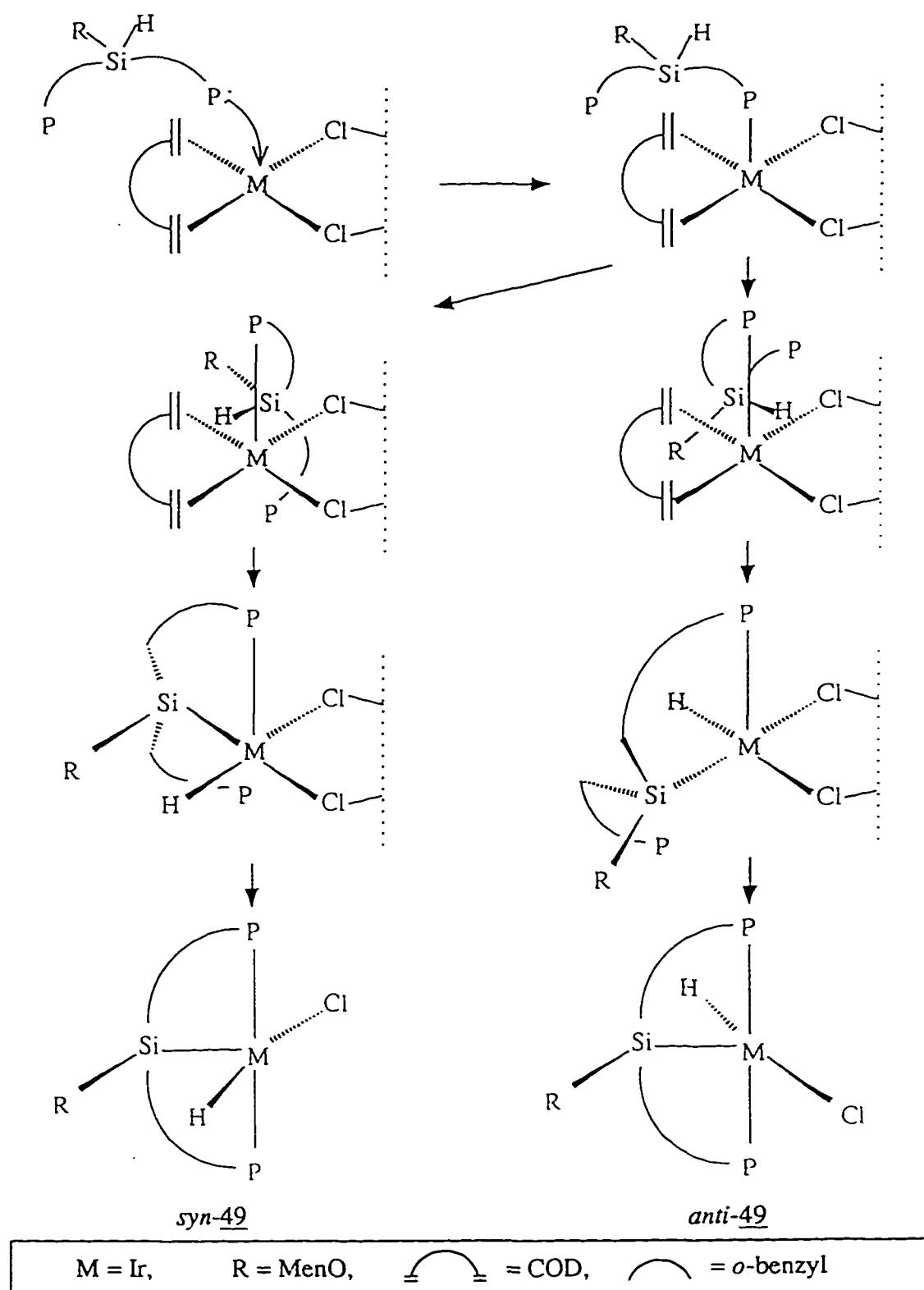
Scheme 5-5. Proposed mechanism for the formation of IrH(mcbiPSi˙)Cl, <u>49</u>.

factors. A likely pathway for the reaction between $[M(COD)(\mu-Cl)]_2$ (M = Ir or Rh) and mcbiPSi˙H ligand precursor (47) is proposed in Scheme 5-5, in which the reaction is viewed as occurring in three sequential steps. Firstly, one of the phosphorus donors coordinates to the metal centre through the apical site only, with the rest of the donor sites remaining free. Next, the oxidative addition of the Si-H bond to the metal centre takes place, replacing cyclooctadiene, but prior to the attack of the Si-H bond, the dangling ligand can be oriented in two different ways. If the remaining free phosphinoalkyl group is positioned pointing away from the metal centre, the product will be a *anti* isomer. Alternatively, the *syn* isomer will be formed if the menthoxy group attached to silicon is placed away from the metal centre. At this position, the free phosphorus donor is close to the metal centre so that the second P-M bond can be readily formed to complete the reaction (the third step). It is probably due to this interaction between the metal centre and the free phosphino group that one orientation in the second stage of the reaction is more favourable, resulting in the *syn* isomer as the kinetic product.

The ratio between the two isomers of IrH(mcbiPSi˙)Cl (49) changes gradually in the solution and therefore is not the thermodynamic distribution. This process was monitored by ^{1}H NMR spectroscopy in C_6D_6 solution at ambient temperature (Figure 5-7). The plot of integration ratio *vs.* time was fitted to determine equilibrium constant K and the forward and backward rate constants k_1 and k_{-1} (Figure 5-8). The results are: K = 7 ± 3, k_1 = (1.69 ± 0.07) × 10^{-6} s^{-1}, k_{-1} = (2.5 ± 1.1) × 10^{-7} s^{-1}. The free energy difference between the two isomers, ΔG^0_{298}, is obtained from the following calculation: ΔG^0_{298} = -RTln$K$ = -(5 ± 2) kJmol^{-1}.
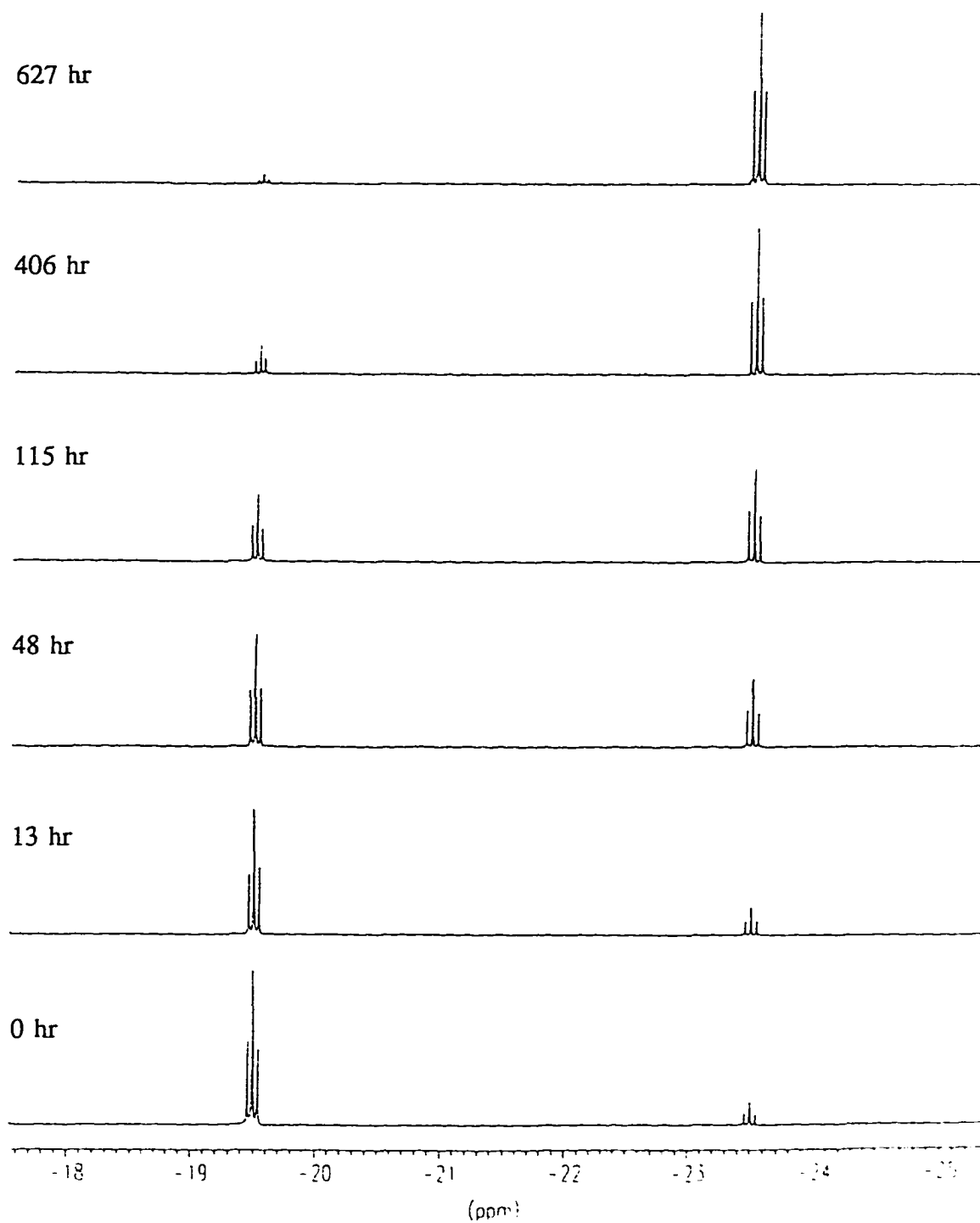
Figure 5-7. Isomerization process monitored by the ^{1}H NMR spectra of IrH(mcbiPSi*)Cl.

$$\textit{syn}\text{-mcbiPSi}^{\bullet}\text{IrHCl } (\textit{syn-}\underline{49}) \quad \underset{k_{-1}}{\overset{k_1}{\rightleftharpoons}} \quad \textit{anti}\text{-mcbiPSi}^{\bullet}\text{IrHCl } (\textit{anti-}\underline{49})$$

$K = 7 \pm 3$

$k_1 = (1.69 \pm 0.07) \times 10^{-6} \text{ s}^{-1}$

$k_{-1} = (2.5 \pm 1.1) \times 10^{-7} \text{ s}^{-1}.$
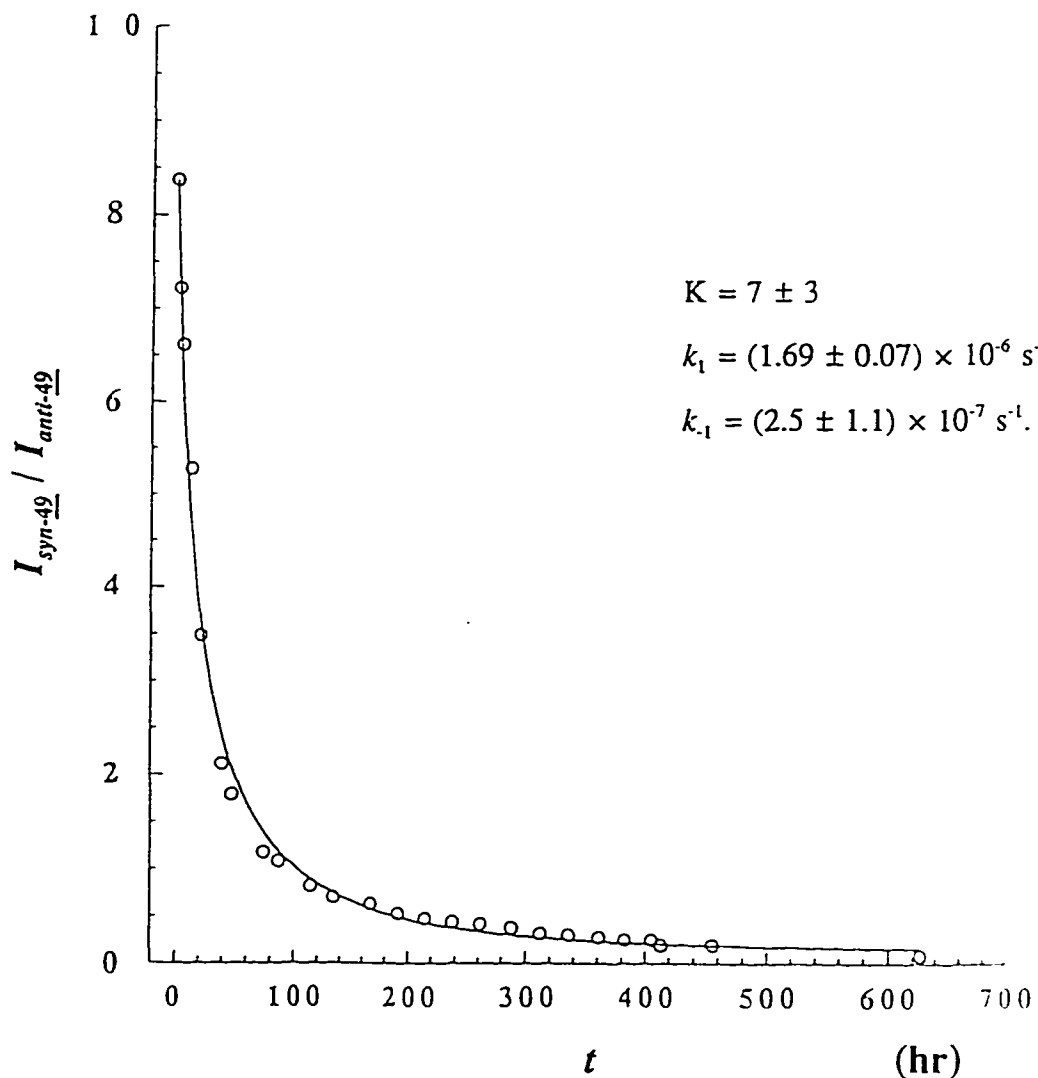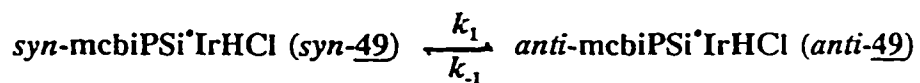
Figure 5-8. Plot of the integration ratio of *syn* and *anti* isomers in $\underline{49}$ vs. time.
I: integration. Equation used for curve-fitting:

$$\frac{I_{syn-\underline{49}}}{I_{anti-\underline{49}}} = \frac{k_{-1} - [k_{-1} - (k_1 + k_{-1}) \dfrac{1}{[I_{anti-\underline{49}}/I_{syn-\underline{49}}]_0 + 1}] e^{-(k_1 + k_{-1})t}}{k_1 - [k_1 - (k_1 + k_{-1}) \dfrac{1}{[I_{syn-\underline{49}}/I_{anti-\underline{49}}]_0 + 1}] e^{-(k_1 + k_{-1})t}} \tag{5-10}$$

where $[I_{syn-\underline{49}}/I_{anti-\underline{49}}]_0$ is the initial integration ratio.

Similar processes were also observed for the rhodium compounds RhH(biPSi)Cl (52), RhH(mcbiPSi)Cl (53), and RhH(mcbiPSi*)Cl (54).[177] For complex 53, the initial ratio of 7:1 between the *syn* and *anti* isomers shifted to 1:10, the thermodynamic distribution, in approximately one day. The isomerization process for 52 was more interesting because an intermediate was observed. The kinetic profile of this process is in good accordance with that of a consecutive reaction:

$$syn\text{-}52 \xrightarrow{\ k_1\ } \text{intermediate} \xrightarrow{\ k_2\ } anti\text{-}52,$$

where k_1 (determined experimentally as 4.6×10^{-3} s^{-1}) and k_2 are comparable. The 40:60 (*syn:anti*) kinetic distribution was eventually shifted to 5:5:90 (*syn:intermediate:anti*). By the NMR spectroscopic data, the intermediate was identified as a distorted square pyramidal species (Figure 5-9). This provided evidence for a possible general mechanism for the isomerization processes of the same type (Scheme 5-6). Theoretical calculations carried out by Kepert and co-workers show evidence that such a intermediate is energetically viable.[201] No intermediate was observed during the isomerization of 54. However, the conversion rate ($k_1 = (1.7 \pm 0.5) \times 10^{-6}$ s^{-1}, $k_{-1} = (2 \pm 5) \times 10^{-7}$ s^{-1}) is much slower than those of 51 and 52, and very close to that of 49.

Diastereoisomerization of the rhodium complexes, 52 and 53 is faster than that of IrH(mcbiPSi*)Cl (49), but each still takes days to complete. The isomerization rate
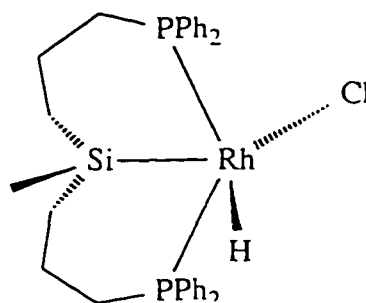
Figure 5-9. The intermediate in the isomerization process of RhH(mcbiPSi)Cl.
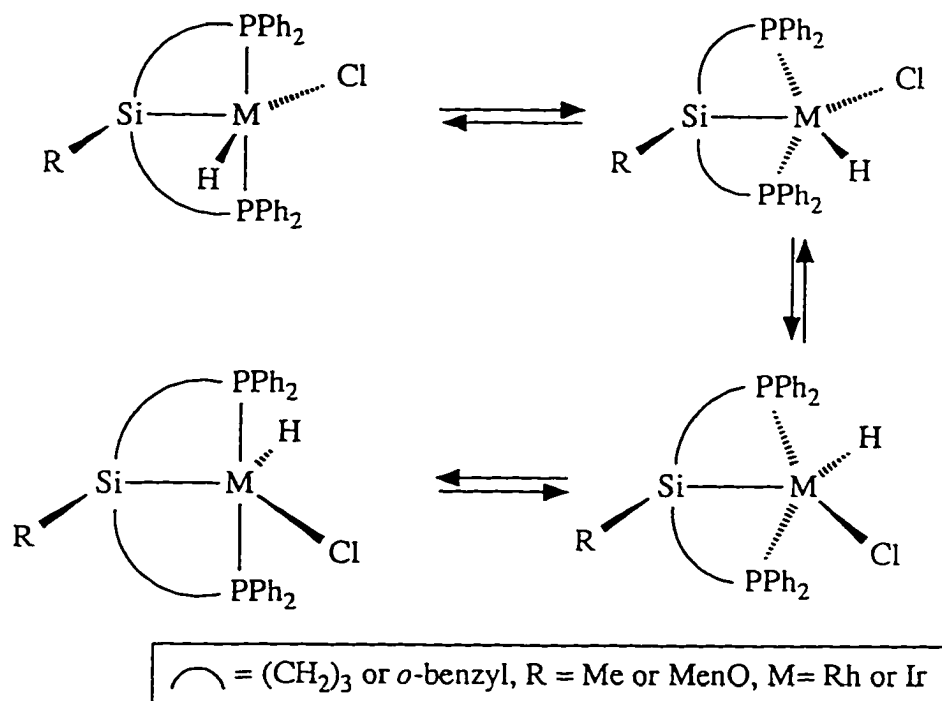
Scheme 5-6. Proposed mechanism for isomerization of complexes $\underline{49}$ - $\underline{53}$.

of IrH(mcbiPSi)Cl ($\underline{51}$) was qualitatively observed to be slow,[177] possibly also of the same order of magnitude as that of $\underline{52}$ or $\underline{53}$. However, the rate for IrH(biPSi)Cl ($\underline{50}$) is believed to be extremely fast in comparison with those of $\underline{49}$ and $\underline{51}$ - $\underline{53}$, resulting in *syn*-$\underline{50}$ being never detected.[159] The rate difference between $\underline{49}$ and $\underline{50}$, $\underline{51}$ is ascribed to the steric difference between ligands biPSi, mcbiPSi, and mcbiPSi*. Since the aromatic groups that connects the phosphors donors and the silyl group in mcbiPSi and mcbiPSi* are much bulkier than the aliphatic chains in biPSi, and the three rotationally flexible carbon atoms connecting the silicon centre with the phosphorus donors in biPSi are reduced to one in mcbiPSi and mcbiPSi*, the constraints in the metallocycle rings in mcbiPSi and mcbiPSi* are much higher than that in biPSi, and so are the activation energies for the conversion process. The similar trend in the isomerization rate of the rhodium complexes $\underline{52}$ - $\underline{54}$ is supportive of this analysis.

Complex $\underline{49}$ (*anti*- and *syn*-IrH(mcbiPSi*)Cl) is subject to addition reactions since
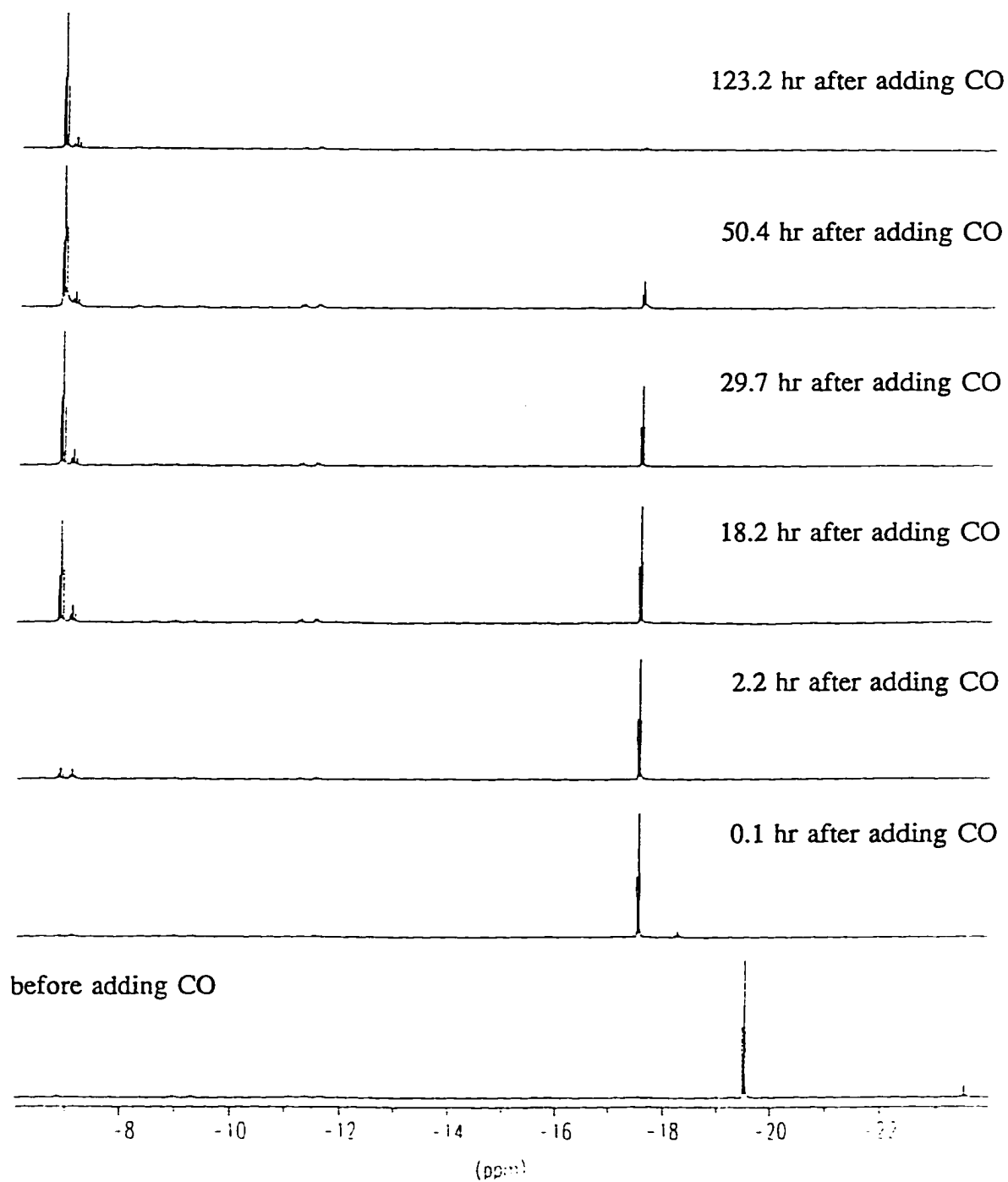
Figure 5-10. CO addition to IrH(mcbiPSi*)Cl (49) monitored by ¹H NMR spectroscopy.

its coordination sphere is unsaturated. The addition of carbon monoxide to this complex revealed a series of interesting ligand rearrangement processes. The reaction was carried out in an NMR tube containing a C_6D_6 solution of <u>49</u> at an isomeric ratio of about 5:1 (*syn:anti*), through which a stream of CO was bubbled. The solution was then monitored by NMR spectroscopy. The ^1H NMR spectra are shown in Figure 5-10. Five minutes after the CO addition, the two hydride resonances due to the five-coordinate species were completely absent and new triplets at -17.55 ppm ($^2J_{PH}$ = 11.9 Hz) and -18.28 ppm ($^2J_{PH}$ = 16.0 Hz) had appeared in a ratio of 16:1. The high field chemical shifts indicate that these hydrides are *trans* to a weak ligand, *i.e.* chloride in the new octahedral species IrH(mcbiPSi*)(CO)Cl, <u>55</u>. The resonance at -17.55 ppm is assigned to the hydride in the *syn* isomer (*syn-*<u>55</u>), since this is the major product. The triplet at -18.28 ppm is therefore due to *anti-*<u>55</u>. These kinetic products (*syn-* and *anti-*<u>55</u>) are not stable in solution. As shown in Figure 5-10, as the reaction progressed, *anti-*<u>55</u> completely disappeared and the amount of *syn-*<u>55</u> decreased. This was accompanied by the emerging of two new resonances at -6.88 ppm ($^2J_{PH}$ = 15.7 Hz) and -7.09 ppm ($^2J_{PH}$ = 20.8 Hz). These low field hydride signals suggest that strong ligands, such as carbonyl or silyl groups, are *trans* to hydride. Based on the comparison with the structurally analogous biPSi system (*vide infra*), these resonances are assigned to a pair of new

syn-<u>55</u>   *anti-*<u>55</u>
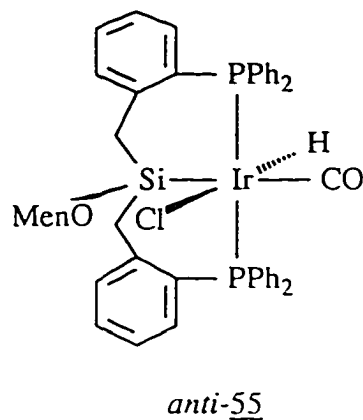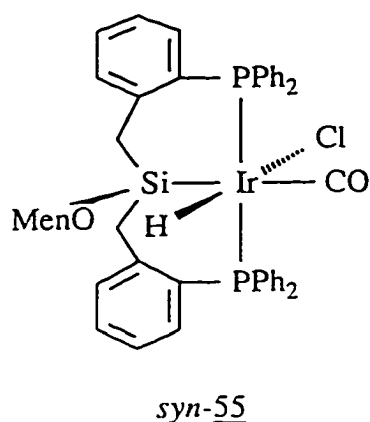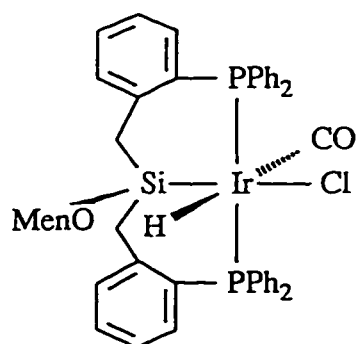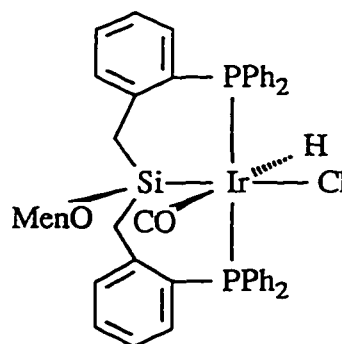
syn-56   *anti*-56

isomers, *syn-* and *anti*-IrH(mcbiPSi*)(CO)Cl (*syn-* and *anti*-56), with the CO group *trans*

to the hydride. Based on the intensity difference of the hydride resonances, the signal

at -6.88 ppm is assigned to *syn*-56, and the signal at -7.09 ppm to *anti*-56. The

integration ratio between the two resonances (-6.88 ppm *vs*. -7.09 ppm) reached 11:1

after 5 days, when *syn*-56, the kinetic product, was almost depleted. It is also noticed

that the conversion from *anti*-56 to *anti*-56 is much faster than the conversion from *syn*-

55 to *syn*-56, since all *anti*-55 was converted within two hours.

The $^{31}P\{^1H\}$ NMR spectra for the same isomerization process were also recorded.

The resonances due to *syn-* and *anti*-55, *syn-* and *anti*-56 are located at 0.1, -1.4, -3.1,

and -6.0 ppm, respectively. Although the two phosphorus nuclei in each molecule are

inequivalent to each other because of the optically active menthoxy groups, all signals

are singlets, due to the coincidental equal chemical shifts arising from the two

phosphorus atoms. The identical chemical shift values of the two phosphorus atoms

confirms that the tridentate mcbiPSi*H ligand adopts a *mer* conformation (*i.e.* the two

phosphorus donors are *trans* to each other and *cis* to silicon). In a *fac* geometry, where

silicon and two phosphorus are all *cis* to each other, the chemical shifts of the two

phosphorus atoms would be differentiated by the various functional groups *trans* to

them.
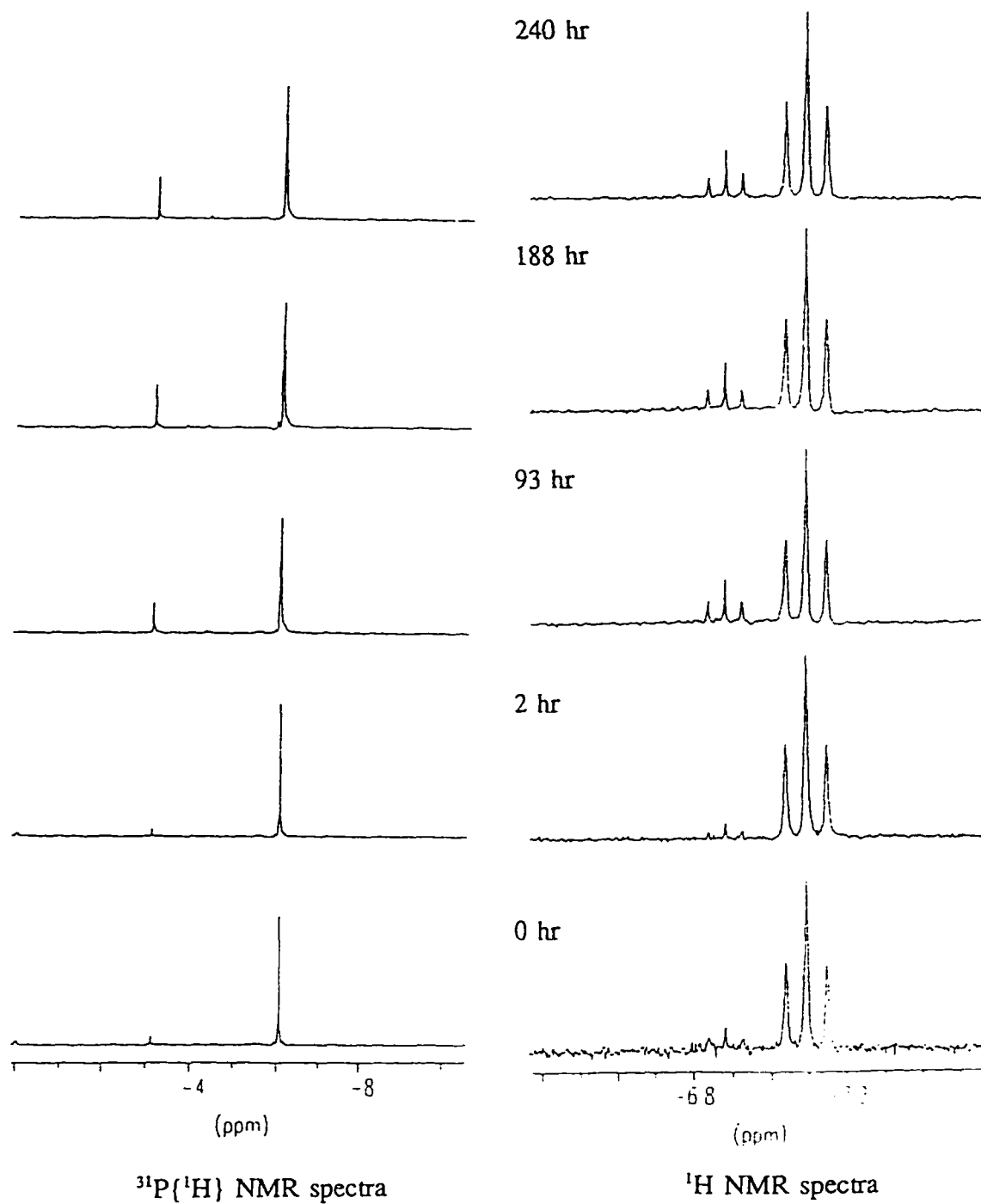
Figure 5-11. The interconversion in <u>56</u> monitored by $^{31}P\{^1H\}$ and ^1H NMR spectroscopy.

The isomerization process is not completed, however, with conversion of the kinetic cabonyl adducts (55) to the isomeric products (56). When 56 is left in solution, *syn*-56 slowly isomerises to *anti*-56 (Figure 5-11. In the experiment, CO was reacted with an aged sample of IrH(mcbiPSi⁺)Cl (49), in which the thermodynamically favored *anti*-isomer was already dominant). In about 10 days, the hydride resonance due to *syn*-56 becomes barely detectable.

With a *mer* tridentate ligand in the coordination sphere, there are six possible structures for the CO adducts of IrH(mcbiPSi⁺)Cl (49) (Figure 5-12). Structures (a) and (b) can be assigned to the kinetic adducts (*syn* and *anti*-55, respectively) because of the high field hydride resonances observed in the ¹H NMR spectra, *i.e.* putting H *trans* to Cl (*vide supra*). However, the chemical shifts of the hydride signals in the NMR spectra of the thermodynamic adducts (*syn*- and *anti*-56) imply that the hydride is *trans* to a strong donor which could be either a silyl or a carbonyl group. This ambiguity is
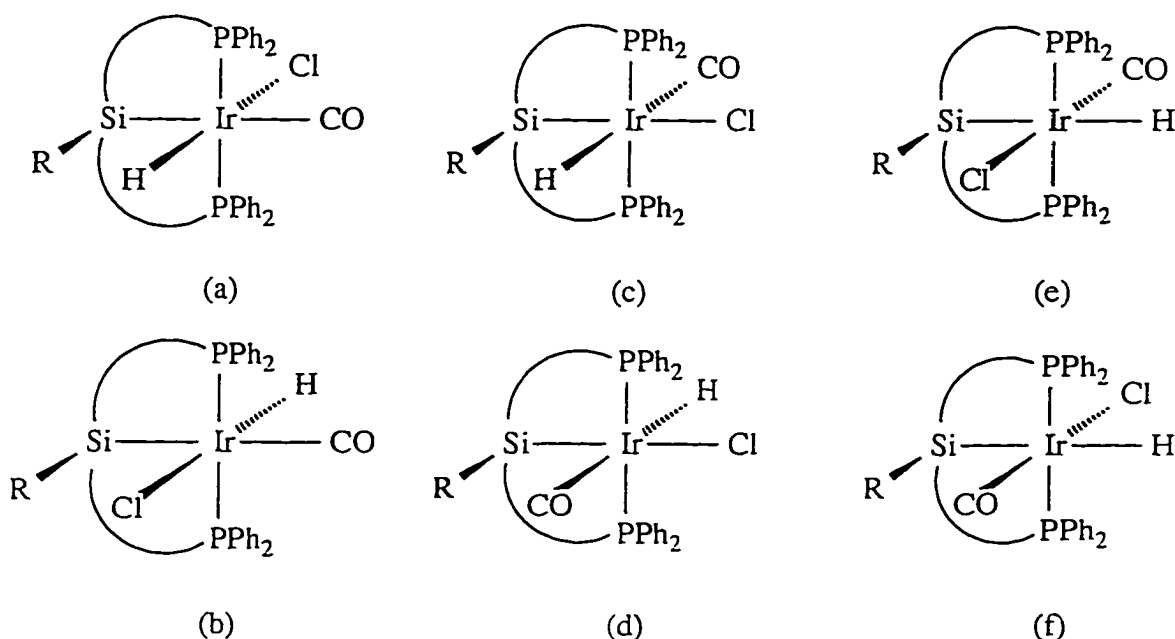
Figure 5-12. Possible structures for CO adducts of IrH(mcbiPSi⁺)Cl, 49.
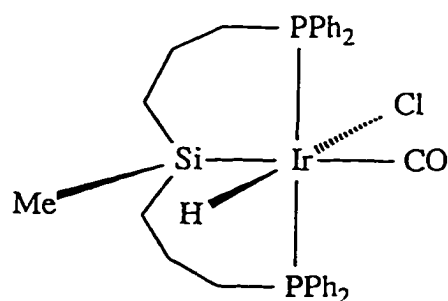
syn-57
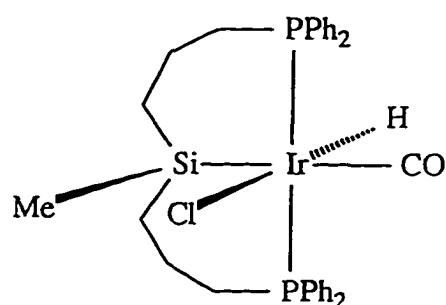
anti-57
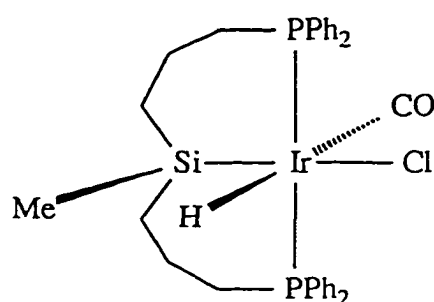
syn-58
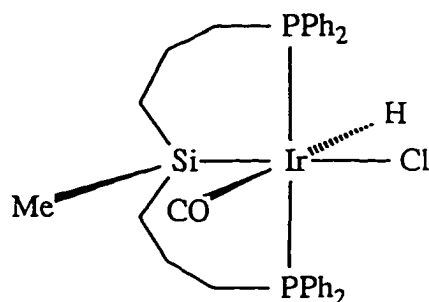
anti-58

resolved by comparison with the behaviour of analogues formed when the unmodified biPSiH ligand precursor reacts at an Ir(I) center: the reaction between CO and IrH(biPSi)Cl (50) produces a pair of kinetic adducts, *syn-* and *anti-57*, which subsequently rearrange to the thermodynamic adducts, *syn-* and *anti-58*.[159] Compounds *syn-57* and *syn-58* have identical spectroscopic data to those of the products of the reaction between biPSiH (45) and Vaska's complex, *trans*-Ir(PPh$_3$)$_2$(CO)Cl (Equation 5-11). Because oxidative addition of Si-H bond to a metal centre is viewed as a concerted process,[109] the silyl group and the hydride should be *cis* to each other in the product. This has been verified by measuring the nuclear Overhauser enhancement difference spectra of *syn-57* and *syn-58*, thereby showing that the distance between the hydride and the silicon atom in either molecule is within 3 Å[177] and establishing that

complex <u>58</u> possesses structure (c) and (d) of Figure 5-12, *i.e.* with H *trans* to CO (not Si). Since the mcbiPSi* and biPSi are structurally analogous, structures (c) and (d) are also assigned to the *syn-* and *anti* diastereomers of compound <u>56</u>.

$$\textit{trans-}Ir(PPh_3)_2(CO)Cl + \underline{45} \longrightarrow \textit{syn-}\underline{57} + \textit{syn-}\underline{58}$$

$$75\% \qquad 25\% \qquad (5\text{-}11)$$
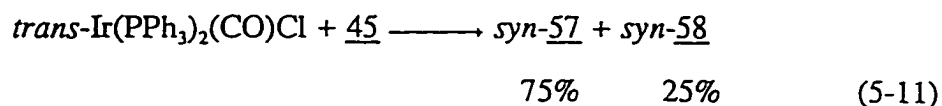
It is plausible that carbon monoxide can attack the metal centre of the five-coordinate IrH(mcbiPSi*)Cl (<u>49</u>) from three directions to form six-coordinate adducts, see Scheme 5-7. Since the CO adducts with structures (e) and (f) in Figure 5-12 are not detected, the CO addition to the metal centre through the Si-Ir-H angle is disfavoured. This is probably because (a) sterically, this angle is smaller than the other two (Si-Ir-Cl and Cl-Ir-H angles, *vide supra*), and (b) in the adducts two strong σ-donors (silyl group
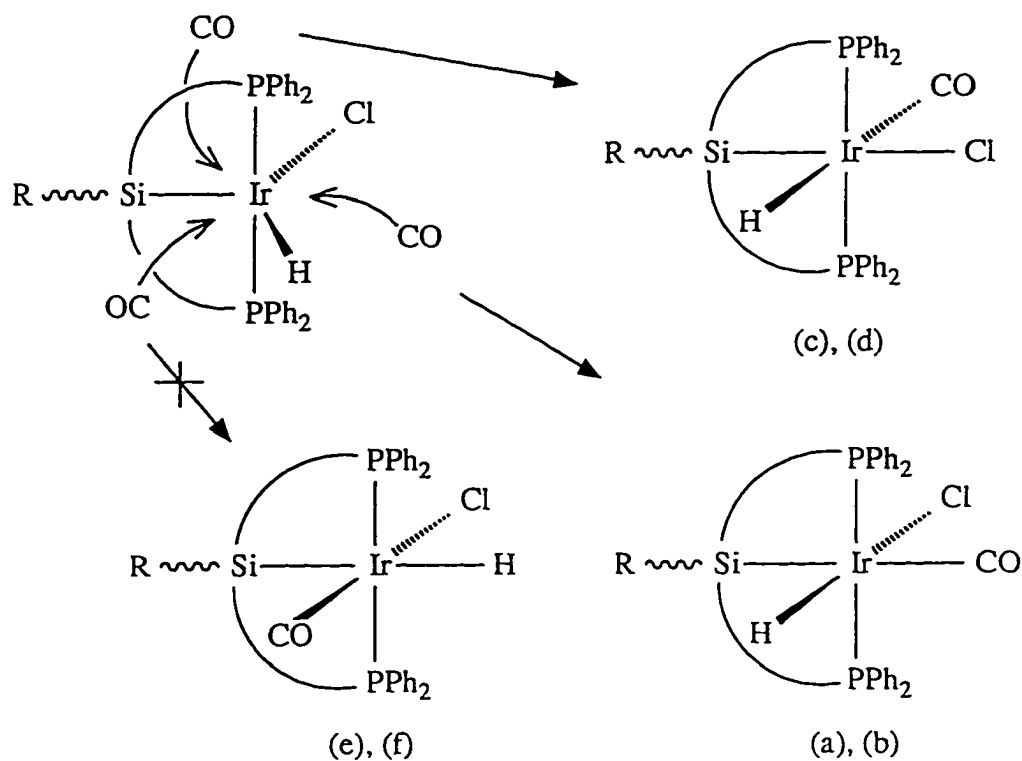
Scheme 5-7. Possible CO attack directions during its addition to IrH(mcbiPSi*)Cl. <u>49</u>.

and hydride) will be *trans* to each other, which is a unstable configuration likely to isomerize rapidly to other structures.

Similar CO addition processes were also observed for IrH(biPSi)Cl (50) and IrH(mcbiPSi)Cl (51), analogues of IrH(mcbiPSi*)Cl (49) (Scheme 5-8).[177] The first of these (50) generates two octahedral carbonyl adducts, *syn-* and *anti-57*, in 1:1 ratio, then further rearrangement occurs to form the thermodynamic adducts *syn-* and *anti-58* also in 1:1 ratio. It is believed that *syn-57* results from CO addition to *syn-50*, which, although never observed, may be in rapid equilibrium with *anti-50*. The reaction between mcbiPSiIrHCl (51) and carbon monoxide also follows subsequential steps. Initial formation of unstable kinetic adducts (*syn-* and *anti-59*), analogues of 57 and 55, is followed by subsequent rearrangement, giving rise to the thermodynamic isomers
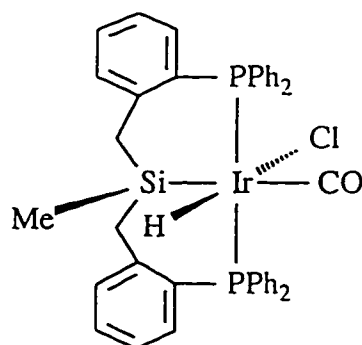
syn-59
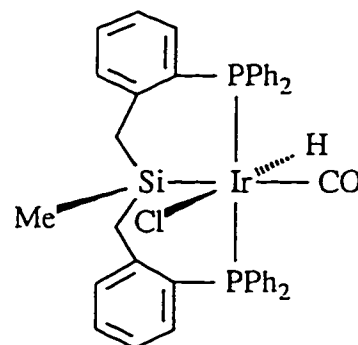
anti-59
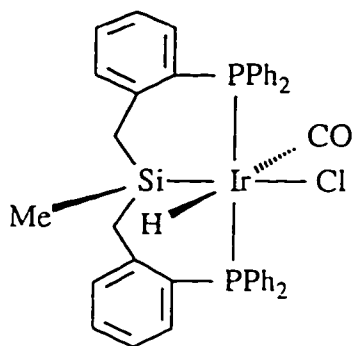
syn-60
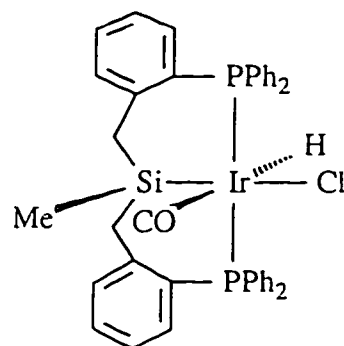
anti-60
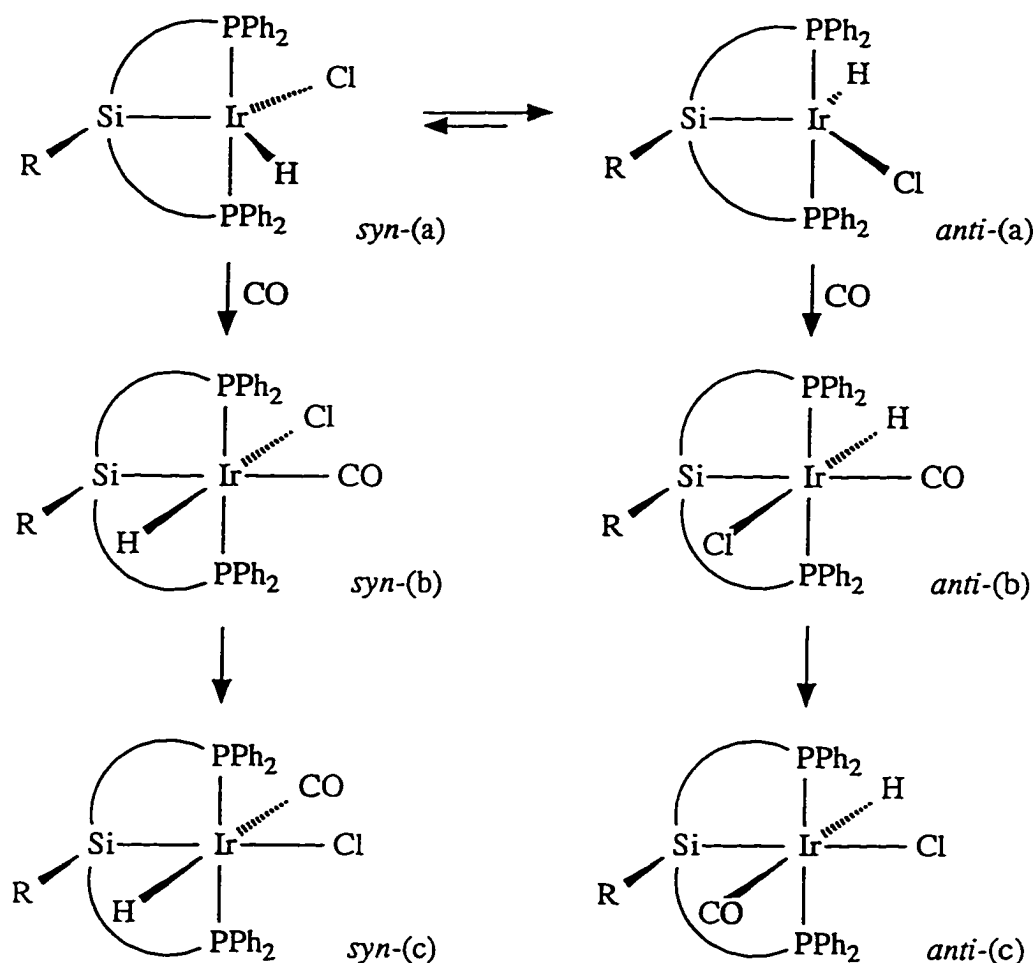
$$(a) = \underline{49}, (b) = \underline{55}, (c) = \underline{56}: \quad PSi = mcbiPSi^{*};$$

$$\underline{50} \qquad \underline{57} \qquad \underline{58}: \quad PSi = biPSi;$$

$$\underline{51} \qquad \underline{59} \qquad \underline{60}: \quad PSi = mcbiPSi.$$

Scheme 5-8. CO addition to five-coordinate Ir complexes ($\underline{49}$ - $\underline{51}$).

(*syn*- and *anti*-$\underline{60}$), analogues of $\underline{56}$ and $\underline{58}$. The difference between the two systems (biPSi *vs*. mcbiPSi) is that for the latter, the ratio between the *anti* and *syn* isomers is kept same throughout the whole process (*i.e. anti*-$\underline{51}$:*syn*-$\underline{51}$ = *anti*-$\underline{59}$:*syn*-$\underline{59}$ = *anti*-$\underline{60}$:*syn*-$\underline{60}$ = 10:1).

In the ^{1}H NMR spectra of the CO adducts of IrH(biPSi)Cl ($\underline{50}$) and

Table 5-2. ^{1}H NMR data of the hydride resonances of the six-coordinate complexes and their starting materials.

Compound	Chemical Shift (ppm)		$^2J_{PH}$ (Hz)	
	syn	*anti*	*syn*	*anti*
IrH(mcbiPSi*)Cl, __49__	-19.52	-23.51	13.9	16.2
IrH(biPSi)Cl, __50__		-22.38		14.7
IrH(mcbiPSi)Cl, __51__	-20.56	-23.54	14	16
IrH(mcbiPSi*)(CO)Cl,__55__	-17.55	-18.28	11.9	16.0
IrH(mcbiPSi*)(CO)Cl,__56__	-6.88	-7.09	15.7	20.8
IrH(biPSi)(CO)Cl, __57__	-18.06	-18.50	16	15
IrH(biPSi)(CO)Cl, __58__	-6.09	-7.27	15	16
IrH(mcbiPSi)(CO)Cl, __59__	-17.40	-18.06	14	16
IrH(mcbiPSi)(CO)Cl, __60__	-7.41	-6.09	16	18

IrH(mcbiPSi)Cl (__51__) (Table 5-2), the hydride resonances of the kinetic products (__57__ and __59__) are located at about -18 ppm, in the same region where the hydride resonances of __55__ are observed (-17.55 and -18.28 ppm), indicating similar structures among __55__, __57__, and __59__. The signals due to the hydrides in the thermodynamic adducts (__58__ and __60__) are found at a much lower field about -7 ppm, again suggesting comparable configurations to that of __56__, since the resonances due to the hydrides in __56__ are also identified in the same region (-6.88 and -7.09 ppm). All hydride resonances are triplets, with $^2J_{Ph}$ values in the range of 10-20 Hz (also comparable to those of __55__ and __56__), implying *cis*

couplings to two equivalent phosphorus nuclei.

The conversion from the kinetic CO adducts (55, 57, and 59) to the thermodynamic adducts (56, 58, and 60) retains the structural relationships (*syn* or *anti*) between the R-Si (R = Me or MenO) bond and the Ir-H bond. A possible mechanism for this process is illustrated in Scheme 5-9, where the kinetic products are transformed into the thermodynamic products through dissociation of carbon monoxide and subsequent re-addition of CO from a different site. An isomerization mechanism for a similar process that converts the SnCl$_2$ derivative of *anti*-IrH(biPSi)(CO)Cl (57) to its thermodynamic isomer, SnCl$_2$ derivative of *anti*-IrH(biPSi)(CO)Cl (58) was proposed by Joslin.[159] As shown in Scheme 5-10, this mechanism involves reductive elimination of Si-H, followed by rotation of the four-coordinate species along the P-Ir-P axis, and oxidative re-addition of Si-H. Another mechanism for the isomerisation of *syn*- and *anti*-IrH(biPSi)(CO)Cl (*syn*- and *anti*-57) suggested that the six-coordinate species could
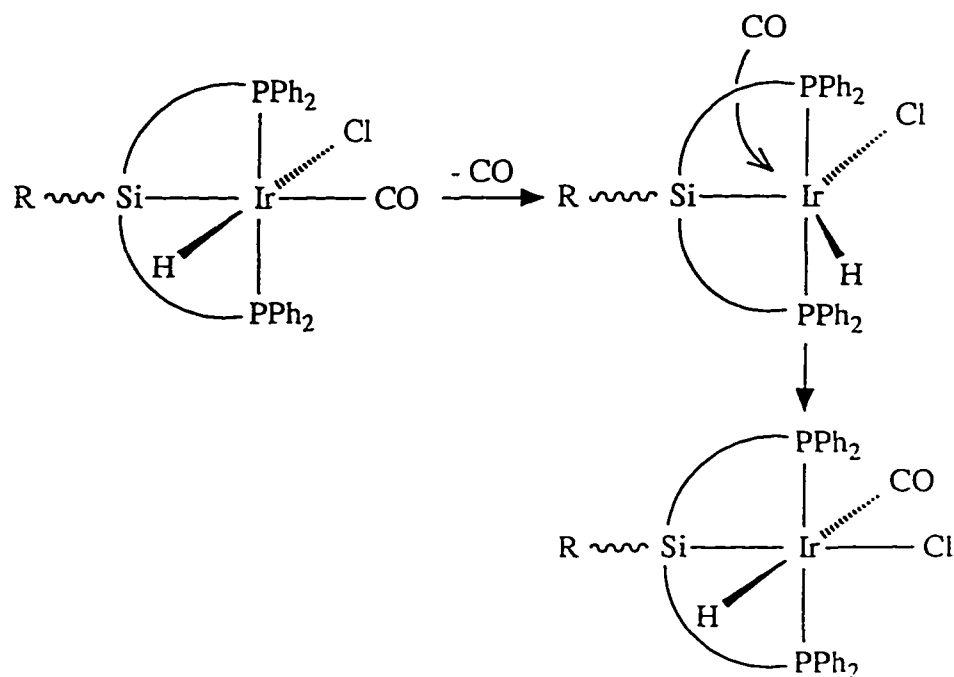
Scheme 5-9. Possible isomerization mechanism involving dissociation of CO.
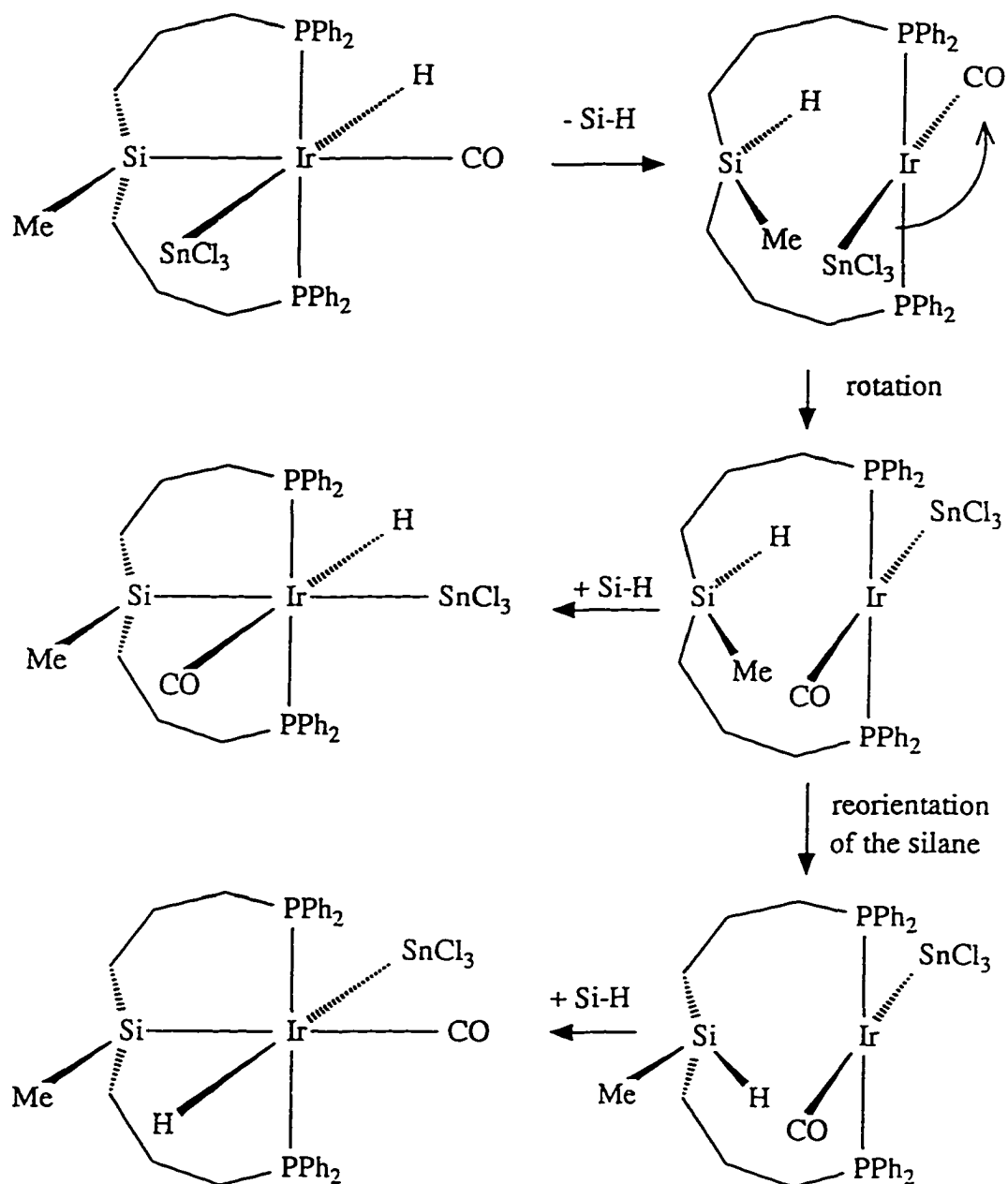
Scheme 5-10. Isomerization mechanism proposed for *anti*-IrH(biPSi)(*t*-SnCl₃)(CO).

undergo reductive elimination of HCl, generating a square planar four-coordinate intermediate. The re-addition of HCl could then produce the rearranged isomers (Scheme 5-11).[159] However, in both of these mechanisms (elimination and re-addition of Si-H or
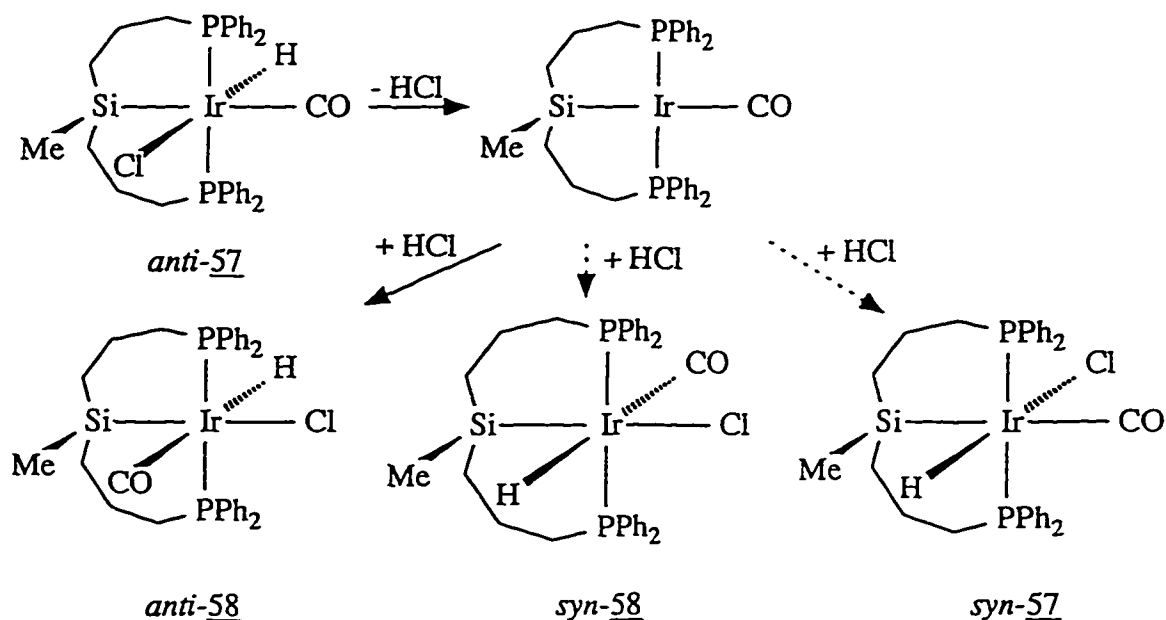
Scheme 5-11. Possible isomerization mechanism involving dissociation of HCl.

H-Cl), the "cross isomerization" between the *syn* and *anti* isomers could occur (Schemes 5-10 and 5-11). For the former, this could be due to a slight rotation of the orientation of the silane in the intermediate; and for the latter, the re-addition of HCl from the other face of the square planar intermediate could cause the same effect, which is contradictory to the retention of the isomeric ratio from the kinetic adducts to the thermodynamic adducts. The CO dissociation and re-addition mechanism (Scheme 5-9), however, will not have the same problem, since none of the hydride, chloride, or silyl groups is involved in the isomerization, thus the relative geometries (*i.e. syn vs. anti*) are retained.

Unlike the IrH(mcbiPSi⁺)(CO)Cl (56) system, no change in the isomeric ratios in Ir(biPSi)(CO)Cl (58) or IrH(mcbiPSi)(CO)Cl (60) in solutions was observed at room temperature. The interconversion between the *syn-* and *anti*-56 may occur through the rearrangement between the five-coordinate species, *syn-* and *anti*-IrH(mcbiPSi⁺)Cl (49), which are generated by CO dissociation of the six-coordinate complexes, as shown in

Scheme 5-9. The fact that the rate of the interconversion between *syn-* and *anti-* $\underline{56}$ is about same as that between *syn-* and *anti-*$\underline{49}$ is supportive of such a mechanism. Thus an overall mechanism for the CO addition reaction can be obtained (Scheme 5-12). According to this mechanism, the magnitude of the rate constants should be in the order:

$$k_2 \sim k_3 > k_4 \sim k_5 > k_1 \gg k_{-1}.$$
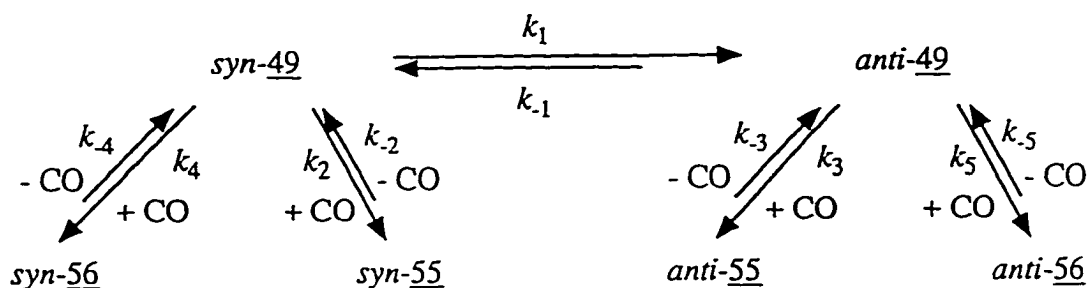
Scheme 5-12. Overall mechanism for the CO addition reaction.

The investigation on the reactivity of mcbiPSi*H ($\underline{47}$) and related ligand precursors (biPSiH ($\underline{45}$) and mcbiPSiH ($\underline{46}$)) shows that a) the asymmetric fragment was successfully introduced into the tridentate organophosphinoalkylsilane system; b) the presence of the aromatic groups in the ligand framework and the bulky menthoxy substitution on silicon make the complexes derived from $\underline{47}$ more rigid systems than their analogues from $\underline{45}$ or $\underline{46}$; c) the asymmetric influence of the optically active menthoxy group is reflected in the NMR spectroscopic data, showing potentials of ligand $\underline{47}$ in asymmetric catalysis, since complexes containing structural related $\underline{45}$ are known catalysts for hydroformylation reactions.[156] The mechanistic study of the CO addition reaction of IrH(mcbiPSi*)Cl $\underline{49}$ in comparison to that of IrH(biPSi)Cl ($\underline{50}$) and IrH(mcbiPSi)Cl ($\underline{51}$) shows interesting stereochemistry of the six-coordinate species ($\underline{55}$-$\underline{60}$), and may provide insight to the mechanism of the catalytic cycle of the hydroformylation reaction.

Chapter 6

EXPERIMENTAL

6.A. General

All synthetic operations were carried out under an atmosphere of dry nitrogen gas, with the use of standard bench-top inert atmosphere (Schlenk) techniques. Solvents were degassed, dried with a suitable reagent and redistilled immediately before use:

(i) THF, diethyl ether, hexanes, pentane, and toluene from sodium/benzophenone;

(ii) dichloromethane from calcium hydride.

All starting materials were either purchased or synthesized using straightforward literature methods (Table 6-1).

Table 6-1. Starting materials.

Compound	Reference
$[Ir(COD)(\mu\text{-}Cl)]_2$	202
endo-Norbornyl iodide	151
exo-Norbornyl iodide	153
$o\text{-}Ph_2C_6H_4CH_2Li$	203
$(COD)PtCl_2$	204

Microanalytical data were supplied by Canadian Microanalytical Services Ltd., Vancouver. All instruments employed in this work are listed in Table 6-2.

Table 6-2. Instruments.

Technique	Spectrometer[a]
IR	Perkin-Elmer 1330
	Bruker IFS25
^{1}H NMR	Bruker WM250 (250.1 MHz)
	Bruker AMX360 (360.1 MHz)
^{13}C NMR	Bruker WM250 (62.9 MHz)
	Bruker AMX360 (90.6 MHz)
^{31}P NMR	Bruker WM250 (101.3 MHz)
	Bruker AMX360 (145.8 MHz)
Mass Spec.	Kratos Concept-H
	Finnigan-3300

[a] Operating frequencies of the NMR spectrometers are given in parentheses.

6.B. Synthesis of Compounds

6.B.a. Chiral Phosphinites

General Procedure

All chiral phosphinites were synthesized in a similar fashion. One mol. equiv. of Ph_2PCl in 40 mL of ether was added to the solution of a chiral alcohol in 20 mL of ether. The clear solution was usually stirred at room temperature for 5-10 hr, following which the solvent was removed under vacuum. The product was typically a colourless or pale yellow viscous liquid. The yields ranged from 80-85%. Analytical data are shown in Tables 6-3 ($^{13}C\{^{1}H\}$ NMR), 6-4 (^{1}H and $^{31}P\{^{1}H\}$ NMR) and 6-5 (Elemental Analysis and Mass Spec.).

MenOPPh$_2$, 1

According to the general procedure, MenOH (2.0 g, 12.8 mmol) and Ph_2PCl (2.3 mL, 2.83 g, 12.8 mmol) were used, yielding a clear viscous liquid product (3.5 g, 10.3 mmol, 80% yield).

BorOPPh$_2$, 2

According to the general procedure, BorOH (2.0 g, 13.0 mmol) and Ph_2PCl (2.4 mL, 2.95 g, 13 mmol) were used, yielding a white crystalline product (3.5 g, 10.3 mmol, 82% yield).

IpcOPPh$_2$, 3

According to the general procedure, IpcOH (2.0 g, 13.0 mmol) and Ph_2PCl (2.4 mL, 2.95 g, 13 mmol) were used, yielding a clear viscous liquid product (3.6 g, 10.6

mmol, 82% yield).

Attempted synthesis of fenchyl diphenylphosphinite.

Fenchyl alcohol (2.0 g, 13.0 mmol) and PPh$_2$Cl (2.4 mL, 2.95 g, 13 mmol) were reacted according to the general procedure. However, the NMR spectra of the product showed a mixture of unidentifiable compounds.

Attempted synthesis of cedryl diphenylphosphinite.

Cedrol (2.0 g, 9.0 mmol) and PPh$_2$Cl (1.6 mL, 1.97 g, 8.9 mmol) were reacted following the general procedure. The product, however, was proven by the NMR spectra to be a mixture of unidentifiable compounds.

6.B.b. Chiral Phosphonites

General Procedure

All chiral phosphonites were synthesized according to the following route: Two-fold excess of triethylamine was added to the ethereal solution (20 mL) of a chiral alcohol followed by dropwise addition of 0.5 mol. equiv. of PhPCl$_2$ in 40 mL of ether at 0 °C. A white precipitate formed immediately. The mixture was usually stirred at room temperature for 5-10 hr, and the solid was then filtered off. The solvent was removed from the filtrate under vacuum. The yields varied from 82-92%. Analytical data are shown in Tables 6-3 (^{13}C{^{1}H} NMR), 6-4 (^{1}H and ^{31}P{^{1}H} NMR) and 6-5 (Elemental Analysis and Mass Spec.).

(MenO)$_2$PPh, 4

According to the general procedure, MenOH (2.0 g, 12.8 mmol), triethylamine

(3.6 mL, 2.62 g, 25.9 mmol) and PhPCl$_2$ (0.84 mL, 1.14 g, 6.36 mmol) were used, yielding a clear viscous liquid product (2.3 g, 5.5 mmol, 86% yield).

(BorO)$_2$PPh, 5

According to the general procedure, BorOH (2.0 g, 13.0 mmol), triethylamine (3.6 mL, 2.62 g, 25.9 mmol) and PhPCl$_2$ (0.86 mL, 1.17 g, 6.52 mmol) were used, yielding a clear viscous liquid product (2.2 g, 5.3 mmol, 82% yield).

(IpcO)$_2$PPh, 6

According to the general procedure, IpcOH (2.0 g, 13.0 mmol), triethylamine (3.6 mL, 2.62 g, 25.9 mmol) and PhPCl$_2$ (0.86 mL, 1.17 g, 6.52 mmol) were used, yielding a clear viscous liquid product (2.5 g, 6.0 mmol, 92% yield).

6.B.c. Chiral Phosphites

General Procedure

All chiral phosphites were synthesized according to the following route: five-fold excess of triethylamine was added to a ethereal solution (20 mL) of one mol. equiv. of chiral alcohol followed by dropwise addition of one-third mol. equiv. PCl$_3$ in 60 mL of ether at -70 °C. resulting in immediate formation of white precipitate. After the addition, the mixture was slowly warmed up to room temperature and stirred for 5-10 hr. The precipitate was then filtered off and the solvent was removed from the filtrate under vacuum. The yields varied from 75-85%. Analytical data are shown in Tables 6-3 (^{13}C{^{1}H} NMR), 6-4 (^{1}H and ^{31}P{^{1}H} NMR) and 6-5 (Elemental Analysis and Mass Spec.).

(MenO)₃P, 7

According to general procedure, MenOH (2.0 g, 12.8 mmol), triethylamine (9.0 mL, 6.54 g, 64.7 mmol) and PCl₃ (0.46 mL, 0.72 g, 4.3 mmol) were used, yielding a clear liquid product (2.0 g, 4.0 mmol, 94% yield).

(BorO)₃P, 8

According to general procedure, BorOH (2.0 g, 13.0 mmol), triethylamine (9.0 mL, 6.54 g, 64.7 mmol) and PCl₃ (0.46 mL, 0.72 g, 4.3 mmol) were used, yielding a white crystalline product (1.6 g, 3.3 mmol, 75% yield).

(IpcO)₃P, 9

According to general procedure, IpcOH (2.0 g, 13.0 mmol), triethylamine (9.0 mL, 6.54 g, 64.7 mmol) and PCl₃ (0.46 mL, 0.72 g, 4.3 mmol) were used, yielding a clear liquid product (1.8 g, 3.7 mmol, 85% yield).

Reaction between PCl₃ and MenOH

In an NMR tube, 0.03 mL of PCl₃ (0.047 g, 0.34 mmol) was dissolved in 0.5 mL CDCl₃, and the $^{31}P\{^1H\}$ NMR spectrum was recorded. To this solution, 0.1 mL of a 3.4 M CDCl₃ solution of MenOH was added, and the $^{31}P\{^1H\}$ NMR spectrum was recorded. The addition of MeOH was repeated for two more times, each followed by recording of a $^{31}P\{^1H\}$ NMR spectrum.

Reaction between PCl₃ and MenOH in presence of Et₃N

To a CDCl₃ solution (0.5 mL) containing 0.03 mL of PCl₃ (0.047 g, 0.34 mmol) and 0.2 mL Et₃N (0.15 g, 1.4 mmol) in an NMR tube, 0.1 mL of a 3.4 M CDCl₃ solution of MenOH was added. The $^{31}P\{^1H\}$ NMR spectrum was then recorded. The

addition of MeOH was repeated for two more times, each followed by recording of a $^{31}P\{^1H\}$ NMR spectrum.

Table 6-3. $^{13}C\{^1H\}$ NMR[a] data for compounds 1 - 9.

Compound		δ C_{Ar}	δ $\underline{C}HOP^b$	δ C_{alk}
P(OMen)Ph₂,	1	128-144	81.28(18.6)	15-50
P(OBor)Ph₂,	2	127-144	86.34(19.3)	13-51
P(OIpc)Ph₂,	3	128-144	81.31(18.6)	20-48
P(OMen)₂Ph,	4	126-144	79.58(17.3), 78.87(7.3)	15-50
P(OBor)₂Ph,	5	127-143	84.12(15.7), 82.09(8.2)	13-51
P(OIpc)₂Ph,	6	127-143	78.91(13.4), 77.84(11.8)	20-48
P(OMen)₃,	7	-[c]	73.46(12.3)	17-50
P(OBor)₃,	8	-[c]	77.89(10.4)	13-50
P(OIpc)₃,	9	-[c]	72.94(11.5)	20-48

[a] Chemical shifts are given in δ(ppm) relative to internal $CDCl_3$ with the middle branch of $CDCl_3$ signal set at 77.0 ppm. All spectra were recorded in $CDCl_3$ solution. [b] $^2J_{CP}$ values are given in parentheses. [c] Not applicable.

Table 6-4. ^{1}H NMR and ^{31}P{^{1}H} NMR data for compounds $\underline{1}$ - $\underline{9}$.

Compound		^{1}H NMR[a]			^{31}P{^{1}H} NMR[b]
		δ H$_{Ar}$	δ C$\underline{H}$OP[c]	δ H$_{alk}$	δ P/ppm
P(OMen)Ph$_2$,	$\underline{1}$	7.2-7.6	3.728	0.6-2.2	107.27
P(OBor)Ph$_2$,	$\underline{2}$	7.2-7.9	4.256	0.8-2.4	110.57
P(OIpc)Ph$_2$,	$\underline{3}$	7.2-7.6	4.312	0.9-2.6	109.88
P(OMen)$_2$Ph,	$\underline{4}$	7.3-7.9	3.802, 3.707	0.6-2.4	160.12
P(OBor)$_2$Ph,	$\underline{5}$	7.3-7.7	4.380, 4.179	0.7-2.3	157.91
P(OIpc)$_2$Ph,	$\underline{6}$	7.3-7.9	4.389, 4.313	0.8-2.6	158.37
P(OMen)$_3$,	$\underline{7}$	-[d]	3.721	0.6-2.2	147.54
P(OBor)$_3$,	$\underline{8}$	-[d]	4.325	0.8-2.3	143.44
P(OIpc)$_3$,	$\underline{9}$	-[d]	4.446	0.8-2.6	142.84

[a] Chemical shifts are given in δ(ppm) relative to internal CDCl$_3$ with CHCl$_3$ signal set at 7.24 ppm. All spectra were recorded in CDCl$_3$ solution. [b] Chemical shifts are given in δ(ppm) relative to external 85 phosphoric acid solution. All spectra were recorded in CDCl$_3$ solution. [c] All peaks are multiplets. [d] Not applicable.

Table 6-5. Elemental Analysis and Mass Spec. data for compounds 1 - 9.

Compound	Calc. (%)		Found (%)		Mass Spec.[a]
	C	H	C	H	
P(OMen)Ph$_2$, 1	77.62	8.59	77.23	8.50	341(9)
P(OBor)Ph$_2$, 2	78.08	8.04	77.73	8.15	339(24)
P(OIpc)Ph$_2$, 3	78.08	8.04	78.23	8.17	339(8)
P(OMen)$_2$Ph, 4	74.60	10.35	75.03	10.72	419(18)
P(OBor)$_2$Ph, 5	75.33	9.48	75.44	9.74	415(16)
P(OIpc)$_2$Ph, 6	75.33	9.48	75.75	9.80	415(25)
P(OMen)$_3$, 7	72.54	11.57	72.83	11.46	497(5)
P(OBor)$_3$, 8	73.43	10.48	73.58	10.63	491(1)
P(OIpc)$_3$, 9	73.43	10.48	72.97	10.45	491(3)

[a] Relative intensity values are given in parentheses. All spectra were recorded with chemical ionization method.

6.B.d. Mono-substituted Iron Carbonyl Complexes with Chiral Phosphorous Ligands

General Procedure

All mono-substituted iron carbonyl complexes were synthesized according to the method described by M. O. Albers et al[70]. A stirred solution of one mol. equiv. phosphorous ligand and 0.05-0.1 mol. equiv. of $CoCl_2 \cdot 2H_2O$ in 30 mL of toluene was brought to reflux. Two mol. equiv. of pentacarbonyliron was then added and the reflux was continued for about 10 hr before the reaction solution was cooled. Cobalt catalyst and traces of excess ligand were removed by eluting the concentrated reaction solution through a column containing three layers: $CoCl_2 \cdot 6H_2O$ (3 g), neutral alumina (10 g) and silica gel (10 g). Benzene was used as eluant. The solvent and excess pentacarbonyliron were removed under reduced pressure yielding an orange product. The products were either solids or very viscous liquids. Solid products were recrystallized from hexanes. The yield was typically around 85%. Analytical data are shown in Tables 6-6 ($^{31}P\{^1H\}$ NMR and IR), 6-7 ($^{13}C\{^1H\}$ NMR), 6-8 (^1H NMR) and 6-9 (Elemental Analysis and Mass Spec.).

$(CO)_4Fe[P(OMen)Ph_2]$, **10**

According to the general procedure, MenOPPh$_2$ (2.10 g, 6.17 mmol), Fe(CO)$_5$ (1.6 mL, 2.38 g, 12.2 mmol) and $CoCl_2 \cdot 2H_2O$ (86.1 mg, 0.52 mmol) were used, yielding 2.90 g product (5.70 mmol, 92.4%). The product was a deep orange viscous liquid which could not be solidified at room temperature.

$(CO)_4Fe[P(OBor)Ph_2]$, **11**

According to the general procedure, BorOPPh$_2$ (3.30 g, 9.75 mmol), Fe(CO)$_5$ (2.6

mL, 3.87 g, 19.8 mmol) and $CoCl_2 \cdot 2H_2O$ (150 mg, 0.90 mmol) were used, yielding 4.2 g product (8.3 mmol, 86%). The product was a pale brown solid which was then crystallized from hexanes.

$(CO)_4Fe[P(OIpc)Ph_2]$, 12

According to the general procedure, $IpcOPPh_2$ (2.50 g, 7.39 mmol), $Fe(CO)_5$ (1.9 mL, 2.83 g, 14.5 mmol) and $CoCl_2 \cdot 2H_2O$ (120 mg, 0.72 mmol) were used, yielding 2.81 g product (5.5 mmol, 75%). The product was a deep orange viscous liquid which could not be solidified at room temperature.

$(CO)_4Fe[P(OMen)_2Ph]$, 13

According to the general procedure, $(MenO)_2PPh$ (2.40 g, 5.73 mmol), $Fe(CO)_5$ (1.5 mL, 2.24 g, 11.4 mmol) and $CoCl_2 \cdot 2H_2O$ (95.0 mg, 0.57 mmol) were used, yielding 2.70 g product (4.6 mmol, 80%). The product was a deep orange viscous liquid which could not be solidified at room temperature.

$(CO)_4Fe[P(OBor)_2Ph]$, 14

According to the general procedure, $(BorO)_2PPh$ (3.01 g, 7.26 mmol), $Fe(CO)_5$ (1.9 mL, 2.84 g, 14.5 mmol) and $CoCl_2 \cdot 2H_2O$ (94.4 mg, 0.57 mmol) were used, yielding 3.41 g product (5.85 mmol, 80.6%). The product was a pale brown solid which was crystallized from hexanes.

$(CO)_4Fe[P(OIpc)_2Ph]$, 15

According to the general procedure, $(IpcO)_2PPh$ (1.12 g, 2.70 mmol), $Fe(CO)_5$ (0.7 mL, 1.04 g, 5.3 mmol) and $CoCl_2 \cdot 2H_2O$ (44.6 mg, 0.27 mmol) were used, yielding 1.15 g product (2.0 mmol, 73%). The product was a deep orange viscous liquid which

could not be solidified at room temperature.

$(CO)_4Fe[P(OMen)_3]$, **16**

According to the general procedure, $(MenO)_3P$ (1.10 g, 2.2 mmol), $Fe(CO)_5$ (0.6 mL, 0.89 g, 4.56 mmol) and $CoCl_2 \cdot 2H_2O$ (33.0 mg, 0.20 mmol) were used, yielding 1.05 g product (1.58 mmol, 72%). The product was a yellow solid which was crystallized from hexanes.

$(CO)_4Fe[P(OBor)_3]$, **17**

According to the general procedure, $(BorO)_3P$ (0.45 g, 0.92 mmol), $Fe(CO)_5$ (0.25 mL, 0.37 g, 1.9 mmol) and $CoCl_2 \cdot 2H_2O$ (14.8 mg, 0.089 mmol) were used, yielding 0.54 g product (0.82, 89%). The product was a yellow solid which was crystallized from hexanes.

$(CO)_4Fe[P(OIpc)_3]$, **18**

According to the general procedure, $(IpcO)_3P$ (1.04 g, 2.12 mmol), $Fe(CO)_5$ (0.6 mL, 0.89 g, 4.56 mmol) and $CoCl_2 \cdot 2H_2O$ (33.0 mg, 0.20 mmol) were used, yielding 0.71 g product (1.1 mmol, 51%). The product was a yellow solid which was crystallized from hexanes.

Table 6-6. $^{31}P\{^{1}H\}$ NMR and IR data for complexes 10 - 18.

Compound		$^{31}P\{^{1}H\}$ NMR[a] δ ^{31}P/ppm	IR[b]/cm^{-1} $\nu(CO)$
$(CO)_4Fe[P(OMen)Ph_2]$,	10	164.11	2054, 1983, 1950, 1940
$(CO)_4Fe[P(OBor)Ph_2]$,	11	167.90	2054, 1983, 1949, 1942
$(CO)_4Fe[P(OIpc)Ph_2]$,	12	167.92	2054, 1983, 1949, 1940
$(CO)_4Fe[P(OMen)_2Ph]$,	13	188.08	2055, 1983, 1949, 1946
$(CO)_4Fe[P(OBor)_2Ph]$,	14	197.38	2056, 1985, 1950, 1943
$(CO)_4Fe[P(OIpc)_2Ph]$,	15	194.04	2056, 1985, 1950, 1942
$(CO)_4Fe[P(OMen)_3]$,	16	163.72	2056, 1983, 1953, 1940
$(CO)_4Fe[P(OBor)_3]$,	17	173.59	2058, 1986, 1955, 1939
$(CO)_4Fe[P(OIpc)_3]$,	18	169.36	2058, 1986, 1956, 1938

[a] Chemical shifts are given in δ(ppm) relative to external 85% phosphoric acid solution. All spectra were recorded in $CDCl_3$ solution. [b] All spectra were recorded in hexane solution. All peaks are strong.

Table 6-7. $^{13}C\{^1H\}$ NMR[a] data for complexes 10 - 18.

Compound		δ $\underline{C}O$[b]	δ C_{Ar}	δ $\underline{C}HOP$[c]	δ C_{alk}
$(CO)_4Fe[P(OMen)Ph_2]$,	10	212.99(19.2)	125-142	79.26(4.2)	15-50
$(CO)_4Fe[P(OBor)Ph_2]$,	11	212.86(19.4)	125-141	84.34(3.9)	13-51
$(CO)_4Fe[P(OIpc)Ph_2]$,	12	212.99(19.4)	124-141	78.80(4.3)	19-49
$(CO)_4Fe[P(OMen)_2Ph]$,	13	213.40(21.1)	125-139	80.61(13.3), 80.43(5.4)	15-50
$(CO)_4Fe[P(OBor)_2Ph]$,	14	212.96(21.4)	128-141	84.69(6.3), 83.79(6.9)	13-51
$(CO)_4Fe[P(OIpc)_2Ph]$,	15	213.28(21.1)	125-141	79.37(6.7), 78.82(8.6)	19-48
$(CO)_4Fe[P(OMen)_3]$,	16	213.23(23.8)	-[d]	78.70(8.0)	15-50
$(CO)_4Fe[P(OBor)_3]$,	17	212.88(23.6)	-[d]	83.23(6.3)	13-50
$(CO)_4Fe[P(OIpc)_3]$,	18	213.19(23.2)	-[d]	77.71(7.0)	20-48

[a] Chemical shifts are given in δ(ppm) relative to internal $CDCl_3$ with the middle branch of $CDCl_3$ signal set at 77.0 ppm. All spectra were recorded in $CDCl_3$ solution. [b] All peaks are doublets. $^2J_{CP}$ values are given in parentheses. [c] All peaks are doublets. $^2J_{CP}$ values are given in parentheses. [d] Not applicable.

Table 6-8. ^{1}H NMR^a data for complexes <u>10</u> - <u>18</u>.

Compound		δ H$_{Ar}$	δ C<u>H</u>OP^b	δ H$_{alk}$
(CO)$_4$Fe[P(OMen)Ph$_2$],	<u>10</u>	7.2-7.9	4.210	0.6-2.4
(CO)$_4$Fe[P(OBor)Ph$_2$],	<u>11</u>	7.1-7.8	4.622	0.8-2.4
(CO)$_4$Fe[P(OIpc)Ph$_2$],	<u>12</u>	7.1-7.8	4.774	0.8-2.5
(CO)$_4$Fe[P(OMen)$_2$Ph],	<u>13</u>	7.1-8.0	4.367, 3.689	0.4-2.4
(CO)$_4$Fe[P(OBor)$_2$Ph],	<u>14</u>	7.4-8.0	4.705, 4.519	0.7-2.3
(CO)$_4$Fe[P(OIpc)$_2$Ph],	<u>15</u>	7.1-8.1	4.696, 4.664	0.8-2.9
(CO)$_4$Fe[P(OMen)$_3$],	<u>16</u>	-^{c}	4.144	0.7-2.4
(CO)$_4$Fe[P(OBor)$_3$],	<u>17</u>	-^{c}	4.610	0.8-2.4
(CO)$_4$Fe[P(OIpc)$_3$],	<u>18</u>	-^{c}	4.446	0.8-2.5

^{a} Chemical shifts are given in δ(ppm) relative to internal CDCl$_3$ with CHCl$_3$ signal set at 7.24 ppm. All spectra were recorded in CDCl$_3$ solution. ^{b} All peaks are multiplets. ^{c} Not applicable.

Table 6-9. Elemental Analysis and Mass Spec. data for complexes 10 - 18.

Compound		Calc. (%)		Found (%)		Mass Spec.[a]
		C	H	C	H	
$(CO)_4Fe[P(OMen)Ph_2]$,	10	61.43	5.75	61.22	5.92	$508(9)^c$
$(CO)_4Fe[P(OBor)Ph_2]$,	11	61.68	5.37	61.61	5.33	$506(7)^c$
$(CO)_4Fe[P(OIpc)Ph_2]$,	12	61.68	5.37	62.06	5.48	$507(12)^b$
$(CO)_4Fe[P(OMen)_2Ph]$,	13	61.44	7.39	61.62	7.73	$586(14)^c$
$(CO)_4Fe[P(OBor)_2Ph]$,	14	61.86	6.75	61.56	6.61	$582(26)^c$
$(CO)_4Fe[P(OIpc)_2Ph]$,	15	61.86	6.75	62.31	6.99	$583(12)^b$
$(CO)_4Fe[P(OMen)_3]$,	16	61.44	8.64	61.10	8.35	$665(11)^b$
$(CO)_4Fe[P(OBor)_3]$,	17	62.01	7.80	61.55	7.84	$659(16)^b$
$(CO)_4Fe[P(OIpc)_3]$,	18	62.01	7.80	62.36	7.91	$659(5)^b$

[a] Relative intensity values are given in parentheses. [b] The spectrum was recorded with chemical ionization method. [c] The spectrum was recorded with electron impact method.

6.B.e. Di-substituted Iron Carbonyl Complexes with Chiral Phosphorous Ligands

General Procedure

Di-substituted Iron carbonyl complexes were synthesized via a two-step process.[90] An ethanolic solution (30 mL) of $K[FeH(CO)_4]$ was produced by stirring a mixture of one mol. equiv. of $Fe(CO)_5$ and KOH in ethanol until the precipitation of $KHCO_4$ and the change in the colour of the solution from yellow to red were observed. This solution was then used *in situ* for the next step, during which one mol. equiv. phosphorus ligands was added into the solution. The mixture was then refluxed for 2 to 10 hr, during which period evolution of gas and precipitation were observed. After cooling to room temperature, the solid was filtered in air on a sintered glass, and thoroughly washed with distilled water up to neutrality of the filtrate. This was followed by washes with three portions of EtOH. Dissolution of the solid on the sintered glass with CH_2Cl_2 with simultaneous filtration afforded a clear solution. The solvent was then removed on a rotatory evaporator to leave a solid which was in turn dried under vacuum. The colour of the products varied from pale yellow to deep orange. The yields were in the range between 55% to 90%. Analytical data are shown in Tables 6-10 ($^{31}P\{^1H\}$ NMR and IR), 6-11 ($^{13}C\{^1H\}$ NMR), 6-12 (^1H NMR) and 6-13 (Elemental Analysis and Mass Spec.).

$(CO)_3Fe[P(OMen)Ph_2]_2$, 19

Following the general procedure, $MenOPPh_2$ (1.90 g, 5.58 mmol), $Fe(CO)_5$ (0.37 mL, 0.55 g, 2.8 mmol) and KOH (0.313 mg, 5.58 mmol) were used, yielding 2.04 g product (2.49 mmol, 89%). The deep orange product was recrystallized from hexanes.

(CO)$_3$Fe[P(OBor)Ph$_2$]$_2$, <u>20</u>

According to the general procedure, BorOPPh$_2$ (2.24 g, 6.62 mmol), Fe(CO)$_5$ (0.44 mL, 0.66 g, 3.3 mmol) and KOH (0.37 g, 6.6 mmol) were used, yielding 2.42 g product (3.01 mmol, 90%). The product was a pale brown solid which was then crystallized from hexanes.

(CO)$_3$Fe[P(OIpc)Ph$_2$]$_2$, <u>21</u>

According to the general procedure, IpcOPPh$_2$ (2.23 g, 6.59 mmol), Fe(CO)$_5$ (0.43 mL, 0.64 g, 3.3 mmol) and KOH (0.370 g, 6.61 mmol) were used, yielding 2.17 g orange product (2.66 mmol, 81%), which was recrystallized from hexanes.

(CO)$_3$Fe[P(OMen)$_2$Ph]$_2$, <u>22</u>

According to the general procedure, (MenO)$_2$PPh (2.24 g, 5.35 mmol), Fe(CO)$_5$ (0.35 mL, 0.52 g, 2.7 mmol) and KOH (0.30 g, 5.3 mmol) were used, yielding 2.07 g product (2.12 mmol, 78%). The product was recrystallized from hexanes solution as an yellow crystalline solid.

(CO)$_3$Fe[P(OBor)$_2$Ph]$_2$, <u>23</u>

According to the general procedure, (BorO)$_2$PPh (2.65 g, 6.39 mmol), Fe(CO)$_5$ (0.42 mL, 0.63 g, 3.2 mmol) and KOH (0.359 g, 6.40 mmol) were used, yielding 2.49 g product (2.57 mmol, 80%). The product was a pale brown solid which was crystallized from hexanes.

(CO)$_3$Fe[P(OIpc)$_2$Ph]$_2$, <u>24</u>

As described in the general procedure, (IpcO)$_2$PPh (2.35 g, 5.67 mmol), Fe(CO)$_5$ (0.37 mL, 0.55 g, 2.8 mmol) and KOH (0.318 g, 5.67 mmol) were reacted, yielding 1.63

g product (1.68 mmol, 60%). The yellow solid was recrystallized from hexanes solution.

(CO)$_3$Fe[P(OMen)$_3$]$_2$, <u>25</u>

According to the general procedure, (MenO)$_3$P (2.12 g, 4.27 mmol), Fe(CO)$_5$ (0.28 mL, 0.42 g, 2.1 mmol) and KOH (0.239 g, 4.26 mmol) were reacted, producing a yellow solid. The product was then crystallized from hexanes, yielding 1.3 g (1.15 mmol, 55%) yellow crystals.

(CO)$_3$Fe[P(OBor)$_3$]$_2$, <u>26</u>

According to the general procedure, 1.77g (BorO)$_3$P (3.61 mmol), 0,24 mL Fe(CO)$_5$ (0.36 g, 1.8 mmol) and 0.187 g KOH (0.333 mmol) were used, yielding 1.53 g product (1.36 mmol, 76%). The product was a very pale yellow solid which was crystallized from hexanes.

(CO)$_3$Fe[P(OIpc)$_3$]$_2$, <u>27</u>

According to the general procedure, (IpcO)$_3$P (1.49 g, 3.04 mmol), Fe(CO)$_5$ (0.20 mL, 0.30 g, 1.5 mmol) and KOH (0.171 g, 3.05 mmol) were used, yielding 1.35 g product (1.20 mmol, 80%). The product was a yellow solid which was crystallized from hexanes.

Table 6-10. $^{31}P\{^1H\}$ NMR and IR data for complexes 19 - 27.

Compound		$^{31}P\{^1H\}$ NMR[a] δ ^{31}P/ppm	IR[b]/cm^{-1} v(CO)
(CO)$_3$Fe[P(OMen)Ph$_2$]$_2$,	19	171.2	1898
(CO)$_3$Fe[P(OBor)Ph$_2$]$_2$,	20	175.1	1897
(CO)$_3$Fe[P(OIpc)Ph$_2$]$_2$,	21	175.3	1888
(CO)$_3$Fe[P(OMen)$_2$Ph]$_2$,	22	199.9	1898
(CO)$_3$Fe[P(OBor)$_2$Ph]$_2$,	23	210.4	1898
(CO)$_3$Fe[P(OIpc)$_2$Ph]$_2$,	24	207.4	1890
(CO)$_3$Fe[P(OMen)$_3$]$_2$,	25	177.9	1901
(CO)$_3$Fe[P(OBor)$_3$]$_2$,	26	188.9	1895
(CO)$_3$Fe[P(OIpc)$_3$]$_2$,	27	184.7	1890

[a] Chemical shifts are given in δ(ppm) relative to external 85% phosphoric acid solution. All spectra were recorded in CDCl$_3$ solution. [b] All spectra were recorded in hexane solution. All peaks are strong.

Table 6-11. $^{13}C\{^1H\}$ NMR[a] data for complexes <u>19</u> - <u>27</u>.

Compound		δ $\underline{C}O$[b]	δ C_{Ar}	δ $\underline{C}HOP$[c]	δ C_{alk}
$(CO)_3Fe[P(OMen)Ph_2]_2$,	<u>19</u>	213.0 (t, 30.0)	127-144	77.7 (s)	16-50
$(CO)_3Fe[P(OBor)Ph_2]_2$,	<u>20</u>	212.6 (t, 30.1)	127-143	82.9 (s)	13-51
$(CO)_3Fe[P(OIpc)Ph_2]_2$,	<u>21</u>	213.0 (t, 30.1)	127-143	77.4 (s)	20-49
$(CO)_3Fe[P(OMen)_2Ph]_2$,	<u>22</u>	213.3 (t, 34.3)	127-142	78.8 (d, 9.8), 78.7 (d, 13.7)	16-50
$(CO)_3Fe[P(OBor)_2Ph]_2$,	<u>23</u>	212.4 (t, 33.5)	127-143	83.1 (s), 82.1 (s)	13-50
$(CO)_3Fe[P(OIpc)_2Ph]_2$,	<u>24</u>	213.1 (t, 33.5)	127-144	77.8 (s), 77.2 (s)	19-49
$(CO)_3Fe[P(OMen)_3]_2$,	25	213.2 (t, 38.9)	-[d]	77.3 (s)	16-50
$(CO)_3Fe[P(OBor)_3]_2$,	<u>26</u>	212.2 (t, 38.4)	-[d]	81.6 (s)	13-50
$(CO)_3Fe[P(OIpc)_3]_2$,	<u>27</u>	213.2 (t, 38.4)	-[d]	76.4 (s)	20-48

[a] Chemical shifts are given in δ(ppm) relative to internal $CDCl_3$ with the middle branch of $CDCl_3$ signal set at 77.0 ppm. All spectra were recorded in $CDCl_3$ solution. [b] $^2J_{CP}$ values are given in parentheses. [c] $^2J_{CP}$ values given in parentheses. [d] Not applicable.

Table 6-12. ¹H NMR* data for complexes 19 - 27.

Compound	δ H$_{Ar}$	δ C$\underline{H}$OP	δ H$_{alk}$
(CO)$_3$Fe[P(OMen)Ph$_2$]$_2$, 19	7.2-7.9	4.36 (s, b)	0.5-2.5
(CO)$_3$Fe[P(OBor)Ph$_2$]$_2$, 20	7.3-7.8	4.82 (s, b)	0.8-2.3
(CO)$_3$Fe[P(OIpc)Ph$_2$]$_2$, 21	7.3-7.8	4.96 (s, b)	0.8-2.5
(CO)$_3$Fe[P(OMen)$_2$Ph]$_2$, 22	7.4-8.1	4.46 (m), 3.84 (m)	0.5-2.5
(CO)$_3$Fe[P(OBor)$_2$Ph]$_2$, 23	7.4-8.0	4.83 (s, b), 4.66 (s, b)	0.6-2.5
(CO)$_3$Fe[P(OIpc)$_2$Ph]$_2$, 24	7.4-8.1	4.93 (m), 4.74 (m)	0.8-2.8
(CO)$_3$Fe[P(OMen)$_3$]$_2$, 25	-^{b}	4.18 (s, b)	0.7-2.6
(CO)$_3$Fe[P(OBor)$_3$]$_2$, 26	-^{b}	4.62 (d, b, 4.8)	0.8-2.4
(CO)$_3$Fe[P(OIpc)$_3$]$_2$, 27	-^{b}	4.81 (sept, 4.7)	0.9-2.7

* Chemical shifts are given in δ(ppm) relative to internal CDCl$_3$ with CHCl$_3$ signal set at

7.24 ppm. All spectra were recorded in CDCl$_3$ solution. ^{b} Not applicable.

Table 6-13. Elemental Analysis and Mass Spec. data for complexes 19 - 27.

Compound		Calc. (%)		Found (%)		Mass Spec.[a]
		C	H	C	H	
$(CO)_3Fe[P(OMen)Ph_2]_2$,	19	68.78	7.12	67.65	6.72	$822(11)^b$
$(CO)_3Fe[P(OBor)Ph_2]_2$,	20	69.12	6.66	68.80	6.73	$818(9)^b$
$(CO)_3Fe[P(OIpc)Ph_2]_2$,	21	69.12	6.66	68.21	6.29	$818(23)^b$
$(CO)_3Fe[P(OMen)_2Ph]_2$,	22	67.61	8.87	67.53	8.99	$-^c$
$(CO)_3Fe[P(OBor)_2Ph]_2$,	23	68.17	8.11	67.08	7.93	$-^c$
$(CO)_3Fe[P(OIpc)_2Ph]_2$,	24	68.17	8.11	68.51	8.27	$-^c$
$(CO)_3Fe[P(OMen)_3]_2$,	25	66.76	10.14	66.66	9.62	$-^c$
$(CO)_3Fe[P(OBor)_3]_2$,	26	67.48	9.17	68.29	9.62	$-^c$
$(CO)_3Fe[P(OIpc)_3]_2$,	27	67.48	9.17	67.21	9.12	$-^c$

[a] Relative intensity values are given in parentheses. [b] Spectrum was recorded with chemical ionization method. [c] Spectrum was not acquired.

6.B.f. Cobalt Carbonyl Dimers with Chiral Phosphorous Ligands

General Procedure

A typical procedure for the synthesis of cobalt carbonyl dimers with di-substituted phosphorus ligands was described by Manning.[99] Two mol. equiv. of phosphorus ligand

was added to a benzene solution (30 mL) of $Co_2(CO)_8$. The solution was then refluxed for 2 to 5 hr, during which time evolution of gas was observed. After cooling to room temperature, the volume of the solution was reduced to about 5 mL under vacuum. Decomposition products and traces of excess ligand were removed by running this solution through a column containing two layers: neutral alumina (10 g) and silica gel (10 g) eluted by ethyl acetate/hexanes (1:2). The solvent was removed on a rotatory evaporator and the resulting solid was dried under vacuum. The products were usually deep orange brown solids, with yields ranging from 40% to 80%. Analytical data are shown in Tables 6-14 ($^{31}P\{^1H\}$ NMR and IR), 6-15 ($^{13}C\{^1H\}$ NMR), 6-16 (^1H NMR) and 6-17 (Elemental Analysis).

$\{(CO)_3Co[P(OMen)Ph_2]\}_2$, **28**

According to the general procedure, MenOPPh$_2$ (1.51 g, 4.44 mmol) and $Co_2(CO)_8$ (0.758 g, 2.22 mmol) were used, yielding 1.63 g product (1.69 mmol, 76%). The product was a dark brown solid.

$\{(CO)_3Co[P(OBor)Ph_2]\}_2$, **29**

According to the general procedure, BorOPPh$_2$ (0.88 g, 2.6 mmol) and $Co_2(CO)_8$ (0.42 g, 1.2 mmol) were used, yielding 0.82 g product (0.85 mmol, 71%). The product was a pale brown solid which was then crystallized from hexanes.

$\{(CO)_3Co[P(OIpc)Ph_2]\}_2$, **30**

According to the general procedure, IpcOPPh$_2$ (1.02 g, 3.01 mmol) and $Co_2(CO)_8$ (0.48 g, 1.4 mmol) were used, yielding 0.87 g product (0.90 mmol, 64%). The dark brown solid product was recrystallized from hexanes.

{(CO)₃Co[P(OMen)₂Ph]}₂, 31

{(CO)$_3$Co[P(OMen)$_2$Ph]}$_2$, **31**

According to the general procedure, (MenO)$_2$PPh (0.96 g, 2.3 mmol) and Co$_2$(CO)$_8$ (0.387 g, 1.13 mmol) were used, yielding 1.01 g product (0.899 mmol, 80%). The product was a dark red brown solid.

{(CO)$_3$Co[P(OBor)$_2$Ph]}$_2$, **32**

According to the general procedure, (BorO)$_2$PPh (1.33 g, 3.21 mmol) and Co$_2$(CO)$_8$ (0.530 g, 1.55 mmol) were used, yielding 1.2 g product (1.1 mmol, 70%). The product was a pale brown solid which was crystallized from hexanes.

{(CO)$_3$Co[P(OIpc)$_2$Ph]}$_2$, **33**

According to the general procedure, (IpcO)$_2$PPh (0.897 g, 2.16 mmol) and Co$_2$(CO)$_8$ (0.379 g, 1.11 mmol) were used, yielding 0.75 g product (0.67 mmol, 61%). The deep orange product was recrystallized from hexanes solution.

{(CO)$_3$Co[P(OMen)$_3$]}$_2$, **34**

According to the general procedure, (MenO)$_3$P (1.42 g, 2.86 mmol) and Co$_2$(CO)$_8$ (0.489 g, 1.43 mmol) were used, yielding 0.74 g product (0.58 mmol, 40%). The product was a yellow solid which was crystallized from hexanes.

{(CO)$_3$Co[P(OBor)$_3$]}$_2$, **35**

According to the general procedure, (BorO)$_3$P (0.426 g, 0.868 mmol) and Co$_2$(CO)$_8$ (0.136 g, 0.400 mmol) were used, yielding 0.28 g product (0.22 mmol, 55%). The product was a yellow solid which was crystallized from hexanes.

{(CO)₃Co[P(OIpc)₃]}₂, **36**

According to the general procedure, (IpcO)₃P (0.82 g, 1.7 mmol) and Co₂(CO)₈ (0.286 g, 0.836 mmol) were used, yielding 0.58 g product (0.46 mmol, 55%). The product was a yellow solid which was crystallized from hexanes.

Table 6-14. $^{31}P\{^1H\}$ NMR and IR data for cobalt dimers (Complexes **28** - **36**).

Compound		$^{31}P\{^1H\}$ NMR[a] $\delta\ ^{31}P$/ppm	IR[b]/cm^{-1} ν(CO)
{(CO)₃Co[P(OMen)Ph₂]}₂,	**28**	160.8	2042, 1982, 1965, 1935
{(CO)₃Co[P(OBor)Ph₂]}₂,	**29**	164.8	2040, 1982, 1964, 1937
{(CO)₃Co[P(OIpc)Ph₂]}₂,	**30**	165.2	2040, 1982, 1965, 1936
{(CO)₃Co[P(OMen)₂Ph]}₂,	**31**	187.4	2042, 1982, 1965, 1939
{(CO)₃Co[P(OBor)₂Ph]}₂,	**32**	196.1	2042, 1982, 1966, 1940
{(CO)₃Co[P(OIpc)₂Ph]}₂,	**33**	193.5	2041, 1980, 1966, 1937
{(CO)₃Co[P(OMen)₃]}₂,	**34**	159.8	2040, 1980, 1960, 1933
{(CO)₃Co[P(OBor)₃]}₂,	**35**	171.1	2041, 1982, 1963, 1936
{(CO)₃Co[P(OIpc)₃]}₂,	**36**	167.7	2042, 1982, 1962, 1938

[a] Chemical shifts are given in δ(ppm) relative to external 85% phosphoric acid solution. All spectra were recorded in CDCl₃ solution. [b] All spectra were recorded in hexane solution. The four bands in each spectrum follow the pattern: weak, medium strong, very strong, medium strong.

Table 6-15. ^{13}C{^{1}H} NMR[a] data for cobalt dimers (Complexes 28 - 36).

Compound		δ $\underline{C}O$[b]	δ C_{Ar}	δ $\underline{C}HOP$[c]	δ C_{alk}
{(CO)$_3$Co[P(OMen)Ph$_2$]}$_2$,	28	201.8 (19.0)	128-141	79.3 (s)	15-50
{(CO)$_3$Co[P(OBor)Ph$_2$]}$_2$,	29	201.6 (19.4)	128-141	84.5 (s)	13-51
{(CO)$_3$Co[P(OIpc)Ph$_2$]}$_2$,	30	201.8 (19.0)	128-141	79.1 (s)	19-49
{(CO)$_3$Co[P(OMen)$_2$Ph]}$_2$,	31	202.1 (26.5)	128-141	78.1 (s), 77.5 (s)	15-50
{(CO)$_3$Co[P(OBor)$_2$Ph]}$_2$,	32	201.7 (25.2)	128-141	84.3 (s), 83.0 (s)	13-50
{(CO)$_3$Co[P(OIpc)$_2$Ph]}$_2$,	33	202.1 (23.3)	128-142	78.9 (s), 78.5 (s)	20-48
{(CO)$_3$Co[P(OMen)$_3$]}$_2$,	34	201.7 (28.8)	-[d]	77.6 (s)	16-50
{(CO)$_3$Co[P(OBor)$_3$]}$_2$,	35	201.4 (29.4)	-[d]	82.4 (s)	13-50
{(CO)$_3$Co[P(OIpc)$_3$]}$_2$,	36	201.8 (29.8)	-[d]	78.2 (d, 5.8)	20-48

[a] Chemical shifts are given in δ(ppm) relative to internal CDCl$_3$ with the middle branch of CDCl$_3$ signal set at 77.0 ppm. All spectra were recorded in CDCl$_3$ solution. [b] All CO resonances are "virtual triplets" (see Chapter 4). $^3J_{PP}$ values are given in parentheses. [c] $^2J_{CP}$ values are given in parentheses. [d] Not applicable.

Table 6-16. ^{1}H NMR^a data for cobalt dimers (Complexes 28 - 36).

Compound		δ H$_{Ar}$	δ C$\underline{H}$OP	δ H$_{alk}$
{(CO)$_3$Co[P(OMen)Ph$_2$]}$_2$,	28	7.2-7.8	4.21 (m)	0.5-2.3
{(CO)$_3$Co[P(OBor)Ph$_2$]}$_2$,	29	7.3-7.8	4.70 (s, b)	0.8-2.2
{(CO)$_3$Co[P(OIpc)Ph$_2$]}$_2$,	30	7.3-7.8	4.85 (s, b)	0.7-2.6
{(CO)$_3$Co[P(OMen)$_2$Ph]}$_2$,	31	7.2-8.0	3.81 (m), 4.27(m)	0.3-2.5
{(CO)$_3$Co[P(OBor)$_2$Ph]}$_2$,	32	7.0-8.0	4.70 (s, b), 4.59 (s, b)	0.3-2.5
{(CO)$_3$Co[P(OIpc)$_2$Ph]}$_2$,	33	7.1-8.0	4.74 (s, b), 4.69 (s, b)	0.6-2.7
{(CO)$_3$Co[P(OMen)$_3$]}$_2$,	34	-^{b}	4.11 (s, b)	0.7-2.5
{(CO)$_3$Co[P(OBor)$_3$]}$_2$,	35	-^{b}	4.61 (s, b)	0.8-2.4
{(CO)$_3$Co[P(OIpc)$_3$]}$_2$,	36	-^{b}	4.78 (s, b)	0.8-2.7

^{a} Chemical shifts are given in δ(ppm) relative to internal CDCl$_3$ with CHCl$_3$ signal set at 7.24 ppm. All spectra were recorded in CDCl$_3$ solution. ^{b} Not applicable.

Table 6-17.   Elemental Analysis data for Cobalt dimers (Complexes <u>28</u> - <u>36</u>).

Compound		Elemental Analysis			
		Calc. (%)		Found (%)	
		C	H	C	H
{(CO)₃Co[P(OMen)Ph₂]}₂,	<u>28</u>	62.12	6.05	61.47	6.04
{(CO)₃Co[P(OBor)Ph₂]}₂,	<u>29</u>	62.38	5.65	62.44	5.58
{(CO)₃Co[P(OIpc)Ph₂]}₂,	<u>30</u>	62.38	5.65	62.26	5.69
{(CO)₃Co[P(OMen)₂Ph]}₂,	<u>31</u>	62.03	7.72	62.56	7.50
{(CO)₃Co[P(OBor)₂Ph]}₂,	<u>32</u>	62.48	7.05	62.36	7.03
{(CO)₃Co[P(OIpc)₂Ph]}₂,	<u>33</u>	62.48	7.05	62.66	6.94
{(CO)₃Co[P(OMen)₃]}₂,	<u>34</u>	61.96	8.98	61.21	8.65
{(CO)₃Co[P(OBor)₃]}₂,	<u>35</u>	62.55	8.11	61.91	7.92
{(CO)₃Co[P(OIpc)₃]}₂,	<u>36</u>	62.55	8.11	62.12	8.35

6.B.g. Pyrazolyl-bridged Diiridium Complexes

$[Ir(COD)(\mu\text{-}pz)]_2$, <u>37</u>[121,205]

$[Ir(COD)(\mu\text{-}Cl)]_2$ (1.2 g, 1.8 mmol) was dissolved in THF (20 mL) and one mol. equiv. pyrazole (0.12 g, 1.8 mmol) was added, resulting in formation of a bright yellow solution. Addition of excess triethylamine (1 mL, 7 mmol) caused an immediate colour change to deep red/purple. After stirring for 10 minutes, the solution was filtered through

a short, neutral alumina column (7×3 cm^2) using THF as the eluant. Removal of the solvent *in vacuo* to dryness afforded the product as deep red-purple powder (1.2 g, 1.6 mmol, 91%).

[Ir(CO)$_2$(μ-pz)]$_2$, <u>38</u>[126]

Through a stirred solution of [Ir(COD)(μ-pz)]$_2$ (100 mg, 0.14 mmol) in THF (20 mL) was passed a stream of carbon monoxide resulting in a graduate colour change from deep red to bright yellow. The reaction is usually completed within 5 min.. This solution was used directly for subsequent reactions.

{Ir(CO)[P(OMen)Ph$_2$](μ-pz)}$_2$, <u>40</u>

Addition of 47.7 mg P(OMen)Ph$_2$ (0.14 mmol) to a 20 mL THF solution of <u>38</u> (0.070 mmol) caused immediate colour change of the solution from bright yellow to orange. The solution was stirred for 30 min. before the solvent was removed under vacuum. The resulting solid was then recrystallized from hexanes/THF to yield orange crystals (72 mg, 0.057 mmol, 82%). Analytical data are listed in Tables 4-1 (^{31}P{^{1}H} NMR), 4-2 (^{1}H NMR), 6-18 (IR). MS: M$^+$, 1254(11%), 1255(6%), 1256(10%), 1257(5%).

{Ir(CO)[P(OBor)Ph$_2$](μ-pz)}$_2$, <u>41</u>

Addition of P(OMen)Ph$_2$ (97.8 mg, 0.289 mmol) to a 20 mL THF solution of <u>38</u> (0.145 mmol) resulted an instant colour change of the solution from bright yellow to orange. The solution was stirred for 30 min. before the solvent was removed under vacuum. The yellow orange solid product was then recrystallized from hexanes/THF to yield orange crystals (137 mg, 0.109 mmol, 75%). Analytical data are listed in Tables 4-1 (^{31}P{^{1}H} NMR), 4-2 (^{1}H NMR), 6-18 (IR). MS: M$^+$, 1250(8%), 1251(5%), 1252(8%), 1253(5%). Anal. Calc. for Ir$_2$C$_{52}$H$_{60}$P$_2$O$_4$N$_4$ (1251.46 g/mol): C, 49.91; H, 4.83; N, 4.48.

Found: C, 49.58; H, 4.79; N, 4.58.

{Ir(CO)[P(OMen)₂Ph](µ-pz)}₂, 42

{Ir(CO)[P(OMen)$_2$Ph](µ-pz)}$_2$, **42**

P(OMen)$_2$Ph (78.4 mg, 0.187 mmol) and **38** (0.093 mmol) were stirred in 20 mL THF for 30 min. The colour of the solution changed from bright yellow to orange. Following the removal of solvent *in vacuo*, the solid product was washed with three portions of 5 mL cold hexanes. Recrystallization from hexanes/THF yielded red-orange crystalline solid product (81.3 mg, 0.0576 mmol, 62%). Analytic data are listed in Tables 4-1 (^{31}P{^{1}H} NMR), 4-2 (^{1}H NMR), 6-18 (IR). MS: M$^+$, 1250(8%), 1251(5%), 1252(8%), 1253(5%).

Table 6-18. IR data^a of compounds 40 - 42.

Compound	v(CO) (cm^{-1})
{Ir(CO)[P(OMen)Ph$_2$](µ-pz)}$_2$, **40**	1970
{Ir(CO)[P(OBor)Ph$_2$](µ-pz)}$_2$, **41**	1971
{Ir(CO)[P(OMen)$_2$Ph](µ-pz)}$_2$, **42**	1977

^{a} All spectra were recorded in THF solution. All bands are medium strong.

Kinetic studies on the ring-inversion process in 41

About 25 mg (~ 0.02 mmol) of crystalline **41** (consisting of both diastereomers with 1:1 ratio) was dissolved in a C$_6$D$_6$ solution of MeI (0.1 mL, 0.23 g, 1.6 mmol) in an NMR tube. The solution was monitored by the ^{1}H NMR spectrum. The resonances at 5.83, 5.76, 5.73, and 5.66 were repeatedly integrated until the equilibrium was reached.

The integration ratios of the two pairs of resonances at 5.83, 5.66, and 5.73, 5.76 are averaged and used as ratio between the two diastereomers. A plot of this ratio *vs.* time was fitted according to Equation 4-8 to obtain the rate constants and the equilibrium constant.

Ir$_2$(CO)$_2$[P(OBor)Ph$_2$]$_2$(µ-pz)$_2$(Me)(I), <u>43</u>

Excess MeI (0.5 mL, 1.14 g, 8.03 mmol) was added to a 20 mL THF solution of <u>41</u> (33.5 mg, 0.0268 mmol). The colour of the solution darkened slightly, while the solution was stirred for 20 min.. The solvent and excess MeI were then removed under vacuum. The resulting solid was then washed with portions of 5 mL hexanes to yield a deep orange product (23 mg, 0.016 mmol, 62%). IR (hexane), v_{CO}: 2017, 1983 cm^{-1}; ^{31}P{^{1}H} NMR δ(ppm) (C$_6$D$_6$): 82.0, 81.0, 81.9, and 80.4. ^{1}H NMR δ(ppm) (C$_6$D$_6$): 7.39 (d, $^3J_{HH}$ = 2.20 Hz, 1H), 7.37 (s, 1H), 7.34 (s, 1H), 7.31 (d, $^3J_{HH}$ = 2.15 Hz, 1H), 6.46 (s, 1H), 6.28 (s, 1H), 5.65 (q, $^5J_{PH}$ = $^3J_{HH}$ = 2.12 Hz, 1H), 5.49 (q, $^5J_{PH}$ = $^3J_{HH}$ = 2.16 Hz, 1H), 5.42 (q, $^5J_{PH}$ = $^3J_{HH}$ = 2.11 Hz, 1H), 5.37 (q, $^5J_{PH}$ = $^3J_{HH}$ = 2.13 Hz, 1H), 4.42 (m, 1H), 4.22 (m, 2H), 4.07 (m, 1H), 1.75 (d, $^3J_{PH}$ = 1.73 Hz, 3H), 1.70 (d, $^3J_{PH}$ = 1.89 Hz, 3H), 6.8-8.4 (Ph), 0.3-1.65 (alkyl). MS: (M + 1), 1391.2(16%), 1392.2(19%), 1393.2(24%), 1394.2(20%), 1395.2(19%), 1396.2(11%), 1397.2(6%). Anal. Calc. for Ir$_2$C$_{53}$H$_{63}$IN$_4$O$_4$P$_2$ (1393.40 g/mol): C, 45.69; H, 4.56; N, 4.02. Found: C, 44.23; H, 4.43; N, 4.93.

Kinetic studies on the equilibrating process between the two diastereomers in <u>43</u>

About 30 mg of <u>43</u> (consists of the two diastereomers in their kinetic distribution) was dissolved in C$_6$D$_6$ in an NMR tube. The solution was monitored by the ^{1}H NMR over a period of 10 days. The three pairs of resonances at 6.46, 6.28; 5.65, 5.49; and 5.37, 5.42 were integrated, and the integration ratios between the two resonances in each pair ar

averaged to give the ratio between the two diastereomers. The plot of this ratio *vs.* time was fitted according to Equation 4-10 to obtain observed rate constants and the equilibrium constant. The attempt to establish a rate law according to the proposed mechanism in Scheme 4-8 was unsuccessful due to the mathematical difficulties.

$Ir_2(CO)_4(\mu\text{-pz})_2(exo\text{-norbornyl})(I)$, __44__

(a) Addition of 48 mg of *exo*-norbornyl iodide (0.22 mmol) to a 15 mL THF solution of __38__ (0.21 mmol) resulted in slight darkening of colour of the solution. After stirring for 30 min., the solvent was removed under vacuum. The orange brown solid reaction mixture was then washed with hexanes (3 × 5 mL) and dried *in vacuo* to yield a orange crystalline product (97 mg, 0.11 mmol, 52%). $^{13}C\{^1H\}$ NMR: see Table 4-4, additional resonances: δ(ppm) (C_6D_6): 169.0, 168.9, 167.4, 167.1, 143.44, 143.39, 137.3, 135.3, 107.1, and 107.0. ^1H NMR: see Figure 4-22, additional resonances: δ(ppm) (C_6D_6): 7.9671 (d, $^3J_{HH}$ = 2.2 Hz, 1H), 7.9666 (d, $^3J_{HH}$ = 2.2 Hz, 1H), 7.14 (d, $^3J_{HH}$ = 2.4 Hz, 1H), 7.09 (d, $^3J_{HH}$ = 2.3 Hz, 1H), 5.593 (t, $^3J_{HH}$ = 2.0 Hz, 1H), 5.589 (t, $^3J_{HH}$ = 2.0 Hz, 1H).

(b) Same results was obtained when *exo*-norbornyl iodide was replaced by *endo*-norbornyl iodide and exact same procedure as described in (a) was followed.

6.B.h. BiPSi Ligand and Its Complexes

Dichloromenthoxysilane

A 20 mL ethereal solution containing 3.14 g MenOH (20 mmol) was added dropwise to excess $HSiCl_3$ (5.0 mL, 6.7 g, 50 mmol) in 25 mL ether at 0 °C. The solution was then stirred at room temperature for about 2 hr, before the volatiles were removed under vacuum, yielding a clear liquid product (4.93 g, 19.3 mmol, 96%). IR (neat), v_{SiH}: 2245 cm^{-1}; $^{13}C\{^1H\}$ NMR δ(ppm) $(CDCl_3)$: 76.4, 49.2, 44.2, 34.1, 31.6, 25.5, 22.8, 22.8,

21.0, and 15.8. ^{1}H NMR δ(ppm) (CDCl$_3$): 5.61 (s, 1H), 3.91 (t of d, J(d) = 4.4, J(t) = 10.6 1H), 0.7-2.2 (alkyl). MS (M$^+$) 254(40%), 256(22%).

(o-Ph$_2$PC$_6$H$_4$CH$_2$)$_2$(MenO)SiH, $\underline{47}$

The yellow o-Ph$_2$PC$_6$H$_4$CH$_2$Li powder (4.4 g, 15.6 mmol) was weighed into a Schlenk tube under Ar, before a mixture of benzene/hexane (25 mL, 1:1) was added. Dichloromenthoxysilane (2.0 g, 7.8 mmol) was then added dropwise at -78 °C. After being stirred overnight, the mixture was eluted with benzene through a short celite/silica gel column. The solvent was removed under vacuum to yield 3.6 g (4.9 mmol, 63%) of product as a white powder. IR (KBr), ν_{SiH}: 2117 cm^{-1}. ^{31}P{^{1}H} NMR δ(ppm) (CDCl$_3$): -13.9 and -14.0. ^{13}C{^{1}H} NMR δ(ppm) (CDCl$_3$): see Table 5-1. Additional data: 24.2 (d, $^3J_{PC}$ = 19.5 Hz), 23.5 (d, $^3J_{PC}$ = 19.5 Hz), 115-145 (aromatic). ^{1}H NMR δ(ppm) (CDCl$_3$): 4.62 (s, 1H), 3.40 (t of d, J(d) = 4.3, J(t) = 10.8 1H), 2.3 (m, 2H), 0.7-2.2 (alkyl). MS (M+1) 735(9%), 736(6%), 737(3%). Anal. Calc. for C$_{48}$H$_{52}$OP$_2$Si (734.97 g/mol): C, 78.44; H, 7.13. Found: C, 77.95; H, 7.10.

[(o-Ph$_2$PC$_6$H$_4$CH$_2$)$_2$(MenO)Si]PtCl, $\underline{48}$

Compound $\underline{47}$ (150 mg, 0.20 mmol) was added to a 20 mL benzene solution containing Pt(COD)Cl$_2$ (76.2 mg, 0.20 mmol) and excess EtN$_3$ (0.5 mL, 0.36 g, 3.6 mmol). The solution was stirred for 2 hr before the volatile was removed. The solid was washed with 5 mL portions of hexanes for 3 times and was dried *in vacuo*. A white solid product (139 mg, 0.14 mmol, 70%) was yielded. ^{31}P{^{1}H} NMR δ(ppm) (CDCl$_3$): 20.9 (1:4:1 t, $^2J_{PtP}$ = 2921.4 Hz). ^{13}C{^{1}H} NMR δ(ppm) (CDCl$_3$): 74.2 (1:4:1 t, $^3J_{PtC}$ = 13.4 Hz) 28.8 (m), 28.4 (m), 124-147 (aromatic), 16-51 (alkyl). ^{1}H NMR δ(ppm) (CDCl$_3$): 2.90 (t of d, J(d) = 4.2, J(t) = 10.0 1H), 1.96 (m, 2H), 6.5-8.0 (aromatic), -0.1-2.7 (alkyl). MS (M$^+$) 963(4%), 964(7%), 965 (8%), 966(5), 967(4%). Anal. Calc. for PtC$_{48}$H$_{51}$ClOP$_2$Si

(964.51 g/mol): C, 59.77; H, 5.33; found: C, 57.10; H, 5.15.

[(o-Ph$_2$PC$_6$H$_4$CH$_2$)$_2$(MenO)Si]IrClH, 49

Compound 47 (271 mg, 0.369 mmol) and [Ir(COD)(μ-Cl)]$_2$ (123 mg, 0.183 mmol) were weighed into a Schlenk tube and 20 mL of benzene was added. The yellow solution was stirred for 2 hr at room temperature before the solvent was removed. The solid was extracted with hexanes, and evaporation of the solvent yielded a yellow solid which was then washed with 2 mL portions of MeOH and dried under vacuum. The product was a yellow solid (213 mg, 0.221 mmol, 60%). Anal. Calc. for IrC$_{48}$H$_{52}$ClOP$_2$Si (962.64 g/mol): C, 59.89; H, 5.44; found: C, 60.31; H, 5.58. NMR data for *syn*-53: ^{31}P{^{1}H} NMR δ(ppm) (CD$_6$Cl$_6$): 27.6, 26.3 (AB pattern, $^2J_{PP}$ = 333.4 Hz). ^{1}H NMR δ(ppm) (CD$_6$Cl$_6$): -19.52 (t, $^2J_{PH}$ = 13.9 Hz, 1H), 3.07 (t of d, J(d) = 3.6 Hz, J(t) = 9.9 Hz, 1H), 2.99 (d, $^2J_{HH}$ = 14.4 Hz, 1H), 2.67 (d, $^2J_{HH}$ = 14.4 Hz, 1H), 2.44 (d, $^2J_{HH}$ = 5.4 Hz, 1H), 2.40 (d, $^2J_{HH}$ = 5.4 Hz, 1H), 6.5-8.4 (aromatic), 0.1-1.8 (alkyl). NMR data for *anti*-53: ^{31}P{^{1}H} NMR δ(ppm) (CD$_6$Cl$_6$): 19.0, 17.5 (AB pattern, $^2J_{PP}$ = 336.3 Hz). ^{1}H NMR δ(ppm) (CD$_6$Cl$_6$): -23.51 (t, $^2J_{PH}$ = 16.2 Hz, 1H), 3.18 (t of d, J(d) = 3.8 Hz, J(t) = 6.2 Hz, 1H), 2.99 (d, $^2J_{HH}$ = 11.7 Hz, 1H), 2.56 (d, $^2J_{HH}$ = 11.7 Hz, 1H), 2.56 (d, $^2J_{HH}$ = 16.2 Hz, 1H), 2.47 (d, $^2J_{HH}$ = 16.2 Hz, 1H), 6.5-8.4 (aromatic), 0.1-1.8 (alkyl).

Kinetic studies on the isomerization process in 49

About 25 mg (~ 0.03 mmol) of solid 49 (kinetic product, consisting of both *syn* and *anti* isomers with about 8:1 ratio) was dissolved in a C$_6$D$_6$ in an NMR tube. The solution was monitored by the ^{1}H NMR spectrum. The resonances at -19.52 and -23.51 ppm were repeatedly integrated. The integration ratios of these two resonances were used as ratio between the two isomers. A plot of this ratio *vs.* time was fitted according to Equation 5-8 to obtain the rate constants and the equilibrium constant.

Reaction of 49 with CO

(a) About 25 mg (~ 0.03 mmol) of 49 consisting of both *syn* and *anti* isomers at about 5:1 ratio was dissolved in C_6D_6 in an NMR tube. After recording both the $^{31}P\{^1H\}$ and ^1H NMR spectra of this solution, a stream of carbon monoxide was bubbled through it. This solution was then monitored by both the $^{31}P\{^1H\}$ and ^1H NMR spectroscopy. Important NMR data: $^{31}P\{^1H\}$ NMR δ(ppm): 0.1 (*syn*-54), -1.4 (*anti*-54), -3.1 (*syn*-55), and -6.0 (*anti*-55). ^1H NMR δ(ppm): -17.55 ($^2J_{PH}$ = 11.9 Hz, *syn*-54), -18.28 ($^2J_{PH}$ = 16.0 Hz, *anti*-54), -6.88 ($^2J_{PH}$ = 15.7 Hz, *syn*-55), and -7.09 ($^2J_{PH}$ = 20.8 Hz, *anti*-55).

(b) Same procedure as described in (a) was followed using about 25 mg (~ 0.03 mmol) of 49 consisting of both *syn* and *anti* isomers at about 1:6 ratio. The CO flushed solution was monitored by $^{31}P\{^1H\}$ and ^1H NMR spectroscopy until the *syn*-55 almost disappeared completely.

References

1. C. Masters, "Homogeneous Transition-metal Catalysis - a gentle art", Chapman and Hall, London (1981).

2. F. Nixon, *Adv. Inorg. Chem. Radiochem.*, **29**, 42 (1985).

3. H.W. Choi and E.L. Muetterties, *J. Am. Chem. Soc.*, **104**, 153 (1982).

4. M. Baudler, *Angew. Chem. Int. Ed. Engl.*, **26**, 419 (1987).

5. M.M.T. Khan and A.E. Martell, *Inorg. chem.*, **14**, 676 (1975).

6. R.A. Aitken and S.N. Kilenyi, "Asymmetric Synthesis", Blackie Academic & Professional, an imprint of Chapman & Hall, Wester Cleddens Road, Bishopbriggs, Glasgow (1992).

7. (a) R.S. Cahn, C.K. Ingold, and V. Prelog, *Angew. Chem., Int. Ed. Engl.*, **5**, 385 (1982); (b) R.S. Cahn, C.K. Ingold, and V. Prelog, *Experientia*, **12**, 81 (1956).

8. H. Brunner, *J. Organomet. Chem.*, **300**, 39 (1986).

9. (a) P.A. Chaloner, "Handbook of Coordination Catalysis in Organic Chemistry", Butterworths, London, **1985**, pp. 403; (b) M. Orchin, *Adv. Catal.*, **16**, 1 (1966).

10. R. Noyori and H. Takaya, *Acc. Chem. Res.*, **23**, 345 (1990).

11. W.S. Knowles, *Acc. Chem. Res.*, **16**, 106 (1983).

12. N. Sakai, S. Mano, K. Nozaki, and H. Takaya, *J. Am. Chem. Soc.*, **115**, 7033, (1993).

13. H. Brunner, *Angew. Chem. Int. Ed.*, **22**, 897 (1983).

14. (a) P.S. Elmes and W.R. Jackson, *Aust. J. Chem.*, **35**, 2041 (1982); (b) M. Hodgson, D. Parker, R.J. Taylor, and G. Ferguson, *Organometallics*, **7**, 1761 (1988); (c) M.J. Baker and P.G. Pringle, *J. Chem. Soc., Chem. Commun.*, 1292 (1991); (d) T.V. RajanBabu and A. Casalnuovo, *J. Am. Chem. Soc.*, **114**, 6265 (1992).

15. (a) K.B. Sharpless, *Chemtech*, 692 (1985); (b) Y. Gao, M. Hanson, J.M. Klunder, S.M. Ko, H. Masamune, and K.B. Sharpless, *J. Am. Chem. Soc.*, **109**, 5765 (1987).

16. (a) T. Aratani, *Pure Appl. Chem.*, **57**, 1839 (1985). (b) T. Aratani, H. Yoshihara, and G. Susukamo, *U.S. Patent*, 4,552,972 (1985).

17. L. Horner, H. Winkler, A. Rapp, A. Mentrup, H. Hoffmann, and P. Beck, *Tetrahedron Lett.*, 161 (1961).

18. A. Bader, M. Pabel, and S.B. Wild, *J. Chem. Soc., Chem. Commun.*, 1405 (1994).

19. L. Horner, H. Siegel, and H. Buthe, *Angew. Chem. Int. Ed. Engl.*, **7**, 942 (1968).

20. W.S. Knowles and M.J. Sabacky, *J. Chem. Soc., Chem. Commun.*, 1445 (1968).

21. For example: (a) R. Noyori, I. Tomino, Y. Tanimoto, and M. Nishizawa, *J. Am. Chem. Soc.*, **106**, 6709 (1984); (b) R. Noyori, I. Tomino, M. Yamada, and M. Nishizawa, *ibid*, **106**, 6717 (1984).

22. For example: (a) M. Kitamura, T. Ohkuma, S. Inoue, N. Sayo, H. Kumobayashi, S. Akutagawa, T. Ohta, H. Takaya, and R. Noyori, *J. Am. Chem. Soc.*, **110**, 629 (1988); (b) H. Takaya, T. Ohta, N. Sayo, H. Kumobayashi, S. Akutagawa, S. Inoue, I. Kasahara, and R. Noyori, *ibid*, **109**, 1596 (1987); (c) R. Noyori, M. Ohta, Y. Hsiao, M. Kitamura, T. Ohta, and H. Takaya, *ibid*, **108**, 7117 (1986).

23. K.M. Pietrusiewicz and M. Zablocka, *Chem. Rev.*, **94**, 1375 (1994), and references therein.

24. D. Valentine, Jr., "Asymmetric Synthesis", J.D. Morrison, J.W. Scott, Eds.; Academic Press: Orlando, FL, Vol. 3, Chapter 3 (1984).

25. T. Imamoto; "Handbook of Organophosphorus Chemistry", R. Engel, Ed., Marcel Dekker: New York, Chapter 1 (1992).

26. A. Miyashita, A. Yasuda, H. Takaya, K. Toriumi, T. Ito, T. Souchi, and R. Noyori, *J. Am. Chem. Soc.*, **102**, 7932 (1980).

27. (a) H.B. Kagan and T.-P. Dang, *J. Am. Chem. Soc.*, **94**, 6492 (1972); (b) T.-P. Dang and H.B. Kagan, *J. Chem. Soc., Chem. Commun.*, 481 (1971).

28. H. Brunner, *Angew. Chem., Int. Ed. Engl.*, **10**, 1301 (1971).

29. H. Brunner and J. Doppelberger, *Chem. Ber.*, **111**, 673, (1978).

30. J. Beneš and J. Hetflejš, *Collection Czechoslov. Chem. Commun.*, **41**, 2256 (1976).

31. T. Milobedzki and J.H. Kolitowska, *Rocz. Chem.*, **6**, 67 [*Chem. Zentralbl.*, **1926/II**, 2898].

32. J. Neuffer and W.J. Richter, *J. Organomet. Chem.*, **301**, 289 (1986).

33. S. Otsuka, K. Tani, I. Kato, and O. Teranaka, *J. Chem. Soc., Dalton Tran.*, 2216 (1974).

34. A.k. Bhattacharya and G. Thyagarajan, *Chem. Rev.*, **81**, 415 (1981).

35. J.C. Tebby, "Handbook of Phosphorus-31 Nuclear Magnetic Resonance Data", CRC Press: Boca Raton (1991).

36. J.H. Letcher and J.R. Van Wazer, *Topics in Phosphorus Chemistry*, **5**, 75 (1967).

37. (a) K. Hiroi, Y. Arinaga, and T. Ogino, *Chem. Lett.*, 2329, (1992); (b) W. Keim, A. Koehnes, T. Roethel, and D. Enders, *J. Organomet. Chem.*, **382**, 295 (1990); (c) M. Hidai, H. Mizuta, H. Yagi, Y. Nagai, K. Hata, and Y. Uchida, *J. Organomet. Chem.*, **232**, 89 (1982); (d) K. Yamamoto, Y. Kiso, R. Ito, K. Tamao, and M. Kumada, *J. Organomet. Chem.*, **210**, 9 (1981), and references therein.

38. (a) J.D. Morrison and W.F. Masler, *J. Org. Chem.*, **39**, 270 (1974); (b) J.D. Morrison, R.E. Burnett, A.M. Aguiar, C.J. Morrow, and C. Phillips, *J. Am. Chem. Soc.*, **93**, 1301 (1971).

39. A.M. Aguiar and T.G. Archibald, *Tetrahedron Lett.*, 5541 (1966).

40. L. Horner, H. Oedinger, and H. Hoffman, *Justus Liebigs Ann. Chem.*, **626**, 26 (1959).

41. J.G. Smith and G.F. Wright, *J. Org. Chem.*, **17**, 1116 (1952).

42. M. Tanaka and I. Ogata, *Bull. Chem. Soc. Jpn.*, **48**, 1094 (1975).

43. H.M. Walborsky and A.E. Young, *J. Am. Chem. Soc.*, **86**, 3288 (1964), and the references therein.

44. C.A. Tolman, *J. Am. Chem. Soc.*, **92**, 2956 (1977), and references therein.

45. (a) C.A. Tolman, *Chem. Rev.*, **77**, 313 (1977), (b) C.A. Tolman, W.C. Seidel, and L.W. Gosser, *J. Am. Chem. Soc.*, **96**, 53 (1974).

46. M.P. Schutzenberger, *Annales*, **15**, 100 (1868).

47. L. Mond, *J. Chem. Soc.*, **57**, 749 (1890).

48. M.J.S. Dewar, *Bull. Soc. Chim. Fr.*, C71 (1951).

49. J. Chatt and L.A. Duncanson, *J. Chem. Soc.*, 2939 (1953).

50. O. Roelen, *Angew. Chem. A*, **60**, 62 (1948).

51. W. Reppe, *Liebigs Ann. Chem.*, **582**, 1 (1953).

52. C.D. Wood and P.E. Garrou, *Organometallics*, **3**, 170 (1984).

53. L. Mond and F. Quincke, *J. Chem. Soc.*, **59**, 604 (1891).

54. M. Berthelot, *C. R. Hebd. Seances Acad. Sci.*, **112**, 1343 (1891).

55. D.K. Liu, C.G. Brinkley, and M.S. Wrighton, *Organometallics*, **3**, 1449 (1984).

56. D.F. Shriver and K.H. Whitmire, "Comprehensive Organometallic Chemistry", Eds. G. Wilkinson, F.G.A. Stone, and E.W. Abel, Pergamon Press, Oxford, England, **4**, 243 (1982), and the references therein.

57. J.P. Jesson and P. Meakin, *J. Am. chem. Soc.*, **95**, 1344 (1973).

58. R.D. Adams and F.A. Cotton, "Dynamic Nuclear Magnetic Resonance Spectroscopy", ed. L.M. Jackman and F.A. Cotton, Academic Press, New York, 1975, p. 489.

59. E.L. Muetterties, *Acc. Chem. Res.*, **3**, 266 (1970).

60. R.S. Berry, *J. Chem. Phys.*, **32**, 933 (1960).

61. G.G. Sumner, H.P. Klug, and L.E. Alexander, *Acta Crystallogr.*, **17**, 732 (1964).

62. R.L. Sweany and T.L. Brown, *Inorg. Chem.*, **17**, 1381 (1978).

63. R.D.W. Kemmitt and D.R. Russell, "Comprehensive Organometallic Chemistry", Eds. G. Wilkinson, F.G.A. Stone, and E.W. Abel, Pergamon Press, Oxford, England, **5**, 1 (1982), and the references therein.

64. J. Newman and A.R. Manning, *J. Chem. Soc., Chem. Commun.*, 2549 (1974).

65. R.F. Bryan, and A.R. Manning, *J. Chem. Soc., Chem. Commun.*, 1316 (1968).

66. J.A. Ibers, *J. Organomet. Chem.*, **14**, 423 (1968).

67. J.A.M. Case, *Diss. Abstr. B.*, **28**, 2786 (1968).

68. F.W.B. Einstein and R. Kirkland, *Acta Crystallogr., Sect. B*, **34**, 1690 (1978).

69. D.J. Thornhill and A.R. Manning, *J. Chem. Soc., Dalton Trans.*, 6 (1974).

70. M.O. Albers, E. Singleton, and N.J. Coville, *Inorg. Synth.*, 168, **28**, (1990).

71. F.A. Cotton and R.V. Parish, *J. Chem. Soc.*, 1440 (1960).

72. W. Strohmeier and F.-J. Müller, *Chem. Ber.*, **102**, 3613 (1969).

73. (a) A.F. Clifford and A.K. Mukherjee, *Inorg. Chem.*, **2**, 151 (1963); (b) A.F. Clifford and A.K. Mukherjee, *Inorg. Synth.*, **8**, 185 (1966).

74. T.A. Manuel, *Inorg. Chem.*, **2**, 854 (1963).

75. M.O. Albers and N.J. Coville, *J. Organomet. Chem.*, **217**, 385 (1981).

76. E. Weiss, K. Stark, J.E. Lancaster, and H.D. Murdoch, *Helv. Chim. Acta*, **46**, 288 (1963).

77. D.J. Darensbourg, H.H. Nelson, III, and C.L. Hyde, *Inorg. Chem.*, **13**, 2135 (1974).

78. L.H. Jones, R.S. Mcdowell, M. Goldblatt, and B.I. Swanson; *J. Chem. Phys.*, **57**, 2050 (1952).

79. L. Vaska, *J. Am. Chem. Soc.*, **88**, 4100 (1966)

80. J.R. Van Wazer and J.H. Letcher; *Topics in Phosphorus Chemistry* **5**, 169 (1967).

81. J.A.S. Howell, M.G. Palin, P. McArdle, D. Cunningham, Z. Goldschmidt, H.E. Gottlieb, and D. Hezroni-Langerman, *Inorg. Chem.*, **32**, 3493 (1993).

82. D.L. Lichtenberger and T.L. Brown, *J. Am. Chem. Soc.*, **99**, 8187 (1977).

83. W.S. Sheldrick, S. Morton, and O. Stelzer, *Z. Anorg. Allg. Chem.*, **475**, 232 (1981).

84. R.H. Neilson, R.J. Thoma, I. Vickovic, and W.H. Watson, *Organometallics*, **3**, 1132 (1984).

85. J. Pickardt, L. Rosch, and H. Schumann, *J. Organomet. Chem.*, **107**, 241 (1976).

86. (a) J.R. Shapley and J.A. Osborn, *Acc. Chem. Res.*, **6**, 305 (1973); (b) M.R. Churchill and K.G. Lin, *J. Am. Chem. Soc.*, **96**, 76 (1974); (c) S.A. Goldfield and K.N. Raymond, *Inorg. Chem.*, **13**, 770 (1974).

87. (a) A.R. Rossi and R. Hoffmann, *Inorg. Chem.*, **14**, 365 (1975); (b) J.K. Burdett, *Inorg. Chem.*, **15**, 212 (1976).

88. E.J. Forbes, D.L. Jones, K. Paxton, and T.A. Hamor, *J. Chem. Soc., Dalton Trans.*, 879 (1979).

89. L.R. Martin, F.W.B. Einstein, and R.K. Pomeroy, *Inorg. Chem.*, **24**, 2777 (1985).

90. J.-J. Brunet, F.B. Kindela, and D. Neibecker, *Inorg. Synth.*, **29**, 151 (1992).

91. A.F. Clifford and A.K. Mukherjee, *Inorg. Synth.*, **8**, 115 (1966).

92. M.J. Therien and W.C. Trogler, *Inorg. Synth.*, **25**, 151 (1989).

93. W.O. Siegl, *J. Organomet. Chem.*, **169**, 191 (1975).

94. R.L. Keiter, E.A. Keiter, K.H. Hecker, and C.A. Boecker, *Organometallics*, **7**, 2466 (1988).

95. J.J. Brunet, *Chem. Rev.*, **90**, 1041 (1990).

96. R. Holderegger and L.M. Venanzi, *Helv. Chim. Acta*, **62**, 2154 (1977).

97. D.S. Brown and G.W. Bushnell, *Acta Crystallogr.*, **22**, 296 (1967).

98. F.A. Cotton, K.I. Hardcastle, and G.A. Rusholme, *J. Coord. Chem.*, **2**, 217 (1973).

99. A.R. Manning, *J. Chem. Soc. (A).*, 1136 (1968).

100. H. Behrens, R. Hüller, A. Jungbauer, P. Merbach, and M. Moll, *Z. Naturforsch., Teil B*, **32**, 1217 (1977).

101. O. Vohler, *Chem. Ber.*, **91**, 1235 (1958).

102. A.R. Manning, *J. Chem. Soc. (A)*, 1018 (1968).

103. (a) K. Noack, *Spectrochim. Acta*, **19**, 1925 (1963); (b) K. Noack, *Helv. Chim. Acta*, **47**, 1555 (1964).

104. F.M. Asseid, "The Synthesis And Reactivity Of Triangular Phosphido-bridged Rhodium And Iridium Clusters", Ph.D. Dissertation, University of Victoria (1995).

105. O. Roelen, *Gar. P.*, 849 548 (1938).

106. (a) B. Cornils, "New Syntheses with Carbon Monoxide", Ed., J.Fable, Springer-Verlag, Berlin (1980); (b) C.A. Tolman and J.W. Faller, "Homogeneous Catalysis with Metal Phosphine Complexes", Ed., L.H. Pignolet, Plenum, London (1983).

107. For recent results, see (a) N. Sakai, K. Nozaki, and H. Takaya, *J. Chem. Soc., Chem. Commun.*, 395 (1994); (b) K. Totland and H. Alper, *J. Org. Chem.*, **58**, 3326 (1993); and (c) L. Kollar, T. Kegl, and J. Bakos, *J. Organomet. Chem.*, **453**, 155 (1993).

108. F.A. Cotton and G. Wilkinson, "Advanced Inorganic Chemistry", Fifth Ed. (1988).

109. J.P. Collman and L.S. Hegedus, "Principles and Applications of Organotransition Metal Chemistry"; University Science Books: Mill Valley, CA, 1980.

110. (a) P. Powell, "Principles of Organometallic Chemistry", 2nd Ed., Chapman and Hall, New York (1988); (b) J.D. Atwood, "Inorganic and Organometallic Reaction Mechanisms", Brooks/Cole, Monterey, CA. (1985). (c) C.M. Lukehart, "Fundamental Transition Metal Organometallic Chemistry", Brooks/Cole, Monterey CA. (1985).

111. R. Frank and H. Schmidbauer, *Inorg. Chim. Acta*, **13**, 85 (1976).

112. N.J. Lewis, K.R. Mann, J.G. Gordon, and H.B. Gray, *J. Am. Chem. Soc.*, **98**, 7461 (1976).

113. R.G. Finke, G. Gaughan, J.H. Noordik, and C. Pierpoint, *Organometallics*, **2**, 1481 (1983), and references therein.

114 J.J. Bonnet, A. Thorez, A. Maisonnat, J. Galy, and R. Poilblanc, *J. Am. Chem. Soc.*, **101**, 5940 (1979).

115. D.O.K. Fjeldsted and S.R. Stobart, *J. Chem. Soc., Chem. Commun.*, 908 (1985).

116. M.H. Chisholm, C.C. Kirkpatrick, and J.C. Huffman, *Inorg. Chem.*, **20**, 871 (1981).

117. I.R. Jobe, S.S.M. Ling, L. Manojlovic-Muir, K.W. Muir, and R.J. Puddephatt, *Organometallics*, **4**, 1198 (1985).

118. J.J. Bonnet, J. Galy, P. Kalck, A. Mayanza, and R. Poilblanc, *J. Chem. Res. (S)*, 146 (1980).

119. (a) M.H. Chisholm, C.C. Kirkpatrick, and J.C. Huffman, *Inorg. chem.*, **20**, 871 (1981); (b) M.H. Chisholm and D.A. Haitko, *J. Am. Chem. Soc.*, **101**, 6984 (1979); (c) F.A. Cotton and W.T. Hall, *Inorg. Chem.*, **19**, 2354 (1980).

120. E.L. Muetterties, T.N. Rhodin, E. Band, C.F. Brucker, and W.R. Pretzer, *Chem. Rev.*, **79**, 91, (1979).

121. A.W. Coleman, D.T. Eadie, S.R. Stobart, M.J. Zaworotko, and J.L. Atwood, *J. Am. Chem. Soc.*, **104**, 922 (1982).

122. K.A. Beveridge, G.W. Bushnell, K.R. Dixon, D.T. Eadie, S.R. Stobart, J.L. Atwood, and M.J. Zaworotko, *J. Am. Chem. Soc.*, **104**, 920 (1982).

123. G.W. Bushnell, D.O.K. Fjeldsted, S.R. Stobart, and M.J. Zaworotko, *J. Chem. Soc., Chem. Commun.*, 580 (1983).

124. M.J. Decker, D.O.K. Fjeldsted, S.R. Stobart, and M.J. Zaworotko, *J. Chem. Soc., Chem. Commun.*, 1525 (1983).

125. K.A. Beveridge, G.W. Bushnell, S.R. Stobart, J.L. Atwood, and M.J. Zaworotko, *Organometallics*, **2**, 1447 (1983).

126. J.L. Atwood, K.A. Beveridge, G.W. Bushnell, K.R. Dixon, D.T. Eadie, S.R. Stobart, and M.J. Zaworotko, *Inorg. Chem.*, **23**, 4050 (1984).

127. G.W. Bushnell, S.R. Stobart, R. Vefghi, and M.J. Zaworotko, *J. Chem. Soc., Chem. Commun.*, 282 (1984).

128. G.W. Bushnell, D.O.K. Fjeldsted, S.R. Stobart, M.J. Zaworotko, S.A.R. Know, and K.A. Macpherson, *Organometallics*, **4**, 1107 (1985).

129. D.O.K. Fjeldsted and S.R. Stobart, *J. Chem. Soc., Chem. Commun.*, 908 (1985).

130. G.W. Bushnell, M.J. Decker, D.T. Eadie, S.R. Stobart, R. Vefghi, J.L. Atwood, M.J. Zaworotko, *Organometallics*, **4**, 2106 (1985).

131. J.L. Marshall, S.R. Stobart, and H.B. Gray, *J. Am. Chem. Soc.*, **106**, 3027 (1984).

132. D.O.K. Fjeldsted, S.R. Stobart, and M.J. Zaworotko, *J. Am. Chem. Soc.*, **107**, 8258 (1985).

133. D.G. Harrison and S.R. Stobart, *J. Chem. Soc., Chem. Commun.*, 285 (1986).

134. R.D. Brost and S.R. Stobart, *J. Chem. Soc., Chem. Commun.*, 498 (1989).

135. R.D. Brost, D.O.K. Fjeldsted, and S.R. Stobart, *J. Chem. Soc., Chem. Commun.*, 488 (1989).

136. R.D. Brost and S.R. Stobart, *Inorg. Chem.*, **28**, 4307 (1989).

137. B.F. Fieselmann and G.D. Stucky, *Inorg. Chem.*, **17**, 2074 (1978).

138. K.S. Chong, S.J. Rettig, A. Storr, and J. Trotter, *Can. J. Chem.*, **57**, 3090 (1979).

139. J.A. Bailey, S.L. Grundy, and S.R. Stobart, *Organometallics*, **9**, 536 (1990).

140. D.G. Harrison, "Oxidative Addition At Di-iridium Centres", Ph.D. Dissertation, University of Victoria (1987).

141. K.A. Beveridge, G.W. Bushnell, K.R. Dixon, D.T. Eadie, S.R. Stobart, J.L. Atwood, and M.J. Zaworotko; *J. Am. Chem. Soc.*, **104**, 920, (1982).

142. T.W.G. Solomons, "Organic Chemistry", 5th Ed., John Wiley & Sons, New York (1992).

143. C.H. Bushweller, J. Golini, G.U. Rao, and J.W. O'Neil, *J. Am. Chem. Soc.*, **92**, 3055 (1970).

144. L. Vaska, *Accts. Chem. Res.*, **1**, 335 (1968).

145. M.F. Lappert and P.W. Lednor, *Adv. in Organometal. Chem.*, **14**, 345 (1976).

146. R.G. Finke, G. Gaughan, J.H. Noordik, and C. Peirpont, *Organometallics*, **2**, 1481 (1983).

147. K.A. Azam, M.P. Brown, R.H. Hill, R.J. Puddephatt, and A. Yarari, *Organometallics*, **3**, 697 (1984).

148. R.D. Brost, "Structural Properties Of Pyrazolyl-bridged Diiridium Complexes", Ph.D. Dissertation, University of Victoria (1984).

149. R.J. Fessende and J.S. Fessenden, "Organic Chemistry", Willard Grant Press, Boston, (1980) pp 175.

150. H.C. Brown and K.T. Liu, *J. Am. Chem. Soc.*, **97**, 600 (1975).

151. H.C. Brown and N.R. De Lue, *J. Am. Chem. Soc.*, **98**, 1292 (1976).

152. K.B. Wiberg, W.E. Pratt, and W.F. Bailey, *J. Org. Chem.*, **45**, 4936 (1980).

153. R.J. Abraham, A.P. Barlow, and A.E. Rowan, *Magn. Reson. Chem.*, **27**, 1074 (1989).

154. L.M. Jackman and S. Sternhell, "Applications of NMR Spectroscopy in Organic Chemistry", 2nd ed., Pergamon, Oxford (1969).

155. (a) M. Karplus, *J. Chem. Phys.*, **30**, 11 (1959); (b) M. Karplus, *J. Am. Chem. Soc.*, **85**, 2870 (1963); (c) A.A. Bothner-By, *Adv. Magn. Resonance*, **1**, 195 (1965).

156. S.R. Stobart, S.L. Grundy, and F.L. Joslin, U.S. Patent 4,950,798 (1990).

157. G. Bruce and S.R. Stobart, *Inorg. Chem.*, **27**, 3880 (1988).

158. F.R. Hartley and P.N. Vesey, *Adv. Organomet. Chem.*, **15**, 189 (1977).

159. F.L. Joslin, "Transition-Metal Poly-(phosphinoalkyl)silyl Complexes", Ph.D. Dissertation, University of Victoria (1989).

160. J. Grobe and U. Möller, *J. Organomet. Chem.*, **17**, 263 (1969).

161. J. Grobe and U. Möller, *J. Organomet. Chem.*, **31**, 157 (1969).

162. Z.C. Brzezinska and W.R. Cullen, *Inorg. Chem.*, **18**, 3132 (1979).

163. R.D. Holmes-Smith, R.D. Osei, and S.R. Stobart, *J. Chem. Soc., Perkin Trans. I*, 861 (1983).

164. F.L. Joslin and S.R. Stobart, *Inorg. Chem.*, **32**, 2221 (1993).

165. R.D. Holmes-Smith, S.R. Stobart, T.S. Cameron, and K. Jochem, *J. Chem. Soc., Chem. Commun.*, 937 (1981).

166. S.L. Grundy, R.D. Holmes-Smith, S.R. Stobart, and M.A. Williams, *Inorg. Chem.*, **30**, 3333 (1991).

167. M.J. Auburn and S.R. Stobart, *J. Chem. Soc., Chem. Commun.*, 281 (1984).

168. M.J. Auburn, S.L. Grundy, S.R. Stobart, and M.J. Zaworotko, *J. Am. Chem. Soc.*, **107**, 267 (1985).

169. M.J. Auburn, R.D. Holmes-Smith, and S.R. Stobart, *J. Am. Chem. Soc.*, **106**, 1314 (1984).

170. M.J. Auburn and S.R. Stobart, *Inorg. Chem.*, **24**, 318 (1985).

171. F.L. Joslin and S.R. Stobart, *J. Chem. Soc., Chem. Commun.*, 504 (1989).

172. M.J. Auburn, R.D. Holmes-Smith, S.R. Stobart, M.J. Zaworotko, T.S. Cameron, and A. Kumari, *J. Chem. Soc., Chem. Commun.*, 1523 (1983).

173. G. Bruce and S.R. Stobart, *Inorg. Chem.*, **27**, 3880 (1988).

174. R.D. Brost, G.C. Bruce, S.L. Grundy, and S.R. Stobart, *Inorg. Chem.*, **32**, 5195 (1993).

175. R.D. Holmes-Smith, S.R. Stobart, R. Vefghi, And M.J. Zaworotko, *J. Chem. Soc., Dalton Tran.*, 969 (1987).

176. R.A. Gossage, G.D. McLennan, S.R. Stobart, *Inorg. Chem.*, in the press.

177. R.A. Gossage, "Synthesis And Characterization of Si Containing Organometallics", Ph.D. Dissertation, University of Victoria (1996).

178. D. Barton and W.D. Ollis, "Comprehensive Organic Chemistry", ed. I.O. Sutherland, Pergamon Press, Vol. 2 (1979)

179. D.J. Peterson, *J. Organomet. Chem.*, **8**, 199 (1967).

180. N.E. Schore, L.S. Benner, and B.E. LaBelle, *Inorg. Chem.*, **20**, 3200 (1981).

181. (a) H.G. Ang and P.T. Lau, *J. Organomet. Chem.*, **291**, 285 (1985); (b) H.G. Ang, B. Chang, and W.L. Kwik, *J. Chem. Soc., Dalton Tran.*, 2161 (1992).

182. E. Negishi and T. Takahashi, *Aldrichimica Acta*, **18**, 31 (1985), and the references therein.

183. R.A. Gossage, S.R. Stobart, and X. Zhou, Unpublished results.

184. B.M. Kingston and M.F. Lappert, *J. Chem. Soc., Dalton*, 69 (1972).

185. N.J. Archer, R.N. Haszeldine, and R.V. Parish, *J. Chem. Soc., Chem. Commun.*, 524 (1971).

186. J. Chatt, C. Eaborn, S.D. Ibekwe, and P.N. Kapoor, *J. Chem. Soc., (A)*, 1343 (1970).

187. F. Glockling and K.A. Hooton, *J. Chem. Soc., Chem. Commun.*, 218 (1966).

188. A.J. Oliver and W.A.G. Graham, *Inorg. Chem.*, **10**, 1 (1971).

189. R.A. Gossage, G. McLennon, and S.R. Stobart, *Inorg. Chem.*, in press.

190. J. Chatt, C. Eaborn, S.D. Ibekwe, and P.N. Kapoor, *J. Chem. Soc. (A)*, 1343 (1970).

191. T.G. Appleton, H.C. Clark, and L.E. Manzer, *Coord. Chem. Rev.*, **10**, 335 (1973).

192. C.R. Crocker, R.J. Errington, R. Markham, C.J. Moulton, K.J. Odell, and B.L. Shaw, *J. Am. Chem. Soc.*, **102**, 4373 (1980).

193. H.D. Kaesz and R.B. Saillant, *Chem. Rev.*, **72**, 231 (1972).

194. R.A. Gossage, Ph.D. Dissertation, University of Victoria (1995).

195. (a) B.E. Mann, C. Masters, and B.L. Shaw, *J. Chem. Soc., Dalton Tran.*, 48 (1972); (b) B.E. Mann, C. Masters, and B.L. Shaw, *J. Chem. Soc., Dalton Tran.*, 704 (1972).

196. F.L. Joslin, "Transition-Metal Poly-(phosphinoalkyl)silyl Complexes", Ph.D. Dissertation, University of Victoria (1989).

197. D.L. Thorn and R. Hoffmann, *Nouv. J. Chim.*, **3**, 39 (1979).

198. A. Albinati, V.I. Bakhmutov, K.G. Caulton, E. Clot, J. Eckert, O. Eisenstein, D.G. Gusev, V.V. Grushin, B.E. Hauger, W.T. Klooster, T.F. Koetzle, R.K. McMullan, T.J. O'Loughlin, M. P'lissier, J.S. Ricci, M.P. Sigalas, and A. B. Vymenits, *J. Am. Chem. Soc.*, **115**, 7300 (1993).

199. J.-F. Riehl, Y. Jean, O. Eisenstein, and M. P'lissier, *Organometallics*, **11**, 729 (1992).

200. (a) M.D. Fryzuk, P.A. MacNeil, R.L. Massey, and R.G. Ball, *J. Organomet. Chem.*, **368**, 231 (1989); (b) H. Werner, A. Höhn, and M Dziallas, *Angew. Chem. Int. Ed. Engl.*, **25**, 1090 (1986); (c) M.D. Fryzuk, P.A. MacNeil, and R.G. Ball, *J. Am. Chem. Soc.*, **108**, 6414 (1986); (d) K.W. Muir and J.A. Ibers, *Inorg. Chem.*, **9**, 440 (1970).

201. M.C. Favas and D.L. Kepert, *Prog. Inorg. Chem.*, **27**, 325 (1980).

202. D.O.K. Fjeldsted, "Pyrazolyl-bridged Binuclear Complexes Of Rhodium And Iridium", Ph.D. Dissertation, University of Victoria (1988).

203. G. Longoni, P. Chini, F. Canziani, and P. Fantucci, *Gazz. Chim. Ital.* **104**, 249 (1974).

204. D. Drew and J.R. Doyle, *Inorg. Synth.*, **13**, 48 (1970).

205. D.T. Eadie, "Transition Metal Complexes Of Pyrazole And Related Ligands", Ph.D. dissertation, University of Victoria (1981).

Appendices

A. Derivation of Equation 4-8

For reactions in the form of the following equation:
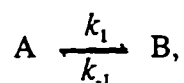
$$A \xrightleftharpoons[k_{-1}]{k_1} B,$$

the rates of the concentration change of the reactant and product are:

$$\frac{d[A]}{dt} = k_{-1}[B] - k_1[A] \qquad\qquad (A-1)$$

$$\frac{d[B]}{dt} = k_1[A] - k_{-1}[B]$$

where [A] and [B] are the concentration of A and B respectively and t is time. Suppose [T] is the total concentration of A and B at any time, and K is the equilibrium constant, then A-1 can be rewritten as:

$$\frac{d[A]}{dt} = k_{-1}([T] - [A]) - k_1[A]$$

$$= \frac{k_1}{K}([T] - [A]) - k_1[A] \qquad \left(\text{since } K = \frac{k_1}{k_{-1}}\right)$$

$$= \frac{k_1}{K}[[T] - (1+K)[A]]$$

$$\therefore \quad \frac{d[A]}{[T] - (1+K)[A]} = \frac{k_1}{K}dt$$

$$\frac{d[[T] - (1+K)[A]]}{[T] - (1+K)[A]} = -(1+K)\frac{k_1}{K}dt$$

Integrating both sides:

$$\ln[[T] - (1 + K)[A]] = -(1 + K)\frac{k_1}{K}t + C$$

In this experiment, the initial concentrations of the two isomers (*i.e.* A and B) are equal. Thus, when $t = 0$, $[A] = [B] = 1/2[T]$. Then

$$C = \ln[[T] - (1 + K)\frac{1}{2}[T]]$$

$$= \ln[\frac{[T]}{2}(1 - K)]$$

Therefore,

$$\ln\frac{[T] - (1 + K)[A]}{\frac{[T]}{2}(1 - K)} = -\frac{(1 + K)}{K}k_1 t$$

$$\frac{[T] - (1 + K)[A]}{\frac{[T]}{2}(1 - K)} = e^{-\frac{(1 + K)}{K}k_1 t}$$

$$[A] = \frac{[T] - \frac{[T]}{2}(1 - K)e^{-\frac{(1 + K)}{K}k_1 t}}{1 + K}$$

$$= \frac{[T]}{1 + K}[1 - \frac{1}{2}(1 - K)e^{-\frac{(1 + K)}{K}k_1 t}]$$

Similarly,

$$[B] = \frac{[T]}{1 + K}[K + \frac{1}{2}(1 - K)e^{-\frac{(1 + K)}{K}k_1 t}]$$

In this experiment, the concentrations of A and B were monitored by the integrations of their NMR signals. The sample was continuously scanned and integrations were taken at various number of scans. Thus each integration is proportional to the average

concentration of A or B over time, and the integration ratio (I_A/I_B) of the NMR signal is equal to the ratio of A and B concentrations integrated over time:

$$\frac{I_B}{I_A} = \frac{\int_0^t [B]dt}{\int_0^t [A]dt} = \frac{\int_t^0 \frac{[T]}{1+K}[K + \frac{1}{2}(1-K)e^{-\frac{1+K}{K}k_1 t}]dt}{\int_t^0 \frac{[T]}{1+K}[1 - \frac{1}{2}(1-K)e^{-\frac{1+K}{K}k_1 t}]dt}$$

$$= \frac{[Kt - \frac{1}{2}(1-K)\frac{K}{(1+K)k_1}e^{-\frac{1+K}{K}k_1 t}]\Big|_0^t}{[t + \frac{1}{2}(1-K)\frac{K}{(1+K)k_1}e^{-\frac{1+K}{K}k_1 t}]\Big|_0^t}$$

$$= \frac{2K(1+K)k_1 t - K(1-K)(e^{-\frac{1+K}{K}k_1 t} - 1)}{2(1+K)k_1 t + K(1-K)(e^{-\frac{1+K}{K}k_1 t} - 1)}$$

B. Derivation of Equations 4-10 and 5-10

For reactions in the form of the following equation:
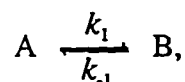
$$A \underset{k_{-1}}{\overset{k_1}{\rightleftharpoons}} B,$$

the rates of the concentration change of the reactant and product are:

$$\frac{d[A]}{dt} = k_{-1}[B] - k_1[A] \qquad\qquad (A-1)$$

$$\frac{d[B]}{dt} = k_1[A] - k_{-1}[B]$$

where [A] and [B] are the concentration of A and B respectively and t is time. Suppose

[T] is the total concentration of A and B at any time, then A-1 can be rewritten as:

$$\frac{d[A]}{dt} = k_{-1}([T] - [A]) - k_1[A]$$

$$= k_{-1}[T] - (k_1 + k_{-1})[A]$$

$$\therefore \quad \frac{d[A]}{k_{-1}[T] - (k_1 + k_{-1})[A]} = dt$$

$$\frac{d[k_{-1}[T] - (k_1 + k_{-1})[A]]}{k_{-1}[T] - (k_1 + k_{-1})[A]} = -(k_1 + k_{-1})dt$$

Integrating both sides:

$$\ln[k_{-1}[T] - (k_1 + k_{-1})[A]] = -(k_1 + k_{-1})t + C$$

When $t = 0$, $[A] = [A]_0$, where $[A]_0$ is the initial concentration of A, then

$$C = \ln[k_{-1}[T] - (k_1 + k_{-1})[A]_0]$$

Therefore,

$$\ln \frac{k_{-1}[T] - (k_1 + k_{-1})[A]}{k_{-1}[T] - (k_1 + k_{-1})[A]_0} = -(k_1 + k_{-1})t$$

$$\frac{k_{-1}[T] - (k_1 + k_{-1})[A]}{k_{-1}[T] - (k_1 + k_{-1})[A]_0} = e^{-(k_1 + k_{-1})t}$$

$$[A] = \frac{k_{-1}[T] - [k_{-1}[T] - (k_1 + k_{-1})[A]_0]e^{-(k_1 + k_{-1})t}}{k_1 + k_{-1}}$$

$$= \frac{[T]}{k_1 + k_{-1}}\{k_{-1} - [k_{-1} - (k_1 + k_{-1})\frac{[A]_0}{[T]}]e^{-(k_1 + k_{-1})t}\}$$

where

$$[T] = [A]_0 + [B]_0$$

$$\frac{[A]_0}{[T]} = \frac{[A]_0}{[A]_0 + [B]_0}$$

$$= \frac{1}{1 + \dfrac{[B]_0}{[A]_0}}$$

Thus,

$$[A] = \frac{[T]}{k_1 + k_{-1}} \{ k_{-1} - [k_{-1} - (k_1 + k_{-1}) \frac{1}{[B]_0/[A]_0 + 1}] e^{-(k_1 + k_{-1})t} \}$$

Similarly,

$$[B] = \frac{[T]}{k_1 + k_{-1}} \{ k_1 - [k_1 - (k_1 + k_{-1}) \frac{1}{[A]_0/[B]_0 + 1}] e^{-(k_1 + k_{-1})t} \}$$

Therefore, at any time,

$$\frac{[B]}{[A]} = \frac{k_1 - [k_1 - (k_1 + k_{-1}) \dfrac{1}{[A]_0/[B]_0 + 1}] e^{-(k_1 + k_{-1})t}}{k_{-1} - [k_{-1} - (k_1 + k_{-1}) \dfrac{1}{[B]_0/[A]_0 + 1}] e^{-(k_1 + k_{-1})t}}$$

Because the integration ratio (I_A/I_B) of the NMR signals of A and B is equal to their concentration ratio,

$$\frac{I_B}{I_A} = \frac{k_1 - [k_1 - (k_1 + k_{-1}) \dfrac{1}{I_{A_0}/I_{B_0} + 1}] e^{-(k_1 + k_{-1})t}}{k_{-1} - [k_{-1} - (k_1 + k_{-1}) \dfrac{1}{I_{B_0}/I_{A_0} + 1}] e^{-(k_1 + k_{-1})t}}$$

where I_{A0}/I_{B0} is the initial integration ratio.

C. Crystallographic data for compound 41

formula: $C_{52}H_{60}N_4O_4P_2Ir_2$ molecular weight: 1251.46

space group: monoclinic, A2 (No. 5)   a = 22.451(6) Å

b = 10.054(3) Å   c = 25.085(7) Å

β = 115.59(3)°   V = 5107(2) Å^3

Z = 4   diffractometer: Nonius CAD4-F11

λ = 0.71069 Å   T = 295 K

R = 0.0539 R_w = 0.0582

Table A-1. Fractional atomic coordinates and temperature parameters for 41.

Atom	x/a	y/b	z/c	U_{eq}
Ir(1)	2047(5)	0(0)	7150(5)	505(5)
Ir(2)	52011(6)	9688(10)	7199(5)	507(5)
P(1)	1033(3)	1344(8)	1262(3)	57(3)
P(2)	6037(3)	-344(8)	1285(3)	50(3)
O(1)	-753(11)	1271(30)	1075(11)	125(6)
O(2)	4310(8)	-365(34)	1155(8)	109(5)
O(5)	1439(9)	980(29)	1958(7)	93(6)
O(6)	6434(6)	-25(16)	1983(6)	43(4)
N(1)	548(5)	-1094(15)	-214(4)	87(6)
N(2)	770(5)	-1095(15)	409(4)	44(4)
C(3)	1328(5)	-1946(15)	659(4)	56(5)
C(4)	1451(5)	-2472(15)	190(4)	69(6)
C(5)	969(5)	-1945(15)	-349(4)	92(6)
N(4)	5572(5)	2243(12)	-155(5)	39(5)
N(5)	5787(5)	2066(12)	463(5)	81(6)
C(6)	6370(5)	2827(12)	761(5)	72(6)

Atom	x/a	y/b	z/c	U_{eq}
C(7)	6516(5)	3475(12)	328(5)	74(6)
C(8)	6022(5)	3114(12)	-238(5)	51(5)
C(11)	1732(6)	1421(20)	1079(6)	56(5)
C(12)	1667(6)	1948(20)	543(6)	80(6)
C(13)	2202(6)	1922(20)	399(6)	85(6)
C(14)	2802(6)	1371(20)	792(6)	76(6)
C(15)	2866(6)	844(20)	1329(6)	116(7)
C(16)	2331(6)	869(20)	1473(6)	80(6)
C(21)	818(7)	3112(12)	1235(7)	55(6)
C(22)	1237(7)	3880(12)	1713(7)	101(7)
C(23)	1112(7)	5234(12)	1733(7)	98(7)
C(24)	568(7)	5819(12)	1275(7)	111(7)
C(25)	150(7)	5051(12)	796(7)	65(6)
C(26)	274(7)	3698(12)	776(7)	78(6)
C(31)	6727(6)	-332(19)	1091(7)	63(6)
C(32)	6575(6)	-805(19)	524(7)	79(6)
C(33)	7056(6)	-806(19)	311(7)	88(6)
C(34)	7689(6)	-333(19)	666(7)	87(6)
C(35)	7841(6)	140(19)	1233(7)	66(6)
C(36)	7361(6)	141(19)	1445(7)	76(6)
C(41)	5852(8)	-2090(12)	1295(7)	59(6)
C(42)	6255(8)	-2993(12)	1719(7)	67(6)
C(43)	6097(8)	-4343(12)	1660(7)	107(7)
C(44)	5535(5)	-4791(12)	1176(7)	88(6)
C(45)	5131(8)	-3888(12)	751(7)	123(7)
C(46)	5290(8)	-2538(12)	810(7)	75(6)
C(50)	1952(7)	-1309(15)	2790(7)	179(9)'
C(51)	1584(7)	-125(15)	2876(7)	90(6)'

Atom	x/a	y/b	z/c	U_{eq}
C(52)	1092(7)	526(15)	2289(7)	62(6)'
C(53)	628(7)	1394(15)	2463(7)	117(7)'
C(54)	957(7)	1107(15)	3136(7)	141(8)'
C(55)	1615(7)	1916(15)	3382(7)	144(8)'
C(56)	2087(7)	1033(15)	3233(7)	115(7)'
C(57)	1178(7)	-384(15)	3221(7)	59(5)'
C(58)	1566(7)	-802(15)	3865(7)	97(7)'
C(59)	575(7)	-1287(15)	2942(7)	95(6)'
C(60)	6373(8)	-1167(12)	3058(7)	198(9)'
C(61)	6419(8)	305(12)	2941(7)	116(7)'
C(62)	6085(8)	653(12)	2266(7)	74(7)'
C(63)	6000(8)	2192(12)	2266(7)	138(8)'
C(64)	6224(8)	2457(12)	2938(7)	198(9)'
C(65)	6977(8)	2328(12)	3096(7)	132(8)'
C(66)	7152(8)	828(12)	3188(7)	96(6)'
C(67)	6058(8)	1188(12)	3209(7)	100(7)'
C(68)	6406(8)	1241(12)	3888(7)	94(6)'
C(69)	5310(8)	988(12)	2930(7)	151(8)'
C(1)	-366(10)	998(23)	935(9)	51(5)'
C(2)	4662(11)	347(26)	1020(11)	66(6)'

Note: Estimated standard deviations are given in parentheses. Coordinaties $\times 10^n$, where $n = 5$ for Ir and $n = 4$ otherwise. Temperature parameters $\times 10^n$, where $n = 4$ for Ir and $n = 3$ otherwise. U_{eq} = the equivalent isotropic temperature parameter = $1/3\sum_i\sum_j U_{ij}a_i^*a_j^*(a_i \cdot a_j)$. Primed values indicate that U_{iso} is given. T = exp-$(8\pi^2 U_{iso}\sin^2\theta/\lambda^2)$.

Table A-2. Anisotropic temperature parameters (Å²) for 41.

Atom	U_{11}	U_{22}	U_{33}	U_{23}	U_{13}	U_{12}
Ir(1)	388(5)	804(11)	384(6)	-64(7)	225(4)	18(8)
Ir(2)	5811(7)	624(8)	502(7)	-33(7)	410(6)	32(8)
P(1)	60(4)	84(6)	41(3)	5(4)	36(3)	21(4)
P(2)	45(3)	64(4)	47(3)	7(3)	26(3)	19(3)
O(1)	99(8)	135(9)	179(9)	-76(8)	97(7)	-3(8)
O(2)	58(6)	209(10)	82(7)	66(8)	51(6)	21(8)
O(5)	93(8)	145(9)	42(6)	-24(8)	31(6)	-39(8)
O(6)	45(5)	53(6)	51(6)	-19(5)	39(4)	-18(5)
N(1)	77(8)	161(9)	45(7)	1(8)	48(6)	-28(8)
N(2)	15(5)	72(8)	34(6)	-25(6)	1(4)	12(5)
C(3)	39(7)	85(9)	30(6)	25(7)	2(6)	-3(7)
C(4)	41(7)	110(9)	53(8)	-2(8)	17(6)	3(8)
C(5)	58(8)	70(9)	150(9)	22(9)	48(8)	29(8)
N(4)	35(6)	32(6)	50(7)	4(6)	18(5)	-10(5)
N(5)	133(8)	70(8)	87(7)	-27(7)	92(6)	11(8)
C(6)	71(8)	51(8)	114(9)	14(8)	61(7)	-21(7)
C(7)	88(8)	90(9)	57(8)	15(8)	44(7)	-15(8)
C(8)	60(7)	78(8)	41(6)	21(6)	47(5)	9(7)
C(11)	32(6)	88(9)	70(8)	-10(8)	42(6)	-7(7)
C(12)	63(7)	151(10)	49(7)	0(8)	45(6)	-13(8)
C(13)	60(7)	158(10)	61(7)	-18(8)	50(6)	-29(8)
C(14)	63(8)	69(9)	117(9)	-28(8)	60(7)	-16(7)
C(15)	120(9)	132(10)	122(9)	25(9)	76(8)	-30(9)
C(16)	97(9)	82(9)	91(8)	-10(8)	68(7)	4(8)
C(21)	67(8)	54(8)	58(8)	2(7)	40(7)	-11(7)
C(22)	106(9)	74(9)	102(9)	-29(9)	24(9)	-4(9)
C(23)	76(8)	101(9)	111(9)	43(9)	35(8)	14(9)

Atom	U_{11}	U_{22}	U_{33}	U_{23}	U_{13}	U_{12}
C(24)	168(9)	48(9)	171(9)	-3(9)	123(8)	14(9)
C(25)	85(8)	29(7)	92(8)	-1(7)	48(7)	32(7)
C(26)	61(8)	135(10)	30(7)	-18(8)	13(7)	7(9)
C(31)	93(9)	55(8)	57(8)	5(7)	46(7)	11(8)
C(32)	86(8)	96(9)	79(8)	8(8)	60(7)	11(8)
C(33)	75(8)	130(9)	62(8)	18(9)	33(7)	16(9)
C(34)	85(8)	127(9)	75(8)	23(8)	59(7)	34(8)
C(35)	62(7)	63(8)	106(8)	-4(8)	67(6)	-17(7)
C(36)	34(6)	108(9)	94(8)	-17(9)	33(7)	-2(8)
C(41)	67(8)	84(9)	44(7)	3(7)	42(6)	-10(8)
C(42)	65(7)	52(8)	105(8)	-15(8)	56(7)	4(7)
C(43)	159(9)	56(9)	148(9)	35(8)	105(8)	36(8)
C(44)	62(8)	111(9)	104(9)	-29(9)	48(7)	-7(8)
C(45)	1141(9)	200(10)	72(8)	-26(9)	57(8)	5(10)
C(46)	96(8)	45(8)	115(9)	-45(7)	74(7)	-39(7)

Note: Estimated standard deviations are given in parentheses. U values $\times$ 10^n, where $n = 4$ for Ir and $n = 3$ otherwise. $T = exp-2\pi^2(U_{11}h^2a^{*2} + ... + 2U_{23}klb^*c^* + ...)$.

D. Crystallographic data for compound 16

formula: $C_{34}H_{57}FeO_7P$

crystal system: orthorhombic

a = 11.439(2) Å

c = 24.993(4) Å

Z = 4

λ = 0.71073 Å

R = 0.0662

molecular weight: 664.64

space group: $P2_12_12_1$

b = 13.258(3) Å

V = 3790.3(13) Å^3

diffractometer: Siemens P4/PC

T = 293 K

R_w = 0.0662

Table B-1. Atomic coordinates ($\times 10^4$) and temperature parameters ($\times 10^3$ Å^2) for 16.

Atom	x/a	y/b	z/c	U_{eq}
Fe(1)	5404(1)	3203(1)	2195(1)	45(1)
P(1)	6961(3)	3547(2)	1721(1)	37(1)
O(1)	5285(11)	5307(8)	2514(4)	95(5)
O(2)	4133(9)	2629(10)	1225(4)	105(5)
O(3)	6820(8)	1751(8)	2789(4)	95(4)
O(4)	3402(8)	2569(6)	2831(5)	102(5)
C(1)	5311(12)	4501(10)	2395(5)	59(5)
C(2)	4644(12)	2846(10)	1591(6)	68(5)
C(3)	6267(11)	2337(11)	2562(5)	55(5)
C(4)	4183(12)	2837(11)	2586(5)	68(6)
O(5)	7964(7)	4168(5)	2002(3)	46(3)
O(6)	6788(7)	4174(5)	1192(3)	51(3)
O(7)	7649(6)	2613(6)	1501(3)	45(3)
C(5)	8632(11)	3862(9)	2476(5)	53(5)
C(6)	9899(11)	4137(11)	2385(6)	71(6)
C(7)	10570(16)	3918(14)	2899(8)	116(9)

Atom	x/a	y/b	z/c	U_{eq}
C(8)	10061(18)	4412(15)	3383(8)	122(10)
C(9)	8784(18)	4109(13)	3477(6)	95(8)
C(10)	8120(13)	4327(10)	2966(5)	74(6)
C(11)	10444(15)	3712(14)	1872(7)	97(8)
C(12)	11580(14)	4231(16)	1747(9)	155(12)
C(13)	10637(15)	2596(14)	1895(9)	145(11)
C(14)	8246(18)	4602(17)	3948(7)	166(13)
C(15)	6464(12)	5240(9)	1163(5)	59(5)
C(16)	7241(15)	5715(10)	739(5)	74(6)
C(17)	6825(18)	6780(12)	626(7)	105(8)
C(18)	5586(21)	6822(12)	472(6)	118(9)
C(19)	4806(14)	6358(12)	896(6)	91(7)
C(20)	5175(13)	5281(10)	1009(5)	74(6)
C(21)	8538(15)	5671(12)	881(7)	91(8)
C(22)	8896(15)	6334(12)	1347(7)	107(8)
C(23)	9316(16)	5889(13)	419(7)	141(10)
C(24)	3492(16)	6403(13)	771(7)	132(10)
C(25)	7218(9)	1930(9)	1084(4)	45(3)
C(26)	8238(10)	1642(9)	727(5)	56(5)
C(27)	7795(12)	887(10)	300(5)	72(6)
C(28)	7188(12)	5(10)	544(5)	66(5)
C(29)	6219(13)	306(9)	924(5)	61(5)
C(30)	6667(11)	1024(9)	1333(5)	51(5)
C(31)	8838(12)	2556(11)	476(5)	68(6)
C(32)	10062(11)	2260(13)	259(6)	99(7)
C(33)	8161(12)	3101(11)	62(5)	76(6)
C(34)	5620(16)	-597(11)	1155(6)	110(8)

Note: Estimated standard deviations are given in parentheses. U_{eq} = the equivalent isotropic temperature parameter = $1/3\Sigma_i\Sigma_j U_{ij}a_i^*a_j^*(a_i \cdot a_j)$.

Table B-2. Anisotropic temperature parameters ($\times 10^3$ Å^2) for **16**.

Atom	U_{11}	U_{22}	U_{33}	U_{12}	U_{13}	U_{23}
Fe(1)	45(1)	53(1)	37(1)	2(1)	5(1)	-1(1)
P(1)	43(2)	35(2)	32(2)	5(1)	-1(1)	3(1)
O(1)	137(10)	51(6)	96(7)	15(7)	25(8)	-16(6)
O(2)	69(7)	170(12)	77(7)	-14(7)	-27(6)	-24(8)
O(3)	96(7)	89(7)	101(8)	10(7)	-11(7)	43(7)
O(4)	65(6)	147(10)	93(8)	-16(7)	25(6)	6(8)
C(1)	65(9)	60(9)	53(8)	5(9)	18(7)	9(7)
C(2)	49(8)	78(10)	78(10)	0(8)	0(8)	-12(8)
C(3)	49(8)	77(10)	38(7)	-14(7)	11(7)	9(7)
C(4)	56(9)	89(12)	58(9)	10(8)	3(7)	-18(8)
O(5)	50(5)	43(5)	44(5)	0(4)	-7(4)	2(4)
O(6)	74(6)	38(5)	40(4)	8(5)	2(4)	0(4)
O(7)	48(5)	48(5)	38(4)	7(4)	-3(4)	-5(4)
C(5)	66(9)	34(7)	59(9)	-9(6)	-23(8)	-4(6)
C(6)	54(9)	60(9)	99(13)	-6(7)	-36(9)	8(8)
C(7)	103(15)	101(13)	144(18)	-23(12)	-58(16)	0(14)
C(8)	133(20)	109(16)	124(17)	-6(13)	-79(15)	-15(13)
C(9)	145(18)	84(12)	54(10)	-3(12)	-39(12)	6(9)
C(10)	87(11)	74(10)	62(10)	-26(10)	-20(9)	-7(8)
C(11)	59(10)	112(14)	120(15)	5(12)	3(11)	-17(12)
C(12)	79(14)	184(21)	200(26)	18(14)	33(15)	24(19)
C(13)	76(13)	155(20)	204(24)	16(13)	-23(14)	-43(49)
C(14)	196(23)	231(28)	69(13)	-52(22)	-55(15)	-22(16)

Atom	U_{11}	U_{22}	U_{33}	U_{12}	U_{13}	U_{23}
C(15)	98(11)	43(8)	35(7)	9(8)	-10(7)	8(6)
C(16)	122(15)	49(9)	50(9)	8(10)	23(9)	6(7)
C(17)	190(20)	59(10)	66(11)	22(15)	27(13)	24(9)
C(18)	255(25)	47(9)	53(9)	58(16)	-27(15)	-1(8)
C(19)	116(14)	88(12)	68(10)	40(11)	-56(10)	-18(9)
C(20)	111(13)	63(9)	47(8)	14(9)	-33(8)	2(7)
C(21)	117(15)	49(10)	107(13)	-7(10)	63(12)	24(10)
C(22)	119(14)	67(11)	135(16)	-21(11)	18(13)	3(12)
C(23)	170(20)	110(15)	144(18)	-26(15)	96(16)	3(13)
C(24)	185(22)	117(16)	95(14)	65(15)	-61(14)	-32(13)
C(26)	62(8)	51(8)	56(7)	-4(7)	12(6)	-17(7)
C(27)	72(10)	79(10)	64(9)	9(9)	37(8)	-14(8)
C(28)	80(11)	49(8)	70(9)	14(8)	-5(8)	-20(7)
C(29)	89(10)	39(8)	56(8)	-1(8)	7(8)	2(7)
C(30)	65(9)	39(7)	51(8)	7(7)	8(7)	0(6)
C(31)	70(9)	78(11)	57(9)	8(9)	14(8)	-13(8)
C(32)	71(11)	124(14)	102(13)	0(10)	30(9)	22(11)
C(33)	90(10)	90(11)	49(8)	-4(11)	25(8)	9(9)
C(34)	187(20)	61(10)	82(11)	-19(13)	-1(14)	-24(9)

Note: Estimated standard deviations are given in parentheses. $T = exp-2\pi^2(U_{11}h^2a^{*2} + ... + 2U_{12}hka^*b^*)$.

Table B-3. H-Atom coordinates ($\times 10^4$) and temperature parameters ($\times 10^3$ Å^2) for 16.

Atom	x/a	y/b	z/c	U_{eq}
H(5A)	8574	3143	2511	80
H(6A)	9909	4857	2341	80

Atom	x/a	y/b	z/c	U_{eq}
H(7A)	11360	4146	2854	80
H(7B)	10584	3203	2962	80
H(8A)	10078	5126	3320	80
H(8B)	10511	4279	3700	80
H(9A)	877	3394	3538	80
H(10A)	7324	4107	3003	80
H(10B)	8109	5045	2916	80
H(11A)	9875	3829	1596	80
H(12A)	11887	3973	1417	80
H(12B)	11413	4937	1709	80
H(12C)	12146	4137	2026	80
H(13A)	10925	2353	1558	80
H(13B)	11209	2472	2168	80
H(13C)	9924	2252	1983	80
H(14A)	7462	4353	3980	80
H(14B)	8666	4467	4273	80
H(14C)	8229	5315	3884	80
H(15A)	6583	5567	1502	80
H(16A)	7156	5335	415	80
H(17A)	7236	7078	330	80
H(17B)	6959	7190	936	80
H(18A)	5467	6441	150	80
H(18B)	5313	7496	407	80
H(19A)	4936	6738	1217	80
H(20A)	4718	5006	1296	80
H(20B)	5045	4880	695	80
H(21A)	8692	4985	980	80
H(22A)	9717	6234	1405	80

Atom	x/a	y/b	z/c	U_{eq}
H(22B)	8750	7032	1270	80
H(22C)	8473	6143	1663	80
H(23A)	10114	5861	537	80
H(23B)	9194	5400	142	80
H(23C)	9148	6551	284	80
H(24A)	3260	7087	705	80
H(24B)	3341	6002	459	80
H(24C)	3055	6140	1068	80
H(25A)	6641	2268	870	80
H(26A)	8804	1295	943	80
H(27A)	8418	668	70	80
H(27B)	7227	1231	84	80
H(28A)	7766	-356	746	80
H(28B)	6895	-438	271	80
H(29A)	5659	672	715	80
H(30A)	6038	1224	1565	80
H(30B)	7246	685	1546	80
H(31A)	8978	3028	760	80
H(32A)	10466	2817	98	80
H(32B)	10516	2003	552	80
H(32C)	9951	1738	-2	80
H(33A)	8583	3675	-69	80
H(33B)	8007	2645	-228	80
H(33C)	7434	3319	216	80
H(34A)	5011	-339	1381	80
H(34B)	5280	-982	869	80
H(34C)	6128	-1023	1361	80